A Pretreatment Process for Wood Based on Ionic Liquids

Von der Fakultät für Maschinenwesen der Rheinisch-Westfälischen Technischen Hochschule Aachen zur Erlangung des akademischen Grades eines Doktors der Ingenieurwissenschaften genehmigte Dissertation

vorgelegt von

Jörn Viell

Berichter: Univ.-Prof. Dr.-Ing. Wolfgang Marquardt

Univ.-Prof. Dr. rer. nat. Bodo Saake

Tag der mündl. Prüfung: 31.01.2014

Fortschritt-Berichte VDI

Reihe 3

Verfahrenstechnik

Dipl.-Ing. Jörn Viell,
Aachen

Nr. 942

A Pretreatment Process for Wood Based on Ionic Liquids

Berichte aus der
Aachener Verfahrenstechnik - Prozesstechnik

RWTH Aachen University

Viell, Jörn
A Pretreatment Process for Wood Based on Ionic Liquids
Fortschr.-Ber. VDI Reihe 3 Nr. 942. Düsseldorf: VDI Verlag 2014.
212 Seiten, 61 Bilder, 17 Tabellen.
ISBN 978-3-18-394203-9, ISSN 0178-9503,
€ 76,00 / VDI-Mitgliederpreis € 68,40.

Keywords: Pretreatment – Ionic Liquid – EMIMAc – Wood – Dissolution – Disintegration – Process Development – Process Analysis

The future chemical utilization of biomass as a renewable raw material requires a pretreatment to gain access to these macromolecules. This work describes the systematic development of such a pretreatment process using ionic liquids to convert wood into fermentable sugars. During the exploration of the effects of several ionic liquids on wood, a disintegration effect is discovered in this work, which is identified as the most promising pretreatment mechanism. Its benefit is demonstrated by a high yield of 65 % of sugars after a short enzymatic hydrolysis. Moreover, the experimental results are exploited in a process simulation to assess the energy demand and the economic prospect of the developed pretreatment concept. This analysis identifies advantages and bottlenecks of the biomass pretreatment with concentrated solvents such as ionic liquids. A discussion outlines the challenges to be tackled by further research to tailor pretreatment processes to biomass and economy.

Bibliographische Information der Deutschen Bibliothek
Die Deutsche Bibliothek verzeichnet diese Publikation in der Deutschen Nationalbibliographie; detaillierte bibliographische Daten sind im Internet unter http://dnb.ddb.de abrufbar.

Bibliographic information published by the Deutsche Bibliothek
(German National Library)
The Deutsche Bibliothek lists this publication in the Deutsche Nationalbibliographie (German National Bibliography); detailed bibliographic data is available via Internet at http://dnb.ddb.de.

D 82 (Diss. RWTH Aachen University, 2014)

ISSN 0178-9503
ISBN 978-3-18-394203-9

Vorwort

Die vorliegende Arbeit ist das Ergebnis meiner bisherigen Zeit am Lehrstuhl für Prozesstechnik von Herrn Prof. Dr.-Ing. Wolfgang Marquardt. Herrn Marquardt möchte ich an dieser Stelle besonders für das Projekt, das in mich gesetzte Vertrauen und seine wissenschaftliche Expertise bedanken, was diese Ergebnisse überhaupt erst ermöglicht hat.

Durch die interdisziplinären Fragestellungen dieses Projektes kam ich darüber hinaus mit diversen Kooperationspartnern in Kontakt. In diesem Zusammenhang bin ich dankbar für die Zusammenarbeit mit Herrn Dr. Roberto Rinaldi vom Max-Planck-Institut für Kohlenforschung in Mühlheim und für die Unterstützung durch Herrn Dr. Jürgen Puls vom Thünen-Institut für Holzforschung in Hamburg. Ebenso möchte ich Herrn Prof. Dr. rer. nat. Bodo Saake für die Übernahme des Koreferats danken.

In Aachen hätte ich die Ideen jedoch nicht allein umsetzen können und möchte daher meinen Kollegen danken. Insbesondere bin ich froh, mit Gerd Spalding immer einen Ansprechpartner in Fragen zu Analytik gehabt zu haben. Weiterhin gebührt an dieser Stelle meinen zahlreichen Studenten ein großes Dankeschön, da sie mich durch viele studentische Arbeiten und auch durch viele Stunden studentische Arbeitskraft auf der experimentellen Seite vielfältig unterstützt haben. Die langjährigen studentischen Mitarbeiter Caroline Marks und Jan Seiler sind an dieser Stelle besonders hervorzuheben.

Nicht zuletzt möchte ich auch meinen Eltern und meiner Partnerin für die immerwährende Unterstützung danken.

Jörn Viell

Content

Nomenclature

a,b,c,s	regression parameters	[J/mol]
G	molar Gibbs energy	[J/mol]
H	molar enthalpy	[J/mol]
$E_T(30)$	electronic transition energy of dye 30	[kcal/mol]
$E_T(33)$	electronic transition energy of dye 33	[kcal/mol]
m	mass	[kg]
n	refractive index	[-]
pH	logarithmic hydronium activity	[-]
pK_a	acid dissociation constant	[-]
P	power	[kW]
p	pressure	[bar]
Q	heat stream	[kW]
R	gas constant	[J/K/ mol]
T	temperature	[°C]
u	moisture	[-]
w	weight fraction	[-]
x	mole fraction	[-]

Greek symbols:

α	Kamlet-Taft acidity, activity	[-]
β	Kamlet-Taft basicity	[-]
δ_H	Hildebrand solubility parameter	[$MPa^{0.5}$]
π^*	Kamlet-Taft polarity/polarizability	[-]
μ	chemical potential	[-]
v	molar volume	[m^3/mol]
γ	activity coefficient	[-]

Indices:

$solv$	solvation
i,j	component i,j
vap	vaporization
res	residual material after pretreatment/dissolution
sup	supernatant
sd	solid
liq	liquid

Abbreviations:

AFEX	ammonia fiber explosion
AMIMCl	1-allyl-3-methylimidazolium chloride
BMIMCl	1-butyl-3-methylimidazolium chloride
DMSO	dimethyl sulfoxide
DMIMDMP	1,3-dimethylimidazolium dimethylphosphate
DP	degree of polymerization
EMIMAc	1-ethyl-3-methylimidazolium acetate
HPLC	high pressure liquid chromatography
IL	ionic liquid
MD	molecular dynamics
NaOH	sodium hydroxide
SEM	scanning electron microscopy
UV/Vis	ultraviolet/visible
XRD	X-ray diffraction

Zusammenfassung

Die Fähigkeit zur Lösung von Cellulose in ionischen Flüssigkeiten initiierte die Idee einer vollständigen Auflösung von Holz zur weiteren enzymatischen Hydrolyse der Makromoleküle. Die physikalisch-chemischen Effekte dieser neuen Stoffklasse der ionischen Flüssigkeiten sind bisher nur bruchstückhaft verstanden und weiterhin gibt es für einen derartigen Holzaufschluss keine ausgearbeiteten Prozesskonzepte. In dieser Arbeit soll daher vom Experiment bis zur Simulation ein Prozess für die Vorbehandlung von Holz mittels ionischer Flüssigkeiten entwickelt werden.

Erstens wurden umfangreiche experimentelle Untersuchungen zu den Lösungsmechanismen mit ionischen Flüssigkeiten mit dem Ziel einer effizienten enzymatische Hydrolyse durchgeführt. Zur Charakterisierung werden neben detaillierten Massenbilanzen die Mikroskopie, die Röntgenstreuung und die Raman-Spektroskopie eingesetzt. Zweitens wurde mit den gewonnenen Daten ein konzeptioneller Prozessentwurf mit Hilfe eines Prozesssimulators (Aspen Plus) erstellt. Die energetische und ökonomische Bewertung identifiziert die Potentiale des entwickelten Prozesses.

Die experimentellen Ergebnisse im ersten Teil der Arbeit zeigen, dass die Auflösung sehr langsam verläuft. Bei 115°C wird ein gelöster Anteil von 80 m-% nach 48 bis 72 Stunden erreicht. Weiterhin geht eine Fraktionierung mittels Fällung aus dem gelösten Zustand mit deutlichen Verlusten in der Ausbeute einher. Die Konzepte zur vollständigen Auflösung von Holz erscheinen deshalb unrealistisch für eine technische Umsetzung.

Allerdings zeigen die untersuchten ionischen Flüssigkeiten deutliche Unterschiede im Lösungsverhalten mit unterschiedlichen Hölzern. Mit Fichtenholz ist in 1-Butyl-3-methylimidazolium Chlorid (BMIMCl) eine selektive Lösung von Cellulose zu beobachten, während Buche in 1-Ethyl-3-methylimidazolium Acetat (EMIMAc) zwar ohne Selektivität für eine Holzkomponente, dafür aber ungefähr mit der doppelten Rate aufgelöst wird. Tatsächlich kann mit EMIMAc diese Lösungsrate für mehrere Partikelgrößen von Abmessungen im Mikrometerbereich bis hin zu Holzchips mit 10 mm Länge beobachtet werden. Diese partiell größenunabhängige Lösung wird auf einen Desintegrationseffekt von EMIMAc zurückgeführt, der ein zerfasertes Material mit deutlich höherer spezifischer Oberfläche erzeugt.

Dieser Desintegrationseffekt ist durch systematische Analyse genutzt worden, um ein schnelles und effektives Vorbehandlungsverfahren zu entwickeln. Mikroskopische Untersuchungen weisen eine Desintegration der Spätholztracheiden in Fichte nach; in Buchenholz wird darüber hinaus eine komplette Desintegration die einzelnen Holzzellen innerhalb kurzer Zeit beobachtet.

Der Mechanismus der Desintegration wird mit verschiedenen analytischen Technologien untersucht. Der Vergleich mit Lösungsparametern zeigt, dass die Basizität zwar die Celluloselösung in ionischen Flüssigkeiten beeinflusst, nicht direkt jedoch den Desintegrationseffekt erklärt. Die weitere Analyse zeigt eine Deacetylierung der Hemicellulosen, eine Reduktion der Cellulosekristallinität und eine Verringerung des Syringylgehaltes im Lignin. Eine mögliche Erklärung für die Desintegration ist daher die Schwächung der Mittellamelle und Ablösung der einzelnen Zellen durch Quellung der Sekundärwand aufgrund der Solvatisierung der Cellulose.

Das damit erarbeitete Prozesskonzept zur Vorbehandlung von Buchenholzschnitzeln hat eine Verweilzeit von 1,5 h bei 115°C bei einem maximalen Wassergehalt in EMIMAc von 8,5 m-%. In Kombination mit einer enzymatischen Hydrolyse zu Zuckern ergibt sich bereits nach 5 h eine Ausbeute von bis zu 65 m-% in Form löslicher Zucker. Sowohl die Verweilzeit als auch die Ausbeute ist damit im Vergleich zu unvorbehandelter Biomasse um eine Größenordnung verbessert worden.

Das Prozesskonzept wird im zweiten Teil der Arbeit in einen konzeptionellen Entwurf eines technischen Prozesses überführt. Die Prozesssimulation wurde inklusive geschlossener Rückführungen und Energieintegration durchgeführt, was die Analyse des technischen Energiebedarfs und des ökonomischen Potentials ermöglicht.

Der gesamte Energiebedarf ist niedriger als beim Organosolv-Verfahren mit organischen Lösungsmitteln, wird aber ähnlich von der Wiederaufbereitung des Lösungsmittels dominiert. Dabei begründet die Thermodynamik der hygroskopischen ionischen Flüssigkeiten mit Wasser eine schlechtere Effizienz der Wärmeintegration. Es ergibt sich mit 7 $MJ/kg_{Biomasse}$ ein Bedarf von 34% des Energieinhaltes des eingesetzten Holz zur Produktion von Zuckern mit Lignin als potentiellem Nebenprodukt.

Die wirtschaftliche Analyse zeigt einen hohen Einfluss der Rückgewinnungsrate der ionischen Flüssigkeit und deren Kosten auf die Ökonomie. Trotz sehr niedrig

angenommener Preise für die ionische Flüssigkeit lassen nur sehr hohe Rückgewinnungsraten eine wirtschaftliche Arbeitsweise möglich erscheinen. Wesentlich für eine wirtschaftliche Attraktivität ist daher eine höhere Inwertsetzung durch hochwertigere Produkte aus Lignin und Kohlenhydraten und die Entwicklung von effektiveren Abtrennkonzepten zur Abtrennung der Lösungsmittel und der Produkte. Die Kapitalkosten des entwickelten Prozesses sind jedoch im Vergleich zum Organosolv-Verfahren halbiert, was Vorteile bei der dezentralen Umsetzung bei kleinen Anlagengrößen ergibt. Die maßgeschneiderte Applikation der zugrundeliegenden ionischen Wechselwirkungen in reaktiven Aufschluss- und Konversionsprozessen stellt daher weiteres Potential in biobasierten Wertschöpfungsketten in Aussicht.

1 Introduction

The current supply chain of consumer goods in terms of energy, chemicals, and fuels depends strongly on the processing of crude oil. The expected depletion of fossil resources and the awareness of the anticipated effects of its utilization foster the exploration of more sustainable resources to cover the growing world-wide demand. A renewable feedstock is clearly favored in this regard.

The shift of raw materials for chemical processing offers the possibility for innovative products and more efficient production routes (Marquardt et al., 2010). In this line, the exploitation of biorenewables also involves new process synthesis problems in contrast to the established refining strategies in petroleum-based processing in order to develop sustainable processes based on mild and selective conversion steps. Such an approach is followed by the cluster of excellence “Tailor-made Fuels from Biomass” at RWTH Aachen University, which integrates the design of a bio-based, zero-emission fuel with the research of biomass conversion.

Concerning the availability, the largest potential of biorenewable carbohydrates is expected from lignocellulosic biomass that is estimated at several billion tons per year (Tuck et al., 2012; Pauly & Keegstra, 2008). The most prominent example of lignocellulosic feedstock is wood. It does not compete with edible plants, thus, it can potentially provide a feedstock for sustainable value chains in terms of chemicals from wood. On the other hand, wood is highly recalcitrant against biological, chemical, and mechanical attack due to its composite-like structure. A selective and efficient conversion process to chemical intermediates is therefore challenging.

Wood can be utilized as a fuel directly or for synthesis gas production, but this does not meet the envisaged strategy of chemical utilization while preserving the molecular structure. It must also be mentioned that pulp and paper production also does not match the objectives of producing chemical intermediates and involves harmful emissions and significant degradation of biomass compounds. Rather, mild and selective processing concepts are desired to comprehensively utilize all biomass constituents in integrated fractionation and conversion schemes to be materialized in a biorefinery operation (Kamm et al., 2006). Hence, novel pretreatment, fractionation and conversion routes are required for the processing of wood for fuels and chemicals.

In 2002, the dissolution of cellulose was discovered in ionic liquids at mild temperatures (Swatloski et al., 2002). This presents an outstanding capability because common solvents do not enable its dissolution and processing in the homogeneous phase. Moreover, ionic liquids are non-volatile in contrast to organic solvents which emissions contribute to global warming. Several years later, the first reports on the dissolution of wood were published (Kilpeläinen et al., 2007; Fort et al., 2007). Dissolution envisioned homogeneous processing routes and an all-purpose pretreatment. However, knowledge about the mechanisms of dissolution is still scarce, first, with respect to the complex and diverse structure of wood, and second because of the new material class of ionic liquids. Furthermore, none of the process ideas has been thoroughly evaluated. Hence, a systematic process development and design is required to assess the potential of ionic liquids in biorefinery schemes.

This thesis presents the results of a systematic investigation of an ionic liquid-based pretreatment of wood and the simulation and analysis of an industrial-scale pretreatment process. The work started in 2008 shortly after the seminal paper of Kilpeläinen et al. (2007) and Fort et al. (2007) and therefore reflects the chronological development in the scientific community worldwide as well as in our laboratory starting from dissolution to the more general term of a pretreatment of wood. The latter can clearly involve many more effects than anticipated by simple dissolution. The investigative development of a beneficial process concept thus also addresses the mechanisms to gain further understanding that can be possibly exploited in the design of tailored reaction media for wood pretreatment and conversion.

The thesis is structured as follows: First, the fundamentals of wood composition and structure are presented to delineate the complexity of the raw material. The challenge of its pretreatment becomes obvious by an overview on established wood pretreatment processes, which also depict the challenges and serve as a benchmark for the pretreatment concept with ionic liquids. Afterwards, the development in the field of ionic liquid processing of (ligno-)cellulose is briefly reviewed. This overview of the raw material, the challenges in pretreatment and the known abilities of ionic liquids thus leads to the objectives of this thesis in Section 2.4. Chapter 3 then presents the experimental protocols and analytical methods which were developed in order to quantify the changes induced by the processing in ionic liquids. The presentation of results is split into Chapters 4 and 5 presenting first the experimental results about dissolution and pretreatment of wood and next the design and analysis of an innovative pretreatment process for wood employing an ionic liquid.

2 Wood and its chemical processing

Chemical processing depends on the state and composition of the material to be converted. Wood in particular is not only a simple mélange of several constituting biopolymers, but in fact, exhibits embedded and interwoven structures on the molecular, supramolecular, and morphological level (Fengel & Wegener, 1989; Klemm et al., 1998). These fundamental differences to a liquid feedstock like petroleum have to be observed when the conversion of wood into chemicals is aimed at.

This chapter gives an overview of the chemical composition of wood and its structural assembly. Afterwards, industrial processes on wood pretreatment and conversion are reviewed with a focus on the underlying molecular mechanisms and on the process yields. The review includes pulping processes for paper production, wood saccharification processes for sugar production and briefly a dissolution process to produce viscose. This is then the basis on which to discuss the pretreatment of lignocellulose with ionic liquids (ILs) and its development in recent years.

2.1 Composition and structure of wood

Wood mainly consists of ~45 wt % cellulose, ~25 wt % hemicelluloses and ~25% lignin. As these biopolymers exhibit a sophisticated structure, the composition and structure is described comprehensively starting with the individual molecules. Afterwards, their assembly in the cell wall is discussed. The final stage in this bottom-up approach is the macroscopic morphology of the wooden material.

2.1.1 Wood components and supramolecular structure

A c*ellulose* macromolecule consists of several glucose monomers that are linked by the elimination of one water molecule to two successive glucose entities (Fengel & Wegener, 1989). The repeating unit of cellulose is thus the anhydroglucose

monomer, which consists of a 6-membered ring of carbon atoms and one oxygen atom (Figure 2.1). While the C(2), C(3), and the C(6) atoms are functionalized with hydroxyl groups, the C(1) and the C(4) atoms are connected with the next monomer via β-1,4 glycosidic bonds. At one end of the chain, the C(1) atom bears an aldehyde hydrate group with reducing properties (Fengel & Wegener, 1989). This is the reducing end, in contrast to the hydroxyl at the C(4) as the non-reducing end.

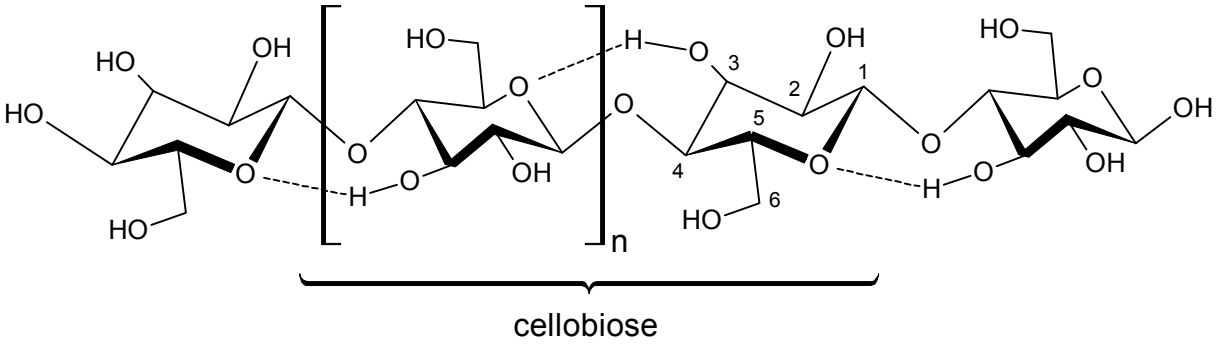

Figure 2.1. The cellulose polymer with its base unit of anyhdroglucose and the structurally repeating unit of cellobiose. The numbers depict the numbering of carbon atoms and the dashed line shows some important intra-molecular hydrogen bonds. The reducing end of the chain is on the right and the non-reducing end is on the left.

The precise molecular formula of cellulose is $C_{6n}H_{10n+2}O_{5n+1}$ (Belitz et al., 2008). Neglecting one water molecule leads to the common formula $(C_6H_{10}O_5)_n$ with a molecular mass of 162 per unit building block. The formula and Figure 2.1 introduce the number of monomers, n, which is equal to the degree of polymerization (DP). The β-1,4 glycosidic bond requires an alternating configuration of the anydroglucose units such that the structural repeating unit is the cellobiose. It results in the linear chains of cellulose with DP ≥ 10,000 in native celluloses (Fengel & Wegener, 1989).

The numerous hydroxyl groups enable intra- and intermolecular hydrogen bonding. While the intramolecular bonds are stabilizing the chains as shown in Figure 2.1, the intermolecular hydrogen bonds enable a close, parallel packing of neighboring linear cellulose chains. Several patterns of a regular hydrogen bonding network are possible, which are characterized by different crystal structures of cellulose. They all show the same chemical composition and only differ in their particular intra- and intermolecular hydrogen bonding network.

The native crystalline cellulose is referred to as cellulose I (Zugenmaier, 2008). It can be differentiated into cellulose Iα from algae and bacteria and cellulose Iβ from higher plants. Only the latter is considered in this work. An investigation by combined X-ray and neutron diffraction reveals the lattice structure of the cellulose crystals (Nishiyama et al., 2002). Briefly, the rather planar glucose rings are organized in sheets with their plane perpendicular to the axes of the cellulose chains (depicted Figure 2.2, left). The intermolecular hydrogen bonds of cellulose Iβ are only formed to adjacent chains within the sheet. The resulting crystal exhibits a monoclinic unit cell with the unit vectors a, b and c.

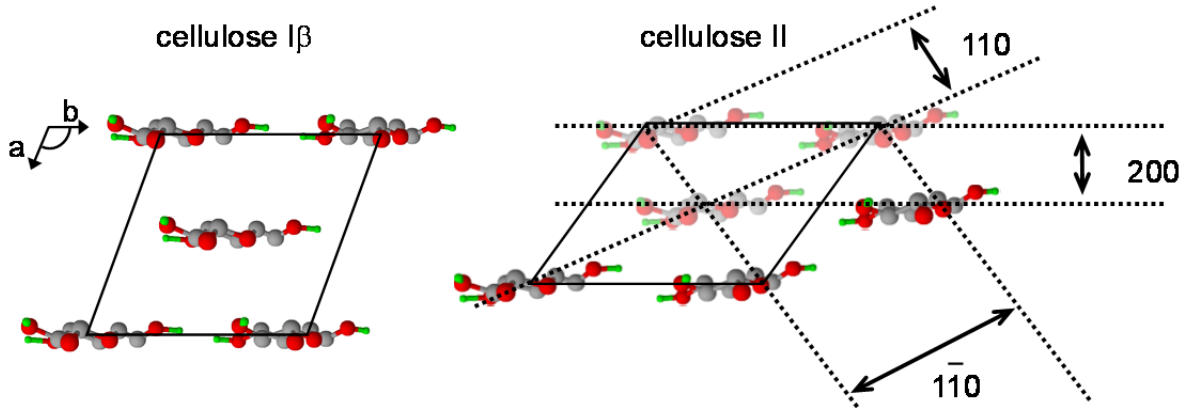

Figure 2.2. The different crystal unit cells of the cellulose polymorphs Iβ (left) and II (right). The cellulose chains form a fibril along the unit cell axis c. The lattice planes of the crystalline unit cell are exemplarily depicted for cellulose II including the corresponding Miller indices; they apply to cellulose Iβ accordingly. Hydrogen bonds are not shown for clarity.

The other crystalline polymorph of cellulose considered in this work is cellulose II. In addition to cellulose Iβ, it constitutes inter-sheet hydrogen bonds of anti-parallel direction (Langan et al., 1999) due to the smaller distance in the unit cell as depicted in Figure 2.2. This configuration results in a more stable polymorph compared to cellulose Iβ from a thermodynamic point of view (Beckham et al., 2011). The transition from cellulose Iβ to cellulose II is thus irreversible. It is usually carried out by a treatment of cellulose Iβ in alkaline aqueous solutions (mercerization) followed by neutralization and washing.

The cellulose polymorphs are commonly identified by wide angle X-ray diffractometry. The lattice planes of the cellulose crystal result in the characteristic reflections that are labeled in Figure 2.2 according to Sugiyama et al. (1991) and Matthews et al. (2011). As can be seen in the figure, the cellulose crystals differ in space between the lattice planes, which therefore cause reflections of the X-ray beams at different angles. Other man-made polymorphs of crystalline cellulose are not considered in this thesis (cf. Zugenmaier, 2008).

The native crystalline cellulose forms elementary fibrils or microfibrils. Electron microscopic investigations indicate that they likely comprise of 36 cellulose chains width a cross-section of 3–4 nm (Klemm et al., 2005; Ding & Himmel, 2006). The crystallites are of the same diameter (Hon, 2000) and occur intermittently with amorphous cellulose. This term describes cellulose without crystalline planes or a regular hydrogen bonding network.

Another group of carbohydrates in wood, the *hemicelluloses,* are also polysaccharides but constitute of hexoses and pentoses, i.e., xylose, mannose, glucose, rhamnose galactose, and arabinose (Fengel & Wegener, 1989). They are organized into a chain as the main backbone, which is frequently branched and substituted with sugars. The particular amount, composition and structure vary with the type of tissue and species. While glucomannans are dominating in softwoods, e.g. spruce (*Picea abies)*, xylans are the major hemicellulose in hardwoods such as beech (*Fagus sylvatica)*.

The hemicelluloses in hardwoods consist mainly of xylose and contain a rather high amount of acetyl groups (Fengel & Wegener, 1989). The xylose units form a xylan chain with methylglucuronic acid side groups called O-acetyl-4-O-methylglucuronoxylan (Timell, 1967). Its repeating structure is shown in Figure 2.3. The xylose backbone is linked by β-1,4-glycosidic bonds and the acetyl groups are located at the C(2) and C(3) atom of the xylose. In beech, roughly half the xylose backbone is substituted with acetyl groups. Furthermore, the xylan is branched with 4-O-methylglucuronic acid groups linked via α-1,2-glycosidic bonds. The methylglucuronic acid is present at an average molar ratio of xylose:methylglucuronic acid of 10:1 (Fengel & Wegener, 1989).

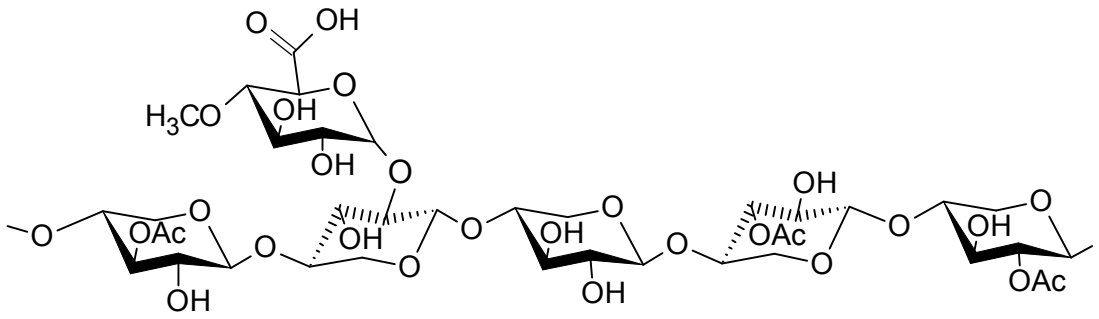

Figure 2.3. The repeating structure of O-acetyl-4-O-methylglucuronoxylan as found in hardwood hemicelluloses (after Fengel & Wegener (1989)).

In softwoods, the hemicelluloses consist mainly of mannose, xylose, galactose, and arabinose, i.e., O-acetyl-galactoglucomannan and arabino-4-O-methylglucuronoxylan (Figure 2.4). The latter shows a xylan backbone but no acetyl groups. Instead, it is substituted with arabinose at the C(3) atom and 4-O-methylglucuronic acid at the C(2) atom. The molar ratio of xylose to arabinose to 4-O-methylglucuronic acid in spruce is 7.4:1:1.25 (Fengel & Wegener, 1989). The most common hemicellulose in softwood is O-acetyl-galactoglucomannan (Figure 2.4). Its backbone consists of glucose and mannose at a ratio of 1:3. Galactose is observed to branch away via α-1,6 glycosidic links. It can occur in similar amounts as glucose in the backbone (Sjostrom, 1993). Few acetyl groups are also found at the C(2) and C(3) atoms of either glucose or mannose at roughly every third to fourth hexose unit. This is about half the amount found in hardwood xylan.

All hemicelluloses are macromolecules with DP = 100–200 (Fengel & Wegener, 1989), which is relatively low in comparison to cellulose. Nevertheless, they are mainly insoluble in water and require sophisticated extraction schemes (Ishii & Shimizu, 2000; Timell, 1967). Their heteropolymeric and branched nature also prevents the formation of crystalline regions. Further details on hemicellulose structure and composition can be found elsewhere (Fengel & Wegener, 1989; Ishii & Shimizu, 2000; Willför et al., 2005a; Pauly & Keegstra, 2008; Willför et al., 2009).

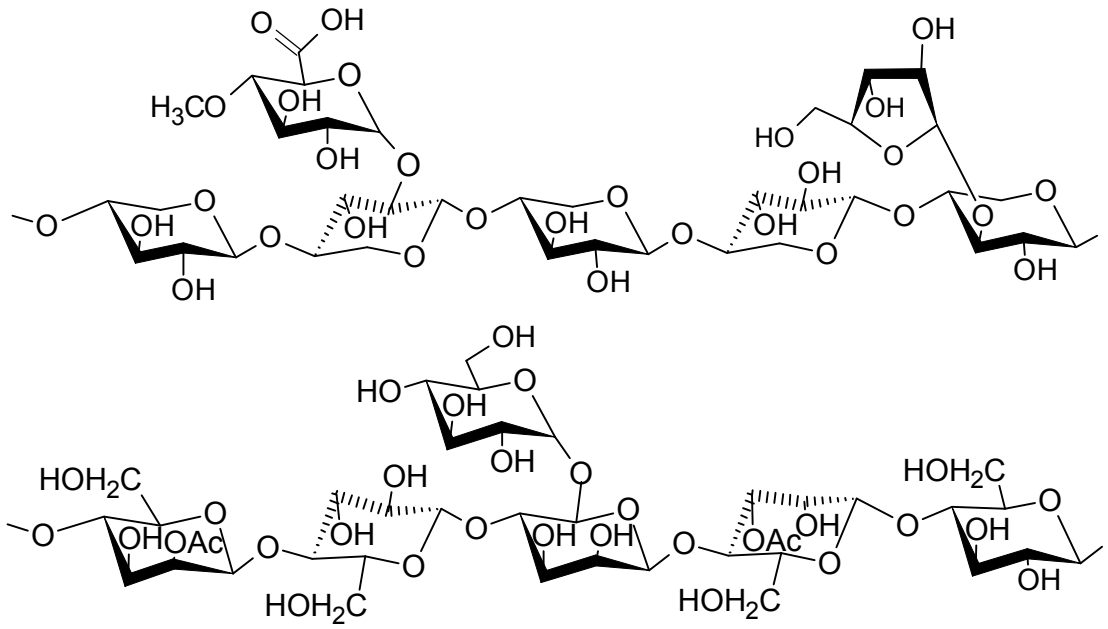

Figure 2.4. The structure of arabino-4-O-methylglucuronoxylan (top) and of O-acetyl-galactoglucomannan (bottom) of softwood (after Fengel & Wegener (1989) and Willför et al. (2008)).

Another fraction of matrix polysaccharides besides hemicelluloses are the pectins. There is some evidence that they are involved in the crosslinking of cellulose, hemicellulose and bound covalently to lignin (Caffall & Mohnen, 2009). The links of pectins are established by small ions, i.e., Ca^{+}, to support the tissue structure. In beech wood, the pectins are highly methylated thus preventing the ionic crosslinking to other macromolecules. In consequence the pectins are mainly water-soluble (poly-)galacturonic acids (Willför et al., 2005b).

Altogether, the content of galacturonic acids, 4-O-methylglucuronic acids and glucuronic acids make up 2.5 wt % in spruce in decreasing order, while beech wood has a higher overall content of acidic carbohydrates (i.e., methylglucuronic acids and galacturonic acids) of approximately 6 wt % (Willför et al., 2005b).

Lignin, the third structural polymer in wood, consists of aromatic moieties with a rather random structure. Lignin biosynthesis starts with the three precursors depicted in Figure 2.5 of coumaryl, sinapyl and coniferyl alcohol. During biosenthisis, these precursors form para-hydroxyphenyl, guaiacyl, and syringyl units in the polymerized lignin molecule (Argyropoulos & Menachem, 1997) shown in Figure 2.6. The phenylpropanoid units are linked to each other by C-C bonds or, more often, by ether

bonds at the α- or β-carbon atom of the side chain (Sjostrom, 1993). The occurrence of β-O-4 bonds differs from species to species. The lignin in beech shows 39 to 48% β-O-4 bonds and 11 to 16% α-O-4 bonds, while the same total fraction of ether bonds is rather equally distributed between α- and β-ether bonds in spruce (Saake & Lehnen, 2007).

The different plant species also show characteristic differences in the distribution of the three base units. Beech wood demonstrates mixed lignins of guaiacyl, syringyl and very few para-hydroxyphenyl lignin units (56%:40%:4%), whereas spruce consists almost completely of guaiacyl lignin (G:H:S 94%:1%:5%, Fengel & Wegener (1989)). Due to the mixture of guaiacyl and syringyl monomers, the lignin of hardwoods is regarded as less crosslinked and less condensed due to fewer bonds between the aromatic rings (Saake & Lehnen, 2007). An arsenal of analytical techniques has been applied to further quantify lignin and its molecular structures, but the knowledge is still not satisfactory (Hon, 2000). The unavoidable isolation of the labile macromolecules in wood still limits the comprehensive characterization, which becomes obvious by the considerable differences between lignins obtained by different extraction techniques (Holladay et al., 2007). An exemplary molecular structure is shown in Figure 2.6.

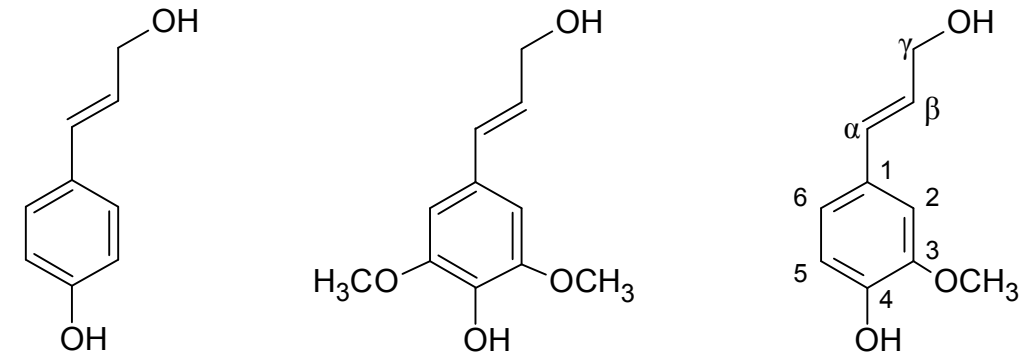

Figure 2.5. The lignin precursor units of coumaryl, sinapyl and coniferyl alcohol. The latter also shows the numbering and lettering of the phenylpropane moiety (Saake & Lehnen, 2007).

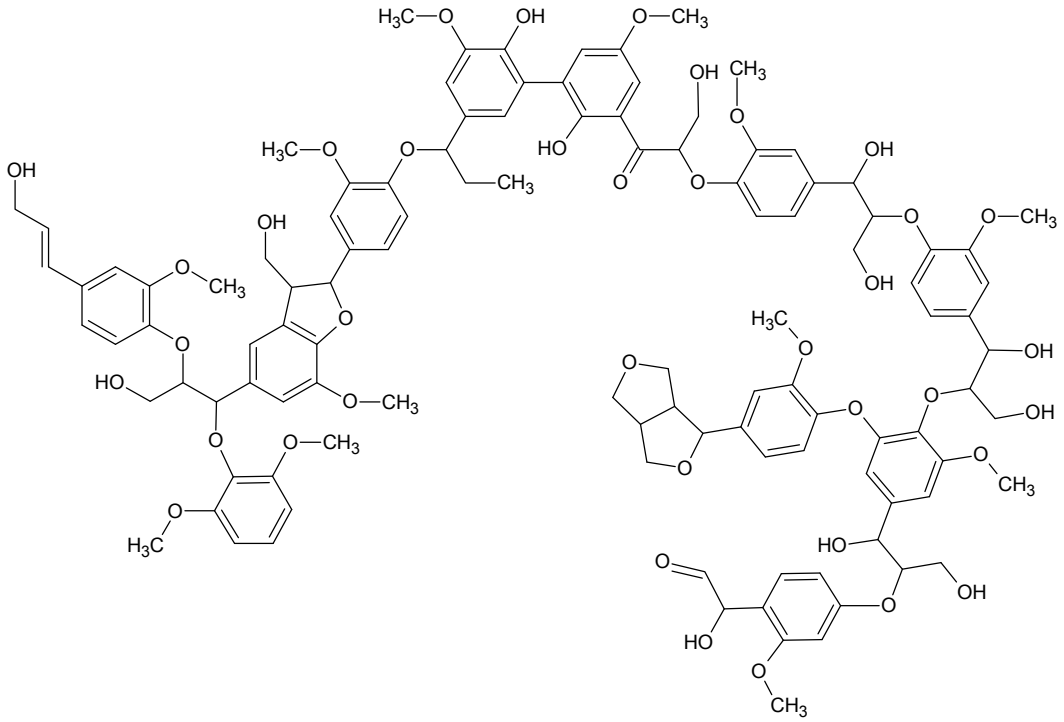

Figure 2.6. A possible structure of lignin. The phenylpropanoid units are linked by α-O-4, β-O-4 and C-C bonds. Note that the number of lignin units does not correspond to the statistical distribution in wood (modified after Zakzeski et al. (2010).

In addition to the structural carbohydrates, several non-structural compounds are present in wood, commonly referred to as extractives and inorganic components. Although extractives like fats, waxes, tannins, acids, oils, etc. are existent only in a few percent (to a greater extent in softwood), they determine smell, color, and resistance of wood against degradation (Fengel & Wegener, 1989). The definition is based on extraction with organic solvents, which is therefore a sum parameter. Extractives are not a major constituent of wood but might prove beneficial sources for specialty chemicals and pharmaceuticals (Hon, 2002). The inorganic components turn into ash after combustion and consist of calcium, magnesium, and potassium and the like. They amount to less than 1 wt % with the highest concentration in leaves or needles, bark and roots.

2.1.2 Cell wall architecture

The cells are assembled by the main components described in Section 2.1.1 to give strength and stability to the wood cells (Salmén & Burgert, 2009). The elementary

fibrils of cellulose are coated with hemicelluloses to become microfibrils without a considerable increase in size. They are further grouped into aggregates or macrofibrils of about 10 to 30 nm and are embedded in a stabilizing matrix of hemicellulose and lignin (Hon, 2000; Salmén & Burgert, 2009). From a molecular point of view, the versatile structure of hemicelluloses is crucial in bonding to lignin and carbohydrates. On the one hand, the linear backbone of the hemicelluloses can link very well to celluloses via hydrogen bonding. Lignin, on the other hand, is connected to hemicellulose or pectic substances by covalent links, namely ether, ester, and glycosidic bonds (Fengel & Wegener, 1989). Although there is progress in the description of the xylan-glucan interactions on an atomistic level (e.g. Hanus & Mazeau, 2006), the lignin-carbohydrate complex is, however, still not understood satisfactorily (Salmén & Burgert, 2009).

The complex of cellulose, hemicellulose and lignin is built during biosynthesis to form the plant cell wall. The so-called middle lamella encompasses each cell and is the most outer layer, which is shared between the adjacent cells. It is virtually free of cellulose (Fengel & Wegener, 1989) and mainly consists of pectins and lignin (Ishii & Shimizu, 2000; Pauly & Keegstra, 2008). During cell growth, cellulose is deposited at the inside of the middle lamella in a disordered state and results in the primary wall. It is hardly differentiable on microscopic images from the middle lamella, which is why it is often called ‘compound middle lamella’ (Fujita & Harada, 2000). Then, on the inside of the primary wall, the cellulose fibrils are synthesized in distinct angles layer-by-layer similar to a composite material (Salmén & Burgert, 2009). The matrix of hemicellulose and lignin then finally combines the compressive stiffness of lignin with the tensile strength of the cellulose fibrils.

A brief overview of the composition of the cell wall is given in Table 2.1. It demonstrates that the concentration of the different wood constituents does not necessarily correspond to the overall composition of wood. The absolute amount of lignin and cellulose is highest in the thick secondary wall. The compound middle lamella consists of nearly two thirds of lignin and a considerable amount of pectins (Fromm et al., 2003). Despite this high lignin concentration, the contribution of lignin in the primary wall to the overall composition is rather low due to its small size. It was also found that the primary wall differs in the distribution of methoxy groups, carbonyl moieties, and α- and β-O4 bonds (Sorvari et al., 1986; Donaldson, 2001), which demonstrates particular differences in lignin composition and structure in comparison to the secondary wall.

Table 2.1. The distribution of the main components in the cell wall layers of softwood tracheids (Kadla & Dai, 2006). The values in brackets refer to the mass fraction of the individual components relative to the total amount in softwood. The difference is caused by the different thickness of the layers, which are given with respect to earlywood and latewood (Fengel & Wegener, 1989).

layer	component mass fraction and fraction of total component				layer thickness	
	lignin	cellulose	hemi-cellulose	pectin	early-wood	late-wood
compound middle lamella	65% (21%)	12% (3%)	8% (4%)	15% (75%)	0.09 µm	0.09 µm
secondary wall	25% (79%)	45% (97%)	30% (96%)	<1% (25%)	1.92 µm	3.07 µm

2.1.3 Morphology of wood

The cells form the tissue of wood. It provides for the strength of trees, or in technical terms, for the mechanical support and allows for storage and transport. Generally, wood consists of mainly vertical, empty (dead) cells, whose organization, morphology, and type varies in the different species. Softwood tissue shows two types of cells, approximately 90–95% are tracheids and 5–10% are parenchyma cells (Fengel & Wegener, 1989). Tracheids are on average 2.9 mm in length and 30 µm in diameter. They are responsible for conducting liquids and give mechanical stability. The parenchyma consists of non-differentiated cells and is a repository for biochemicals. Additionally, certain species like pine, spruce, fir, or larch exhibit a three-dimensional network of radial and vertical resin canals surrounded by parenchyma.

Hardwood has a much more diversified structure and consists of fibers and vessels instead of only one cell type in softwood. The fibers in hardwood are much smaller than the tracheids in softwoods, approximately 1 mm in length and 18 µm in diameter (Fengel & Wegener, 1989). While fibers stabilize the tissue, the wide-lumened vessel

cells are specialized in conducting liquids. The length can reach up to several hundred millimeters with a diameter of a few hundred microns.

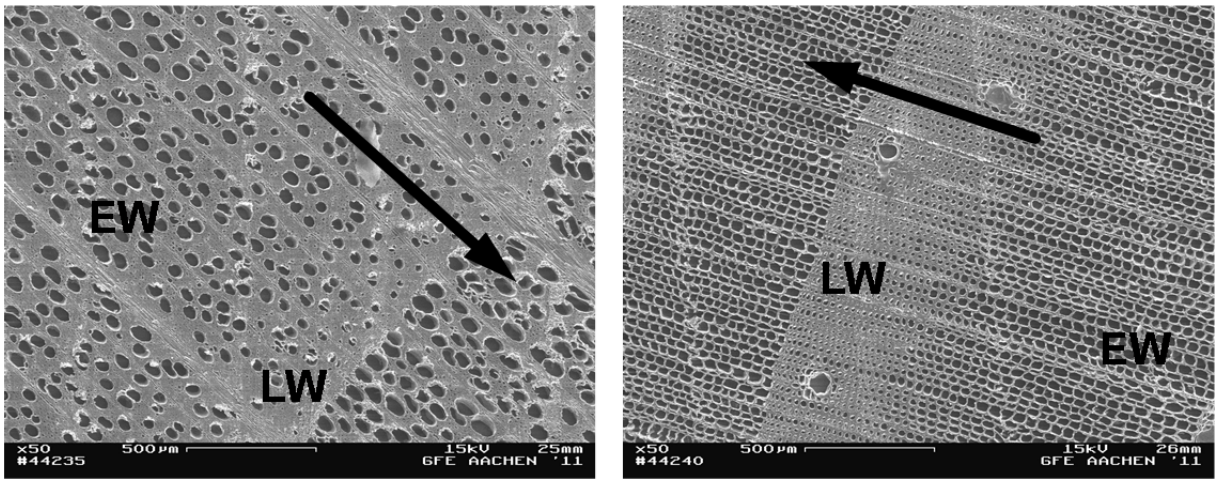

Figure 2.7. The different tissue of a hardwood (beech, left) and a softwood (pine, right) as observed with scanning electron microscopy of cross-sections. The arrow indicates the direction of radial growth. Additionally, the structures of earlywood (EW) and latewood (LW) are marked.

The morphologic differences between hardwood and softwood can be easily observed in photographs taken from scanning electron microscopy (SEM) in Figure 2.7. Beech, as an exemplary hardwood, exhibits large vessels, which are diffusely distributed over the tissue and surrounded by fibers and parenchyma cells. In contrast, the softwood tracheids of for example pine (Figure 2.7, right) are regularly arranged in the tissue and vary only in size. These variations form the structures of earlywood and latewood, which occurs in both species but less pronounced in beech (Figure 2.7, left).

The difference between earlywood and latewood is due to the seasonal vegetation. During growth of the tree, new cells are formed concentric around the existing cells in the layer beneath the bark, i.e., the region of the greatest metabolic activity. Formerly active cells slowly decay and form heartwood. The initially low lignin concentration increases during heartwood formation and results in higher stability of the tissue. Macroscopically, these changes in annual growth are visible as growth rings of the tissue. The fact that latewood consists of much denser tracheids formed in fall with a thicker secondary wall. In contrast, the faster growth rates in spring and summer

create open-lumened earlywood with a smaller cell wall thickness (cf. Table 2.1). In hardwood, the differences in size due to seasonal growth are less pronounced and lead to only a small growth ring.

The complexity of the structure of the raw material is illustrated in Figure 2.8. The molecules of cellulose, hemicellulose and lignin that are to be isolated from wood, are embedded in a composite-like structure, which limits the access to the macromolecules. The supramolecular assembly of lignin and carbohydrates and the crystallinity of the cellulose has to be cleaved by gentle and mild processing preserving the functionality of the components. Additionally, the tissue exhibits a sophisticated ultrastructure of cells and tissue that can cause macroscopic effects like limitations in mass transport.

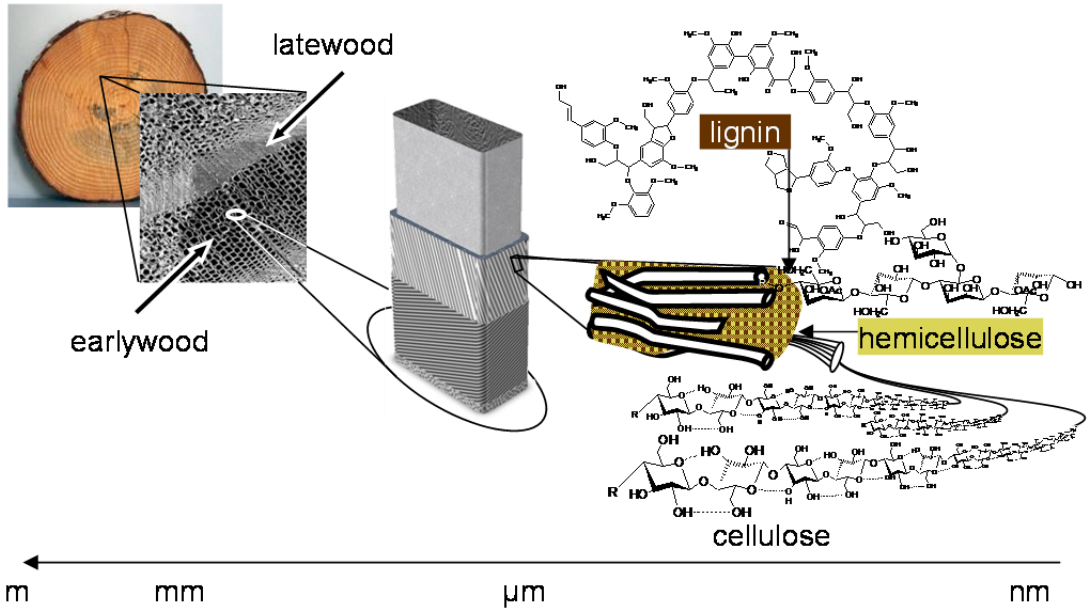

Figure 2.8. The structure of wood at different length scales and levels of complexity (modified after Kadla & Dai (2006) and Marquardt et al. (2010)). At the molecular level, the cellulose forms crystalline regions within the fibrils. They are embedded in a matrix of lignin and hemicellulose that forms the layers of the cell wall. The cell wall is the elementary structure of the cells, which constitute the tissue and determines the macroscopic morphology of wood.

2.2 Chemical processing of lignocellulose

The valorization of wood for a chemical utilization has to deal with the complexity of the wood structure described in the previous chapter. This section focusses on established processes to produce a chemical product from wood. Two concepts are presented; first the production of pulp and second the saccharification of wood.

Pulping processes aim at the delignification of wood to produce lignin-free pulp, either for paper production with high yield and strong fibers or for chemical utilization with high cellulose purity known as “dissolving pulp”. In this field, a huge amount of knowledge has been gathered in the last centuries with regard to how lignin can be cleaved and removed to minimize its residual content in pulp.

In contrast to pulp production, the saccharification of wood aims at depolymerization of the carbohydrates in wood, hence, a conversion of insoluble carbohydrates into soluble sugars is carried out, while the lignin remains as a solid residue. The employed processes involve dissolution of the carbohydrates at different stages during saccharification. The dissolution of cellulose or wood with ionic liquids is then discussed in Section 2.3.

2.2.1 Pulping processes

Pulping can be carried out by either mechanical or chemical means. Sixta et al. (2006) provide an extensive compilation on that field, which is the basis for the following discussion unless otherwise noted. The simplest way is mechanical pulping by pressurized grinding of the wood, favorably at temperatures slightly above 100°C to soften the lignin. The cells are liberated by cracking along the compound middle lamella or along the cell wall layers the cells are basically peeled off. The result is a low-strength pulp suitable for magazine paper when blended with chemical pulps of higher strength. The components of wood are thus not separated during mechanical pulping, but it is cheaper than chemical pulping and results in high yields of 85 - 95 wt %.

Chemical pulps are produced in large batch or continuous digesters at a cooking temperature of 130–170°C for 4–5 h and a liquid to wood ratio of approximately 3:1 to 4:1 (w/w). At least 80% of the lignin is removed this way and the fibers can be

disintegrated. There are two predominant industrial processes, the *sulfite process* and the *Kraft* or *sulfate process*, which both utilize sulfur-containing chemicals.

The *sulfite process* is based on sulfur dioxide SO_2 and a cooking base. SO_2 in water forms hydrogensulfite HSO_3^- that can break the α-O-4 bonds of lignin by protonation and nucleophilic addition. The stronger β-O-4 bonds are cleaved by stronger nucleophiles at higher pH (neutral or alkaline) forming water-soluble lignosulfonates. An concentration of approximately 17 g SO_2 per kg of dry wood is prepared initially. The SO_2 and HSO_3^- is consumed during cooking and has to be compensated by continuous addition of chemicals. Magnesium bisulfite $Mg(HSO_3)_2$ is commonly utilized as a base because it is easier to recover than the calcium or sodium salt and it also allows operation in a wider range of pH without precipitation of the salt.

Such conditions with variable pH are realized in multistage pulping. The range of operating conditions enables adjustment of the process to a broad variety of feedstock. Nevertheless, once the process is set up, it is rather inflexible towards variations in the feedstock. The pulp is separated from the cooking liquor by washing with water. Almost pure cellulose can be obtained in yields of 40–50 wt %.

The lignin, hemicelluloses, and the active chemicals are dissolved in the cooking liquor, which is sent to recovery. The lignosulfonates can be separated by precipitation, ultrafiltration or ion-exchange (Lebo et al., 2001). Evaporation of the liquor removes the water and leaves a residue of sugars, remaining lignosulfonates and salts. This solid is then burned to recover the active chemicals such as magnesium oxide and SO_2. The exhaust fumes cause the main emissions of this pulping process. Its drawback in recovery, the rather low strength of the fibers, and the inflexibility in feedstock utilization are the reasons why sulfite pulping plays only a minor role in worldwide fiber production despite the highly pure fibers.

The most widely used pulping process is the *Kraft or sulfate process,* which accounts for more than two thirds of worldwide pulp production. It is a basic process with OH^- and HS^- ions in aqueous sodium solution. The OH^- ions ionize the phenolic groups of the lignin moieties (cf. Figure 2.6) by nucleophilic attack. This enables cleavage of α-O-4 bonds of lignin and the stronger nucleophiles HS^- then subsequently cleave the β-O-4 bonds. While the former process is taking place mainly during initial delignification, the stronger β-O-4 bonds and in particular the etherified phenolic groups are broken during the consecutive stages of bulk and residual delignification. The strongly nucleophilic HS^- can also demethylate the methoxy groups of lignin. A

fundamental difference to sulfite pulping is that the sulfur is bound only temporarily to lignin in these reactions.

Despite the higher amount of β-O-4 bonds in hardwoods, the progress of Kraft delignification is much faster with hardwoods than with softwoods. This is considered to be due to the guaiacyl lignin which shows a higher degree of cross-linked units in softwood. An additional advantage of hardwoods in Kraft processing is due to the fact that xylan is stable under basic conditions. It results in rather high yields of 50 to 60 wt % of the wood as fibers, which is considerably more than the cellulose content. The final yield is a tradeoff between the beginning degradation of carbohydrates and the residual delignification. The lignin is therefore not completely removed in the Kraft process with a residual lignin fraction of a few percent at maximum fiber yield. The fibers are therefore subject to subsequent bleaching. The main advantage of the Kraft process is the robustness to variations in feedstock.

Although the sulfur is not considerably consumed during Kraft pulping, it is lost with the black liquor or with volatile and odorous mercaptanes. The recovery of OH^- and HS^- is realized similarly to the sulfite process, i.e., by evaporation and burning of the dissolved organics. Combustion and recausticizing with calcium to purge carbonate as insoluble $CaCO_3$ finally yields $NaOH$ and NaS_2 that can be reused for the next cook. The losses during the process and the neutralizing action of acidic groups in wood require the addition of $Na_2SO_4^-$, which explains its alternative name *sulfate process.* The cooking liquor has a concentration of approximately 18 wt % of active alkali per kg dry wood. Further details of these pulping processes are given by Fengel & Wegener (1989), Sakakibara & Sana (2000) and Sixta (2006, pp 109–510).

The difficult recovery of chemicals and the interest in sustainable processes have fostered the development of more environmentally-friendly pulping processes reviewed by Schliephake (1990). One example is the alkaline sulfite-anthraquinone-methanol (ASAM) process, where the gaseous SO_2 is substituted by Na_2SO_3. The concerted action of sulfur, methanol and water leads to an enhanced delignification without volatile sulfuric molecules. Despite the proven applicability of the pulp, a demonstration at technical scale could not be realized due to a research agenda that despite more than 50 man-years of development did not consider the recycling of solvents and the separation steps at the process level (Schubert, 2006).

Another alternative of an as yet also not commercially proven pulping process is the Organosolv process. It was developed by Kleinert and Tayenthal (1931) and utilizes

an organic solvent to dissolve the lignin at approximately 170–200°C for a few hours. The aim is to cleave lignin until it dissolves without derivatization in an aqueous mixture of an organic solvent, e.g., ethanol and water (Phillips, 1934; McDonough, 1992).

The cleavage of wood macromolecules in Organosolv processing can be either induced by bases or acids. The formation of acids from wood lowers the pH by auto-catalysis even if no additional acid catalyst is added. The higher acetyl content of hardwoods therefore results in faster delignification compared to softwoods (McDonough, 1992). The delignification seems to follow a first order kinetics with the consecutive stages of initial, bulk, and residual delignification (Oliet et al., 2000). In case of softwoods, the performance of Organosolv processing ceases and it requires additional catalysts (Yawalata & Paszner, 2004), e.g., divalent metal salts of chlorides, to liberate fibers with 60% yield and a lignin content of 10 wt %. Trivalent metal salts cause degradation of carbohydrates and reduce the yield.

Basic Organosolv processing can be realized with methanol and anthraquinone as catalyst but it comes at the expense of a complicated recovery. If run under acidic conditions, the process also extracts and dissolves the hemicelluloses. While the cellulose-rich solid remains, the dissolved lignin and hemicelluloses have to be separated by precipitation and solvent exchange. An extensive overview of the developments of Organosolv processing is given by Hergert (1997) and Zhao et al. (2009).

The Organosolv process is often claimed to be economically attractive because of easier solvent recovery only by evaporation in contrast to the more complicated combustion and recausticizing recovery cycle in Kraft processing (Hergert, 1997). Avoiding sulfur also makes it potentially environmentally benign in view of the environmental problems with sulfuric emissions. However, technical problems have prevented industrial application. In fact, the utilization of volatile organic solvents causes a relatively high pressure during digestion, which creates a possible safety hazard. Together with the slightly lower fiber strength, the Organosolv concept has thus never been a threat to established Kraft processes (Sixta, 2006).

It can be stated that pulping processes in general do not aim at a fractionation of wood as it is desired in biorefineries. Rather, they aim at the production of strong fibers with low lignin content. The delignification reactions are relatively well understood. Either acidic or basic conditions are applied to cleave the lignin at the

ether bonds to eventually remove soluble fragments of lignin from the fiber. Hemicelluloses are preserved at high pH, which explains the higher fiber yield. In contrast, acidic conditions depolymerize hemicelluloses as well, which benefits from the auto-acidification by the cleavage of acidic groups in wood. The recovery of the inorganic chemicals is realized by combustion and regeneration cycles that produce heat as a co-product. However, pulping processes are claimed to be too expensive for the production of chemicals from wood (Fan et al., 1987), which might be due to the fact that glucose, as the constituent of cellulose, sells only at approximately half the price compared to cellulose pulp (cf. Annex F).

Concerning the envisaged biorefinery schemes, the Organosolv process concepts seem to meet the demands of biorefinery applications fairly well. Although it does not change the recalcitrant cellulose structure, it enables wood to be fractionated into its major components without derivatization and without the problems due to the utilization of sulfur. The applicability of Organosolv processing for the production of chemicals is currently under investigation at pilot-plant scale (Michels & Wagemann, 2010). Nevertheless, recent process simulations unveiled several economic bottlenecks (Viell et al., 2013b) that limit industrial success and need to be improved for viable processing. A serious issue is still the high energy demand for solvent recovery and the loss of the costly organic solvent.

2.2.2 Wood saccharification processes

The discussion of pulping processes indicate that simpler processes are required if saccharification of wood is the objective. Such processes were employed to overcome the shortages during World War I and II and during the energy crisis in the late 1970s. Several industrial-scale plants were in operation to produce sugars and alcohols from wood in particular in the US and in Germany (Locke et al., 1945). As the enzymatic hydrolysis of cellulose has been just discovered at that time (Reese, 1976), it was still in its infancy, and the developed processes are consequently based on chemical hydrolysis of the wood carbohydrates. Although the potential of lignin as a chemical co-product was already recognized at that time (Faith, 1945; Locke et al., 1945), no use other than as a fuel was reported. In general, the wood saccharification processes can be differentiated based on the utilization of dilute or concentrated acids (Katzen & Othmer, 1942; Kamm et al., 2006).

Processes based on dilute acids typically employ acid concentrations of 0.4 - 1.5 wt % based on the liquid phase (Fengel & Wegener, 1989). During the first half of the 20th century a technical process named the Scholler process was developed in Germany (Lüers, 1930). Typically, a dilute aqueous solution of 0.4 wt % sulfuric acid is utilized to hydrolyze the polysaccharides of lignocellulosic material at temperatures between 130 and 190°C (Fengel & Wegener, 1989). The maximum yield is obtained at short residence times, and a high sugar concentration can only be achieved at low liquid to solid ratios. This is realized in the original Scholler process by intermittent percolation of the acid through several reactors packed with wood in a counter-current mode (Lüers, 1930; Lüers, 1937). Afterwards, lime is added to neutralize the acidic mixture and precipitate as insoluble gypsum that can be separated.

The product of the Scholler process is an aqueous sugar stream with a concentration of approximately 4 wt %. The yield is approximately 50 wt % based on the original dry wood (Lüers, 1937; Locke et al., 1945; Goldstein & Easter, 1992) because a considerable fraction of carbohydrates decomposes at the high temperatures. Despite short residence times of the hot liquor, a rather long overall processing time of 16–20 h is realized per percolation reactor in the Scholler process to reach high yields. This sophisticated operation is replaced by continuous extraction known as the Madison process (Harris & Beglinger, 1946). The design decreases the residence time to approximately 3 hours but still only results in rather dilute sugar streams of approximately 5 wt %.

The concept of using concentrated acid for cellulose processing is based on the work of Zechmeister (1913), who investigated cellulose dissolution in aqueous HCl at a concentration larger than 40 wt %. This concentration enables cellulose dissolution and hydrolysis at 50°C within 15 min (Goldstein, 1980). The advantage of this concept is the mild dissolution of carbohydrates that results in near-quantitative yields of sugars without any byproduct formation (Lüers, 1937).

The concept of concentrated acid processing has been transferred into an industrial process known as the Bergius process (Bergius, 1933). Prior to processing, drying of the wood to a few percent of moisture is necessary to avoid dilution of the acid and to maximize the sugar concentration (Lüers, 1937). The extraction of carbohydrates from the biomass usually takes several hours at moderate temperature (Taherzadeh & Karimi, 2007). To avoid degradation, the process is run autothermally at temperatures of 40–50°C (Bergius, 1933) and rather long cycle time of 55 h per reactor. The acid to wood ratio is 7:1 (w/w), and a cascade of reactors is operated in

a counter-current flow to minimize the total mass flow of acid. After extraction, the acid is washed off with water from the residual lignin. The liquid product is a concentrated solution of more than 30 wt % oligosaccharides and 28 wt % HCl (Locke et al., 1945).

The sugars then need to be recovered from the acid. As the concentrated acid cannot be neutralized and disposed of for economic reasons, it has to be recovered for the next cycle. In a first step, the sugars are concentrated by evaporation of HCl to approximately 60 wt % with only a few percent of acid left in the liquid mixture. Boiling of this mixture further hydrolyzes the dissolved oligosaccharides to sugars. The second step of acid recovery is realized by vacuum distillation and spray drying with a HCl loss of 1.5–3 wt % based on the wood feedstock (Bergius, 1937; Lüers, 1937; Goldstein & Easter, 1992). In total, a near-quantitative sugar yield of 67 wt % can be obtained from wood (Bergius, 1937; Lüers, 1937; Locke et al., 1945; Fengel & Wegener, 1989).

Alternatively, concentrated sulfuric or phosphoric acid also dissolve cellulose (Ekenstam, 1936; Schulz & Löhmann, 1941), which was also transferred into process concepts (Wenzl, 1970; Goldstein, 1980; Fan et al., 1987, pp 149–187). The downside in comparison to HCl is the more difficult recovery of the non-volatile acid. More sophisticated separation techniques like dialysis are required; the application of ion-exchange membranes (Goldstein, 1980) and electrodialysis (Goldstein & Easter, 1992) has also been investigated. Nevertheless, the combination with electrodialysis still results in an acid loss of 2.5 wt %. After sugar separation, the volatile substances and water have to be removed from the acids for recycling. Evaporation as a simple means for concentration increases the energy demand.

The advantages and disadvantages of the processing with dilute acid in comparison to concentrated acids have been discussed quite often (Lüers, 1937; Katzen & Othmer, 1942; Taherzadeh & Karimi, 2007) and can be summarized as follows: The dilute acid process achieves saccharification of wood with a relatively low amount of acid, which is beneficial in terms of cost. However, the degradation of carbohydrates is difficult to control and results in a loss of overall sugar yield. This lack obviously arises from the application of high temperature to hydrolyze and extract the carbohydrates from wood. A high selectivity cannot be reached due to the similar activation energy in this consecutive reaction (Girisuta et al., 2007; Saeman, 1949).

Furthermore, the dilute acid processing is characterized by a high effort to separate the product stream. The dilute aqueous acid streams need to be neutralized and require evaporation energy to obtain sugar streams of valuable concentration. The use of low-concentrated, non-volatile acids is therefore favorable in view of the input streams, but not in terms of its products. Consequently, all of these plants were shut down in Germany in the 1950s due to economic reasons. Although the dilute acid process is still among the favorable processes today (Taherzadeh & Karimi, 2007), the above-mentioned challenges have not yet been tackled successfully (Mosier et al., 2005).

The concentrated acid processes require thoroughly acid-resistant equipment to process the biomass and in particular to recover the acid. The ambitious technology results in high capital cost. Furthermore, the cost of HCl that is lost with the products is critical. Locke et al. (1945) concluded that “although interesting from a technological point of view, [the concentrated acid processes] can only be useful under the most extraordinary economic circumstances”.

Hence, technological as well as economic problems are encountered with both concepts of wood saccharification. Though the dilute acid process offers more prospect of success in terms of viability, the concentrated acid process defines the benchmark in terms of high yield processing. The coinciding dissolution and hydrolysis to oligomers at mild temperatures obviously prevents degradation of sugars regardless of the crystalline state of the cellulose.

To avoid the utilization of concentrated acids, a solvent might be key for the simple processing to obtain sugars from wood. Unfortunately, there are only few available systems that dissolve cellulose. The viscose process involves derivatization of the cellulose that is dissolved as sodium cellulose xanthate, which has to be recovered after spinning using sulfuric acid. Non-derivatizing solvent systems are clearly more desirable but their mechanisms are not yet fully understood (Liebert, 2010; cf. list of cellulose solvents in Fischer et al., 2003; Rinaldi & Schüth, 2010). Cadoxen, a mixture of cadmium oxide and aqueous ethylenediamine, was employed to obtain quantitative yields of sugars from lignocelluloses using a combined dissolution of cellulose and enzymatic hydrolysis as shown by Ladisch et al. (1978). Although no report on implementation at technical scale could be found, dissolution obviously presents a promising opportunity to process cellulosic material.

2.3 Wood dissolution in ionic liquids (ILs)

Ionic liquids (ILs) consist of ions in a liquid state. Several terms can be found in literature like “molten salts”, “room temperature ionic liquid”, or “organic liquid salt” (Wasserscheid & Welton, 2007). In this work, the definition of ILs given by the mentioned authors as salts with a melting point below 100°C is adopted. This rather low melting point envisages applications similar to those realized with established molecular solvents (Plechkova & Seddon, 2008) but with less environmental impact. A reason for this is the non-volatility of ILs, which avoids losses to the environment in contrast to volatile organic solvents (Rogers & Seddon, 2003). Therefore, Jessop et al. (2012) rank ILs as “green solvents” but Wasserscheid and Welton (2007) have already pointed out that the “greenness” can only be assessed by evaluation of the whole process chain. The following paragraphs briefly introduce the structure and properties of ILs to dissolve cellulose. After an overview of theoretical concepts to describe dissolution and solubility, the relevant facts for wood processing in ILs are discussed in individual sections about dissolution of cellulose, lignin and wood.

Figure 2.9 shows three ILs based on an organic imidazolium cation and the corresponding anion, e.g., 1-butyl-3-methylimidazolium chloride. Several abbreviations can be found in literature like BMIMCl, [BMIM][Cl], or [C4C1im][Cl]. The latter was recently suggested by Hallet et al. (2011) to unambiguously reflect the chemical structure by explicitly naming the number of carbon atoms at the atoms of the imidazolium ring (Figure 2.9). Nonetheless, the literal abbreviations are more intuitive and better to memorize; they will be used in this work.

ILs became attractive for biomass processing when Swatloski et al. (2002) reported the dissolution of cellulose in BMIMCl. The authors speculated that it is caused by an effective interaction of the chloride with the cellulose hydroxyls that disrupt the native hydrogen bonds of cellulose. Indeed, the properties and capabilities of the ILs seem to be mainly due to the interaction of the ions (Weingärtner, 2008).

The next paragraphs will therefore briefly mention the macroscopic properties of melting point, viscosity and miscibility with water in relation to the structure of ions. Although a detailed description of the relation between molecular structure and properties of ILs is beyond the scope of this work, this provides a better understanding of the peculiarities of the ILs in contrast to common solvents.

The interaction between anion and cation in inorganic salts is usually due to Coulomb's law. The small and highly charged ions of chloride exhibit strong electrostatic forces with sodium and result a high melting temperature of 800°C of sodium chloride (Green & Perry, 2008; Dong & Zhang, 2012). In contrast, the interaction of anion and cation in ILs is lower (Sashina & Novoselov, 2009) but still higher than in molecular solvents (Suresh & Naik, 2000). This is a first clue to understand the moderate melting point of ILs in comparison to conventional salts. Longer alkyl chains at the nitrogen atoms of the cation increase the melting point (Weingärtner, 2008); chloride-based ILs melt at higher temperatures than ILs with an acetate anion.

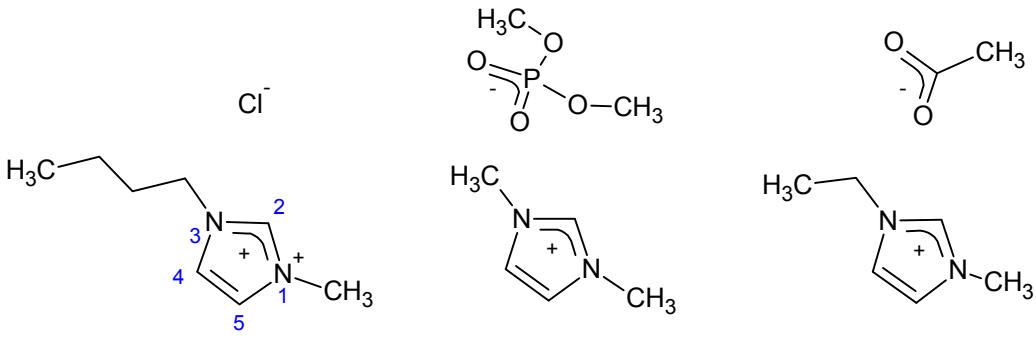

BMIMCl DMIMDMP EMIMAc

Figure 2.9. Names and chemical structures of the ILs investigated for biomass pretreatment: BMIMCl (1-butyl-3-methylimidazolium chloride), DMIMDMP (1,3-dimethylimidazolium dimethylphosphate), and EMIMAc (1-ethyl-3-methylimidazolium acetate). The numbering of carbon atoms of the imidazolium ring is exemplarily given in the case of BMIMCl.

Similarly, the viscosity is higher than experienced with molecular solvents. While the viscosity of water is approximately 0.4 mPas at 80°C (Green & Perry, 2008), BMIMCl and EMIMAc are more viscous by up to two orders of magnitude (i.e., 99.2 mPas and 12.3 mPas, respectively, Remsing, et al. (2008)). A higher degree of electrostatic interactions, hydrogen bonding, localization of the anion's charge, and polarizability of the cation also causes a higher viscosity (Yu et al., 2012). As these effects will also be involved in breaking the hydrogen bonding of cellulose, the rather high viscosity of the neat ILs seems to be an inevitable property.

The localized charge of the anions and the cations depicted in Figure 2.9 enable direct interaction in the anion-cation complex. The cation's charge located within the

imidazolium ring is delocalized between the hetero-nitrogen atoms; the extent of this polarization is also determined by the coordination to the anion (Cremer, et al., 2010). The localized negative charge of Cl^-, DMP^-, or Ac^- anions coordinates well to the C(2)-H (Sashina & Novoselov, 2009). As this complex still exhibits charged surfaces of rather small molecules, the mentioned ILs are completely miscible with water (Klähn et al., 2010). Bulkier and weakly coordinating anions like BF_4^- or PF_6^- do not interact with the cation to that extent (Cremer et al., 2010) that leads to immiscibility with water but also to insolubility of cellulose (Sashina & Novoselov, 2009).

Hence, the properties of ILs are strongly related to the molecular structure and the distribution of the charge within and between the molecules. Polar moieties are clearly interesting for the dissolution of cellulose but the detailed mechanisms of interaction are likely to be more complex. Therefore, a general description of the theory of dissolution and solubility is given before the empirical knowledge about the dissolution and interaction of cellulose and lignocellulosic biomass is presented in the subsequent sections.

2.3.1 Idealized model of solubility

The definition of the International Union of Pure and Applied Chemistry (Nic et al., 2006) categorizes the terms “solvation”, “dissolution” and “solubility” according to different phenomena. The kinetic process to achieve a solvated state is described by the term “dissolution”. “Solvation” generally refers to the state of a solvated molecule (the solute) which is kept in solution by physico-chemical effects like hydrogen bonding or electrostatic interactions. The equilibrium state, i.e., the maximum amount of solute soluble in the solvent is then defined as the “solubility”. The following considerations refer only to the solubility and do not cover kinetic effects.

From the concept of continuum thermodynamics (c.f. Atkins & Julio, 2006), the dissolution of a species (index 2) in a solvent (index 1) corresponds to a change in the Gibbs energy G of the system. The driving force to dissolve a solid solute is described as a difference in the chemical potential μ. The equilibrium at the solubility limit is therefore characterized by the chemical potential of the undissolved solid μ^{sd} being equal to that of the solvated solid μ^{solv},

$$\mu_2^{\mathrm{sd}} = \mu_2^{solv}. \tag{2.1}$$

The definition of the chemical potential $\mu_i = \mu_i^0 + RTln(a_i)$ includes the chemical potential at a standard condition μ_i^0, the temperature T, the ideal gas constant R and the activity $a_i = \gamma_i x_i$ with the activity coefficient γ_i and the mole fraction x_i. Inserting the definition of the chemical potential and the activity in eq. (2.1) enables the calculation of the mole fraction of solute x_2 at the solubility limit as a function of temperature, activity coefficient and the (molar) change of the Gibbs energy of solvation ΔG^{solv},

$$x_2 = \exp\left(\frac{\mu_2^{sd,0} - \mu_2^{solv,0}}{RT}\right)\frac{1}{\gamma_2} = \exp\left(\frac{\Delta G^{solv}}{RT}\right)\frac{1}{\gamma_2}. \quad (2.2)$$

Quantum or molecular mechanic calculations could provide the change in the Gibbs free energy in principle, but it requires a detailed parameterization of the system, which is difficult to validate and quite demanding from a computational point of view, in particular in the case of large, polymeric systems (Politzer & Murray, 2006). The energies of solvation therefore need to be determined by caloric measurements in dedicated experimental setups.

The assumption of the solvent being a continuous phase leads to univariate parameters to characterize the (homogenous) properties of the solvent. In this view, the polarity can be used to categorize a certain solvent and a solute; the polarity is defined as “the sum of all possible (specific and nonspecific) intermolecular interactions between the solvent and any potential solute, excluding those interactions leading to definite chemical changes (reactions) of the solute” (Hallett & Welton, 2011). However, this approach does not yield information about the microenvironment of the solute because the distortion of the solvent molecules in the first solvation shell is neglected (Politzer & Murray, 2006; Reichardt & Welton, 2010, p 82).

To overcome the limitations in the model of polarity, the changes of the Gibbs energy of solvation have been divided into specific solvent-solute interactions. From a mechanistic point of view, the process of dissolution can be split into several sub-processes. First, a cavity has to be formed in the solvent to accommodate the solute. Second, the solute has to be introduced into this cavity and third, the intermolecular interactions are activated (Vitha & Carr, 2006). The latter step includes specific hydrogen bonding and also unspecific polar interactions.

In addition to the molecular and continuum-based models (cf. Politzer & Murray, 2006), numerous empirical scales and parameters have been developed to

quantitatively describe these processes, circumventing the difficulties of molecular simulations (Katritzky et al., 2004; Reichardt & Welton, 2010). The aim is to probe the microenvironment in the solvent directly with selected dyes, whose absorption depends on the interaction in the solvent. The measurement can be carried out using standard analytical ultraviolet/visible (UV/vis) spectroscopy.

A set of these specific parameters has been combined to give quantitative structure-property relationships, called linear-free energy relationships (LFER), e.g. the relationship gibe by Abraham, Kamlet, and Taft (Abraham et al., 1988),

$$\Delta G^{solv} = G_0^{solv} + \overbrace{d\delta_H^2}^{cavity\ formation} + \overbrace{a\,\alpha + b\,\beta}^{hydrogen\ bonding} + \overbrace{s\pi^*}^{dipole\ interactions} . \quad (2.3)$$

Here, G_0 represents a reference state, and a, b, d, and s are regression coefficients. The solvent-specific parameters are the Hildebrand solubility parameter δ_H , the acidity α and basicity β, and the dipolarity π^*. The analysis by Marcus (1993) shows that the properties and interactions of organic solvents are satisfactorily described using four independent parameters. Although both, the solute and the solvent, can be characterized this way, which would add another 4 parameters to eq. (2.3) (cf. Spange et al., 1998), the parameters remain constant if only one particular solute is considered.

Analysis of the solvent parameters in eq. (2.3), namely δ_H , α, β, and π^* yields insight into the mechanisms of solvation. The first step is the endoergic process of cavity formation in the solvent that is described by the Hildebrand solubility parameter δ_H (Hildebrand, 1916). It is based on the assumption that a cavity in the solvent has to disrupt the molecular network of the solvent molecules. The necessary energy is related to the molar potential energy U of a material in a state of ideal vapor at the particular temperature (Barton, 1991) and the molar volume of the liquid molecules. Well below the boiling point of the liquid, U can be substituted by the enthalpy of vaporization ΔH_{vap} reduced by the specific pressure-volume work RT. Division by the molar volume v of the liquid yields the cohesive energy density or Hildebrand solubility parameter (Barton, 1991),

$$\delta_H = \sqrt{\frac{-U}{v}} \approx \sqrt{\frac{\Delta H_{vap} - RT}{v}}. \quad (2.4)$$

The solubility parameter δ_H needs to be multiplied by the volume of the solute to yield units of energy as required in eq. (2.3). As the molar volume of a

macromolecule is difficult to define (Politzer & Murray, 2006), this is included in the regression parameter d. Hence, the molar volume of cellulose as a function of DP will not occur explicitly in eq. (2.3) as long as only one type of cellulose is considered.

The solubility parameter is either determined by eq. (2.4) or by comparison with known solvents and solutes. The latter strategy is feasible in particular in case of non-polar species without any considerable exoergic interaction (e.g. polymers) because the parameters in eq. (2.3) consequently reduce to yield an equation depending on the solubility parameter only. It is therefore standard practice to match δ_H of the solvent and solute for maximum solubility following the aphorism of “like dissolves like” (Barton, 1991). However, the ionic species of interest in this work and the interaction with the long fibers and composite-like structures will likely challenge this simple strategy.

The exoergic interactions of specific hydrogen bonding and unspecific polar interactions are accessed by the (dimensionless) solvatochromic Kamlet-Taft parameters α, β, and π^* in eq. (2.3). The acidity α is related to the capability to donate a proton in hydrogen bonding (Kamlet & Taft, 1976b). Vice versa, the hydrogen bond acceptor abilities are reflected in the basicity β (Kamlet & Taft, 1976a). The basicity or acidity should not be interpreted as protonation or deprotonation because the formation of new charged species is beyond the definition of the solvation model (Marcus, 1993; Hallett & Welton, 2011).

In addition to the specific interactions, the non-specific polar interactions commonly referred to as polarity or polarizability of the solvent molecules are reflected in the parameter π^* (Kamlet et al., 1977; Laurence et al., 1994) defined between cyclohexane and DMSO from zero to unity. It includes the non-specific dipolar interactions due to van der Waals interaction, dispersion forces, etc., and the mutual polarizability of the solvent-solute complex (Politzer & Murray, 2006).

The determination of the Kamlet-Taft parameters is based on certain dyes. Their absorption has been standardized to well-known solvents in order to distinguish between the two modes of hydrogen bonding and dipolarity of the molecules (cf. Marcus, 1993; Reichardt & Welton, 2010). As a prerequisite, the contribution of hydrogen bonding and the nonspecific polarity contribution π^* have to hold for the investigated substances. Further contributions would otherwise compromise the differentiation between specific and non-specific interactions (Katritzky et al., 2004).

Hence, the LFER parameters lack the rigor of thermodynamics and provide only local empirical equations (Kamlet et al., 1987). Nevertheless, the sensitivity towards direct solute-solvent interactions and the simple measurement makes them attractive to give insight into the mechanisms of solvation of biomass components in ILs, which is outlined in the next sections.

2.3.2 Cellulose dissolution

The starting point for the dissolution of cellulose in ILs was the work of Swatloski et al. (2002), who reported the dissolution of cellulose at temperatures between 80 - 100°C in a group of chloride-based ILs incorporating an imidazolium cation. In the meantime, several other ILs have been found to dissolve cellulose (Wang et al., 2012). Swatloski et al. (2002) reported a solubility of up to 25 wt % using microwaves, but solutions of 5–10 wt % were more readily prepared.

The varying data on solubility is on the one hand likely due to very high viscosity of the mixtures. The viscosity increases in a highly non-linear fashion the more macromolecules are dissolved (Zhang et al., 2005), which challenges the determination of an equilibrium. On the other hand, the experimental protocols may also produce irreproducible effects that might be overlooked macroscopically. For instance, the amount of cellulose dissolved within one hour was found to dissolve within two minutes using ultrasonics (Mikkola et al., 2007). However, the temperature was reported to rise in an uncontrolled manner to about 150°C. Such an operation offers no clear insight into the underlying mechanism and seems critical in large-scale applications; the application of ultrasound or microwaves is therefore not considered in this work.

Nonetheless, the fast dissolution in ILs is clearly desired with the high viscosity being one limitation to overcome. The polyatomic anions of phosphates and acetates (Figure 2.9) are 5–6 times less viscous than the ILs with chloride counterparts (Sescousse et al., 2010). Indeed, IL based on phosphates or acetates can dissolve cellulose up to 20 wt % (Köhler et al., 2007; Fukaya et al., 2008; Wang et al., 2012). Polyatomic anions are therefore promising candidates for cellulose dissolution in that respect but it is still not clear whether it is only an issue of mass transport or a more complex interaction due to the different anion.

The molecular interaction of ILs with cellulose in the solvated state has been addressed using molecular simulations and nuclear magnetic resonance (NMR) spectroscopy. Novoselov et al. (2007) simulated a cellobiose complex solvated by BMIMCl and found the chloride coordinating to the C(2) atom of the cation while simultaneously interacting with both the C(6) and C(2) hydroxyls of cellobiose. This predominant action of the anion was verified experimentally by NMR spectroscopy (Remsing et al., 2008). Further results showed that the cation might be involved as well, which is still difficult to demonstrate quantitatively using NMR data (Zhang et al., 2010c). Nonetheless, recent molecular simulations suggest a concerted action of anions and cations in breaking the intramolecular hydrogen bonds with finally the anion being in the first solvation shell around the cellulose (Ding et al., 2012; Xu et al., 2012b).

The solvated state of cellulose could be imagined as individually dissolved cellulose chains interacting closely with the molecules of the solvent. This assumption relates to the common model of linear polymer chains in solution where the volume fractions are statistically distributed lattices of either the polymer or the solvent (Flory, 1942). Michels und Kosan (2005), however, dissolved cellulose in BMIMCl, added water to precipitate the cellulose, and surprisingly recovered a fibrous state. This indicates that the cellulose chains are still organized in the solution to a certain extent, which somehow resembles the original state.

The existence of aggregates in ILs was further confirmed by light scattering experiments, which showed that cellulose solutions in BMIMCl and EMIMAc involve aggregates by far exceeding the size of a single macromolecule (Kuzmina et al., 2010). Polarized light microscopy also revealed an anisotropic effect of cellulose solutions in ILs beyond a certain concentration (Kosan et al., 2010). Hence, the cellulose-IL solution seems to be more complex than resolved by existing models of ideal polymer solutions.

The challenge in dissolving cellulose obviously arises from the long chains of the polymer. In fact, there is experimental evidence that cellulose with smaller DP is dissolved to a larger extent in ILs (Heinze et al., 2005), which is in line with similar observations in sodium hydroxide (Isogai & Atalla, 1998) and also with oligosaccharides in water (Gray et al., 2007; Glasser et al., 2012). The molar volume in the solubility parameter also in LFER (cf. eq. (2.4) in Section 2.3.1) also supports the influence of longer molecules. Native cellulose with the longest DP is thus likely the most difficult substrate to dissolve.

Although Swatloski et al. (2002) reported no significant change of the DP after dissolution of cellulose, the process of dissolution and regeneration seems however not completely reversible. An investigation of Zhang et al. (2005) showed a small decrease in the DP of less than 10% after dissolution of a cellulose pulp with a DP = 650 for 40 min in 1-allyl-3-methylimidazolium chloride (AMIMCl) at 100 to 130°C and regeneration with water. However, a cellulose pulp with more than twice the DP showed a reduction of 50% in the DP after 4 h at 110°C. Lowering the temperature to 100 or 85°C also decreased the DP by only 20 or 10%, respectively, after dissolution in BMIMCl for 1 h and regeneration with water (2009; Kosan et al., 2008). These results show that higher temperatures and longer residence times can result in a reduced DP at least with chloride-based ILs.

The obvious hydrolysis can also proceed to smaller molecules that become water-soluble. Iguchi et al. (2013) found that a treatment of cellulose at 90°C in BMIMCl for 2–5 h results in a 10% reduction of the mass of cellulose recovered in combination with a comparable reduction in the DP. Though this is described as “non-derivatizing”, an increase in time and temperature to 10 h at 120°C, however, showed only 70% recovery with only 20% of the original DP. A comparison of 1-allyl-3-methylimidazolium chloride (AMIMCl) and BMIMCl at 105°C revealed that cellulose is degraded more readily in BMIMCl (Laus et al., 2005), while AMIMCl enabled quantitative recovery of cellulose (Nakamura et al., 2010b).

A possible explanation for the hydrolysis might be the formation of small amounts of acids as observed in BMIMCl upon dissolution of cellulose (Gazit & Katz, 2012). It is likely that such an effect is related to the chemical structure of the cation. The strongest interaction seems to happen via the C(2) atom of the imidazolium ring that can even exhibit a reactive behavior and covalently bind to the reductive end of cellulose (Ebner et al., 2008; Rodriguez et al., 2011).

The result of the dissolution is a reduced or even removed crystallinity. Consequently, an increase of the enzymatic activity by a factor of 6 was observed with cellulases after cellulose dissolution in BMIMCl and regeneration (Dadi et al., 2006). The overall process time of dissolution in BMIMCl at 120°C and subsequent enzymatic hydrolysis could be shortened to 5 h with full conversion of cellulose to sugars (Xiao et al., 2012). This encourages utilizing the dissolving capability of ILs for biomass in combination with an enzymatic hydrolysis step.

A model-based prediction of the solubility of cellulose in ILs would be a convenient way to replace the tedious measurements by fast calculations. MD simulations calculated the interaction energy between IL and cellulose to be -117 to -130 kJ/mol for BMIMAc and -100 kJ/mol for BMIMCl with the former being the better solvent (Sashina & Novoselov, 2009). The results by Guo et al. (2010) also showed an energetically favorable interaction of the acetate with carbohydrates in comparison with the alkylphosphate anion. The inferred solubility of cellulose followed the order of decreasing interaction energy with $Ac^- > Cl^- > DMP^-$ (Pinkert et al., 2010; Sashina & Novoselov, 2009), which is in line with experimental results (Wang et al., 2012).

More advanced predictions are possible using the activity coefficient. Casas et al. (2013) showed that it results in more accurate correlations with the solubility in comparison to enthalpic data. The results by Kahlen et al. (2010) corroborate the fact that acetate and chloride anions in combination with a slightly polar cation are very well suited to dissolve cellulose. Clearly, the 3D structure of the solvent plays an important role in solvation (Pinkert, 2012). However, the entropic effects cannot be resolved very well by the available models (Kahlen et al., 2010). Further, the effect of amorphous and crystalline cellulose has not been explicitly considered up to now.

The specific interaction between ILs and the hydrogen bond donors and acceptors of cellulose have been specifically probed by LFER parameters. Spange et al. (2003) determined the Kamlet-Taft parameters of solid cellulose and concluded that good solvents for cellulose should either exhibit high basicity or acidity. Consequently, the analysis of LFER parameters (cf. eq. (2.3)) is expected to shed further light on the required interactions causing the dissolution of cellulose in ILs.

The Hildebrand solubility parameter is the first of the LFER parameters in eq. (2.3). In principle, it could be calculated straightforward with the enthalpy of vaporization ΔH_{vap}. In the case of the ILs, the enthalpy of vaporization is, however, difficult to access. As the ILs are non-volatile at ambient conditions, the vapor pressure is extremely low and only detectable using high vacuum equipment. Nevertheless, the evaporation of ion pairs has been reported (Earle et al., 2006) and an enthalpy of vaporization between 130 to 200 kJ/mol is determined (Deyko et al., 2009; Reichardt, 2005). The range plausibly exceeds the values of molecular solvents by an order of magnitude but show that ILs are not non-volatile in general. However, the evaporation of the ILs utilized in this thesis was not studied in the literature.

Table 2.2. The reported Hildebrand solubility parameter of the ILs displayed in Figure 2.9 (recalculated in $MPa^{0.5}$ when necessary) at the indicated temperature.

IL	δ_H [$MPa^{0.5}$]	method
BMIMCl	34.95 (T=?)[5]	*unknown*
	24.14 (25°C)[2]	intrinsic viscosity
DMIMDMP	25.08 (25–50°C)[3]	structure-property relationship
	26.54 (40°C)[1]	inverse gas chromatography
EMIMAc	24.79 (40°C)[2]	intrinsic viscosity
	25.16 (25°C)[2]	intrinsic viscosity
	35.22 (27°C)[4]	molecular dynamics
	23.10 (40°C)[6]	inverse gas chromatography

[1] Revelli et al. (2009)
[2] Weerachanchai, et al. (2012)
[3] Wang et al. (2013)
[4] Liu et al. (2010)
[5] Mora-Pale et al. (2011)
[6] Yoo et al. (2012)

Another possibility to circumvent the complicated measurements is offered by strategies from polymer chemistry. In particular, quantitative structure-property relationships, molecular dynamics (MD), or the comparison with other solvents or solutes have been applied to determine the solubility parameter of ILs. In addition to the direct calculation of the enthalpy of vaporization, MD calculations compute the difference between the ion pair in vacuum and within the liquid ensemble. The method of comparing known solvent system is carried out by analysis of the solvent solute interaction. Inverse gas chromatography measures the retention time of a volatile solute in comparison to an insoluble solute, i.e. a gas, in the stationary IL. Another approach is the intrinsic viscosity measurement, which screens for the maximum viscosity in mixtures with the IL and then takes the solubility parameter of the particular solvent. The compiled data are shown in Table 2.2.

Table 2.2 shows that the solubility parameters of the ILs are reported mostly between 23.1 to 26.54 $MPa^{0.5}$ except the values of Liu et al. (2010) and Mora-Pale et al. (2011), which are approximately 35 $MPa^{0.5}$ for BMIMCl and EMIMAc. As the parameters for molecular liquids commonly exhibit an uncertainty of only a few percent (Barton, 1991), this deviation cannot be regarded as an experimental error.

An explanation of this variation points to the utilized method. The value reported by Mora-Pale et al. (2011) originates from a non-reviewed online source, which is obviously not in agreement with the other data. A detailed review of the MD

simulation of Liu et al. (2010) was not possible within the scope of this work but the origin is likely to be due to the MD calculation as it is the only simulation in Table 2.2. If both data points are neglected, the solubility parameters of the investigated ILs are rather close. This remaining data points do not show a reasonable trend; neither the effect of temperature nor of the different chemical structure of the ILs is reflected. Hence, the differentiation of ILs using the solubility parameter seems infeasible at this point.

The ambiguity of this concept in the case of cellulose dissolution is further supported when considering the solubility parameter of cellulose. The parameters of the IL and cellulose should match in principle with ILs as a proven solvent. However, the reported values for cellulose range from δ_H = 25.7±1.4 MPa$^{0.5}$ (Roberts & Rowe, 1993) to δ_H = 55.7 MPa$^{0.5}$ (Bochek, 2003) with several values in between (microcrystalline cellulose: δ_H = 39.3 MPa$^{0.5}$ by Archer (1991); amorphous cellulose: δ_H =38.64 MPa$^{0.5}$ by (Hansen & Björkman, 1998)). The origin of these variations could not be clarified but this range would actually identify water with δ_H = 47.9 MPa$^{0.5}$ (Barton, 1991) as a possible solvent for cellulose. Hence, the solubility parameter does not seem to be a comprehensive parameter in the characterization of cellulose dissolution. A similar conclusion was already drawn for molecular solvents (Hudson & Cuculo, 1980). Moreover, Weingärtner (2008) argued that the available methods to determine the enthalpy of vaporization indirectly might not hold in case of ILs. The solubility parameter will thus not be investigated further in this work.

The other part of LFER might be more suited in characterizing the solubility of cellulose. For instance, its dissolution in dimethylacetamide/lithium chloride could be attributed to an extraordinary high β (Spange et al., 1998). The cellulose hydroxyls and their ability to form hydrogen bonds thus seem to be substantially involved in the dissolution mechanism. Indeed, Rinaldi (2011) found that $\beta \sim 0.8$ is the lower bound to dissolve cellulose in mixtures of ILs with 1,3-dimethyl-2-imidazolidinone as an organic co-solvent, which is supported by the studies of Xu et al. (2013) with EMIMAc and dimethylsulfoxid (DMSO). Additionally, the latter authors and Gericke et al. (2011) identified a high dipole moment to be beneficial for cellulose dissolution. A high β and high polarity ($\pi^* > 0.8$) therefore seems to be a prerequisite for cellulose dissolution. While Rinaldi (2011) could not find a correlation with α, Hauru et al. (2012) suggested the “net basicity”, i.e., the difference $(\beta - \alpha)$, to characterize the dissolution capability of ILs for cellulose.

The specific exoergic interactions described by the Kamlet-Taft parameters have been assigned to the chemical structure of imidazolium ILs as shown in Figure 2.10. The localized negative charge of the anion is related to the basicity β. Its counterpart is the delocalized charge on the C(2)-H of the ring, which is the main hydrogen bond donor (Lungwitz et al., 2008) and thus governs the acidity α. The effect is experimentally confirmed by the observation of a decrease in α on substitution of C(2)-H by a methyl group (Ab Rani et al., 2011). The C(2)-H proton is therefore also called “acidic” in the Brønsted definition or termed as “electron acceptor” according to the Lewis definition (Atkins & Julio, 2006). Its acidic property and also its pK_a in the Brønstedt definition are influenced by the electronic structure of the imidazolium cation and its side groups, i.e., the different length of the alkyl chains attached to the imidazolium ring (Magill et al., 2004; Cremer et al., 2010; Schmeisser et al., 2012).

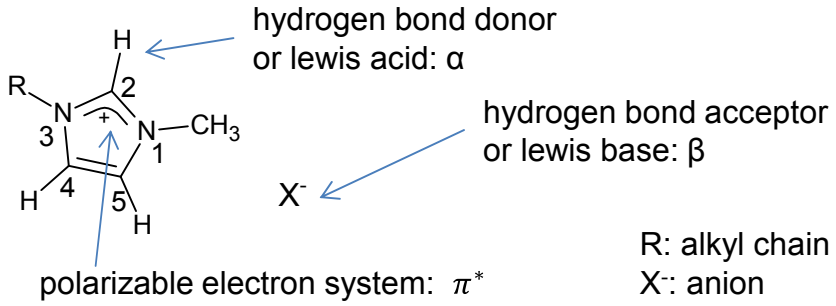

Figure 2.10. The functional groups of imidazolium-based ILs assigned to influence the Kamlet-Taft polarity parameters, predominantly according to Reichardt (2005).

The polarity and polarizability of the IL are covered by the parameter π^*. It depends on the type of ions and their interaction. For instance, π^* decreases with longer alkyl chains on the cation while β increases simultaneously (Lungwitz et al., 2010). Lungwitz et al. (2008) report a linear correlation between α and β which indicates some ambiguity in these parameters in the case of ILs. Hence, the interplay of dipolarity/polarizability and the other Kamlet-Taft parameters has to be analyzed on a case-by-case basis; the assignment in Figure 2.10 is thus likely only a first approximation of the real interaction of anions and cations.

In sum, the mechanisms of solubility are yet not fully understood and literature gives rather broad ranges of the amount of soluble cellulose in the ILs. It might be a result

of the highly viscous mixtures or due to yet unknown physico-chemical interaction of these complex solvent systems. Therefore, the ideas about the relation between structure and properties of the IL in terms of cellulose solubility are only qualitative at this point as summarized by several authors (Pinkert et al., 2010; Zhang et al., 2010a; Rinaldi, 2011; Pinkert, 2012): The anion should be a hydrogen bond acceptor with a high basicity and a delocalized negative charge on a small volume to form multiple hydrogen bonds. The cation on the other hand should be a moderate hydrogen bond donor with a size appropriate for a low melting point and low viscosity. Furthermore, the aromatic heterocycle of the imidazolium seems to be favorable (Pinkert et al., 2010).

The reports on the kinetics of cellulose dissolution are scarce compared to those on the solubility. The macroscopic process happens within a few minutes as observed in in situ viscosity measurements (Cruz et al., 2012). This gives at least an impression of the time-scale of dissolution. On the molecular level, MD simulations showed that breaking the intramolecular hydrogen bond is key in effectively peeling-off cellulose chains from the solid bundle (Rabideau et al., 2013).

Cuissinat et al. (2008a) observed first a swelling and then the subsequent formation of balloons with delignified wood cells at random positions along the fiber. The molecules inside the thin membrane of the balloons were suggested to be already dissolved, while the non-swollen regions are dissolving afterwards. This indicates that the structure and distribution of additional biomass compounds might influence the dissolution and its kinetics.

2.3.3 Lignin dissolution

Pu et al. (2007) investigated the dissolution of Kraft lignin obtained from softwood in several ILs. The most promising ILs are based on the $MeSO_4^-$ anion with a maximum solubility of 344 g/L in $DMIMMeSO_4$ at 50°C. Halide-based ILs like BMIMCl are inferior by an order of magnitude despite a higher processing temperatures of 75°C. Unfortunately, the dissolution time was not reported and the material was not recovered to check for chemical degradation. This might be particularly critical with the $MeSO_4^-$ anion because it can hydrolyze to sulfuric acid as observed with $EtSO_4^-$ (Ficke et al., 2008), which in turn could derivatize lignin (cf. Section 2.2.1).

In spite of using isolated lignin that will possibly influence the results by the method of extraction, Lee et al. (2009) tested the extraction of lignin from maple wood flour in different ILs. The lignin was determined by UV/vis spectroscopy, while solubility of wood was checked visually. After 24 h at 80°C, chloride-based ILs dissolved both, wood and lignin. In contrast, the authors observed no dissolution of wood in EMIMAc but an extraction of lignin. They concluded EMIMAc to be a selective solvent for lignin.

Casas et al. (2013) investigated the dissolution of lignin by comparison with activity coefficients. Similar to cellulose dissolution, a range of activity coefficient values was identified that allows lignin dissolution. However, the difference between the studied model compounds and the lignin that was actually used was not considered. Thus, the predictions are still to be verified, in particular regarding the separation of reactive and physical dissolution. Molecular insight is obtained from density functional theory (DFT) calculations and MD simulations of lignin dissolution in ILs (Ji et al., 2012; Janesko, 2011). The authors identified a stacking of lignin model compounds with the imidazolium rings and hydrogen bonding as the predominant solvation mechanism with the anion. This shows that the aromatic imidazolium might play an important role in lignin dissolution.

Similar to the lack of data on lignin solubility in ILs and its mechanism, there is scarce knowledge on LFER parameters. Systematic investigation of lignin solubility in solvent systems indicates that the Hildebrand solubility parameter of lignin is likely in the range of 20 to 24.6 $(MPa)^{0.5}$ (Schuerch, 1952; Balogh et al., 1992; Lee et al., 2009). Ni and Hu (1995) assessed the solubility parameter of the non-volatile lignin polymer by a group contribution method. Based on the syringyl, guaiacyl and hydroxylphenyl moieties in lignin, $\delta_H = 28.03$ $(MPa)^{0.5}$ was obtained for a hardwood lignin, which is above the other values.

The analysis of Schuerch (1952) already showed that a good lignin solvent should exhibit a particular hydrogen bonding capability. This is in principle included in the extended solubility parameters given by Hansen and Björkmann (1998), which calculate a value of $\delta_H = 31.05$ $(MPa)^{0.5}$. It is clearly the highest value so far, and it neither supports nor disapproves the other values above. Hence, lignin is in the range of the solubility parameters tabulated in Table 2.2 a quantitative differentiation is impossible using the solubility parameter. Kamlet-Taft parameters could not be found in literature for lignin; a screening of the ILs utilized by Pu et al. (2007), however, indicates no clear correlation of lignin solubility with β (Brandt et al., 2013).

George et al. (2011) studied the change in the structure of several technical lignins after dissolution in DMIM-based ILs at 120°C for 3 hours. They found a significant reduction in the molecular weight, and the investigated anions showed an increasing effect in the order dimethylphoshphate < chloride < acetate < lactate < sulfate with a conversion of up to 55% of the lignin to smaller fragments. Although a cleavage of the β-O-4 bond was not directly supported in this study, a cleavage seems plausible as observed in later studies (Papa et al., 2012; Varanasi et al., 2012; Wen et al., 2013).

Hence, solubility data of lignin are scarce and highly uncertain. This is on the one hand due to the fact that lignin is an undefined macromolecule. On the other hand, the theory of solubility cannot accommodate for the chemical reactivity encountered in several solvents. The observed bond cleavage in good solvents for lignin indicates that physico-chemical phenomena other than solubility parameters have to be taken into account in order to understand the extraction or dissolution of lignin (Hansen & Björkman, 1998). The question whether the dissolution of lignin can be described as a physical process or as reactive phenomena has not been conclusively solved.

2.3.4 Hemicellulose dissolution

The dissolution of hemicelluloses is not well studied in comparison to lignin or even cellulose. Hemicellulose dissolved to an extent of 30 wt % during the treatment of poplar with EMIMAc for 3 h at 75°C (Yuan et al., 2012). A further improvement was reported by Froschauer et al. (2013), who achieved the selective dissolution of xylan from pulp by altering the dissolution capabilities of EMIMAc by the addition of water.

Further, phosphate-based ILs could be used to extract hemicelluloses quite selectively from cellulose by varying the structure of the anion to lower the Kamlet-Taft basicity β (Abe et al., 2010; Froschauer et al., 2012). The reaction conditions however need to be controlled carefully because the viscosity limits simple dissolution and the dissolved hemicellulose readily decomposes into a number of unknown components at 110°C and above (Cox & Ekerdt, 2013). Thus, the ILs shown in Figure 2.9 can dissolve hemicellulose as well as cellulose.

2.3.5 Wood dissolution

The idea of wood dissolution in ionic liquids goes back to the reports of Kilpeläinen et al. (2007) and Fort et al. (2007). The first group achieved a dissolution of 8 wt % of spruce sawdust at 110°C in BMIMCl or AMIMCl after 8 h. Fort et al. (2007) studied the dissolution of several hard- and softwoods with processing times up to 24h in BMIMCl and confirmed a superior dissolution of spruce in comparison to oak. However, they diluted BMIMCl with 15 wt % DMSO at 100°C in order to reduce the viscosity that increases during dissolution. None of the samples dissolved completely, though a rough indication of a 2:1 ratio of cellulose to lignin from NMR was interpreted as complete dissolution of the cellulose. Nakamura et al. (2010a) reported dissolution kinetics of wood in EMIMCl. The residue was 5 wt % of beech after 24 h at 120°C, while 17 wt % was obtained in the case of cedar. The lignin content in the undissolved residue was 60 wt % and 82 wt %, respectively. Hence, the dissolution is confirmed to be slow but it seems not to be complete in chloride-based ILs.

In contrast, Sun et al. (2009) report the complete dissolution of wood in EMIMAc. Powdered oak and pine was dissolved at 110°C for 25 and 46 h, respectively. A partial separation was achieved by precipitation with acetone/water to yield a cellulose-rich material, while the lignin stayed in solution. The suggested process scheme discloses an overall yield of 40 wt % of carbohydrates. Thus, a considerable mass fraction must have been lost. Later results questioned the claim of complete dissolution (Viell & Marquardt, 2011; Brandt et al., 2013) but confirm the slow progress of the dissolution.

The slow kinetics of wood dissolution likely encouraged the application of higher processing temperatures. Li et al. (2013) exposed ground biomass of pine, eucalyptus, and switchgrass to EMIMAc for 3 h at 160°C. The IL predominantly dissolved hemicelluloses, which could not be regenerated by precipitation. Similarly, slightly larger particles of eucalyptus of 0.5–1 mm could be recovered to only 65 wt % after processing in EMIMAc for 3 h at 150°C (Papa et al., 2012). The loss was also attributed to lost hemicelluloses. The losses diminish the overall yield to 50 wt %, which is thus inferior to the established processes. The moderate temperatures of approximately 110°C seem more appropriate to realize high yield processing.

Concerning the quantitative description of wood dissolution, there are only few articles reporting comprehensive quantitative results or mechanistic effects in

contrast to singular aspects of the dissolution of wood in an IL (cf. Brandt et al., 2013). Well before IL processing of wood was investigated, Hansen and Björkman (1998) discussed the solubility parameter of wood in view of its components and argued that the difference between them leads to the insolubility of wood. However, the cleavage of the structural complexity of the cell wall likely includes other physico-chemical effects that are not described by the solubility parameters alone. This view is implicitly supported by the work of Yu et al. (2011). The authors designed solvent mixtures of water, ethanol, and an IL based on solubility parameters to selectively dissolve cellulose or lignin and amorphous cellulose but did not observe the desired selectivity in dissolution. This result supports that the solubility parameter likely does not characterize the dissolution of lignin and cellulose thoroughly as discussed in Sections 2.3.2 and 2.3.3.

The exoergic effects of the solvent in wood dissolution have been characterized only roughly by Kamlet-Taft parameters. Doherty et al. (2010) identified a minimal value of $\beta > 0.84$ to enable decrystallizion of cellulose and delignification of biomass with aqueous mixtures of ILs. This is similar to the observed solubility of cellulose in EMIM- and BMIM-based ILs (Brandt et al. (2013) and cf. Section 2.3.2). Padmanabhan et al. (2011) suggested in addition a high polarity/polarizability to be necessary for lignin and biomass dissolution. It might therefore not be a single parameter value for wood dissolution.

The common method to determine dissolution is a macroscopic analysis often carried out visually. Fort et al. (2007) noticed that the wood begins to swell immediately when suspended in BMIMCl and it does not disappear completely. Cuissinat et al. (2008b) made observations of swelling and ballooning of wood fibers in BMIMCl similar to delignified fibers. The swelling was monitored in several reports (Singh et al., 2009; Lucas et al., 2011; Miyafuji & Suzuki, 2011) and Brandt et al. (2010) correlated the swelling of the wood in ILs with basicity. However, the correlation is questionable because it is based only on few meaningful data points.

The observed swelling however points to another issue in the literature. Most of the studies using ILs as a pretreatment chemical neglect the ultrastucture of wood by using milled wood. Excessive ball milling can cause chemical degradation (Ikeda et al., 2002), and it is known that ball-milled wood dissolves better (Kilpeläinen et al., 2007). In view of the envisaged technical application, the dissolution of larger chips is more favorable to avoid the energy costs of comminution (Blanch et al., 2011). The

utilization of larger chips would also enable to investigate the pretreatment mechanisms on the morphological level.

Indeed, we were able to show that EMIMAc results in disintegrated fibers which are then effectively dissolved due to a much higher specific surface area than the initial particles (Viell & Marquardt, 2011). Meanwhile, the fibrous appearance of biomass after pretreatment with EMIMAc was noticed as well by other authors in combination with a reduction of lignin and a reduced crystallinity of the cellulose (da Silva et al., 2011; Xu et al., 2012). This opens up for energy-efficient designs avoiding an energy demanding comminution step.

2.3.6 Effect of water

Wood dissolution in the ILs are usually carried out with fresh ILs in a neat state. Water is thus clearly the most important impurity or co-solvent, which will not evaporate during the pretreatment. The hygroscopic nature of the IL even complicates common drying strategies; 4 h of vacuum drying at 70℃ still leaves 0.22 wt % (Huddleston et al., 2001).

Water can alter the physico-chemical properties of ILs significantly, i.e., the viscosity and density drops and the melting point is reduced (Seddon et al., 2000; Anantharaj & Banerjee, 2012; Chen et al., 2010; Fendt et al., 2011; Hall et al., 2012) even at small amounts of water. Most importantly, water reduces the ability to dissolve wood and induces precipitation of the dissolved molecules. DFT calculations indicate that the solubility of carbohydrates decreases with more than two water molecules per molecule of EMIMAc (Ding et al., 2012). The simulation of Ding et al. (2012) suggested that the introduction of water into an IL/cellulose solution weakens the hydrogen bonds formed between the carbohydrate, the EMIM, and the acetate ion. However, comprehensive quantitative data of energies or entropies in IL/water/cellulose systems are not available and the authors of the aforementioned study also pointed to steric aspects which are possibly involved. Hence, the effect of water is not satisfactorily understood.

The investigation of the LFER parameters appears to be more advanced than the fundamental studies in this regard. Gericke et al. (2011) showed that suitable molecular co-solvents for ILs require high polarity ($\pi^* > 0.8$) and low acidity ($\alpha < 0.5$) to maintain the cellulose in solution. A higher basicity then allows for larger fractions

of the co-solvent in the mixture before the cellulose precipitates. An example is DMSO ($\pi^* = 1$, $\alpha = 0$, $\beta = 0.76$). In contrast, water is not very well suited because it is a moderate hydrogen bond acceptor and a good donor, i.e., $\alpha = 1.17$, $\beta = 0.47$ and $\pi^* = 1.09$ (Reichardt & Welton, 2010).

Hence, mixtures of ILs and water therefore do not maintain the conditions under which cellulose is dissolved. This effect of water had already been noted in the initial paper of Swatloski et al. (2002), who reported a very low water content inhibiting cellulose dissolution. Rayne und Mazza (2007) achieved good results with 0.3 wt % of water in BMIMCl. Additional water seems to alter the basicity of the mixture and causes the insolubility of cellulose and wood at $\beta < 0.84$ (Doherty et al., 2010). Any process concept thus needs to include precise data of how much water can be tolerated.

If considerable amounts of water are added, the dissolved macromolecules will precipitate. Increasing amounts of water lead to larger agglomerates until the cellulose aggregates form a dispersion and finally precipitate (Kuzmina et al., 2010). The observation is supported by the investigation of the intrinsic viscosity of cellulose-EMIMAc mixtures which showed a maximum viscosity at 8–10 wt % of water (Le et al., 2012). The authors reported no complete solvation of cellulose above 15 wt % of water but the formation of a macro-gel. The precipitated cellulose can recrystallize into cellulose II after precipitation (Michels & Kosan, 2005; Iguchi et al., 2013) as the most stable cellulose polymorphs (Beckham et al., 2011).

The precipitation using a mixture of water and acetone (1:1 v/v) resulted in recoveries of 30–60 wt % of the initial dry wood (Fort et al., 2007). A component analysis showed a high content of cellulose in the precipitate. The precipitation works with acetone/ethanol as well (Balensiefer et al., 2008) though different solvents might have an influence of the obtained molecular weight distribution and yield (Nakamura et al., 2010a; Leskinen et al., 2011). Though the precipitation process is still barely understood quantitatively, the benefit is clearly obvious in combination with subsequent enzymatic hydrolysis. The hydrolysis yield from precipitated material increases by a factor of 2–5 compared to untreated wood (Kilpeläinen et al., 2007).

2.4 Objectives of a pretreatment based on ILs

The conversion of wood into chemicals by selective depolymerization with enzymes is a promising way to achieve high yields of sugars without the formation of by-products that inhibit subsequent fermentation. The reaction rate in the case of lignocellulosic material, however, is commonly less than 20% (Lynd et al., 1999) and requires an effective pretreatment. The importance of this process step is demonstrated by the fact that it can account for up to 40% of the overall production cost in biomass conversion processes (Yang & Wyman, 2008), which effectiveness is eventually determined by the combination with subsequent process steps.

The theoretical considerations show that this pretreatment is challenging for two reasons. First, the dense, composite-like structure of wood poses a major obstacle to access the complex molecules. Accessibility is thus key to increase mass transport and kinetics but grinding is prohibited in view of energy efficiency. Second, the pretreatment is usually a concerted action of depolymerization and dissolution. The latter is usually determined by the aqueous solvent. The maximum attainable fraction of water-soluble molecules is thus a tradeoff between kinetics and yield. The harsher the applied conditions the faster the depolymerization to soluble molecules but also at the cost of carbohydrate degradation of dissolved molecules. A quantitative yield and a preserved molecular functionality of the building blocks therefore demands for a pretreatment tailored to the characteristics of the raw material.

Several pretreatment concepts have been suggested in order to overcome the mentioned obstacles. Table 2.3 lists these concepts and the phenomenological effects on native biomass. All concepts increase the accessible surface area of the biomass and remove a significant amount of hemicelluloses. Such effects are even achieved with hot water and steam explosion. However, the simple aqueous pretreatments do not cleave and remove lignin substantially, which seems necessary for efficient enzymatic digestion.

The dilute acid process removes additionally a small amount of lignin due to catalytic cleavage by sulfuric acid. Similar results can be observed when steam explosion is carried out with catalytic amounts of sulfuric acid or in combination with a subsequent extraction step. Nevertheless, the optimized steam explosion concepts reach saccharification yields of approximately 35–56 wt % of the initial wood (Shimizu et al., 1998; Schütt et al., 2011).

Table 2.3. Processing concepts and their effect on the chemical composition and structure of biomass (extended based on Mosier et al., 2005).

method	increases accessible surface area	decrystallizes cellulose	removes hemicellulose	removes lignin	alters lignin structure
steam explosion	✓	×	✓	×	(✓)
AFEX	✓	✓	(✓)	✓	✓
hot water	✓	nd	✓	×	(✓)
dilute acid	✓	×	✓	(✓)	✓
lime	✓	nd	(✓)	✓	✓
Organosolv	✓	×	✓	✓	✓

✓: major effect, (✓): minor effect, ×: no effect, nd: not determined

Considerable lignin removal is accomplished by the application of higher concentrations of chemicals on wood, as realized in the Organosolv processes, lime processing and ammonia fiber explosion (AFEX). The Organosolv process still shows drawbacks for the production of chemicals as described in Section 2.2.1. Moreover, the Organosolv pulp is still highly crystalline and requires long hydrolysis times of 48 h or more (Zhao et al., 2009). Lime treatment requires processing times in the range of days and realizes an alkaline mode of action at lower temperature (Mosier et al., 2005).

In particular, the mentioned processes do not change the crystalline structure of cellulose (Chang & Holtzapple, 2000; Zhao et al., 2009), which is one of the limiting steps in enzymatic hydrolysis. A decrystallization is reported only in the case of AFEX (cf. Table 2.3). The choice of the right additional chemical, likely a base, is therefore required for decrystallization. However, the alkaline methods such as AFEX and lime are reported to decrease in its effectiveness in lignin removal with more lignified feedstocks, in particularly with softwood (McMillan, 1994; Galbe & Zacchi, 2007). Moreover, all the processes described do not reach economic attractiveness for economic realization (Eggemann & Elander, 2005; Viell et al., 2013b).

An ultimate pretreatment would therefore remove the cellulose crystallinity and separate the lignin. The mechanisms should be effective at moderate temperature to ease the problem of carbohydrate degradation in order to reach a near quantitative

yield. At this point, a potential pretreatment could be envisioned based on ILs. Their most intriguing feature is the dissolution of cellulose, which instantaneously removes the crystallinity. The reported temperatures of approximately 100–120°C should enable mild processing without severe degradation. Hemicellulose and lignin can also be expected to dissolve readily. The IL-based concepts that extract only the lignin (Brandt et al., 2013) obviously do not exploit this novel class of solvents and resemble established pulping processes.

The easiest way to process the hypothetical wood solution would be an enzymatic hydrolysis in ILs directly. However, enzymatic hydrolysis in IL/water mixtures does not take place at water fractions below 80–90% (v/v) (Engel et al., 2010; Park et al., 2012). As this is far above the water concentration acceptable for wood or cellulose dissolution in ILs (cf. Section 2.3.6), the dissolution capabilities of ILs for cellulose are not compatible with the conditions of enzymatic hydrolysis; the cellulose therefore has to be hydrolyzed in a separate reaction compartment under aqueous conditions.

The subsequent steps from biomass pretreatment to enzymatic conversion have to be integrated into a feasible process. First process concepts for an IL-based pretreatment have been published in literature (Sun et al., 2009) and in several patents (Balensiefer et al., 2008; Rahman et al., 2009; Jimenez de la Parra et al., 2012). The concepts include milling and drying of the wood, which is thereafter dissolved in EMIMAc at 110°C for at least 16 h and regeneration. The regeneration recovers cellulose-rich material that can be hydrolyzed enzymatically, while the lignin in the acetone/water/EMIMAc solution is recovered by evaporation of the acetone and subsequent precipitation with water. Yields of approximately 70% were claimed this way for glucose (Balensiefer et al., 2008). Drying of the process liquors then removes the volatiles from the IL that is then recycled. The recycling of IL and the energy demand was already identified to be important for the success of the concepts (Fort et al., 2007). The economic prospect thus has to be benchmarked on the process level.

However, the mentioned process concepts already demand for energy prior to the IL pretreatment. The reported utilization of milled wood requires considerable energy for mechanical comminution (Blanch et al., 2011). In contrast, the established processes listed in Table 2.3 have been studied with larger wood chips. In this context, the steam pretreatment was found to be an effective means to reduce the particle size (Schütt et al., 2012). As the particle size is actually related to the accessible surface area, which is mentioned explicitly in Table 2.3, the benchmarking to established

pretreatment concepts essentially requires a technically-relevant particle size in the range of chips.

Moreover, the yields of sugars reported in the references given above are promising figures but do not offer comprehensive mass balances of a pretreatment process. The viability of the IL-based process concepts cannot be assessed without this data and the important process parameters are unknown as well. In addition, there are still many open fundamental questions of the ILs being a complex solvent system despite the progress made since 2007. It is not precisely known whether the ILs completely dissolve wood or its constituents only and if so, to what extent. The situation is illustrated by the different claims of complete (Sun et al., 2009) and insignificant dissolution of wood (Lee et al., 2009) in the very same IL, which clearly contradicts each other. A choice of the most promising combination of IL and wood cannot be made this way.

Further, the effects of the IL in the presence of water are poorly understood. A quantitative description using fundamental thermodynamic parameters of the dissolution processes seems impossible, but LFER and in particular Kamlet-Taft parameters offer a viable means to conveniently describe the interaction in the solvent. However, no systematic investigation of dissolution and pretreatment in the presence of water in ILs has been reported using these parameters.

It can thus be concluded that there is far too little data to start a process design directly. The dissolution of wood and the subsequent precipitation of dissolved macromolecules might not necessarily be the most efficient process concept. To gain insight into the process performance, key parameters are necessary, i.e., residence time, solid to liquid load, feasibility of different wood species in combination with ILs, acceptable water content and the achievable yields from an overall mass balance. A set of target-oriented experiments is required to fill the depicted gaps. Basically, this means a process design from scratch.

The objective of this thesis is therefore the investigation of wood pretreatment in three ILs that are selected to cover a range of anions and cations. The work aims at the selection of a promising combination of wood chips and an IL based on the idea of the dissolution of wood. The investigation and determination of the process parameters is guided by mechanistic understanding, which includes the pretreatment criteria of crystallinity, specific surface area, and dissolution or alteration of the lignin in order to enable efficient enzymatic hydrolysis. The anticipated effects in relation to

the properties of the solvent and the wood can provide a basis for a knowledge-based design of pretreatment processes tailored to the downstream requirements and to the lignocellulosic feedstock.

The structure of the following chapters is as follows: First, the description of the materials and methods are described in the next chapter. Thereafter, the results are presented and split into two main chapters to accomplish (i) a mechanistic and investigative level in Chapter 4 and (ii) a process level in Chapter 5. The experimental part starts with studies on the dissolution of cellulose in ILs. Then the dissolution kinetics of wood in ILs is investigated with a particular focus on the structural changes in wood. The effect of water in the IL is explored with both cellulose and wood. Data from spectroscopy and Kamlet-Taft parameters are analyzed for mechanistic explanations.

After the dissolution studies, the most promising processing strategy is chosen, which is then developed to yield a feasible process concept for the pretreatment of wood based on ionic liquids. The combination with enzymatic hydrolysis infers mass balances for a technical application of this concept. These balances are then utilized in a process simulation in Chapter 5 to assess viability and drawbacks of IL-based pretreatment of wood at technical scale. An economic evaluation completes the investigations, and the advantages and pitfalls of the IL-based processes are discussed in comparison with the known Organosolv pretreatment.

3 Materials and methods

The pretreatment of biomass addresses a composite-like material consisting of different components that also exhibit a complex molecular structure and ultrastructure. On the one hand this thesis therefore investigates the behavior of isolated main components as well as wood particles at several sizes. On the other hand, analytical methods are required to reveal mass balances and to track the changes of the molecular structure in the biomass. Further, Kamlet-Taft parameters in ILs are to be determined. The corresponding materials and techniques are described in the following sections.

3.1 Materials

Microcrystalline cellulose (Avicel PH-101) and α-cellulose were bought from Sigma (Munich, Germany). The material was analyzed by Jäger, et al. (2010), who reported an average DP of 62 and 267 for Avicel and α-cellulose. The authors also measured the crystallinity by X-ray powder diffraction (XRD), which was 82% and 64%, respectively. Xylan from beech wood (purity 95%, isolated by biological means, Sigma-Aldrich, Munich, Germany) was chosen as a representative compound of woody hemicellulose. Lignin was provided by the Federal Research Institute of Rural Areas, Forestry and Fisheries (vTi, Hamburg). It was produced by Organosolv pulping with a mixture of ethanol and water at technical scale.

Wood was obtained from several sources and then processed into defined fractions as shown in Table 3.1. Blocks were made of rods obtained from local hardware stores. Rods of pine had to be used instead of spruce because the latter was not available. The veneer was cut into defined chips manually with a knife, while particles of defined size were obtained by sieving after short swing milling (<1 min). All samples were stored at room temperature in closed flasks prevent changes of the water content in the air-dried material. This way, the masses can be calculated on a dry basis by subtracting the moisture of the wood, which was regularly checked (cf. chapter 3.3). An impression of size and morphology is given in Figure 3.1.

Table 3.1: Wood particles used in the experiments.

name	size	made from/processing	obtained from
beech chips	10 × 2 × 1 mm^3	beech veneer/ cut with to size	Karl Kohl GmbH, Cologne, Germany
spruce chips	10 × 2 × 1 mm^3	spruce veneer/ cut with to size	Karl Kohl GmbH, Cologne, Germany
beech particles	0.1–0.5 mm	beech log/ swing milling and sieved	Sägewerk Heyden, Düren, Germany
spruce particles	0.1–0.5 mm	chips/ swing milling and sieved	vTi, Hamburg, Germany
beech blocks	Ø 5 × 10 mm^2	rods/ sawn to size	local hardware store
pine blocks	Ø 5 × 10 mm^2	rods/ sawn to size	local hardware store

Figure 3.1. The individual fractions of wood utilized in the experiments; beech left, spruce right, the pine blocks are the sample on the right. The particle sizes are 0.1 - 0.5 mm, 10 × 2 × 1 mm^3 and 5 × 10 mm^2 (picture made by Schlüter, 2011).

The ILs utilized in this study were obtained from Iolitec (Heilbronn, Germany). The purity was >99 wt % for BMIMCl, >98 wt % for DMIMDMP and >95 wt % for EMIMAc. All other chemicals not explicitly noted in this work were of pro analysi grade. Deionized water was utilized throughout if not otherwise indicated.

3.2 Pretreatment experiments

The investigation of ILs for the pretreatment of wood was based on the dissolution of cellulose. The experiments therefore aim in particular at the determination of dissolution in these novel solvents. The dissolved state is commonly determined after a particular time by taking samples from the system under investigation to analyze the amount of dissolved solute. A complementary strategy is the quantitative recovery of the undissolved solute (Klemm et al., 1998, p 61). Both strategies have essential downsides if applied to ILs: first, a sampling technique alone can be ambiguous when dissolved substances decompose during processing, which seems possible in view of the long processing times. Second, the non-volatile IL sticks to the solid and virtually yields a higher mass in the residue. A washing step with polar solvents can precipitate dissolved molecules and cause an apparently larger mass. This problem has been circumvented by establishing an overall mass balance of the dissolution of wood in ILs.

Overall mass balances of wood dissolution

To overcome the problems given by the small amounts and the high viscosity of the water-susceptible IL samples, a detailed protocol for quantification of the dissolution step was therefore developed as described elsewhere (Viell & Marquardt, 2011). In a typical experiment, wood and ionic liquid were added to a 50 ml centrifugal tube, which was flushed with nitrogen, sealed and placed in a hot heating block to start the dissolution. A temperature of 115°C was selected because it is an appropriate compromise to prevent IL decomposition and hemicellulose degradation and to soften of the wood matrix (Sixta, 2006; Saake & Lehnen, 2007) for increased dissolution speed. Magnetic stirring at 500 rpm (RET control visc C, IKA, Staufen, Germany) with extra strong stirring bars for efficient mixing (Komet 15, Thermo Scientific, Langenselbold, Germany).

The dissolution was stopped by centrifugation at 10,000 × g and 80°C for 15 min (Rotina 420R, Hettich, Tuttlingen, Germany). Care was taken that undissolved particles effectively settled from the solution even in case of highly viscous samples at extended dissolution times by selecting an appropriate amount of wood according to the dissolution time, i.e., 5% for up to 24 h and 1% for longer dissolution times. The effectiveness of centrifugation was checked by phase-contrast microscopy, which also detects transparent particles more reliably (not shown for brevity).

Dissolution and centrifugation are carried out in a single centrifugal tube in order to avoid any loss of the honey-like solution due to transfer between vessels. Having separated the undissolved particles from the viscous supernatant, a fraction of the latter was then decanted into a second centrifugal tube.

Recovery of dissolved wood was established by precipitation in acetone/ethanol (1:1 v/v) in both centrifugal tubes. The precipitates were washed at least seven times with the precipitation agent in a glass filter crucible (POR4, ROBU, Hattert, Germany). After washing and drying at 105°C overnight, the solid masses $m_{1,solid}$ and $m_{2,solid}$ were obtained from the masses m_1 and m_2, which correspond to the heavy and light phases resulting from centrifugation.

Subsequent evaporation of volatiles and addition of water to the washing liquor induced a second precipitation. The precipitated solid were recovered by subsequent filtration with glass fiber filters (GF/D, Whatman, Dassel, Germany).

All phases were collected in order to close the mass balance of the wood and the IL. The method of calculating the dissolved fraction during dissolution is depicted in Figure 3.2. It shows the consecutive steps of dissolution, phase separation by centrifugation, precipitation, and washing.

The experiment started with the mass of wood m^{wood} and IL m^{IL} forming a suspension of wood particles in the ionic liquid. The centrifugation and decantation gives a residual mass m_{res} and a separate mass from the supernatant m_{sup}. Precipitation and washing of these fractions with liquors of masses $m_{sup,liquor}$ and $m_{res,liquor}$ resulted in two solid fractions of masses $m_{sup,sd}$ and $m_{res,sd}$. It has to be noted that these masses are not the dissolved and undissolved masses because the high viscosity of the mixture and the structure of wood impede complete separation of the liquid supernatant from the solid. For instance, $m_{res,sd}$ also contains dissolved macromolecules that precipitate due to the supernatant sticking on the solid residue.

For quantifying the IL and the dissolved material in the solids, the liquid phase was collected as well to be able to close the mass balance. The IL was recovered as masses m_{sup}^{IL} and m_{res}^{IL} by evaporation of the volatile liquids added for precipitation and washing (masses $m_{sup,liq}$ and $m_{res,liq}$). The remaining water content was determined by FT IR spectroscopy (see Section 3.3). In this way, the mass of the recovered IL in both masses m_{sup} and m_{res} could be determined to allow for balancing of ionic liquid and wood.

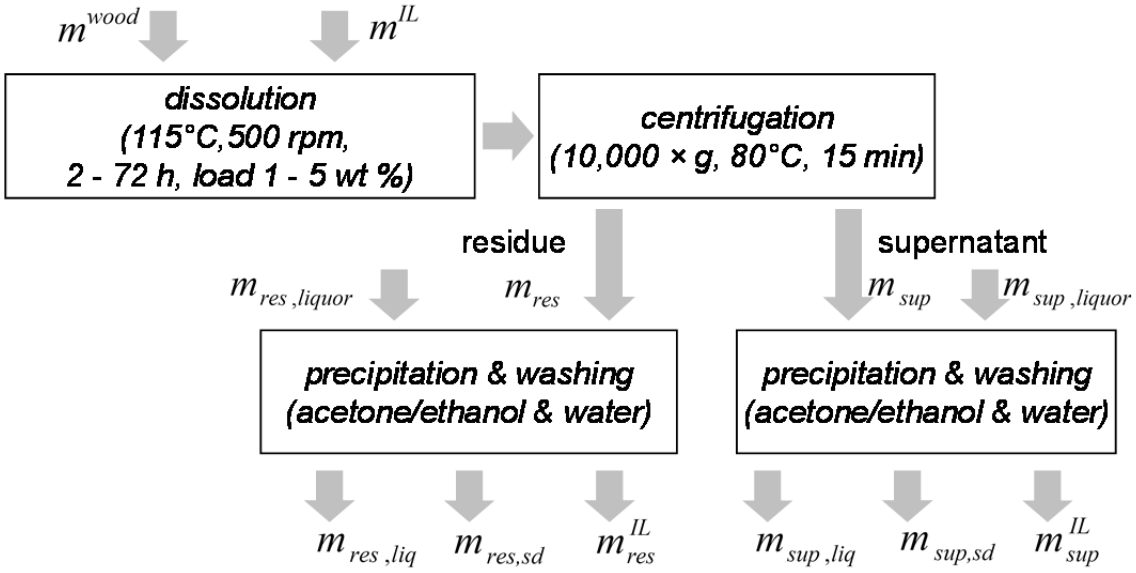

Figure 3.2. Experimental scheme of all solids and liquids considered in dissolution, separation and recovery. The dissolved macromolecules are precipitated by addition of an anti-solvent ($m_{sup,liquor}$ and $m_{res,liquor}$), which was also used to wash the solids (figure adapted from Viell & Marquardt (2011)).

The precise knowledge of the mass of dissolved macromolecules $m_{sup,sd}$ per mass of IL m_{sup}^{IL} allows correction of the mass obtained from the residue. As the mass of IL in the residue m_{res}^{IL} is also known, the truly undissolved mass in $m_{res,sd}$ can be calculated. Further details can be found in the paper of Viell & Marquardt (2011).

The advantage of the described method is that it avoids the addition of further chemicals other than the IL and wood and is based on direct gravimetric measurements. During the course of the work, the tedious work-up procedure of approximately two days per sample was simplified to decrease the work load. This protocol is described next.

Simplified determination of the dissolution kinetics of wood

The general problem of probing the mixture of IL and wood arises from the high viscosity due to dissolved macromolecules. The addition of DMSO has shown not to change the amount of dissolved cellulose (Gericke et al., 2011; Lv et al., 2012; Rinaldi, 2011) thus it should provide for a simpler and less tedious way to determine dissolution quantitatively.

In the simplified protocol, the dissolution was conducted as described above. After the specified dissolution time, 10 ml of DMSO were added, which effectively reduced the viscosity. Centrifugation at 10,000 × g and 80°C for 15 min separated the undissolved solids readily to the bottom of the centrifugal tube so that the supernatant could be decanted through a POR 4 filter crucible. The sediment was washed and the procedure was repeated to wash any dissolved material and IL from the residual wood, while any solid was recovered in the filter. In total, DMSO, acetone, water were utilized three times, respectively, at a volume of 10 ml each as suggested by (Chen et al., 2012). Finally, the solid was flushed out with water into the filter crucible. The liquid was discarded and the residue was dried at 105 °C overnight.

The analysis of dissolved components in ILs could not be established in the IL directly because the ILs contribute a strong signal in established high pressure liquid chromatography (HPLC) analysis. The difficulties were also observed by other groups (Hyvärinen et al., 2010). The dissolution of wood components during processing with IL was therefore detected by analysis of the residue $m_{res.,sd.}(t)$ after distinct experimental times for carbohydrates and lignin (cf. Section 3.3). The dissolved components were calculated as the difference between the initial component concentration w^i and mass m^{wood} and the composition $w^i_{res}(t)$ and mass $m_{res}(t)$ after the dissolution time t. The dissolved fraction was calculated according to

$$w^i_{dissolved}(t) = \frac{w^i \cdot m^{wood} - w^i_{res}(t) \cdot m_{res}(t)}{m^{wood}}. \quad (3.1)$$

3.3 Analytical techniques

In addition to overall mass balances, the detection of carbohydrates and lignin in wood and its structure is fundamental to explore the effect of ILs in pretreatment. While the composition is analyzed using wet chemical analysis, the analysis of the molecular structure is determined by spectroscopy. Furthermore, the ultrastructure of wood is investigated using microscopy in order to monitor the IL-induced changes on the ultrastructure. The determination of the Kamlet-Taft parameters in IL/water mixtures eventually characterize the molecular interaction of ions possibly leading to the observed pretreatment effects.

Compositional analysis of wood

The moisture of wood was checked regularly, because it introduces water in the IL experiments and gives the dry mass of the feedstock. Wood samples of approximately 100 mg were dried overnight at 105°C following the protocol of Sluiter, et al. (2008). The moisture content u was then calculated from the relative difference before and after drying,

$$u = \frac{m_{wet} - m_{dry}}{m_{dry}} \cdot 100\%. \quad (3.2)$$

In this work, u varied between 7 - 9% in the utilized wood before processing.

The content of extractives was determined by extraction with ethanol. After extraction in a soxhlet extractor, the ethanol was evaporated and the residue after mild drying in high vacuum was referred to as extractives. Incineration of the solid at 500°C yielded the inorganic material present in wood. More details and the experimental protocols can be found in the report of Sluiter et al. (2005a,b).

The content of lignin and structural carbohydrates of wood and pretreated wood samples were also determined on the basis of published methods (Sluiter et al., 2011). Briefly, 150 mg of the sample with a particle size <0.5 mm were added to 2.46 g H_2SO_4 (72%). After hydrolysis at 30°C for 1 h, a post hydrolysis with additional 42 g of H_2O was conducted at 117°C for 1 h in a 50 ml centrifugal tube to depolymerize the oligomers. The monomers in the supernatant were analyzed by high pressure liquid chromatography (HPLC, Shodex 0810 column), while the dried solid residue was weighed to determine the lignin fraction.

Table 3.2. Composition of the spruce and beech veneer.

	lignin	cellulose	xylan	galactan/ rhamnan	arabinan	mannan	ash	extracts	sum
	[wt%]	[wt%]	[wt%]	[wt%]	[wt%]	[wt%]	[wt%]	[wt%]	[wt%]
spruce veneer	28.0	47.2	4.1	6.8	0.5	12.3	0.3	3.1	102.3
beech veneer	22.1	42.6	21.6	2.8	0.8	2.3	0.3	2.6	95.1

The composition of the veneer is shown in Table 3.2. The standard error was usually less than 1 wt %. It can be seen that the total sum is close to 100 wt % in the case of spruce veneer but shows larger undetermined fraction in the case of beech veneer. Since the wood analysis is usually quantitatively (Sluiter et al., 2010), this deviation indicates a missing fraction in the analysis. An analysis of acidic groups was not conducted but a maximum of 6.6 wt % can be calculated based on the acetyl content in xylan (cf. section 2.1.1). It is therefore very likely that the missing fraction is therefore due to uronic acids.

Microscopy

A hot stage (LTS120, Linkam, Tadworth, UK) was used in combination with a stereomicroscope (M5, Wild, Wetzlar, Germany) to investigate the dissolution of cellulose and the swelling and dissolution of wood in ILs. The cellulose fiber of α-cellulose was fixed on an object slide by two small droplets of glue. In case of wood, the material was cut into cross-sections of 60 µm thickness with a sliding microtome. The cuttings were positioned on an object slide and fixed with a cover slide.

After placing the sample with the slide on the preheated stage (100–115°C), approximately 100 µl of IL was added from the side and the stage was closed. Argon was used to flush the stage in order to exclude humidity as much as possible. After the start of the experiment, images were recorded at regular intervals.

Scanning electron microscopy was carried out at the Gemeinschaftslabor für Elektronenmikroskopie at RWTH Aachen. Prior to investigation, the samples were dried at 105°C overnight and sputtered with carbon in vacuum.

Raman spectroscopy

Solid samples were analyzed with a Fourier transform Raman spectrometer (Multiram, Bruker, Ettlingen, Germany) with the focus adjusted to the maximum intensity in the range of 1000 cm^{-1}. The samples were measured at a laser power of 100 to 500 mW; the power was set individually to avoid burning of the material. Spectra were recorded at a resolution of 4 cm^{-1} with 250 scans in the range from 50 to 4000 cm^{-1}. The spectral data were processed with OPUS (6.5, Bruker, Ettlingen, Germany) and Peaxact (3.0, S-Pact, Aachen, Germany).

The application of Raman spectroscopy was twofold. First, the crystallinity of cellulose was investigated quantitatively. The calibration was established with a set of samples of different crystallinity prepared by mixing crystalline cellulose I, II and amorphous cellulose. The latter was obtained after ball milling; cellulose II was prepared by treatment with 16 wt % sodium hydroxide (NaOH) in water for 30 min sodium hydroxide (NaOH). The calibrated model enables to determine mass fractions of cellulose polymorphs.

The model was applied to monitor the changes of cellulose crystallinity after the treatment in IL/water mixtures. To this end, approximately 30 mg of Avicel was added to approximately 3 g of solvent, which was either neat IL or a mixture with water. After processing for 24 h at 115°C with magnetic stirring at 500 rpm, water was added to precipitate any dissolved cellulose. The solid was centrifuged and after decanting the liquid, washed 5 times with water. Fluorescence was removed by bleaching in an aqueous solution of 14% sodium hypochlorite (GPR Rectapur, VWR Prolabo, Fontenay-sous-Bois, France) for 30 min at room temperature. Afterwards, the material was washed by the method described above and the cellulose was mildly dried before collection of a Raman spectrum.

The recorded spectra were evaluated quantitatively by a phenomenological modeling using indirect hard modelling (IHM, cf. Alsmeyer et al. (2004)) that was based on the distinct differences between cellulose polymorphs. The transformation of the cellulose polymorph from cellulose I to cellulose II was taken as a reliable indicator

for cellulose dissolution. The maximum water content that enabled transition of cellulose polymorphs was taken as the acceptable water content to enable cellulose dissolution in the IL. Further details can be found elsewhere (Viell et al., in preparation).

The second field of application of Raman spectroscopy was the investigation of wood components before and after the IL pretreatment. The dried material showed only little fluorescence and required no further processing to record a significant Raman spectrum. Due to the complex material and the unknown effects of the IL, the analysis was only qualitative in order to monitor the changes induced by pretreatment on the composition.

X-ray diffraction

Powder X-ray diffraction (XRD) measurements were carried out by Roberto Rinaldi at the Max-Planck-Institut für Kohlenforschung (Mülheim, Germany) to qualitatively determine the crystallinity of the recovered material. Spectra were recorded on a transmission diffractometer in Debye–Scherrer geometry (Stadi P, Stoe, Germany) with a primary monochromator (Cu-Kα_1, λ=0.154060 nm). The diffractograms were obtained at diffraction angles 2θ between 10° and 30° in steps of 0.01° and a counting time of 6 s per step. Details can be found elsewhere (Jäger et al., 2010; Viell et al., in preparation).

Monitoring the water content of ILs

As the water content is critical for the dissolution of biomacromolecules in ILs, the water content of the ILs was monitored repeatedly. It is defined in liquids as the mass of water m_{H2O} relative to the total mass m_{sample}:

$$w_{H2O} = \frac{m_{H2O}}{m_{sample}}. \tag{3.3}$$

The water content of fresh ILs was measured by coulometric Karl-Fischer titration. A sample volume of approximately 100 mg was injected. This method was applied up to 3 wt % of water.

In case the method is applied to recovered ILs after pretreatment, the Karl-Fischer reaction was observed to be compromised by side reactions. It might be due to the

presence of decomposition products like aldehydes and ketones (Cedergren & Oraedd, 1994) or by strong ions competing with the Karl-Fischer reagents (Fidale et al., 2006). In order to overcome the limitations of the Karl-Fischer method, a mid-infrared (IR) spectroscopic method has been developed (Viell & Marquardt, 2012). The method was realized on an FT IR spectrometer (Tensor 27, Bruker, Ettlingen ruggedized by Dr. Bastian GmbH, Wuppertal) equipped with a fiber optic immersion probe. The probe features a diamond ATR element with two reflections, which enables the analysis of samples of less than 0.5 g. Quantification of the spectra was achieved by IHM using Peaxact (3.0, S-Pact, Aachen, Germany). The spectra showed strong nonlinear changes of the investigated peaks but prediction errors of less than 2.3 wt % have been achieved by the calibration over the whole concentration range (Viell & Marquardt, 2012). This method was also established in view of a robust on-line measurement within the developed process.

Solvent characterization

Kamlet-Taft parameters were determined from the maximum intensity of the long-wavelength absorption of 4-nitroaniline (4NA, 98%, Aldrich), N,N-diethyl-4-nitroaniline (DENA, 97%, Chempur), 4-nitroanisole (97%, Aldrich), and 2,6-Diphenyl-4-(2,4,6-triphenylpyridinio) phenolate (Reichardt's dye, 90%, Aldrich) in mixtures of IL and water. The structure and the predominant interaction sites of the dyes are depicted in Figure 3.3.

During preparation of the samples, a sufficient amount of dye was added to a methanol solution in order to achieve an acceptable absorption. The methanol was evaporated in high vacuum and a calculated amount of distilled water was added, mixed and measured in an UV/Vis spectrometer (Multispec USB, Tec5, Oberursel, Germany). Spectra were acquired averaging 10 spectra at 0.3 nm resolution at room temperature to detect the absorption of the particular dye.

The calculation of the Kamlet-Taft parameters is based on the wavelength at the maximum long wavelength absorbance λ_{max} (or the wavenumber $\nu = \frac{10^4}{\lambda}\ [10^{-3} cm^{-1}]$) of the dissolved dye and the following equations (cf. Marcus, 1993):

$$E_T(30) = \frac{28591}{\lambda_{max}(\text{Reichardt's dye})}\ [\frac{kcal}{mol}], \tag{3.3}$$

$$\pi^* = 0.314\ (27.52 - \nu(DENA)_{max}), \tag{3.4}$$

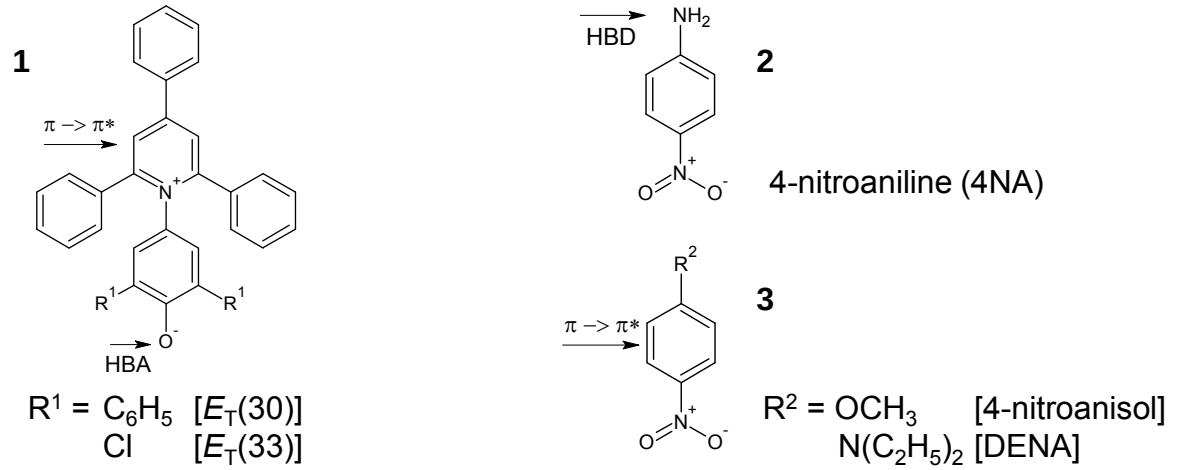

Figure 3.3. The chemical structure of the molecular probes $E_T(30)/E_T(33)$ (1), 4NA (2), and 4-nitroanisol/DENA (3) utilized to determine the molecular interaction in the IL/water mixtures. The arrow depicts the interaction site for hydrogen bond donation (HBD), hydrogen bond acceptance (HBA), and unspecific π^* interaction.

$$\pi^* = 0.427\ (34.12 - \nu(4Nitroanisol)_{max}), \tag{3.5}$$

$$\alpha = 0.0649\ E_T(30) - 2.03 - 0.72\pi^*, \tag{3.6}$$

$$\beta = 0.358\ (31.10 - \nu(4NA)_{max}) - 1.125\pi^*. \tag{3.7}$$

As can be seen from eqs. (3.6) and (3.7), the parameters α and β depend on π^*. To match the concentration of water in IL/water mixtures in the calculation of α and β, the values of π^* were linearly interpolated. Pure water is by definition $E_T(30) = 63.1$ kcal/mol (Reichardt, 1994). A more acid-resistant dye (2,6-Dichloro-4-(2,4,6-triphenyl-1-pyridinio)phenolate, >97%, Aldrich) known as $E_T(33)$, had to be used to analyze DMIMDMP and BMIMCl because Reichardt's dye, $E_T(30)$, was protonated in these ILs and lost the relevant absorption. The corresponding $E_T(30)$ value was calculated using the following equation (Sarkar & Pandey, 2006):

$$E_T(30) = 0.9953 \cdot E_T(33) - 8.1132\ [\frac{kcal}{mol}]. \tag{3.8}$$

As the protonation of the dyes implies an acidic nature of the IL, the ILs were probed with bromothymol blue as a well-established indicator of dissociation in both qualitative and quantitative analysis (Davidson, 1942; Klotz et al., 2011).

Summary of the analytical approach

In addition to the previously described analytical protocols, their envisioned benefit and the novelty of the developed techniques is briefly compiled. The dissolution of wood in the ILs as a novel class of solvents exhibits peculiarities like high viscosity, limited water tolerance and optical properties that make visual assessment difficult. It requires comprehensive mass balances of the liquid and solid phase as a 'gold standard' as reported by Viell & Marquardt (2011). Analysis of the liquid phase by weight also requires the determination of water in the IL to calculate the mass of dry IL. It is measured by in situ IR spectroscopy and a multivariate quantification model published by Viell & Marquardt (2012).

The time-consuming mass balances are complemented by a simplified protocol that aims at the isolation of the solid residue from the IL after dissolution by a multistep washing procedure. It enables screening of different particle sizes with the three ILs for the identification of the most promising combination of IL and wood species and the investigation of compositional changes induced by dissolution. The wet chemical analysis by two-stage hydrolysis to sugars and subsequent HPLC analysis was established at RWTH Aachen University during this project.

The detection of the change in the composition and the structure of wood during dissolution and pretreatment is one of the main characteristics which were addressed during this thesis. X-ray analysis of cellulose is taken as a reference to set up an analytical method that detects the crystallinity of cellulose by Raman spectroscopy (Viell et al., in preparation). The measurement serves to detect the transformation of cellulose polymorphs in the novel solvents and also quantifies a physically justified mass fraction instead of an arbitrary crystallinity index. The molecular interaction leading to dissolution, polymorph transformation and pretreatment is characterized by analyzing the dissociation of ILs and the Kamlet-Taft parameters of IL/water mixtures, which has not been carried out systematically before. Furthermore, the fundamental modes of Raman spectroscopy serve to detect distinct changes in the composition of wood that give insight into the reactive behavior of ILs during the pretreatment. The exceptional work on analytical methods was necessary to provide quantitative understanding in addition to the assessment of pretreatment effectiveness by enzymatic hydrolysis.

4 Pretreatment with ILs

This chapter deals with fundamental investigations of experimental dissolution and pretreatment of wood in ILs. The overall objective of a viable process concept will be achieved by a step-by-step approach. The individual sections resemble a decision tree to identify and develop the most promising process concept. The targeted concept should be characterized by an acceptable water tolerance, an effective operation with larger wood particles, a high yield at short residence times, and effective enzymatic hydrolysis.

Cellulose is the main constituent of biomass, and its molecular structure plays an important role in the recalcitrance of wood. The investigation in Section 4.1 therefore addresses how cellulose dissolves in the imidazolium-based ILs introduced in Section 3.1, what happens when water is added and how this relates to hydrogen bonding. An analysis unveils the induced changes to the structure of cellulose and also determines the water content that limits the dissolution of cellulose in the ILs. The tolerable water content will be a first measure to rank the ILs, and the description of the induced effects is a basis to interpret the effects observed with wood.

In Section 4.2, the investigations are extended to the pretreatment of native wood. The complexity clearly rises in comparison to cellulose fibers. The dissolution of wood in ILs is thus approached by comprehensive mass balances (cf. Section 3.2). The investigations shed light on the dissolution of hard- and softwood in the ILs. A detailed description of the dissolution is further established by testing different particle sizes of wood from the sub-millimeter range to chips. Based on the observations made during dissolution, the processing concept is to be decided. A combined pretreatment and hydrolysis experiment based on the identified operating conditions eventually infers the mass balances and yields of this process concept.

A diverse set of analytical techniques (cf. Section 3.3) is applied to characterize the IL and their effect on cellulose and wood to offer more than simple phenomenological descriptions. It includes microscopy, molecular probing of the solvent environment and several types of spectroscopy. The mechanistic understanding will enable the selection of the most viable strategy of pretreatment and gain insight into the dedicated effects of IL-based pretreatment. The stepwise refinement in this regard is discussed in the individual sections just after the presentation of the results.

4.1 Dissolution of cellulose in ILs

To demonstrate the visual appearance of cellulose dissolution in such a new class of solvents and to provide for a later comparison with wood fibers, a first experiment shows the dissolution of one α-cellulose fiber. The left-hand side of Figure 4.1 shows the α-cellulose at 100°C. Addition of BMIMCl results in the state shown in Figure 4.1 (right) after 3 minutes. The free part of the fiber is not visible anymore. The fiber appears to be completely dissolved within a short period of time.

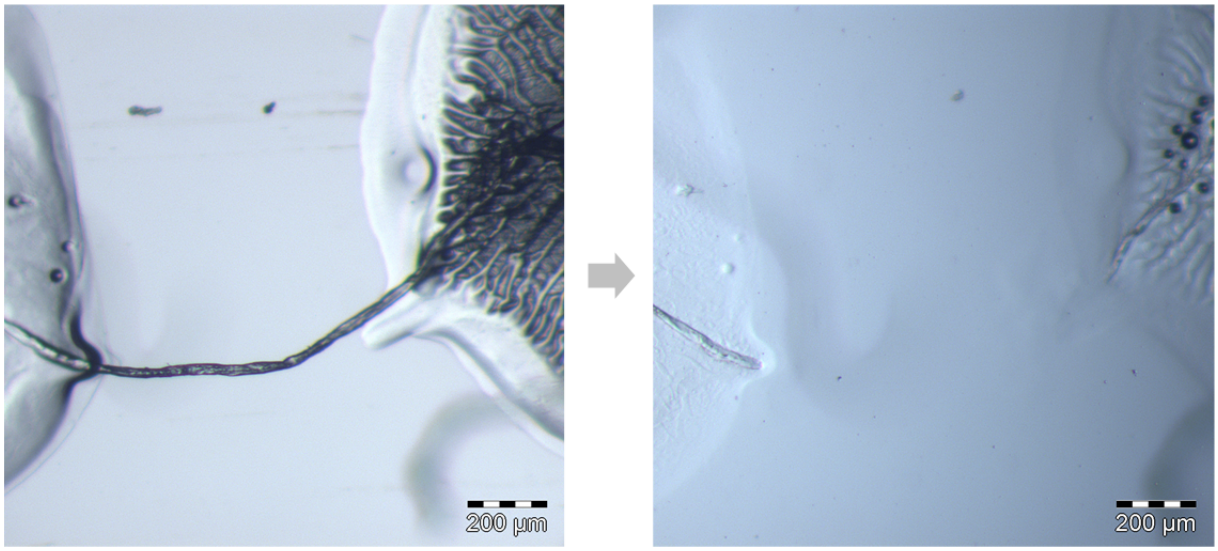

Figure 4.1. A fiber of α-cellulose prior to IL exposure (left) and after less than 3 min in BMIMCl at 100°C (right). The fiber is fixed by two spots of glue, which also remain visible after exposure to IL.

The facile dissolution can be also observed macroscopically. Avicel and α-cellulose dissolve at 115°C in BMIMCl, DMIMDMP and EMIMAc within minutes and form a clear and homogeneous appearance of the mixtures (not shown for brevity). The ILs with polyatomic anions, i.e., DMIMDMP and EMIMAc, have a much lower viscosity and melting point. This enables the cellulose to dissolve even at room temperature but at the expense of a much longer residence time in the order of days. BMIMCl could not be tested under these conditions due to the higher melting point of 69°C (Scurto, et al., 2008). In general, precise times were difficult to determine due to the highly viscous ILs. The impression is that the process is rather fast but sometimes leads to insoluble aggregates.

As one of the few time-resolved studies, Cruz et al. (2012) made viscosity measurements and determined the time when constant viscosity was reached. Their data showed a dissolution within 4 min at 100°C, which is in full agreement with the results described above. The formation of agglomerates has been observed in concentrated mineral acids as well (Schulz & Löhmann, 1941), and thus seem to be an inherent problem in cellulose dissolution.

4.1.1 Cellulose transformation in IL/water mixtures

When the IL/cellulose mixtures are mixed with water, particles are observed forming flocs or a gel, the morphology of which depends on the concentration of dissolved cellulose and the strategy of precipitation. High cellulose concentrations of several wt % can result in the formation of one solid mass upon the addition of water, which greatly complicates the washing. Therefore, the following investigations were carried out at a load of one wt % of cellulose in the mixture to avoid deviations caused by insufficient mixing.

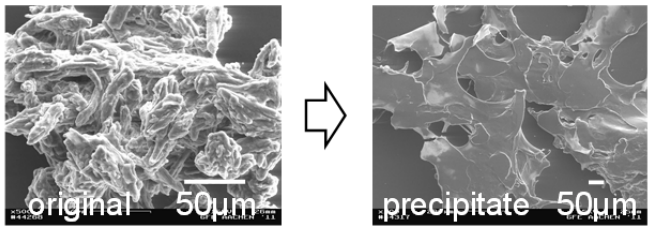

Figure 4.2. SEM pictures of original Avicel (left) and cellulose regenerated from EMIMAc after 24h at 115°C by precipitation (right). The right picture was taken at a lower magnification to demonstrate the difference in surface roughness.

The mixtures then precipitate as small flocs of cellulose. Figure 4.2 shows an image of Avicel and of the material after dissolution, precipitation, washing and drying as observed by scanning electron microscopy (SEM). The original cellulose shows fine, aggregated particles. The dissolution and precipitation result in larger structures with a smoother surface. It supports that structural changes have happened during dissolution.

The molecular structure of the cellulose powder and the dissolved and precipitated cellulose flocs has been investigated by Raman spectroscopy. The spectra in Figure 4.3 show the fingerprint range up to 1600 cm^{-1}, which includes the vibrations of the glucose monomers and the attached hydroxyl groups (Wiley & Atalla, 1987). As the hydroxyl and in particular the CH_2OH groups are sensitive towards changes of the hydrogen bonding network, a change of the peaks reflects a change of the molecular, crystalline structure.

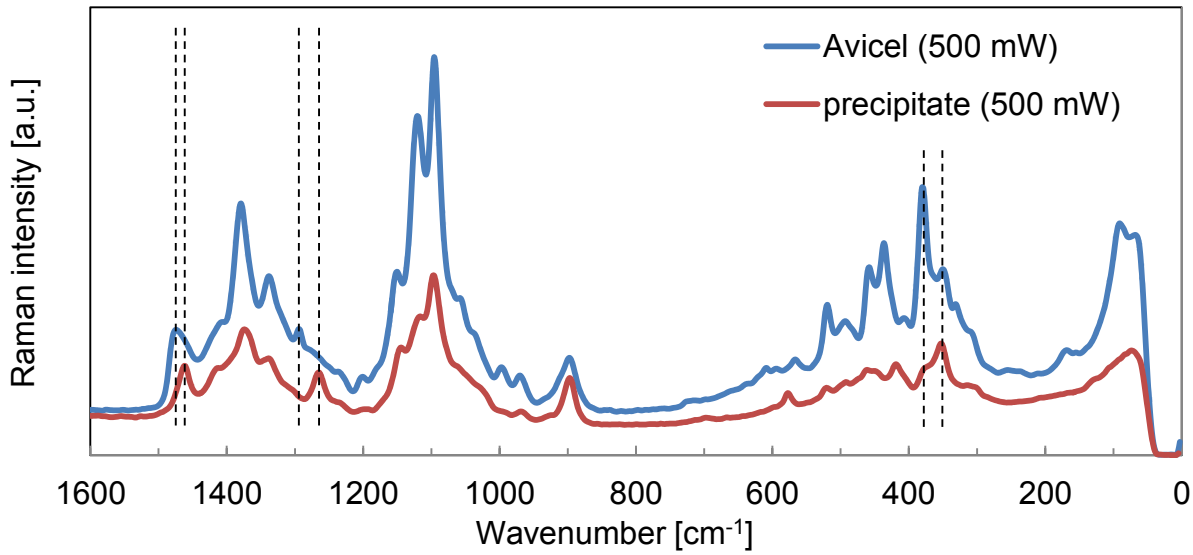

Figure 4.3. Raman spectra collected from Avicel and from the dissolved and precipitated cellulose shown in Figure 4.2. The main differences at the wavenumbers mentioned in the text are indicated with a pair of dashed lines.

The peaks of the microcrystalline Avicel sample at 1472, 1297, and 380 cm^{-1} comprise vibrations of the CH_2OH group at the C(6) atom, a twisting mode of the methylene groups and ring deformation vibrations (Schenzel et al., 2009) that relate to the crystalline polymorph of cellulose I (Agarwal et al., 2009; Schenzel & Fischer, 2001).

The spectrum of precipitated cellulose looks similar but show differences in the position of certain peaks. The peak at 1472 cm^{-1} shifts to 1464 cm^{-1}, while the other peaks appear at 1265 and 355 cm^{-1} instead at their original position. The shift of the CH_2OH group is due to a simpler mono-modal hydrogen bonding network of the secondary alcohol group. In combination with the other changes, a transformation of

cellulose I into cellulose II can be concluded, which is in line to the studies of cellulose after treatment with NaOH or after dissolution in molten inorganic salt hydrates (Schenzel & Fischer, 2001; Schenzel et al., 2009).

A conversion from cellulose Iβ into cellulose II is thus clearly shown by the spectra in Figure 4.3. As the existence of a crystalline structure in the solvated state is rather unlikely, the recrystallization into cellulose II likely happens during precipitation. Such a transformation of the cellulose crystal has already been proven to be a reliable indicator for dissolution and transformation (Marson & El Seoud, 1999). A detection of the transformation of cellulose polymorphs thus elegantly circumvents the optical determination of dissolution reported in literature. Two questions remain at this point, (i) what degree of crystallinity is reached during this precipitation and (ii) how much water is required for precipitation, or more importantly, can be tolerated during dissolution as it will be introduced with biomass into the process.

Several IL/water mixtures have been prepared with a small amount of Avicel to identify the water content of ILs that inhibits cellulose dissolution. The samples were processed for 24 h at 115°C in closed vials to investigate the transformation of cellulose polymorphs in the presence of water (Viell et al., in preparation).

The samples were first inspected visually (Figure 4.4, left). Samples at the left-hand side with large water content show turbid appearance with a sediment of particles. At high concentrations of ILs (right-hand side), the transparent appearance indicates that the cellulose is completely solvated. A first characteristic of all samples is the color. In general, it reflects the purity of the neat IL but it is also an indicator of beginning decomposition. The dissolved samples show a considerably darker color than in the undissolved samples, in particular in the case of BMIMCl and EMIMAc.

A hint towards a beginning degradation is also given the encountered fluorescence in Raman spectra. Though cellulose and ILs do not show fluorescence individually, the regenerated cellulose samples exhibit a strong fluorescence, which is obviously due to the formation of fluorochromes. The ability of the IL to form covalent bonds has already been reported (cf. Köhler et al., 2007; Ebner et al., 2008; Liebert & Heinze, 2008; Du & Qian, 2011). Although, the amount of chromophores might be small, it might decrease the achievable yields.

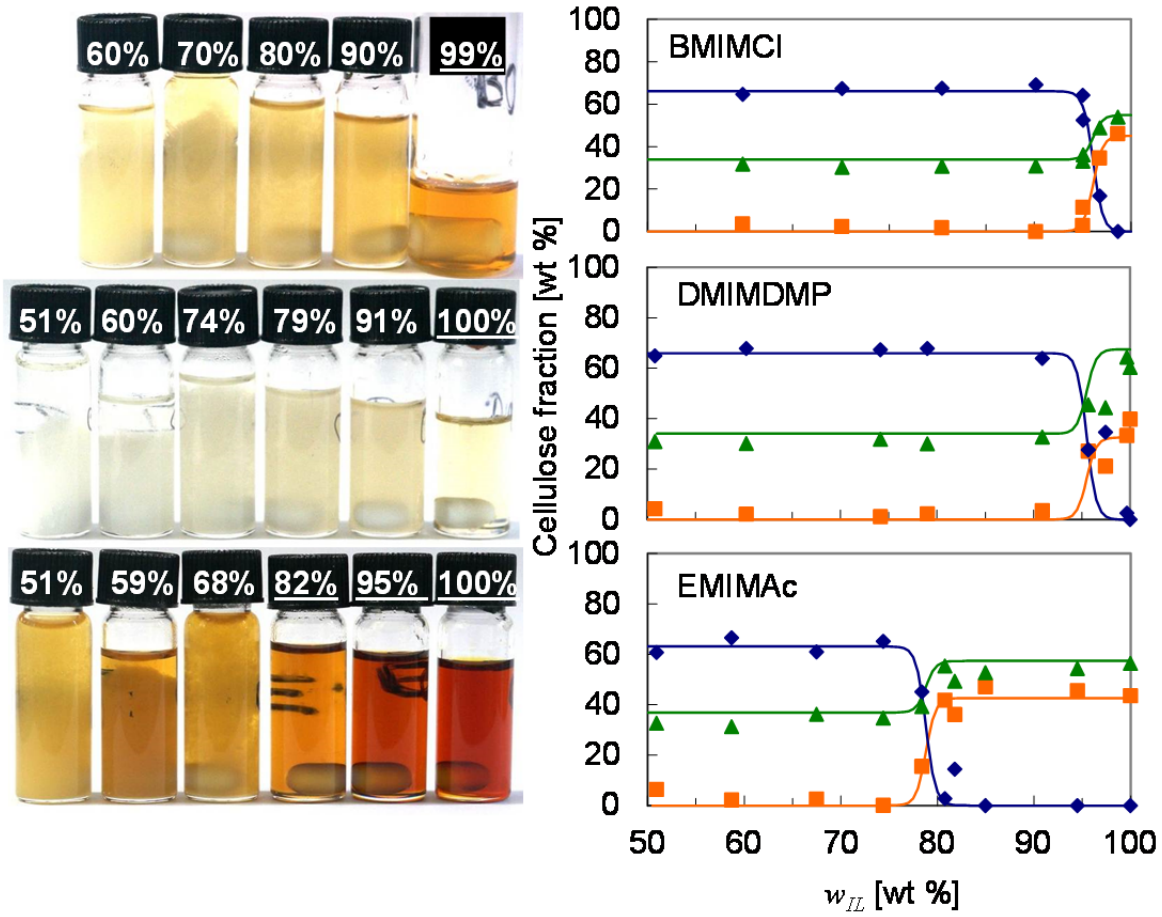

Figure 4.4. Samples with an amount of cellulose (1 wt % per unit solvent mass) in IL/water mixtures (marked by IL concentrations in wt % after processing at 115°C for 24 h (left). The diagrams on the right show the mass fractions of cellulose polymorphs after regeneration including a fit of the mass fractions of cellulose Iβ (◆), cellulose II (■), and amorphous cellulose (▲) (images and data from Viell et al. (in preparation)).

To reduce the fluorescence in Raman spectra, the samples were washed and bleached before spectroscopic analysis. The spectra of bleached samples were then evaluated quantitatively for the mass fraction of crystalline and amorphous cellulose by multivariate analysis of the difference between the spectra introduced in Figure 4.3. The results are shown in Figure 4.4 (right). A simultaneous fit observing the mass balance of crystalline cellulose mass fractions identifies the transition of cellulose polymorphs in the IL/water mixtures.

At low IL content, the cellulose shows a composition of 62 wt % of crystalline cellulose Iβ and 38 wt % of amorphous cellulose. Interestingly, the native crystallinity of microcrystalline Avicel was determined to be 82% by X-ray analysis. However, the overestimation of the crystallinity based on X-ray data is well-known in literature (Röder et al., 2006; Park et al., 2010) and the reported values for Avicel are between 54 % and 93 % using different analytical methods (cf. Tab. 2 in Bansal et al. (2010)), which plausibly fits to the value obtained in this work.

The further analysis of the data in Figure 4.4 shows that the composition of the cellulose samples remains constant with increasing IL content until a transition is noticed. With BMIMCl this is detected at 95 wt % IL. While the fraction of amorphous cellulose increases, cellulose Iβ diminishes accordingly. Simultaneously, cellulose II can be detected in the more concentrated IL mixtures, which eventually accounts for 40 - 50 wt % in the cellulose regenerated from the neat IL. DMIMDMP shows a similar behavior; the date points indicate a transition between 96 and 97 wt % of IL. However, EMIMAc shows a different behavior. The transition is already observed at only 80 wt % of EMIMAc.

It thus has been determined that the acceptable water concentration for cellulose transformation differs according to the employed IL. In case of BMIMCl and DMIMDMP, the maximum water content corresponds to approximately 5 wt % or 30 mol %. EMIMAc still enables dissolution at a water content of 20 wt % or 72 mol %. This ranks the IL/water mixtures according to their molar tolerance against water as EMIMAc > BMIMCl ≥ DMIMDMP.

The values obtained can be compared to only few available data points in literature. While Swatloski et al. (2002) reported insolubility of cellulose in BMIMCl already at 1 wt % of water, a water content of more than 3 wt % was still sufficient for the crystal transformation of cellulose in BMIMCl by Michels & Kosan (2005). However, the latter authors utilized much higher concentrated mixture of 12 wt % of cellulose, which indicates that the water tolerance might depend on the amount of dissolved cellulose.

Mazza et al. (2009) measured an increase in turbidity at 95°C as an indicator for precipitation at rather high water contents of 16.8 wt % in BMIMCl. This value might be due firstly to an influence of temperature and secondly to precipitation and dissolution not likely to happen at the same water content. In this view, the value of 5 wt % observed with 1 wt % cellulose in BMIMCl in Figure 4.4 corresponds to the

reported values. Mazza et al. (2009) also qualitatively mentioned that the dissolution in DMIMDMP is more susceptible to water than BMIMCl on a mass basis.

In the case of EMIMAc/cellulose mixtures, Le et al. (2012) observed a transition from Newtonian to shear-thinning behavior in rheological measurements upon the addition of water at 15 wt % water. The solvation of cellulose will likely not be complete at higher water content, and the cellulose was reported to precipitate when polar solvents like alcohols or water were added at more than 18.1 wt % (Gericke et al., 2011; Hauru et al., 2012). The latter group of authors combined the measurement of viscosity and turbidity and detected an inflection point at 21 - 22 wt % of water. These results are all well in agreement with the the maximum concentration of 20 wt % of water to dissolve cellulose in EMIMAc obtained in this work.

Another finding of this analysis is that still a remarkable fraction of crystalline cellulose is obtained after the pretreatment of cellulose with ILs. Although the overall crystalline mass fraction is decreased by about 30% in comparison to the original Avicel, the dissolution and regeneration obviously involves crystallization of dissolved macromolecules into the thermodynamically more stable polymorph cellulose II. Similar observations have been made in other cellulose-dissolving systems (Kuo & Lee, 2009; Hall et al., 2010).

At first sight, the occurrence of another crystalline polymorph after cellulose dissolution appears a bit odd considering the reported increase in enzymatic hydrolysis after this treatment (cf. Section 2.3.2). However, it is well-known that cellulose II can be much more efficiently hydrolyzed enzymatically as compared to cellulose Iβ (Kuo & Lee, 2009; Wada et al., 2010; Beckham et al., 2011). Therefore, the efficient enzymatic hydrolysis only requires a change in crystallinity and not necessarily the transformation of crystalline cellulose into amorphous material.

Hence, the investigation confirms that cellulose is dissolved only in concentrated ILs. Concerning the choice of IL for biomass pretreatment, the acceptable water tolerance clearly favors EMIMAc because it tolerates twice the amount of water on a molar basis in comparison to the other ILs. The increasing color at longer exposure times at 115°C, however, indicates a beginning decomposition. It is therefore to be clarified whether residence times of 24 h can be tolerated if high yield processing is envisioned.

4.1.2 Descriptors for characterizing the IL/water mixtures

Prior to a more detailed characterization, it is convenient to classify a novel substance according to their acid/base properties (Davidson, 1942). However, the hydrogen ion activity, which is usually described by pH in aqueous systems, is not applicable to ionic liquids (MacFarlane et al., 2006). A first impression of the state of dissociation in the neat ILs is given by dissolved bromothymol blue as a common indicator molecule for pH measurements in aqueous systems with an aqueous pKa = 7.1 (Klotz et al., 2011).

The color of bromothymol blue in the three ILs is shown in Figure 4.5. Although no direct comparison to aqueous pH can be made, the color allows an acid/base classification of the neat ILs. The basic nature of the ILs is in the order of EMIMAc > DMIMDMP > BMIMCl. It becomes obvious that, despite a formally neutral mixture of anions and cations, the ILs show a remarkable difference that could induce reactivity in wood pretreatment.

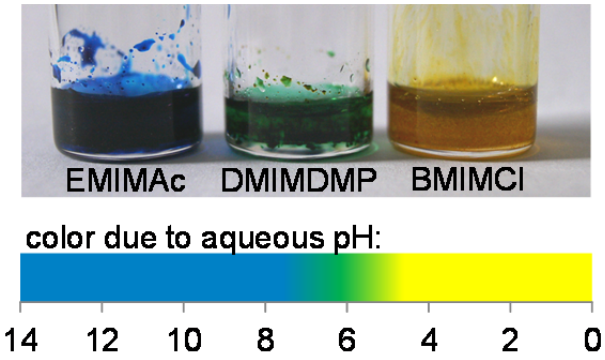

Figure 4.5. Bromothymol blue in the three ILs to establish an acid/base classification of the ILs. Note that the color does not provide quantitative information but reflects the known dissociation of acids or bases in aqueous mixtures of bromothymol blue.

As the cation is similar in the investigated ILs, the attention is drawn to the anion. In fact, the ordering of ILs follows the acid strength of the conjugate acids of the anions, i.e., pK_a = -3 for hydrochloric acid, 1.29 for dimethylphosphoric acid, 4.75 for acetic acid (data from Kumler & Eiler (1943) and MacFarlane et al. (2006)). Although the effect of impurities on the acid/base properties could not be clarified, the analysis

provides a first means of classifying IL hydrogen ion activity, i.e., the base strength of the studied ILs decreases in the order EMIMAc > DMIMDMP > BMIMCl.

Concerning the dissolution process, the numerous hydroxyl groups of wood components imply a preferential interaction with ILs via hydrogen bonds, which are not covered by the concept of proton or electron transfer. MD and density functional theory calculate hydrogen bond interaction energies between cellulose and the anions in the order chloride > acetate > dialkylphosphate, which is claimed to relate to the solubility of cellulose (Sashina & Novoselov, 2009; Zhao et al., 2013). The interaction with a particular solute is therefore investigated by Kamlet-Taft parameters, which are most promising to characterize cellulose dissolution (cf. Section 2.3). The parameters quantify the local molecular environment providing for dissolution and transformation of the cellulose.

Table 4.1 shows the Kamlet-Taft parameters obtained in neat ILs. The data determined in this work can be compared to data from other groups given in the table as well. Comparison of literature values for EMIMAc and BMIMCl shows a good match with own data except for the acidity of BMIMCl. While the other parameter values differ by only a few percent, the acidity of BMIMCl deviates by 40% from the average of the literature values despite replicate measurements. This difference is clearly significant because the measurement error observed to be is less than 5×10^{-3} units.

No Kamlet-Taft parameters could be found in literature for DMIMDMP. Instead, the parameters for 1-ethyl-3-methylimidazolium dimethylphosphate, an IL of similar chemical structure in comparison with DMIMDMP, may be taken for comparison (Fukaya et al., 2008). The reported values, $\pi^* = 1.06$, $\alpha = 0.51$, and $\beta = 1.00$, are in good agreement with the parameter values for DMIMDMP obtained in this work.

The analysis of the ILs regarding π^* shows that it decreases in a row headed by BMIMCl with $\pi^* = 1.11$, followed by DMIMDMP with $\pi^* = 1.08$ and finally $\pi^* = 1.02$ in EMIMAc. In principle, this could be due to either the change of the alkyl chain attached to the cation or the different anions of the ILs. A comparison of π^* for EMIMAc with literature data for 1-butyl-3-methylimidazolium acetate (BMIMAc, cf. Table 4.1) indicates that π^* drops the longer the alkyl chain, which is also observed in literature (Lungwitz et al., 2010). As this is not observed with the other investigated ILs, it can be assumed that the difference in π^* between BMIMCl, DMIMDMP and EMIMAc is mainly caused by the anion.

Furthermore, a high basicity β and a rather low acidity α are observed in all ILs in Table 4.1. These parameters also show the most pronounced variation in the Kamlet-Taft parameters. The simple concept of the basic anion and an acidic moiety on the cation (Figure 2.10, Section 2.3.2) would imply separate trends in these parameters. In fact, the basicity increases in the order BMIMCl < DMIMDMP < EMIMAc while the acidity is decreasing vice versa. Once again, the length of the alkyl chain seems not to cause the change in acidity. If so, it would be rather small as suggested by the acidity of EMIMAc and BMIMAc.

Table 4.1. Kamlet-Taft parameters of the studied ILs measured at room temperature in this work and from literature. The deviation of the results to the average of literature values is given in parentheses (dyes: N,N-diethyl-4-nitroaniline (DENA) for π^*, $E_T(30)$ and $E_T(33)$ in the case of DMIMDMP and BMIMCl for α, 4-nitroaniline (4NA) for β).

IL	π^* (dipolarity/ polarizability)	α (acidity)	β (basicity)	source
BMIMCl	1.11 (+2%)	0.67 (+40%)	0.91 (+8%)	this work
	1.10[g], 1.03[e], 1.08[f], 1.14[h]	0.47[g], 0.49[e], 0.51[f], 0.44[h]	0.87[g], 0.83[e], 0.84[f], 0.84[h]	literature
DMIMDMP	1.08	0.56	1.06	this work
	n/a	n/a	n/a	literature
EMIMAc	1.02 (+3%)	0.49 (-5%)	1.16 (+5%)	this work
	1.01[a], 0.95[b], 1.01[c],	0.56[a], 0.48[b], 0.50[c],	1.08[a], 1.16[b],	literature
BMIMAc	0.96[g], 0.97[e], 0.97[f]	0.57[g], 0.47[e], 0.57[f]	1.10[g],1.20[e], 0.99[f,] 1.16[g]	literature

[a] Doherty et al. (2010)
[b] Varanasi et al. (2012)
[c] Hauru, et al. (2012)
[d] Xu (2010)
[e] Brandt et al. (2010) (75°C, $E_T(30)$, own synthesis)
[f] ElSeoud et al. (2011) ($E_T(33)$, T=?, own synthesis)
[g] Ohno & Fukaya (2009) (T=?, unspec. source)
[h] Fukaya (2006) ($E_T(30)$, supercooled)

The rather high acidity of BMIMCl demands for a brief discussion before the interpretation of the data. A possible explanation for the exclusive deviation of the acidity is obviously related to the measurement of the absorption of $E_T(33)$ as the

respective dye. Other authors have applied both, $E_T(33)$ and $E_T(30)$, successfully to the studied ILs without systematic deviations (cf. footnotes in Table 4.1; Rinaldi, 2011; Zhang et al., 2010b), such that a methodological error seems unlikely.

A source for uncertainty is, however, the purity of BMIMCl. Rinaldi (2011) utilized an ultra-high purity IL (>99.99 wt %) and determined $E_T(30)$ = 49.8 kcal/mol. In comparison, the measurement in this study results in $E_T(30)$ = 53.9 kcal/mol that indicates indeed a higher polarity than expected. Although the utilized BMIMCl in this study was specified by the manufacturer with a purity of 99 wt %, its very hygroscopic nature might have resulted in a small uptake of water, which is the most polar compound of the scale with $E_T(30)$ = 63.1 kcal/mol and thus might erroneously increase the value for neat BMIMCl.

Fidale et al. (2006) also reported that $E_T(33)$ is indeed very sensitive to moisture. Though the water content was monitored regularly by Karl Fischer titration, the origin of the deviation in acidity might be small impurities of water. As the acidity is not an input for further calculation of other Kamlet-Taft parameters, the deviation, likely due to an impurity, was accepted at this point.

The interpretation of the Kamlet-Taft parameters sheds light on the ion interaction that possibly determines cellulose dissolution. The dipolarity/polarizability parameters π^* in Table 4.1 show that all ILs are rather polar. This is not surprising considering that they consist only of coordinated ions (cf. Figure 2.9). The fact that the parameter is nevertheless clearly influenced by the choice of the anion indicates a strong interaction between the ions.

A further indication of the microenvironment being controlled by the anion in the studied ILs is found in the basicity. It is remarkably high in comparison with common organic solvents (cf. Reichardt & Welton, 2010, p 471). The anion thus seems to determe both the basicity and also controlling the polarization of the cation as already reported for other imidazolium-based ILs by Shukla et al. (2012). The concept of net basicity (Hauru et al., 2012) also points towards an interplay between cation and anion in order to describe cellulose dissolution. However, no matter which concept is chosen, the ranking of ILs according to basicity found to be EMIMAc > DMIMDMP > BMIMCl. The order is also maintained if the acidity from literature is considered in the case of BMIMCl.

Consequently, one would be tempted that the basicity of these highly polar compounds determines cellulose solubility. However, the dissolution power of the ILs has been reported to be in the order of the anions of acetate > chloride > dialkylphosphate (Pinkert et al., 2010). MD simulations show a hydrogen bond interaction between cellulose and the IL in the order chloride > acetate > dialkylphosphate (Zhao et al., 2013). Although limitations in ion diffusion could change the macroscopic behavior, the ranking indicated by the solvatochromic parameters is clearly not matched. Hence, the effect of the anion is most pronounced in the basicity and the acidity, which obviously follow the trend given by the pK_a of the conjugate acid. The current understanding from MD and the observed solubility data seem, however, not to fit in that scheme.

In fact, the concept of acidity and basicity of ILs is still under investigation. Lungwitz et al. (2008) obtained a good correlation between acidity and basicity parameters, which supports the observation that both are not independent parameters in the case of ILs. The authors also point out that spurious interactions of anions with dyes and the cations could lead to ambiguous values of α and π^* which is not in agreement with non-IL solvents (Lungwitz et al., 2008; Lungwitz et al., 2010). Thus, one should recall that the concept of Kamlet-Taft parameters is rather empirical and the interaction of ions in ILs and in particular with solutes is still unknown.

A further proof of the more complicated interaction in ILs leading to dissolution can be inferred from an experiment with a similar IL that has been substituted with a methyl group at the C(2)-H group of the imidazolium ring, i.e., 1-ethyl-2,3-dimethylimidazolium acetate. From the discussion above, one would expect a reduced acidity (Crowhurst et al., 2003), while the anion stays the same and provides for high basicity. Surprisingly, this particular IL cannot dissolve cellulose.

It is thus obvious that the microenvironment of ILs likely provides for a more complex interaction than anticipated from the concept of Kamlet-Taft parameters or acid/base properties. The high basicity of the ILs is nevertheless a characteristic feature, which is similarly reported with established solvents like dimethylacetamide/lithium chloride (Liebert, 2010). However, the IL systems might not be generally characterized this way.

Mixtures of IL and water

The complexity increases when water is mixed to the IL. Water is a good proton donor molecule with an acidity $\alpha = 1.17$ and a moderate basicity $\beta = 0.47$ (Marcus, 1993; Reichardt & Welton, 2010), which is counterproductive to the high basicity of the IL. To shed light on the interaction of ILs with water, the Kamlet-Taft parameters have also been determined in mixtures of ILs with water (Figure 4.6). The axes show mole fractions instead of mass fractions to balance the different molecular weight of the molecules.

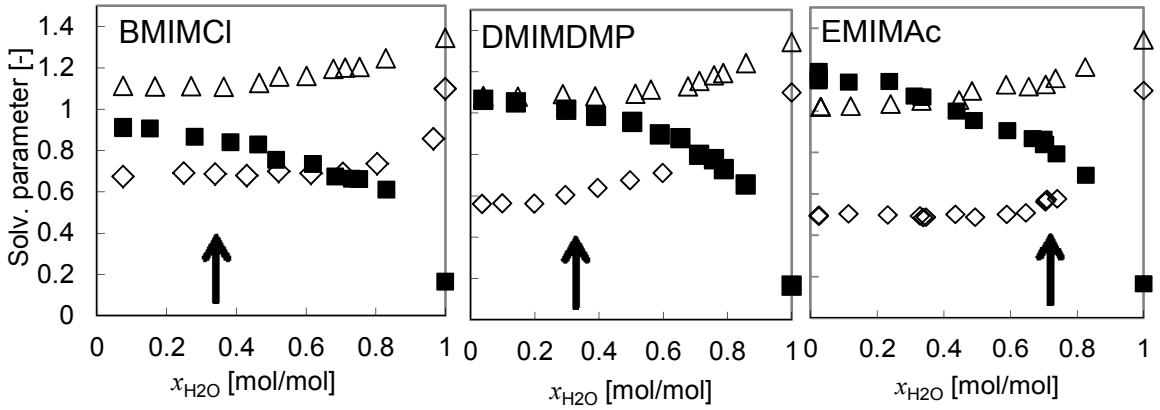

Figure 4.6. The Kamlet-Taft parameters α (◇), β (■), and $\pi*$ (△) for BMIMCl, DMIMDMP, and EMIMAc at varying mole fractions of water. The arrows indicate the maximum water concentration to dissolve cellulose as determined in Section 4.1.1.

The data points of α, β and π^* as a function of water content in Figure 4.6 show a smooth, non-linear trend in all three parameters. The dipolarity/polarizability is nearly constant up to an equimolar composition ($x_{H2O} = 0.5$) but beyond, it increases more and more in all ILs. It reaches a value of $\pi^* = 1.34$ for pure water, which is rather high in comparison to the established value of $\pi^* = 1.09$ (Marcus, 1993; Reichardt & Welton, 2010).

Similar to the dipolarity/polarizability, the acidity of the mixtures with BMIMCl and EMIMAc is constant up to the equimolar concentration. Again, it shows a considerable increase at larger water concentrations. In DMIMDMP/water mixtures, however, the values show an increase at water contents higher than 20 mol % indicating an increased hydrogen bond donor capability. The measurement failed

beyond a water fraction of 60 mol % because the dye got protonated and the relevant absorption could no longer be detected. Pure water gives an acidity of $\alpha = 1.10$.

The basicity decreases gradually in all three IL mixtures. A small amount of water thus results in an instantaneous decrease in basicity in contrast to the other parameters, which seem rather stable as long as more IL molecules are present than water molecules. The decrease in basicity is further enhanced in the aqueous regime, when more and more water molecules are present. The increasing water content causes the basicity to drop quickly to finally reach the moderate value of water at $\beta = 0.16$. Similar to the value of π^*, this deviates from the literature value of $\beta = 0.47$. The water concentration identified as being critical to dissolve cellulose is plotted in Figure 4.6 as an arrow. The concentrations correspond to values of $\beta = 0.86$ in the case of BMIMCl and EMIMAc. DMIMDMP cannot dissolve cellulose when $\beta = 1.00$.

The interpretation of the data first has to address the differences observed in the parameters of pure water. Though the value of $\pi^* = 1.34$ has also been reported in other studies dealing with IL/water mixtures (e.g. Khupse & Kumar, 2011; Trivedi et al., 2010), it is in conflict with relevant literature sources claiming $\pi^* = 1.09$ for water (Marcus, 1993; Reichardt & Welton, 2010). It is the same situation with the other parameters.

The origin of this difference is actually the dye that is utilized to probe the water or the IL/water mixtures. While ILs are probed with DENA due to its more favorable absorption, 4-nitroanisol is the dye of choice in molecular solvents and water. It is confirmed by an additional set of samples with 4-nitroanisol, which resulted in a value of $\pi^* = 1.06$ for pure water and also calculates a value of $\alpha = 1.30$ and $\beta = 0.49$; all of them are close to literature values. Unfortunately, it was not possible to determine π^* in the ILs using 4-nitroanisol because, as expected, the relevant absorptions of the dye are inaccessible in the spectrum.

A mechanistic explanation for the different values of water can be found in the dye molecule itself. In one of their early reports, Kamlet et al. (1973) already noted that DENA is susceptible to hydrogen bonding in protic solvents, which is not accounted for in the established equations (cf. eqs. (3.3) and (3.4)). As π^* is a central parameter in the calculation of the Kamlet-Taft parameters, this issue is more severe than the deviation in acidity of neat BMIMCl and it also causes the deviation of basicity and acidity from literature values.

Hence, Kamlet-Taft data in mixtures with molecular solvents can be easily cross-contaminated by solvatochromic effects that have not been included in the established regressions. This is in particular the case for self-associating, protic solvents (Taft & Kamlet, 1979) and it likely holds for mixtures with ILs as well. The observed increase in acidity in the aqueous regime of all the studied ILs is thus likely a mixed effect of water and the erroneous effect of water on π^*. It is not further investigated quantitatively at this point.

However, two effects of the acidity measurement are observed in mixtures of DMIMDMP and water which warrant discussion. First, the acidity in DMIMDMP/water mixtures was increased at much lower water contents than in the other ILs. An increase of accessible hydrogen bond donors is thus indicated. Second, the acidity could not be measured due to a lack of the relevant absorption in aqueous mixtures of DMIMDMP, which indicates protonation of the $E_T(33)$ dye. Although its pK_a = 4.78 and it allows to probe also weak acids (Kessler & Wolfbeis, 1989), the mixture of DMIMDMP and water forms an acid with a hydrogen ion activity lower than the pK_a of the dye. A mechanism similar to the hydrolysis of alkyl phosphates might be involved (cf. Bunton et al., 1960). It might be a similar mechanism as reported for the hydrolysis of $EtSO_4$ anions (Ficke et al., 2008).

Concerning the description of cellulose dissolution, the lower limit of basicity observed with EMIMAc and BMIMCl in Figure 4.6 is well in agreement with the value reported by Rinaldi (2011) and Gericke (2011). The relation of cellulose dissolution with high basicity can also be observed in other cellulose solvents. Spange et al. (1998) showed that an amount of 0.5 wt % of lithium chloride in dimethylacetamide already results in β = 1.75. In comparison with the lower limit of β = 0.86, a cellulose dissolution should be readily obtained but is observed not before 3 wt % of lithium chloride (Chrapava et al., 2003). This comparison demonstrates that β alone cannot yield a general description of cellulose solvents.

The only IL, which does not fit into that scheme, is DMIMDMP. Its basicity implies that DMIMDMP should be much more tolerant to water than observed in practice. Concerning the effect in DMIMDMP, it can be speculated that the increasing acidity might have an influence as well, which is not explicitly included in the basicity. It is addressed by the concept of net basicity (Hauru et al., 2012) that suggests the range of $0.35 < (\beta - \alpha) < 0.9$ in order to enable cellulose dissolution.

The data in Figure 4.6 calculates lower limits of $(\beta - \alpha)$ as 0.2, 0.4, and 0.27 for BMIMCl, DMIMDMP, and EMIMAc, respectively, at the observed insolubility of cellulose (data in Appendix B, Figure B.7). Although being on the border of the given range, the net basicity also does not predict the insolubility of cellulose in DMIMDMP/water mixtures correctly. Hence, the results roughly agree to the suggested concept of net basicity but also seem to face high uncertainties as long as the individual mechanism of Kamlet-Taft interaction has not been understood.

4.1.3 Conclusion of the cellulose dissolution in ILs

As shown by the results above, a facile dissolution of crystalline cellulose can be reached in each IL at 115°C. The dissolution causes decrystallization of the polymer, which can be recovered by addition of a polar solvent, for instance water. The recovery induces precipitation of a solid, which involves part of the cellulose to crystallize into cellulose II. As this crystalline polymorph is supposed to be more beneficial for enzymatic hydrolysis, the crystalline cellulose Iβ is not necessarily converted into amorphous cellulose for efficient enzymatic hydrolysis during pretreatment.

The investigated ILs show a different tolerance against water in cellulose dissolution. EMIMAc seems to be the substance of choice because amounts of up to 20 wt % of water are tolerated in cellulose processing, while BMIMCl and DMIMDMP already fail to dissolve cellulose above 5 wt % of water.

The characterization of the studied ILs exhibits acid/base properties in line with the strength of the conjugate acid. The base strength of the ILs is in the order EMIMAc > DMIMDMP > BMIMCl, with the later already resembling an acid nature. This order also seems to control the Kamlet-Taft parameters, which cannot explain for the cellulose dissolution mechanism, neither in neat ILs nor in mixtures with water.

The quantitative analysis of the hydrogen bond donor and acceptor capabilities thus leaves a divided result. On the one hand, it could be clarified that the basicity of the anion is the major feature of the investigated ILs and it is very likely a prerequisite for the solvation of cellulose. On the other hand, it became obvious that the interaction of both ions is very complex. Aside from qualitative results, the Kamlet-Taft parameters do not hold for a quantitative description of cellulose solvents in general and even indicate discrepancies within the group of imidazolium ILs.

4.2 Pretreatment of wood in ILs

This section covers the experiments to study dissolution of wood in IL. The work aims not necessarily at complete wood dissolution but rather at the identification of most promising pretreatment effects induced by an ILs that is still to be found. In a first set of experiments, the wood dissolution with EMIMAc as the most promising IL in cellulose dissolution is quantitatively assessed. A comprehensive mass balance allows for the first fundamental kinetics of the dissolution process and enables the investigation of the process of dissolution more thoroughly. Further experiments then reveal the changes in composition and structure that are induced by the particular ILs. The most promising conditions for IL pretreatment of larger wood chips are selected step-by-step. The process parameters are established in Section 4.2.3 in combination with enzymatic hydrolysis after detailed investigation of the possibilities due to dissolution of wood in the ILs.

According to the cellulose experiments, the dissolution is first investigated with a single, manually separated, native spruce fiber (Figure 4.7, left) that is exposed to BMIMCl at 100°C. During the experiment, the fiber becomes transparent as IL enters the lumen and displaces the air from within the fiber. However, the cell wall does not appear to be substantially changed even after an exposure time of 16.5 min. In contrast, the cellulose dissolution was complete within 3 min (Figure 4.1). Although cellulose, lignin, and xylan dissolve individually in the three ILs (cf. the literature review in Section 2.3.3; it was also checked by own experiments), the ultrastructure and the molecular complex of wood obviously inhibits facile dissolution.

Another important aspect is unveiled by Figure 4.7 concerning visual determination of wood dissolution. The optical properties of the spruce fiber obviously change from dark into transparent. At the beginning, air fills the void of the lumen in the dry fiber that has an index of refraction of $n_{589nm} = 1$. ILs have an index of refraction of $n_{632nm} = 1.50$ at 85°C (Kuzmina et al., 2010), which is very close to the one of cellulose and lignin of $n_{588nm} = 1.47$ (Kasarova et al., 2007) and $n_{546nm} = 1.60$ (Donaldson, 1985), respectively.

With the displacement of air from the lumen by penetrating IL, the difference between the refractive indices becomes smaller and the phase boundaries become harder to discern visually. A superficial visual check of a wood solution could erroneously lead

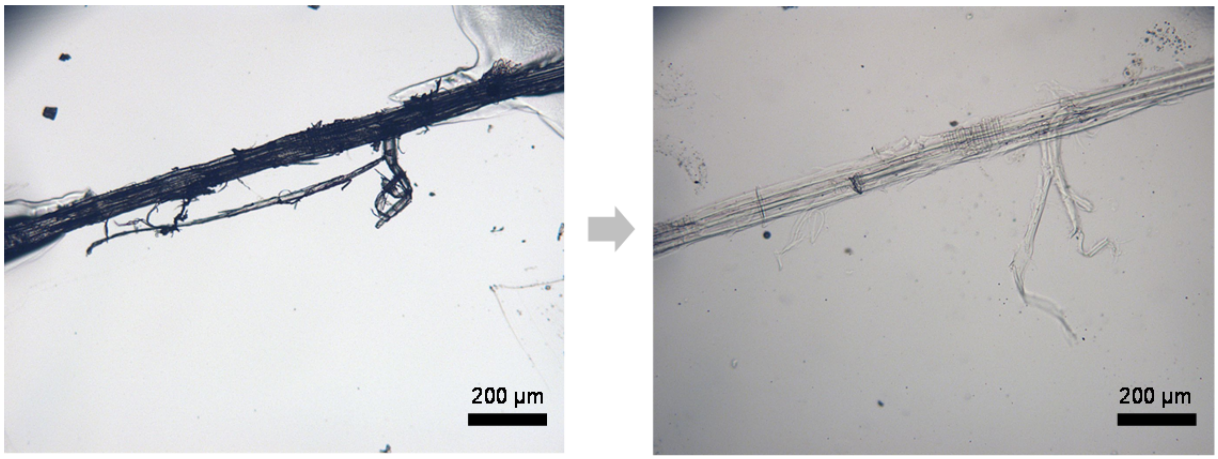

Figure 4.7. A spruce fiber at the start (left) and after 16.5 min in BMIMCl at 100°C (right). The treatment reveals swelling but does not show any substantial dissolution.

to the conclusion of a solvated state. The color of the IL and the continuous darkening of the mixture during dissolution can even enhance the uncertainty as shown in Appendix A (Figure A.1). It has to be noted that optical methods such as Focused Beam Reflectance Measurements (Kail et al., 2009) or scattered light analysis from wood particles (Zavrel et al., 2008) probably do not provide reliable data of the dissolution.

4.2.1 Overall mass balances of wood dissolution

The developed laboratory strategy to assess the amount of dissolved material more precisely is based on the analysis of the supernatant for dissolved material and subsequent weighing of all remaining liquid and solid that has been thoroughly washed (Viell & Marquardt, 2011). The results of several dissolution experiments show that more than 95 wt % of the overall mass has been recovered on average, which was calculated from the overall mass balance. This figure is taken as a convincing validation of the method. At short dissolution times up to 4 hours, a standard error of less than 4 wt % was achieved; longer processing times were not included in the error calculations because decomposition of the macromolecules is likely possible as assessed by the dark appearance of the raw material at long dissolution times (cf. Figure B.1 in Appendix B).

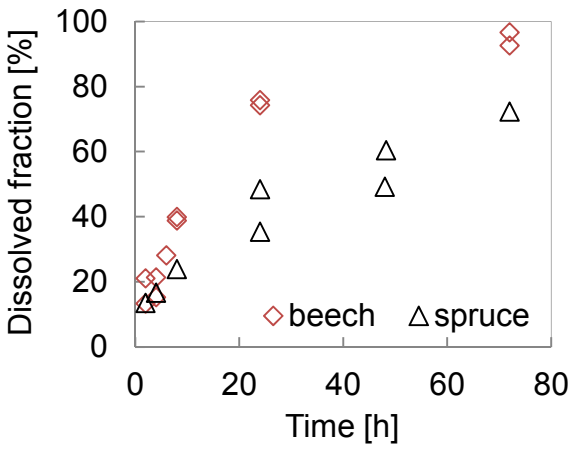

Figure 4.8. The dissolved fraction of small beech and spruce particles (0.1–0.5 mm) in EMIMAc at different processing times measured by mass balancing the IL and the processed wood. Small particles (0.1–0.5 mm) of beech and spruce have been used (EMIMAc, 115°C, 500 rpm, 1–5 wt % solids, precipitated with acetone/ethanol 1:1 (v/v), from Viell & Marquardt (2011)).

With this method, the first approach is to investigate the suggested process concept of wood dissolution in an IL and subsequent precipitation to recover cellulose and lignin separately after solvent exchange. EMIMAc has been selected because it is the most promising IL according to precise cellulose dissolution studies, which coincides to the studies of Sun et al. (2009), who introduced the processing concept followed in this work.

Figure 4.8 shows the time course of the dissolution of two wood species in EMIMAc. First, small particles of 0.1–0.5 mm are used to investigate the course of dissolution. The dissolved fraction increases with time and the data points shows a diminishing slope at extended processing times. 40 wt % of spruce and 75 wt % of beech can be dissolved after 24 h, which increases after 72 h to 70 wt % and 95 wt %, respectively. Therefore, beech is dissolved to a greater extent than spruce.

The second set of experiments with wood chips instead of small particles gives the results shown in Figure 4.9 in comparison with small particles to investigate the effect of specific surface area. A similar time course is indicated by the data points. Beech chips are dissolved to fractions of 75 wt % after 24 h and 90 wt % after 72 h, which are very similar to the values obtained with small particles. Interestingly, the results

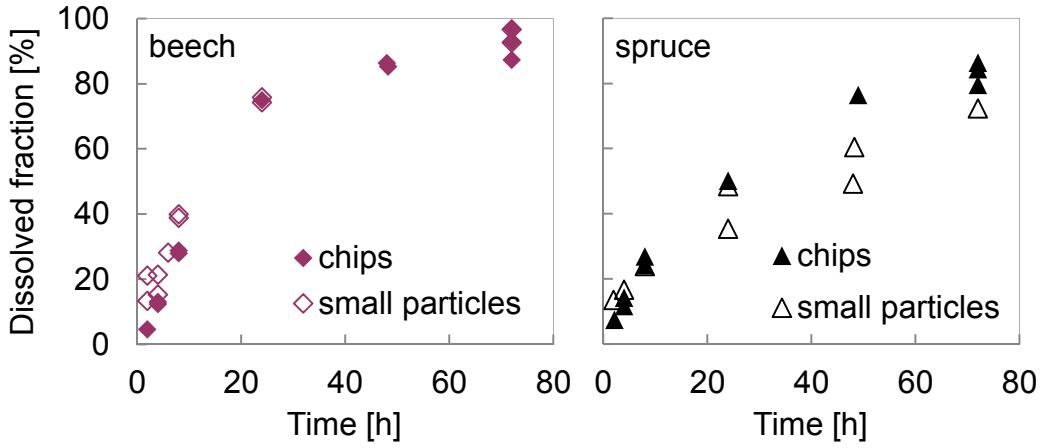

Figure 4.9. The dissolved fraction of beech (left) and spruce (right) in EMIMAc after different processing times at two particle sizes. The results from chips of 10 × 2 × 1 are compared to those from small particles of 0.1–0.5 mm from Figure 4.8 (EMIMAc, 115°C, 500 rpm, 1–5 wt % solids, precipitated with acetone/ethanol 1:1 (v/v), from Viell & Marquardt (2011)).

with spruce chips seem to be even superior to those obtained with small particles, which can be observed after 48 and 72 h of dissolution. In general, the data for wood chips vary to a smaller degree than the data for small particles.

The acetone/ethanol mixture utilized for precipitation in the experiments displayed in Figure 4.9 enables precipitation of dissolved lignin by the addition of water. The obtained lignin mass fractions as per the original dry wood mass are depicted in Figure 4.10. Only a few percent are dissolved during the first 24 h of dissolution; longer dissolution up to 72 h elevates the lignin yield to about 10 wt % for both, beech and spruce chips.

Sun et al. (2009) isolated 10 wt % of lignin from small particles of pine after 48 h by dissolution and precipitation; the results in Figure 4.10 show a yield of 6–8 wt % from spruce chips in the same time period. The results obtained by the developed method are therefore close to those published by the mentioned authors. It can be concluded that the data are consistent with those in literature, also in case of large particles and without a pH adjustment with acids for a little higher recovery of lignin. If the lignin content of the utilized wood was considered, the lignin fraction recovered after 72 h would amount to 36 wt % and 45 wt % of the original lignin content of spruce and beech, respectively.

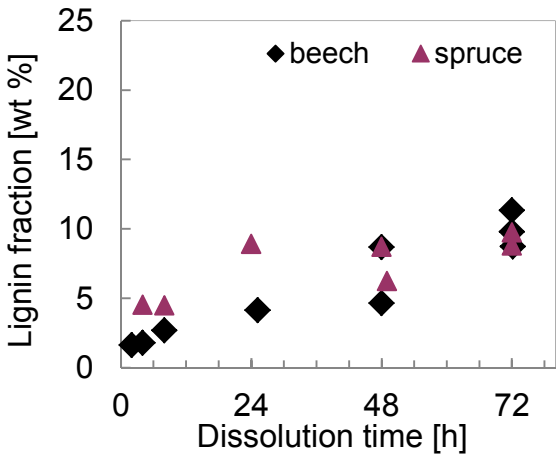

Figure 4.10. The lignin fraction obtained by precipitation from the washing liquors after dissolution of wood chips (10 × 2 × 1 mm^3) of spruce and beech in EMIMAc at the indicated times (EMIMAc, 115°C, 500 rpm 1–5 wt % solids, washed with acetone/ethanol 1:1 (v/v), precipitated in water, filtered with 1.2 µm filter, from Viell & Marquardt (2011)).

Summing up these results, beech shows a faster dissolution than spruce, which agrees with the report of Sun et al. (2009). The isolated amount of lignin also corresponds to the reported values, and a higher relative amount of lignin is extracted and recovered from beech in comparison to spruce. This finding might be due to the different structure of lignin in both species.

The complete dissolution, however, claimed for a similar particle size of 0.125–0.25 mm after 25 h and 46 h with oak and pine, respectively, could not be confirmed, neither for beech nor for spruce. Additional experiments with completely dried beech and spruce particles as used by Sun et al. (2009) did not change these results significantly (not shown for brevity). Several other authors also noted an incomplete dissolution, e.g., in case of corn stover (Xu et al., 2012) and eucalyptus (Leskinen et al., 2011). Hence, it must be acknowledged that, in agreement with several reports from the literature and with the results of this work, dissolution of wood in IL does not seem to proceed to completeness.

Moreover, the average fraction of dissolved wood seems to be independent of particle size. After 72 h, approximately 90 wt % of beech wood is dissolved both with small particles and wood chips. This is surprising because particles in the mm-range have a larger specific surface area by nearly two orders of magnitude in comparison

to the wood chips. In case of spruce, larger particles dissolve even better than small particles. Thus, a closer look at different particle sizes is of interest.

The results of the mass balances enable a first quantitative insight into the progress of dissolution of wood in EMIMAc. The dissolution is very slow and requires a residence time of several days for a considerable fraction of dissolved wood. Interestingly, the involved mechanisms seem to be rather independent of particle size in the range tested. This phenomenon possibly enables processing without or at a reduced effort for mechanical comminution.

Effect of particle size and IL on the dissolution of wood

The tedious protocol for mass balancing of the dissolution in the last section was developed to cope with the high viscosity of IL-wood solutions that limit efficient separation and reliable assessment of residual mass. A simplification of the experimental load for higher throughput is achieved by the consecutive utilization of DMSO, acetone and water to remove the viscous IL from the solid mass. The washed solid is then weighed directly to calculate the dissolved fraction. First, small particles are investigated to validate the method against the rigorous mass balances in the previous section and to identify the most promising combination of IL and wood species. Afterwards, this particular combination is investigated with larger particles of chips and blocks.

The results obtained with small particles in Figure 4.11 show a quick increase of dissolved fraction at the beginning of pretreatment, and the slope diminishes as the processing time increases. With EMIMAc, approximately 70 wt % of beech and 40 wt % of spruce is recovered after 24 h, which increases to 90 wt % after 69 h. This is well in agreement with the dissolved fraction of 75 wt % and 40 wt % obtained with the rigorous method (cf. Viell & Marquardt (2011) and Figure 4.8). Hence, the simplified protocol achieves similar results and is therefore not compromised by erroneous effects of the IL or precipitated macromolecules in case of small particles.

In detail, the combinations of IL and wood show distinct differences in the dissolved fraction. The most inferior performance is observed with DMIMDMP. Beech dissolves only to 22–26 wt % (Figure 4.11, left), which is already achieved after 20 h of dissolution time but without further substantial increase. The beech particles dissolve much faster in BMIMCl or EMIMAc and to a larger extent. EMIMAc is clearly superior

with approximately twice the amount of dissolved wood in the experiments up to 20 h of dissolution in comparison to BMIMCl. To check whether complete dissolution is a matter of time, very long processing times are tested as well. Both ILs achieve similar amounts of dissolved material (approximately ~95 wt %) after 188 h. The incompleteness of the dissolution is demonstrated by a significant amount of residue (cf. Appendix B, Figure B.2 to Figure B.4). Moreover, it looks very dark, which is obviously due to the formation of chromophores that indicate decomposition of the material.

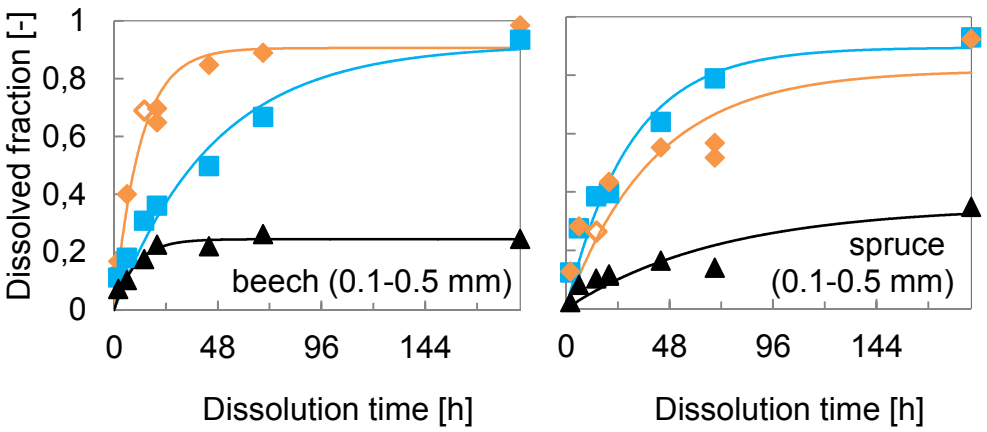

Figure 4.11. The dissolved fraction of small particles (0.1–0.5 mm) of beech (left) and spruce (right) after different processing times in BMIMCl (■), DMIMDMP (▲), and EMIMAc (◆). The lines indicate a pseudo-first order kinetics (115°C, 5 wt % solids, 500 rpm, washed consecutively with DMSO, acetone, water).

In case of spruce, the data for DMIMDMP reveals a similar picture as with beech; the dissolution of spruce progresses only up to a rather minor fraction of 13–16 wt %. A higher fraction of dissolved material is obtained with BMIMCl and EMIMAc. Both ILs show a similar performance in the first hours of dissolution. EMIMAc results in approximately 55 and 50 wt % of dissolved spruce after 44 and 69 h while BMIMCl achieves 64 and 79 wt %, respectively. Eventually, a small amount of residue of 5–10 wt % is detected with both EMIMAc and BMIMCl after 188 h, which is similar to the results with beech for the two ILs.

The data in Figure 4.11 has been fitted to a pseudo first order kinetic of the form $w^{dissolved} = c(1 - \exp(a * t))$. The comparison shows that the data of beech fits quite

well to this model with $R^2 \approx 0.95$. In case of spruce, the R^2 of the fit of EMIMAc and DMIMDMP falls below 0.8 and indicates effects that are not covered by a first order kinetics. Furthermore, the comparison to the calculated kinetics shows two data points at 14 h in the set with EMIMAc that deviate slightly (both marked with an open diamond in Figure 4.11).

Hence, the comparison of the ILs and the dissolution of the two wood species unveiled remarkable differences in the performance of the ILs. DMIMDMP is in general inferior in wood dissolution. The best performance is achieved with BMIMCl and EMIMAc. The latter IL shows in particular a superior progress in the initial time of beech dissolution. In case of spruce, the choice is not that clear. BMIMCl performs better with spruce than with beech, which agrees to a similar observation by Fort et al. (2007). While EMIMAc and BMIMCl perform nearly identical at short dissolution times, the performance of BMIMCl is slightly superior compared to EMIMAc at extended dissolution times.

The results thus imply kinetics of dissolution to depend on the combination of wood and IL. The difference in the goodness of fit indicates that, however, the underlying mechanisms cannot be described by a first order kinetic in case of spruce and EMIMAc. Two promising combinations of IL and wood are identified, i.e. BMIMCl and spruce and EMIMAc and beech. The latter combination is ahead to the other ILs by nearly 50 % in yield after short pretreatment time in comparison

Next, the effect of different particle size is to be investigated with these pairings. The results of three different particle sizes in pretreatment are shown in Figure 4.12. The diagrams include the results obtained for small particles from Figure 4.11 and additionally present results from chips (10 × 2 × 1 mm^3) and cylindrical blocks (5 × 10 mm^2).

The most remarkable peculiarity of these data is the negative data at the beginning of the time course in Figure 4.12. These values are obviously caused by solid mass larger than the initial mass, which contradicts dissolution at first sight. As this occurs in particular with the large blocks at the shorter dissolution times, the cause is probably remaining IL in the wood blocks that withstands the intensive washing procedure. In fact, spectroscopic investigations of the chips showed distinct features of remaining IL supporting this conjecture (cf. Figure B.6 in Appendix B). To account for this effect, the pseudo-first order kinetics applied in Figure 4.11 has been extended by an induction time *b*, i.e., $w^{dissolved} = c\big(1 - \exp\big(-a * (t - b)\big)\big)$.

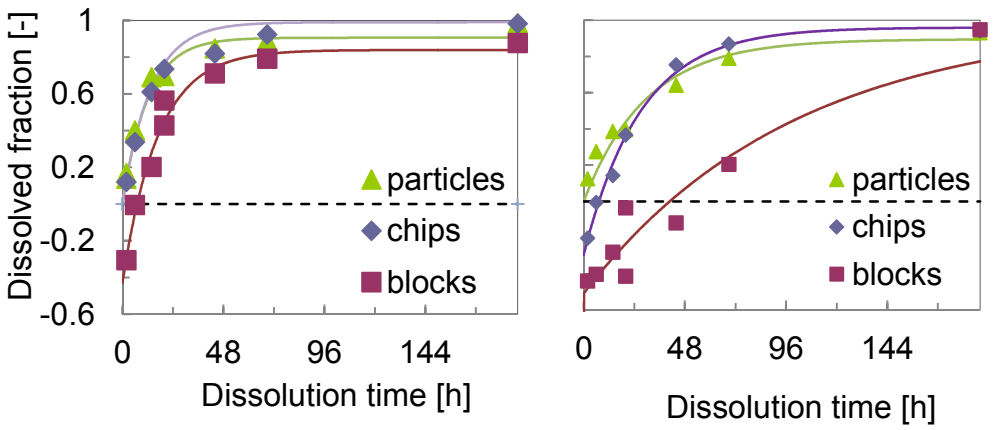

Figure 4.12. The progress of the dissolution in the best pairs of IL and wood: left beech in EMIMAc and right spruce in BMIMCl. Both sets utilize raw material of different size (particles: 0.1–0.5 mm, chips: 10 × 2 × 1 mm^3, blocks 10 × 5 mm^2). The dashed line depicts zero mass change (115°C, 5 wt % solids, 500 rpm, washed consecutively with DMSO, acetone, water).

The results show that beech particles and beech chips in EMIMAc follow the same trend as if there is hardly any difference between them. Even the larger blocks exhibit similar dissolution kinetics after an induction time of 7 h. The processing for 188 h results in approximately 88 wt % of dissolved material, and the finding of a particle-size independent dissolution rate in EMIMAc substantiates.

In contrast, BMIMCl seems much more susceptible to largely increased particle sizes. While chips only result in an induction time of 7 h and yield even slightly higher amounts of dissolved spruce after 48 and 72 h in comparison to small particles, the results are different for blocks. They obviously cause large variations in the data and limit the dissolution to a great extent. Even when remaining BMIMCl is assumed to cause the negative dissolved fraction up to 40 h, as observed with EMIMAc, a different behavior of the two species in the two ILs is quite obvious.

The morphology of the residue after dissolution of the blocks in Figure 4.13 supports this implication. While the beech blocks are completely converted into fines after 14 h, the pine blocks still show a similar size as the original particles. Only a swelling of the latewood is noted. The presence of the original morphology suggests that the dissolution of softwood blocks in BMIMCl is largely limited by mass transport that

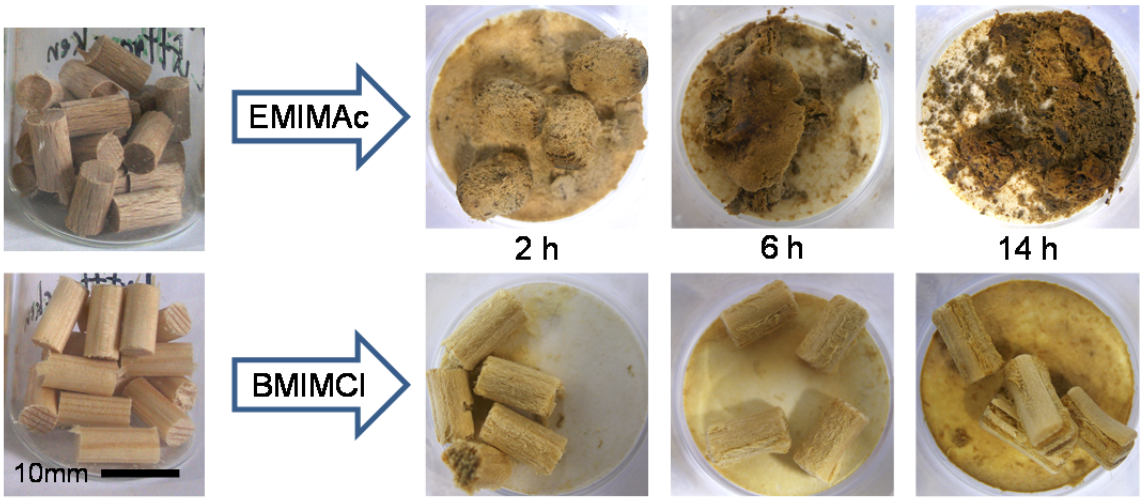

Figure 4.13. Morphology of blocks (10 × 5 mm^2) of beech (top) and pine as representative softwood in this case (bottom) in its native state (left) and after dissolution in the two ILs for the time indicated. The samples are part of the set, for which data is shown in Figure 4.12; the full set of pictures is available in Appendix B, Figure B.5 (washed with DMSO, acetone, water).

might cause the large deviations and slow dissolution presented in Figure 4.12. In contrast, the residue of beech in EMIMAc cannot be differentiated from smaller particles after 14 h. This gives a first explanation of the similar performance independent of beech particle size in EMIMAc.

Only few data are available from literature for comparison and discussion of the own experimental findings. Nakamura et al. (2010a) investigated the dissolution of wood flour in EMIMCl. After 24 h of processing, the authors detected a residue of only 17 and 5 wt % for cedar, a softwood, and beech, respectively. Their work thus shows a better dissolution of beech in comparison to cedar in EMIMCl and in general much smaller residues. Both findings outperform the dissolution determined in this work, where 64 and 60 wt % from beech and spruce are obtained with BMIMCl after the same time.

The difference might be due to the different wood species, particle sizes and the different cations of the utilized ILs. Reflecting the results of spruce in BMIMCl, it seems plausible that the dissolution of wood in BMIMCl is hindered due to issues of mass transport into and out of the wood. Although the blocks are made of pine instead of spruce, the tissue and chemical composition can be regarded to be nearly

identical (Blechschmidt et al., 1986). Rather, the large blocks obviously decrease the dissolution rate. Indeed, the utilized EMIMCl shows a viscosity of 62 mPas at 80°C (Chen et al., 2010), which is 2/3 of the value of BMIMCl utilized here. This could increase the mass transport resistance during dissolution and cause the smaller residue in the study of Nakamura et al. (2010a).

However, the larger chips and the smaller particles show a similar course of dissolution with even higher yields after 48 and 72 h from chips. This observation was already noted in Figure 4.9 and it is again observed in Figure 4.12. A possible explanation could be the method of particle preparation. The swing milling and subsequent sieving into different size classes could result in a fractionation leaving more inaccessible wood in the particle size class. In this context it is interesting to note that the dissolution in EMIMAc does not seem to be affected by the larger particle size. These issues are likely related to the wooden ultrastructure and cannot be further investigated using overall mass balances.

In conclusion, it is shown that dissolution of wood in ILs is not complete within finite processing times and rather slow. It is even slower when larger wood particles are processed. The best solvent among the tested ILs is EMIMAc, which shows good dissolution capabilities for both wood species but in particular with beech. Still, residence times of 72 h are required to obtain an acceptable dissolution. The dissolution kinetics also indicates more complex mechanisms at the beginning of dissolution and during the course of the processing.

4.2.2 Component mass balances during dissolution

The analysis of the overall dissolved fraction of wood turned out to be more complex than anticipated from the concept of simple dissolution. The heterogeneity of wood implies that the individual components could possible cause these effects. Therefore the composition of the residue is analyzed, which correspondingly unveils which components have been removed during dissolution. To do so, the solid material from Figure 4.11 was subjected to wet chemical analysis. The necessary amount of solid material limited the analysis to maximum dissolution times up to 20 or 44 h.

Figure 4.14 to Figure 4.16 show the dissolution kinetics as in Figure 4.11 but resolve the individual wood components. The dissolved material was calculated by the difference between composition of the residue after dissolution and the initial

composition of the wood (cf. eq. (3.1)). All diagrams show the total dissolved mass fraction as topmost line from the course of dissolution in Figure 4.11. The raw composition data can be found in the Appendix B (Figure B.2 to Figure B.4). Arabinan, which is present in wood with less than one wt % in total composition, is not included in this analysis.

Figure 4.14 shows the progressing dissolution of the individual wood fractions of beech in BMIMCl up to 44 h, and up to 20 h in case of spruce. The extraction of glucan from beech shows maximum values of 38 wt % after 44 h. The same value is reached in spruce but after half the residence time. Thus, high fractions of cellulose are dissolved. In contrast, the lignin seems to largely withstand considerable dissolution in the IL. A rather constant amount of only 5–8 wt % of beech lignin is dissolved at all pretreatment times up to 40 h. It seems as if this part of the lignin is dissolved rather instantaneously and no further lignin is extracted at prolonged dissolution times. In case of spruce, the dissolved lignin fraction is always below 1 wt %. Concerning the hemicelluloses of the wood species, the xylan from beech is rather linearly extracted up to 9 wt %; the mannan from spruce shows a similar course although being slightly faster in extraction up to 6.5 wt % already after 20 h.

Hence, the dissolution is highly selective for celluloses from spruce with BMIMCl which is in line with previous reports. For instance, EMIMCl was employed to fractionate spruce by a selective dissolution and hydrolysis to monomeric sugars (Hyvärinen et al., 2010). Despite the higher degree of dissolution in the work of Nakamura et al. (2010, cf. Section 4.2.1), the authors also showed that cellulose was dissolved preferentially by EMIMCl and reported the same component ratios as this work. The lignin from hardwood was also much quicker dissolved in comparison to the softwood lignin from cedar. The same situation is observed in comparison with the results by Miyafuji et al. (2009).

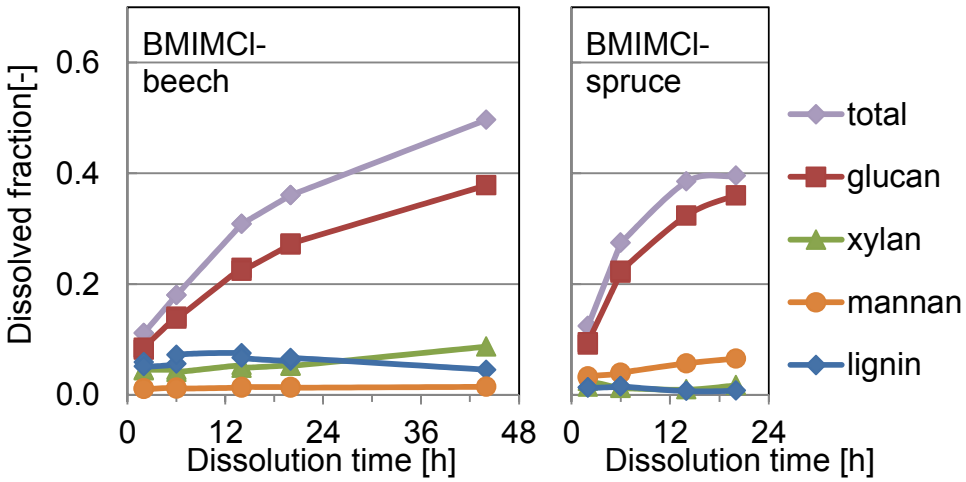

Figure 4.14. The component fraction of beech (left) and spruce (right) dissolved in BMIMCl after different dissolution times as per in Figure 4.11 (lines to guide the eye).

The insolubility of lignin from spruce, however, contradicts the claim of the high dipolarity/polarizability being responsible for lignin dissolution (cf. Padmanabhan et al., 2011). As a matter of fact, BMIMCl cannot extract significant amounts of guaiacyl lignin despite a high π^*. It might be that the temperature of 115°C is too low to cause remarkable depolymerization of lignin as observed by Cox & Ekerdt (2013).

This selectivity might also yield a possible explanation for the higher yield with larger chips at longer dissolution times in Figure 4.9 and Figure 4.12. As the milling results in cell wall debris (Fukazawa et al., 1982) that is sorted out by subsequent sieving, a concentration of lignin-rich material in the fraction of small particles could be the reason why small particles dissolve slightly worse. Alternatively, the swing milling might also cause the ultrastructure to collapse, which should also worsen the mass transport in comparison to the cut chips.

DMIMDMP showed an inferior performance in overall dissolution and does not exhibit a good selectivity as well. The results in Figure 4.15 show that a few percent of all fractions of both wood species dissolve rather unselectively. After 20 h, there seems to be an increase in the dissolution of glucan. It occurs in beech and spruce and may indicate a discrete process that enables dissolution of a little bit more cellulose at extended processing times. However, this does not compensate for the low overall performance of DMIMDMP.

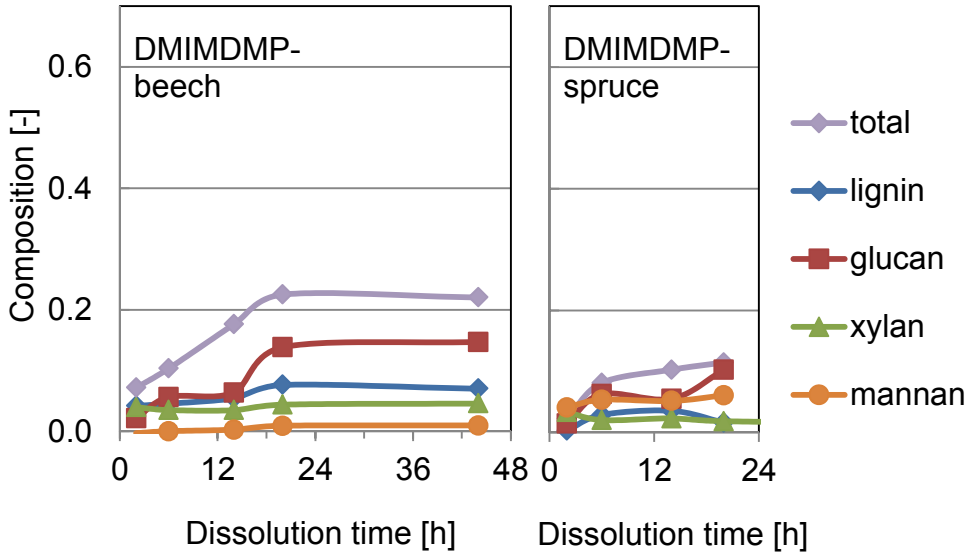

Figure 4.15. Dissolved fractions of beech (left) and spruce (right) during dissolution in DMIMDMP at 115°C after different dissolution times (lines are to guide the eye; samples are experiments shown in Figure 4.11).

The performance of EMIMAc in the overall dissolution is remarkable in that it provides the highest dissolved fractions at the early dissolution times. The dissolved components from beech and spruce are shown in Figure 4.16. Both lignin and carbohydrates are extracted from the wood. After two hours, equal amounts of lignin and glucan of approximately 7 wt % are dissolved from beech. The longer the processing, the more glucans and lignin are dissolved, but the rate of dissolution is different. A final lignin fraction of 11.5 wt % is extracted from beech after 20 h. Although a considerable fraction of xylan is observed first after 6 h in EMIMAc, it continuously increases until nearly all xylan is extracted after 20 h. Similarly, nearly 70 wt % of the cellulose has been dissolved. The data points in both sets at 14 h are likely due to erroneous measurements as already indicated in Figure 4.11; they are therefore excluded from the general trend.

With spruce, a smaller slope is observed in the extraction of all wood fractions. Similar as before, the ambiguous data points after 14 h of treatment are not considered. The amount of extracted glucan increases continuously but does not reach values as high as with beech. Lignin and mannan are dissolved in a rather linear fashion up to 8 wt %, which corroborates that less lignin is extracted in comparison to beech.

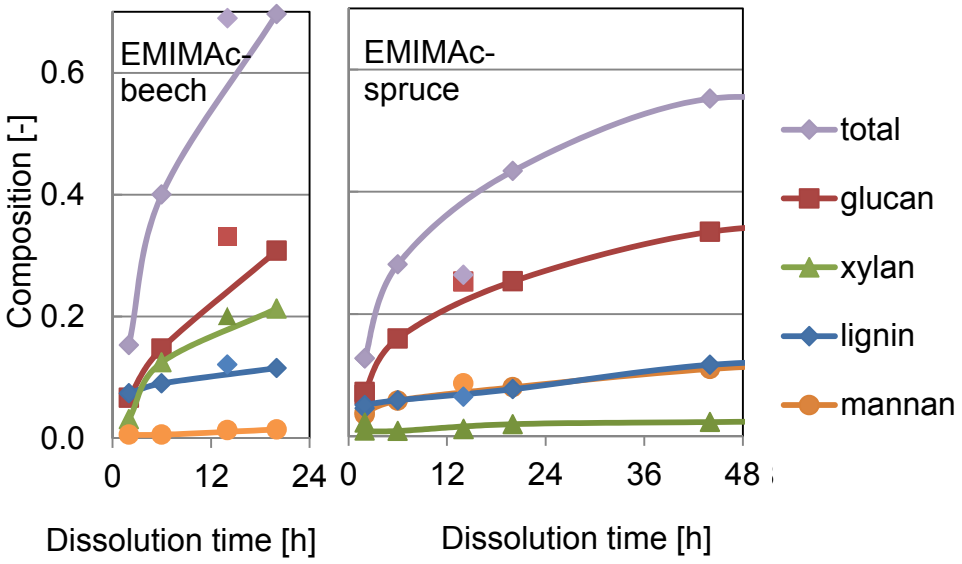

Figure 4.16. Dissolved fractions of beech (left) and spruce (right) during dissolution in EMIMAc at 115°C after different dissolution times (lines are to guide the eye; samples are experiments shown in Figure 4.11).

Interestingly, the precipitated fraction of lignin determined in Figure 4.10 differs from the extracted fraction as determined in Figure 4.16. The latter shows that there is already more dissolved after 20 h than what can be obtained after more than twice the time using precipitation. Losses of approximately 50 wt % of the dissolved material are therefore faced. The missing fraction is likely decomposed to water soluble molecules that cannot be recovered by precipitation.

Despite the common application of EMIMAc in biomass research, the quantitative investigations of wood dissolution in this IL are still scarce. Sun et al. (2009) did not report a compositional analysis of the residual solid, so this study cannot be taken for direct comparison. The yield in precipitable lignin was already compared in the discussion of Figure 4.10. The data were in good agreement but the loss demonstrated by the lignin balance was not addressed.

In contrast to Sun et al. (2009), the report by Lee et al. (2009) claims a preferential extraction of lignin with EMIMAc at a “low solubility of wood flour”. An extraction of 14 wt % of lignin is achieved after 24 h at 90°C. The data presented in Figure 4.16 shows an extraction of 12 wt % after 20 h, but at 115°C. A closer look at the experimental protocol of Lee et al. (2009) reveals that an extraction with 0.1N of sodium hydroxide (NaOH) was carried out after IL treatment. The high solubility of

lignin under alkaline conditions (cf. 2.2.1) is a plausible explanation for the higher selective extraction of lignin mediated by pretreatment with EMIMAc. Later, the same group published another paper without the NaOH washing step and reported roughly half the amount of extracted lignin (Doherty et al., 2010). This is in reasonable agreement concerning the temperature difference between their work and the results in this study.

One recent work could be found that presents data about the carbohydrate composition of the solid after partial dissolution in EMIMAc. Wen et al. (2013) reported that mannan, arabinan and galactan are completely removed from birch wood by treatment in EMIMAc after 16 h at 110°C. Despite the different species of wood in this work, the removal of 70% of mannan from beech after 20 h in this work indicates a similar trend.

Hence, it can be stated at this point that the investigated methods are in agreement with the few reports in literature although the experimental conditions vary. In sum, the results show that the dissolution of wood in ILs depends largely on the combination of IL and raw material. DMIMDMP is clearly inferior in its performance in both the overall dissolution and in selectivity towards particular components. This IL is therefore not considered for an envisaged technical application in further investigations in this work.

BMIMCl is selective for carbohydrates, in particular for cellulose, while only negligible amounts of lignin are extracted from spruce. In view of the dissociation equilibrium resembling an acid (Figure 4.5) and the reported removal and hydrolysis of carbohydrates (Hyvärinen et al., 2010), this indicates an action of the chloride-based ILs similar to the processing with concentrated hydrochloric acid (cf. Section 2.2.2). As the non-solubility of lignin was only observed with spruce and BMIMCl, the selectivity is likely related to the lignin structure. In fact, all experiments above showed that lignin from beech always dissolves better than from spruce; it might by the syringyl which is preferentially dissolved. As spruce-lignin contains mainly guaiacyl lignin, the higher recalcitrance against extraction of spruce lignin is likely due to the condensed structure of guaiacyl lignin.

At first sight, the feature of selective extraction could be promising for a fractionation of wood. However, the process is very slow. A cellulose extraction of larger than 70 to 80% can be achieved from either species at residence times longer than 24 h. Comparison with solubility data of the individual components (Pu et al., 2007; Wang

et al., 2012) demonstrates that the slow progress is not due to reaching the maximum solubility. Limitations in mass transport as experienced with macroscopic particles are likely involved. Hence, it remains for further studies to elucidate whether the selectivity of chloride based ILs can be exploited for technical processing with varying feedstock.

Concerning the technical application, it has to be realized that the idea of pretreating wood into a completely dissolved state is not feasible. Systematic experiments show that a complete dissolution is not observed under technical conditions even with EMIMAc as the best solvent among the investigated ILs. The advantage of a “good” dissolution in EMIMAc among the investigated ILs is, however, gained by a rather unspecific dissolution of the wood components. The higher amount of dissolved beech wood and in particular lignin indicates a small advantage for the processing of hardwoods in contrast to softwoods. Nevertheless, the precipitation yield showed that a certain amount of lignin cannot be recovered. Even the dissolution studies with cellulose in Section 4.1.1 showed first signs of decomposition. Although this has not yet been quantified, it is therefore questionable whether long-time dissolution and subsequent precipitation will be appropriate for high-yield technical processes. Other effects thus have to be exploited in order to establish a viable process concept for wood pretreatment based on ILs.

4.2.3 Investigation of short-time pretreatment

The indication of a pretreatment in EMIMAc which is almost independent of particle size draws the attention to the effects related to the complex ultrastructure of wood on dissolution. Despite being clearly obvious on a macroscopic level, they are often overlooked during chemical investigation at a small scale. The challenge is to bridge phenomenological investigation with identification of chemical fundamentals, which is only addressed by a few studies in general (Lynd et al., 1999). This section therefore deals with the effects of pretreatment and concerns both the chemical aspects and the structural changes of wood. The preceding sections showed no advantage from the longer processing times, so the focus will be on the short-time effects.

The investigations start with the analysis of the particle morphology after an exposure of macroscopic wood particles, i.e., chips, in EMIMAc at 115°C as before. The result

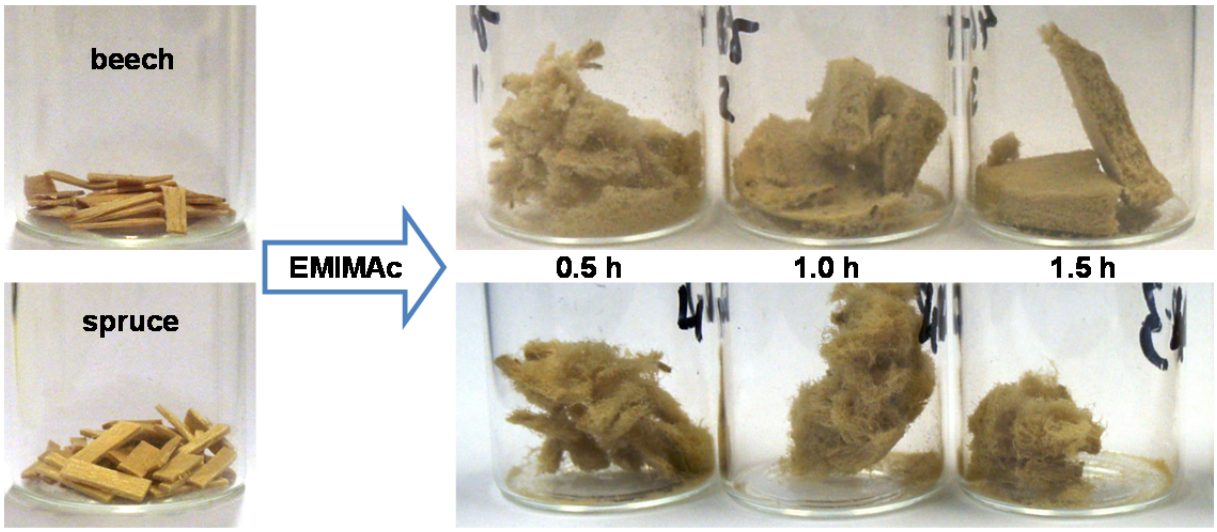

Figure 4.17. Macroscopic effect of EMIMAc on the wood structure of chips (beech on top and spruce at the bottom). The original wood chips (left) were pretreated in EMIMAc after pretreatment times as indicated in the figure (115°C, 500 rpm, washed with acetone/water 1:1 (v/v)).

is shown in Figure 4.17. Surprisingly, the initially dense and compact chips of beech and spruce, which are not dissolved substantially during the experiment, are converted into larger particles with a fibrous appearance. After 0.5 h, beech already shows detangled fibers on the surface of the chips. A processing time of 1.5 h is sufficient to convert the beech chips into a particle material, whose geometry has become a filter cake due to the washing step. In case of spruce, the same process applies. The former chips of spruce resemble a fluffy lump of fibers. However, the residue still shows a few solid particles after 1.5 h, where the integrity of the wood has obviously not been disintegrated (not visible in Figure 4.17).

A more detailed insight can be obtained by microscopy of thin wood slices of 60 µm thickness. The corresponding experiment was published by Viell and Marquardt (2011). Figure 4.18 shows the initial and the final picture of a series taken to visualize the process during exposure of these cross-sections to EMIMAc. Initially, the structure of wood with the dense latewood (LW) and the earlywood (EW) of beech wood (top left) and spruce (bottom left) are visible. Beech wood exhibits the characteristic ray cells in vertical direction; its diffuse porous tissue also shows EW and LW but without the remarkable difference in the cell wall thickness as in spruce.

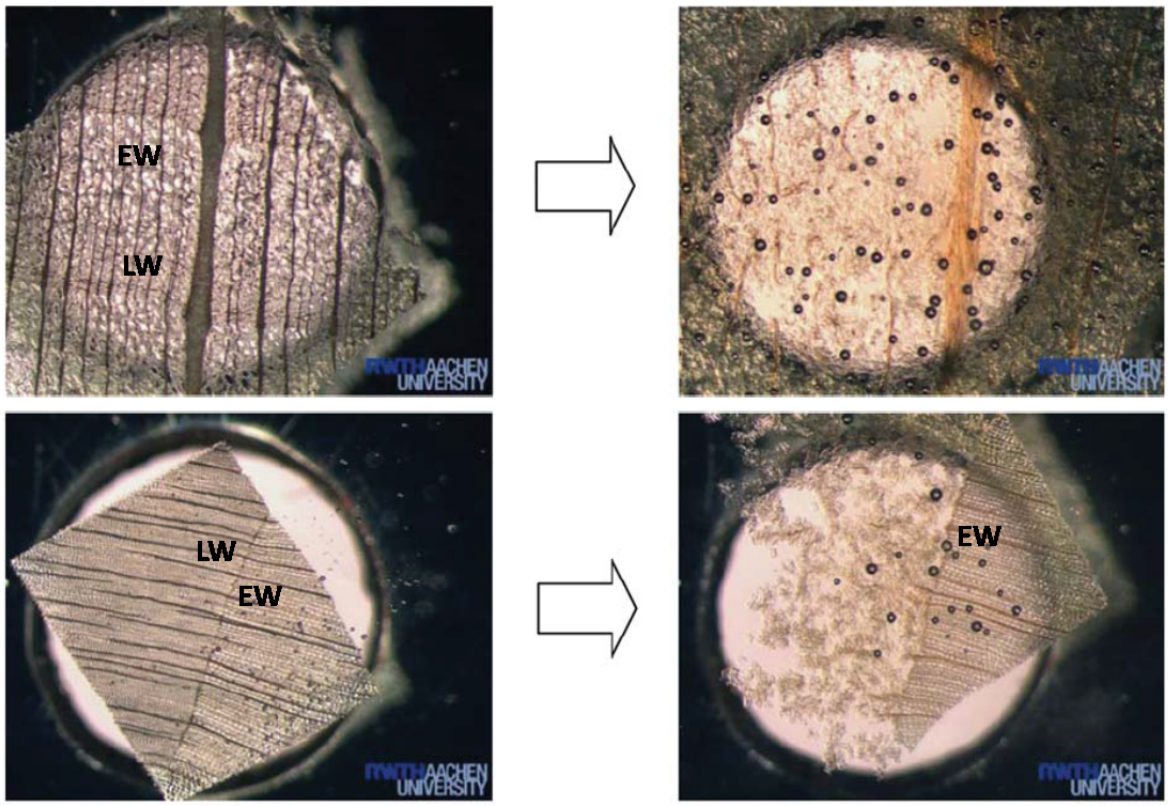

Figure 4.18. Cross-sections (60µm) of beech on top and of spruce below. The pictures show the tissue before (left) and after EMIMAc treatment (right) for 20 min. The disintegration of beech is clearly visible. In spruce, the earlywood (EW) is recalcitrant to disintegration whereas latewood disintegrates completely (115°C; bubbles on the right likely due to accumulation of volatiles below the cover slide; pictures from Viell and Marquardt (2011)).

The cuttings are exposed to EMIMAc at 115°C while being observed microscopically. After 20 minutes, the tissue of beech has completely lost its structure and only the darker ray cells give some orientation. With spruce, a similar process can be observed though restricted to latewood. After swelling of the cutting, the cell fragments of the latewood disintegrate, while the wide-lumened earlywood remains intact and does not show further change. At the end of the experiment, the earlywood is completely free of latewood cells, which have all been separated.

These results imply that the beech chips are completely disintegrated into individual fibers. To prove the existence of single cells after treatment with EMIMAc, SEM pictures of the disintegrated beech wood are shown in Figure 4.19. The background of the image is strewn with cells of approximately 10 µm in diameter that can be

attributed to fibers of the former beech tissue (cf. 2.1.3). Additionally, a few larger cells can be seen. The magnification shows a large lumen and a cross-section of nearly 80 µm, which identifies a vessel cell. It exhibits an intact surface and a couple of simple pits for intercellular fluid exchange. These pits measuring 3.5–7 µm in diameter are likely the former interconnections to radial ray parenchyma cells (cf. Ohtani & Ishaya, 1973). The pits do not show any signs of the original membrane structure (cf. Jayme & Azzola, 1965), so that the primary wall is obviously separated from the cell wall during disintegration.

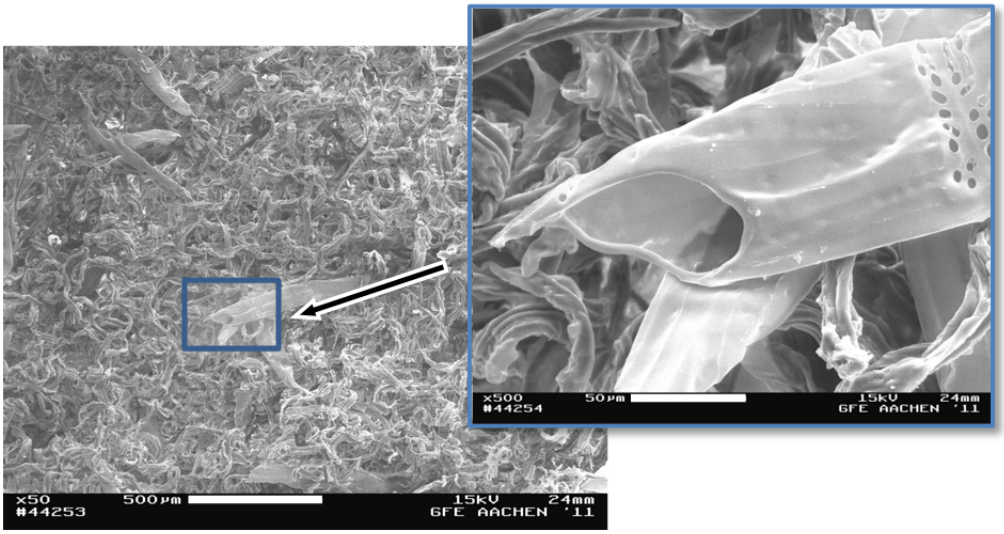

Figure 4.19. SEM pictures of the disintegrated cells of beech chips after 1.5 h in EMIMAc. The vessel cell is shown in the excerpt at higher magnification (115°C, 5 wt % beech, 5 wt % water in IL, 500 rpm, washed with acetone/water 1:1 (v/v) dried at 105°C; the scale bar corresponds to 500 and 50 µm, respectively.).

It can be safely concluded that the dense tissue of the native wood is disintegrated into individual fibers during treatment with EMIMAc. The disordered structure takes a much larger volume and also creates a larger accessible surface area. An estimation of the increase in the surface area between the initial state as a chip and in the disintegrated material indicates an increase by nearly two orders of magnitude.[1] The

[1] The calculation is based on the comparison of the surface area of a chip (10 × 2 × 1 mm^3) with the surface area of cylindrical cells in the chip (fiber:vessel ratio of 2:1) using a fiber diameter of 10 µm, a vessel diameter of 80 µm, and lengths of 1 and 10 µm, respectively (cf. Section 2.1.3).

surface area is still larger by an order of magnitude in comparison to small particles of 0.1–0.5 mm.

These effects of EMIMAc on the ultrastructure of wood give a possible explanation of the peculiarities observed in the dissolution performance. With beech, the treatment not only involves dissolution of a given particle but also involves disintegration to break down the wood structure in the case of EMIMAc. The accessible surface area is therefore determined by the efficiency of disintegration and the size of the wood cells. The rather uniform disintegration of beech wood leads simply to an enhanced dissolution that follows pseudo first-order kinetics as shown in Figure 4.12.

In contrast, the processing of spruce results in disintegrated latewood tracheids and the residual compact earlywood. These distinct fractions will clearly cause more complex kinetics in the case of EMIMAc. The inferior fit of the first-order kinetics to the experimental data of small particles in Figure 4.11 is a first indication that dissolution does not proceed from a uniform regime of particles.

The disintegration was also checked with BMIMCl and DMIMDMP. A similar experiment as in Figure 4.17 reveals that beech chips in BMIMCl showed no changes in the morphology of the chips up to 1.5 h at 115°C (see Figure C.2 Appendix C). In case of spruce, the latewood is disintegrated after longer processing times (cf. Figure 4.13) but the effect is by far not as remarkable as observed in EMIMAc. In agreement with this behavior, Miyafuji & Suzuki (2012) also observed disintegration in the latewood of 15 µm thick slices of softwood but only after 24 h at 120°C. Own experiments also showed that DMIMDMP can also disintegrate spruce at long processing times but the extent is inferior to what is obtained with EMIMAc.

The results reasonably explain the superior dissolution capability of EMIMAc by the largely increased specific surface area due to disintegration that is, within certain limits, independent of the initial particle size. In particular the thin-walled earlywood of softwood is more recalcitrant. Similar processes occur in the other tested ILs but to a much lower degree, which diminish the macroscopic effect of disintegration. The disintegration possibly offers an effective way of processing the natural composite material of wood efficiently.

Pretreatment of wood by disintegration in EMIMAc

The disintegration of wood and subsequent dissolution provides a plausible explanation for the difference observed in ILs and certain wood species. While the application of dissolution under technical conditions was shown to be infeasible, the effect of disintegration could be very interesting for a pretreatment concept because (i) it is much faster than any other process based solely on dissolution and (ii) it results in a large specific surface area. A subsequent heterogeneous process like enzymatic hydrolysis or any other chemo-catalytic conversion could likely benefit from the increased surface area of the solids. The effect of disintegration is therefore explored further.

Prior to the assessment of disintegration as a pretreatment concept, several process parameters need to be determined. First of all, the disintegration has only been studied in neat EMIMAc, whose capabilities are well-known to be susceptible to water. Thus, a key parameter in the process concept is the acceptable concentration of water in EMIMAc for disintegration. Second, the pretreatment should enable high yield processing. In this case, the disintegration has to be operated at low losses of carbohydrates into the IL. Hence, the dissolution needs to be reinvestigated at shorter pretreatment times. The investigations are supported by compositional and spectroscopic analyses and the results are again compared to Kamlet-Taft parameters.

Similar to the dissolution of cellulose (cf. Section 4.1.1), the maximum water content to disintegrate beech wood is effectively determined in experiments with mixtures of EMIMAc and water. Figure 4.20 (top row) shows the solid residue after pretreatment of beech chips in EMIMAc/water mixtures with the indicated water content.

Concentrated EMIMAc easily achieves the disintegration of beech chips as already demonstrated in Figure 4.17, which is therefore not shown again. At 2.9 wt % of water, the material looks similar, so the process is obviously not affected by small amounts of water. At 8 wt % of water, however, the material is only partly disintegrated and some particles still resemble the morphology of the original beech chips. This impression is strengthened when the water content is further increased.

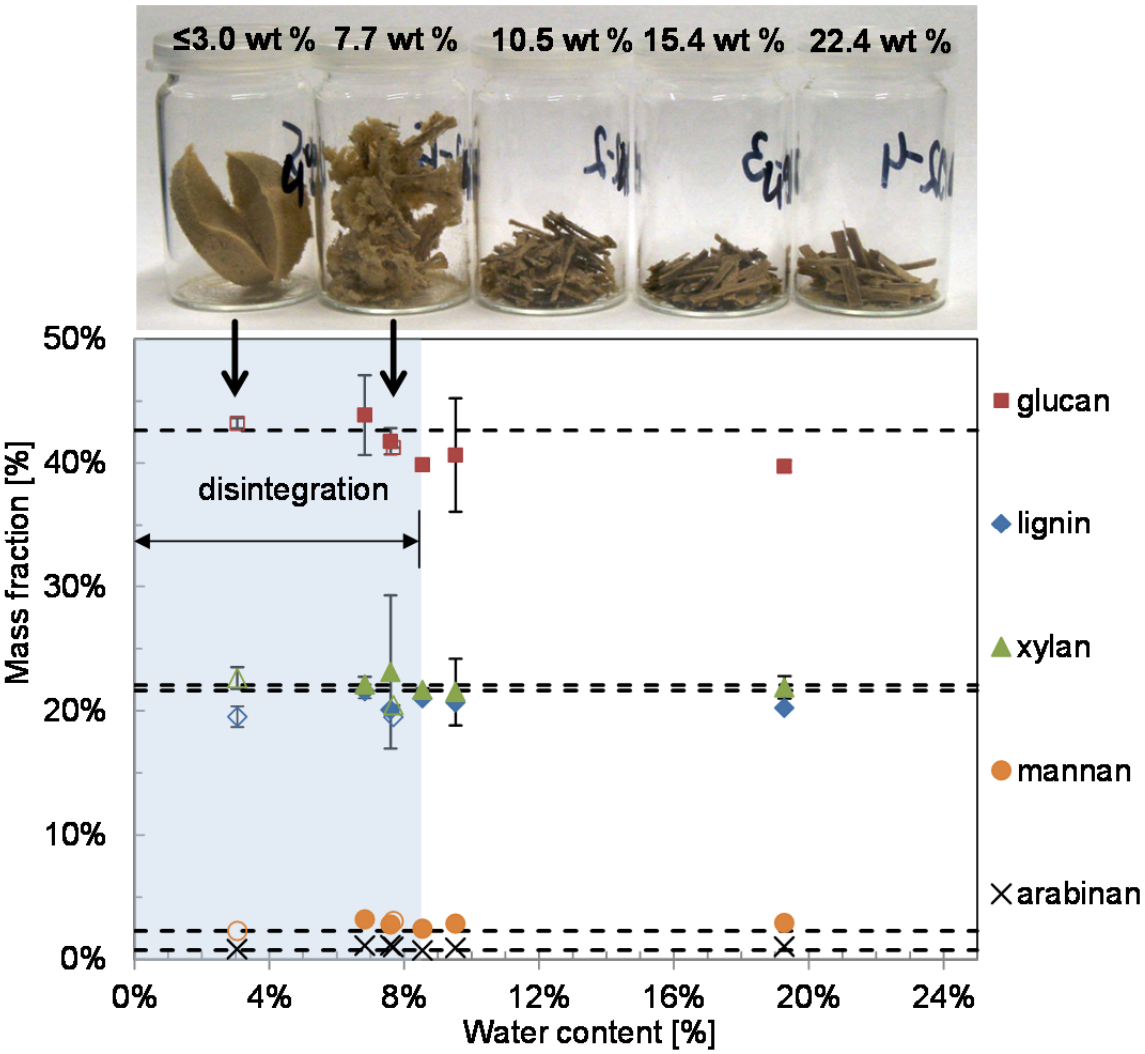

Figure 4.20. The effect of water on the disintegration of beech for 1.5 h at 115°C in EMIMAc (top) and the compositional change of the residue (data below). The dashed lines show the composition of native beech in the order of appearance in the legend. The composition of the depicted material corresponds to open symbols; solid symbols refer to a treatment for 2 h (washed with acetone/water 1:1 (v/v)).

At 13.3 wt % and higher, there is hardly any change in comparison with the original chips (cf. Figure 3.1). The precise water content, up to which disintegration of beech in EMIMAc takes place, was determined in another set of experiments to be 8–9 wt % of water (cf. Appendix C). Hence, the critical water content for disintegration is defined by 8.5 wt %. The fact that the IL does not need to be completely dry for an efficient disintegration facilitates an application in a technical concept.

The composition of the wood treated at different water contents in EMIMAc is also shown in Figure 4.20. Dashed lines depict the initial composition of the native beech wood chip from Table 3.2. As the chromatograms showed a spurious baseline effect that leads to erroneous fractions of galactan and rhamnan, the corresponding fraction was not evaluated in this analysis. The error bars of the points in Figure 4.20 show the range given by the replicate measurements; the difference is, however, not larger than the symbols in most cases. The analysis was carried out with samples treated for 1.5 h (open symbols) and 2 h (solid symbols).

In general, the treatment of beech with EMIMAc/water mixtures seems to result in a certain change of the composition. At high water contents, the fraction of arabinan, mannan and xylan is equal to the original composition. The lignin content and the glucan is, however, slightly less than what is detected in native beech. Thus, despite macroscopic integrity of the wood chip, the EMIMAc/water mixture seems to have a small influence on the wood composition.

In mixtures of higher water content, the data points show in general a small increase in the mass fractions of cellulose and mannan at the determined water content of disintegration. Despite a considerable error, the xylan and lignin content stays the same with the latter being always approximately one percent below the original value. The data points obtained after 1.5 h show no considerable deviation from the trend observed with the samples after 2 h.

The effect of reduced cellulose content could have different origins. First, it could be due to an actual extraction of cellulose. The experiments in Section 4.1.1 showed that Avicel does not dissolve at the tested water content (20.1 wt % of water). Together with the observation that it is similarly reduced at 9 and 10 wt % of water, this seems rather unlikely. A second option would be an amount of EMIMAc that has overcome the washing and is thus part of the probed wood sample. The residual mass would be undetected in the analysis and virtually decrease the fraction of the individual components. As all values would be affected, an unknown mass of residual IL seems also unlikely.

A third possibility would be a better accessibility of the cellulose fraction in the analytical hydrolysis. Since the other fractions show rather constant values, only the cellulose increases at the upper critical concentration of water for disintegration in EMIMAc. A plausible explanation is therefore that the intact wood chips have been hydrolyzed slightly less in the analytical hydrolysis despite the manual comminution.

The disintegration then effectively increases the accessible surface area and likely also the yield in the wood component analysis.

Hence, the data indicate a negligible change in the fractions of wood components during disintegration except a small decrease in lignin at all studied water concentrations. A high yield of main components is therefore envisioned in a conversion of the solid residue after disintegration. The total recovered solid fraction after treatment is thus investigated next. Furthermore, the lignin reduction might be a possible parameter to tune the disintegration since it is also regarded as one main inhibitor in enzymatic hydrolysis (Mosier et al., 2005; Li et al., 2013).

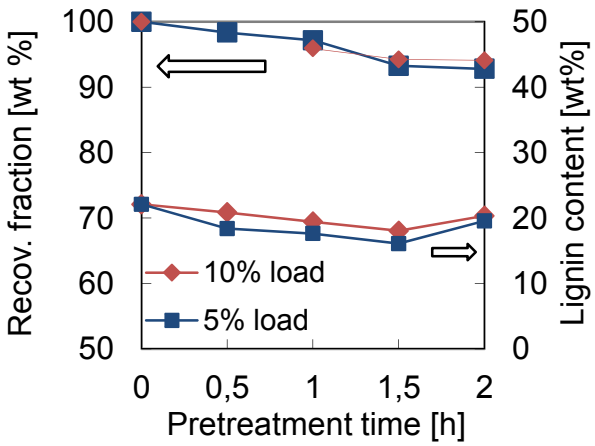

Figure 4.21. Recovered mass fraction (left ordinate) and its lignin content (right ordinate) after short-time pretreatment of beech chips in neat EMIMAc (115°C, washed/precipitated with acetone/water, 1:1 v/v) for two wood loads (Viell et al., 2013a).

The recovered solids relative to the initial dry mass and the lignin content with progressing disintegration up to 2 h was studied in Figure 4.21 (Viell et al., 2013a). The study utilized two wood loads per unit mass of neat EMIMAc. Both the recovered fraction and the lignin content in the solid are a function of pretreatment time. The recovered material decreases continuously with pretreatment time, reaching a value of 93 wt % after 2 h. No effect of the load was detected in the recovered fraction.

In contrast, the delignification is slightly more effective at 5 wt % load compared to 10 wt % load. Interestingly, the lignin concentration of the solid increases again at 2 h

compared to 1.5 h of pretreatment time. The effect was confirmed by repeated measurements (not shown for brevity).

The decrease in the recovered mass implies that certain compounds are removed that are not determined in this compositional analysis. The original material showed a fraction of inorganic salts and extractives of 2.9 wt % in total with an unknown amount of uronic acids estimated to be approximately 5 wt % (Section 3.3). A detailed analysis of ash, extracts and acids could not be carried out with the pretreated wood due to the small amount of mass.

Nevertheless, Figure 4.21 shows a recovered fraction of 93.6 wt %, it can be hypothesized that charged molecules and acidic groups are removed during disintegration. The observation of increasing lignin, however, might also be related to erroneous detection of condensed molecules as Klason lignin (cf. Hu et al., 2012). At this point, an optimal pretreatment time of 1.5 h is chosen in order to reach a high yield of pretreated material at minimum lignin content.

Further insight into the small changes of the composition during disintegration can be gained by Raman spectroscopy. It was applied to four samples from Figure 4.20 to reveal qualitative changes during disintegration. The recorded spectra are shown in Figure 4.22 in the fingerprint region in comparison with a spectrum of the native beech wood.

An obvious difference in all spectra that were subject to EMIMAc treatment is the diminished intensity at around 1744 cm^{-1}. The corresponding vibration is assigned to carboxyl groups (Colthup et al., 1990) and is caused by the acetylated hemicellulose of beech wood. The other vibrations can be mostly assigned to the molecular structure of lignin and carbohydrates. The first strong band next to the acetyl vibration can be found at 1600 cm^{-1}. It is due to the C-C/C=C stretching mode of the aromatic ring of lignin (Takayama et al., 1997) and usually correlates well with the overall lignin content (Agarwal et al., 2003).

The other peaks are similar to those observed in the spectrum of cellulose (Figure 4.3) but distinct contributions from lignin can be identified. The different methoxy groups of syringyl and guaiacyl units (cf. Figure 2.5) can be also differentiated in the spectrum. The C-O vibrations of syringyl and guaiacyl are found at 1333 and 1272 cm^{-1}, respectively (Larsen & Barsberg, 2010). The modes are overlapped with contributions of celluloses (Wiley & Atalla, 1987) and hemicelluloses – mainly xylan –

which has strong contributions at 1090, 1121, 1379, and 1462 cm^{-1} (Kacuráková et al., 1999). The vibration band at 1121 cm^{-1} is in particular a strong one in the spectrum of hemicelluloses and has been assigned to the glycosidic link.

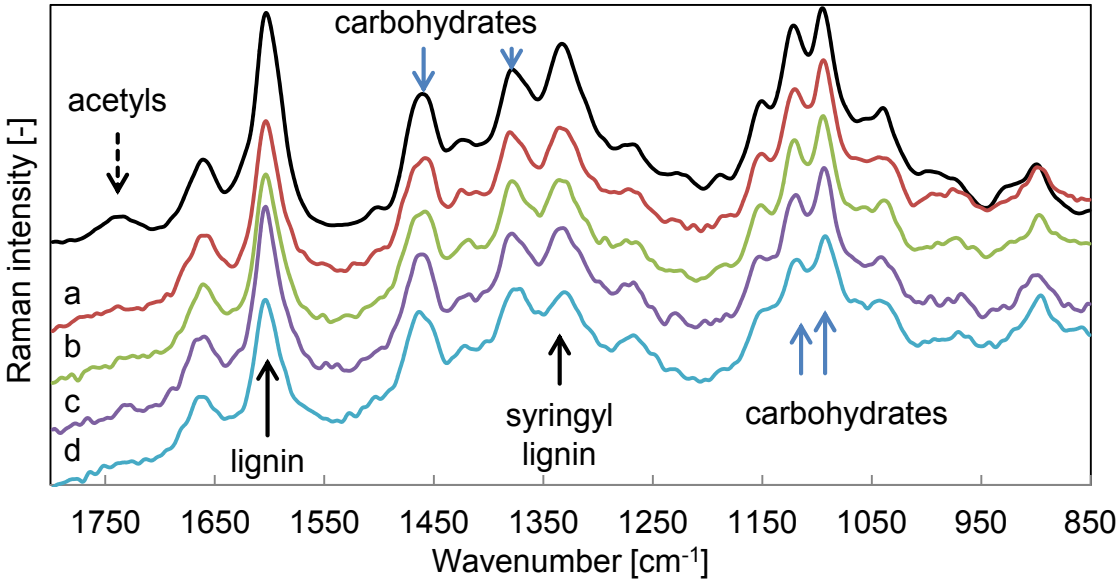

Figure 4.22. Raman spectra of native beech (top) in comparison to samples treated with EMIMAc at decreasing water content (a: 17.5 wt %, b: 13.3 wt %, c: 8.0 wt %, d: 2.9 wt %) in comparison to the spectrum of native beech. The arrows mark contributions from carbohydrates, acetyl groups and lignin, where a significant decrease can be observed (beech chips, disintegrated at 115°C for 1.5 h, 500 rpm, washed with acetone/water 1:1 (v/v), 100 mW laser power, vector standardized, no baseline correction).

The comparison to the spectra of the wood chips after pretreatment also reveals small changes induced by the IL. The missing vibration of the acetyl groups confirms the deacetylation of the hemicelluloses. The process seems to be independent of the water content.

The deacetylation is characteristic for acidic or basic conditions, which agrees to the alkaline conditions in EMIMAc (cf. Figure 4.5) and has been observed in literature quite often. Samples of birch showed no signals of acetylated xylan after 16 h in EMIMAc at 120°C (Wen et al., 2013). Labbe et al. (2012) showed that the deacetylation of xylan can take place in either EMIMAc, BMIMAc, or BMIMCl even at

a temperature of 60°C but only 52% of the acetyl groups were cleaved after 72 h of pretreatment. In general, the assumption of alkaline pretreatment conditions being one driver for the pretreatment is supported by the work of Zanuttini et al. (2005). They report the deacetylation to happen within a few minutes and also observe swelling and higher accessibility afterwards. The effect of acetyl groups on enzymatic hydrolysis is however a bit controversial. While Labbé et al. (2012) were able to correlate the deacetylation in ILs with a higher digestibility by enzymes, the opposite is reported after lime pretreatment (Chang & Holtzapple, 2000).

Further analysis reveals that the lignin peak at 1600 cm^{-1} decreases more and more the less water is present in EMIMAc. The peak at 1465 cm^{-1} changes its shape and seems to shift to 1465 cm^{-1} but at only a small decease in intensity. The change in the peak position and shape indicates a change in crystallinity. A noticeable change in the CH_2OH vibration at the C(6) atom of cellulose at 1465 cm^{-1} supports the presence of less crystalline cellulose Iβ. The small variations in the carbohydrate peaks observed at and 1379, 1121 and 1090 cm^{-1} can be explained by this as well.

The most obvious change in addition to the lignin peak at 1600 cm^{-1} is detected at 1333 cm^{-1}. Its intensity decreases clearly in comparison to the adjacent peak at 1379 cm^{-1} and indicates the reduction of mainly syringyl. The effect seems to enhance the lower the water content. The treatment with EMIMAc therefore actually removes syringyl lignin from wood.

Other pretreatments like dilute acid or Kraft pulping decrease the ratio of syringyl:guaiacyl lignin (Varanasi et al., 2012). In contrast, several authors have reported a rather selective guaiacyl extraction in EMIMAc after pretreatment for 3–16 h at 110–120 °C in EMIMAc (Cetinkol et al., 2010; Wen et al., 2013; Varanasi et al., 2012). At first sight, one would expect a change in the guaiacyl lignin as opposed to the results presented in Figure 4.22. A closer look at the results of Varanasi et al. (2012) reveals an initial decrease of the syringyl content after 1.5 h at 120°C before guaiacyl is also extracted. This is in good agreement with the results obtained here. A short pretreatment in EMIMAc thus leads to deacetylation of hemicelluloses and a decrease in syringyl lignin. Wen et al. (2013) speculated that a preferential extraction of lignin from the middle lamella containing fewer methoxy groups might lead to this observation.

The small variations in vibrational modes of cellulose have already indicated a change in the crystalline cellulose, which would be very desirable for efficient

hydrolysis of cellulose into sugars. The seminal work on wood dissolution by Kilpeläinen et al. (2007) also reported that the recovered wood is obtained in an amorphous state after 8h in Cl-based ILs at 110°C. The state of the cellulose in the disintegrated beech chips is therefore assessed by XRD.

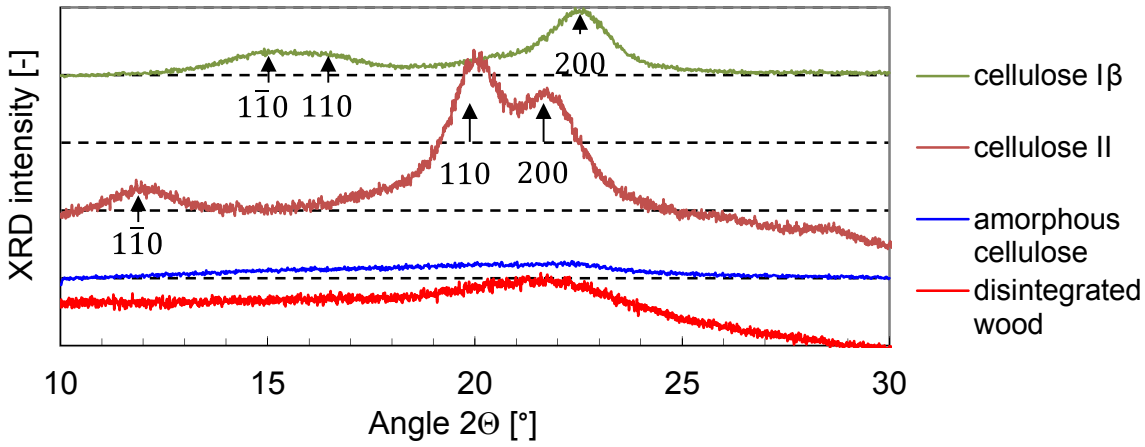

Figure 4.23. XRD diffractograms of disintegrated wood in comparison with different cellulose polymorphs. The disintegrated wood does not show the sharp peaks of crystalline cellulose Iβ (unscaled spectra have been shifted vertically).

The diffractograms of cellulose Iβ and cellulose II in Figure 4.23 show the features of their different crystal lattices. Cellulose Iβ has strong reflections at $2\theta = 15°$ and $2\theta = 22.5°$, which correspond to the crystal planes $1\bar{1}0$ and 200, respectively (cf. Figure 4.23 and Fink et al. (1995)). The 110 plane can be identified as a weak shoulder at approximately 16.5°. In cellulose II, the tighter packing of the cellulose chains results in a different crystal unit cell that causes the 110 plane to shift to 19.8°, while the $1\bar{1}0$ plane is found at 11.8°. The strong reflection at the 200 plane is diminished and slightly shifted to $2\theta = 21.7°$. Amorphous cellulose does not show any distinct reflections as expected without a crystalline structure.

The features of cellulose Iβ in native wood (cf. Andersson et al. (2003) for representative spectrum) are not observed in the signal of the disintegrated wood (Figure 4.23, bottom). The broad signal obtained from the disintegrated wood does not show a clear contribution of cellulose Iβ and does also not match the peaks of cellulose II. A rather amorphous state is thus obviously the result of disintegration, which is in contrast to the recrystallization observed with pure cellulose (Section

4.1.1). It can be deduced that the dissolving capabilities of the IL can disrupt the hydrogen bonding network during disintegration of the wood to form the amorphous cellulose; the recrystallization as observed with pure cellulose in Section 4.1.1 then might be limited due to the presence of hemicelluloses and lignin.

Several other authors also observed the decreasing crystallinity of wood in ILs after the report of Kilpeläinen et al. (2007). A broad XRD peak as in Figure 4.23 was also described by Torr et al. (2012) as a result of the treatment in EMIMAc for 3 h at 120°C. The authors further suggested the pretreatment to convert the organized microfibrils into a disordered structure in the cell wall. Lee et al. (2009) reported a similar decrease in the crystallinity of maple wood after 1.5 h in EMIMAc even at 90°C.

Moreover, the addition of 10 wt % water to EMIMAc no longer results in a change in the crystallinity of maple wood (Doherty et al., 2010). This water concentration is just above the upper critical water concentration for disintegration and it can be assumed that there is a relation between macroscopic disintegration of fibers and cellulose decrystallization on the molecular level. In view of the cellulose conversion by enzymatic hydrolysis, the coinciding decrystallization and disintegration could work out as a favorable pretreatment step because the pretreated material is likely to be readily digested.

The depicted processes again raise the question whether they can be described by a solubility parameter. Doherty et al. (2010) suggested that the pretreatment efficiency with EMIMAc in the presence of water can be “excellently” predicted by the basicity. In order to test this hypothesis, the basicity at different water contents in IL/water mixtures from Figure 4.6 is compared with the regime of beech disintegration and cellulose dissolution in Figure 4.24. In case of EMIMAc, the dissolution of cellulose was accomplished at a value of $\beta = 0.86$ or 0.72 mol % of water. The disintegration of wood is observed, however, only below 8.5 wt % of water (47 mol % of water), where $\beta = 0.95$. If the deterministic value were β, the wood would have been disintegrated at much larger water contents as well.

The curves in Figure 4.24 can also be used to assess the effect of DMIMDMP and BMIMCl. In fact, spruce is disintegrated in the former IL while the experiments with BMIMCl only showed disintegration of the latewood of spruce (cf. Figure B**.** and Miyafuji et al. (2009)). Neither IL is capable of disintegrating beech. Such a behavior is not predicted by the basicity. If disintegration were due to the basicity in general, at

least DMIMDMP would readily disintegrate beech wood up to a water content of approximately 0.5 mol %. Calculation of the net basicity $(\beta - \alpha)$ also does not result in more meaningful correlations (cf. Figure B.7 in Appendix B).

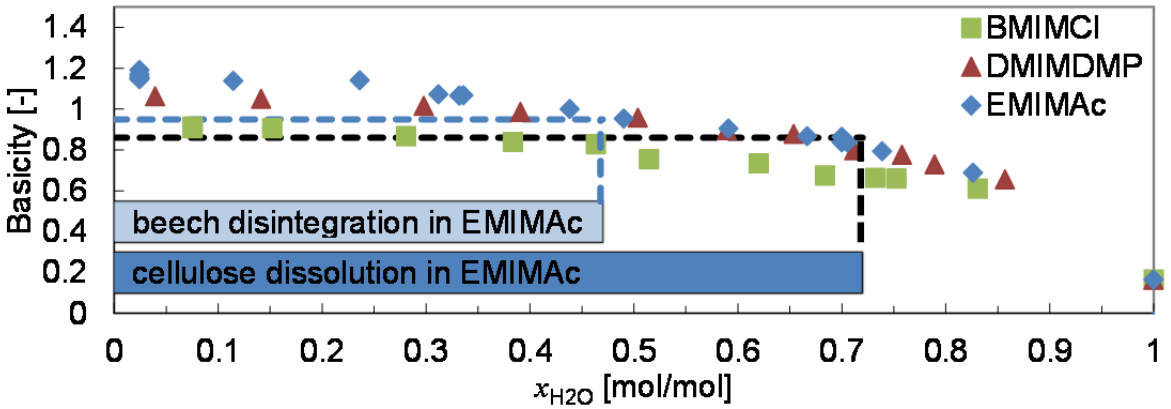

Figure 4.24. The Kamlet-Taft basicity in mixtures with water to compare the disintegration with the change in polar interaction and cellulose solubility, depicted as horizontal bars. The dashed lines indicate the critical basicity of EMIMAc/H_2O solutions to disintegrate beech and dissolve cellulose.

Hence, the prediction of disintegration with the basicity cannot be established. At this point, the observed effects can only be described by a qualitative hypothesis. EMIMAc is the most water-tolerant IL of this study and therefore interacts with cellulose very well. The introduction of ions in the hydrogen bonding network results in a swelling, which largely takes place in the secondary wall of the wood cell wall. A small removal of syringyl lignin facilitates the swelling, but the ultrastructure of the cell limits the mass transport such that neither the cellulose chains may be transported and dissolved in the bulk liquid nor they may recrystallize into cellulose II. The mechanical pressure due to swelling and a weakening of the compound middle lamella thus likely result in the disintegration. The higher pressure in the dense latewood due to swelling plausibly explains the recalcitrance of earlywood against swelling.

The weakening of the compound middle lamella might involve reactive mechanisms that cannot be described by solvation models and solubility parameters. The recently discovered formation of carbenes in basic ILs might play a role in that context

(Holloczki et al., 2010; Magill et al., 2004; Rodriguez et al., 2011; Brehm et al., 2012). The recent studies reporting the cleavage of β-O-4 linkages of lignin also point towards a reactive behavior of the ILs (George et al., 2011; Torr et al., 2012). Clearly, these hypothetical mechanisms need to be proven but provide a first basis to screen ionic solvent systems for the pretreatment of biomass.

4.3 Combined IL-pretreatment and hydrolysis

The efficiency of a short pretreatment with EMIMAc is investigated next in combination with enzymatic hydrolysis following the structure shown in Figure 4.25. Beech wood chips are disintegrated during pretreatment into fibers, which will result in a small amount of extract, namely, everything that is dissolved and not recovered by precipitation during washing. The subsequent hydrolysis is then carried out under aqueous conditions. The resulting product is a sugar stream in water and the non-depolymerized material constituting a solid residue mostly made of lignin.

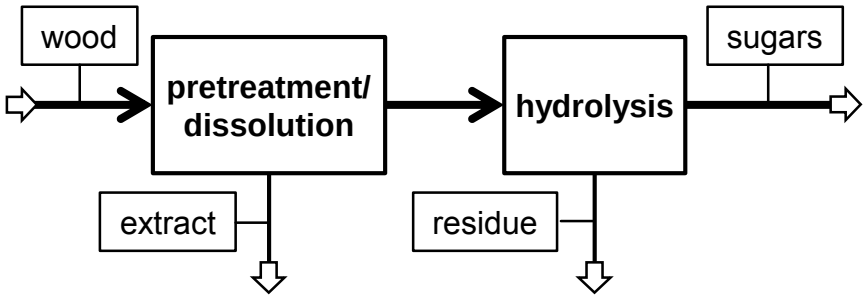

Figure 4.25. Aggregated block flow diagram of a general pretreatment and hydrolysis concept for the chemical valorization of biomass. The solvent streams and other utilities have been omitted for clarity.

4.3.1 Mass balances of pretreatment and hydrolysis

The objective of this subsection is to determine the yield of sugars and to infer mass balances of the combined process for a conceptual design and a process evaluation in the next chapter. This requires larger-scale experiments to yield higher gravimetric precision, and to allow for a more detailed analysis of the saccharification products. The investigations were carried out in collaboration with Helene Wulfhorst from

Biochemical Engineering/Enzyme Process Technology and Thomas Schmidt from the Institute of Biology VII at RWTH Aachen University (Viell et al., 2013a).

The combined experiment utilizes the parameters determined in the previous sections. As the lignin content is known to limit enzymatic hydrolysis, a load of 5 wt % is chosen during pretreatment. Ethanol was used for washing to possibly precipitate any dissolved carbohydrates. The systematic investigation of pretreatment and hydrolysis (Viell et al., 2013a) lead to efficient combination of the pretreatment for 1.5 h at 115°C with a hydrolysis for 5 h at 50°C as a process concept. It was carried out at larger scale in order to determine mass balances.

The compositions of the beech wood, intermediate and final products determined in larger scale experiments are given in a block flow diagram of the combined pretreatment and enzymatic hydrolysis process (Figure 4.26). The mass balance of the pretreatment reveals that only a few percent of the wood chips are dissolved during short pretreatment in EMIMAc. 100 g of beech chips on a dry basis result in 88 g of disintegrated material. Comparison of the composition of the disintegrated and the original wood reveals a near-quantitative recovery of cellulose and most of the xylan, while the lignin content is slightly reduced. A removal of 4 g in absolute mass of lignin can be calculated, which is well in agreement with the delignification observed in Figure 4.21.

Certain dissolved components of the wood were therefore lost as extract in the washing step. The washing with excess ethanol (EtOH) resulted in the precipitation of a solid, which is referred to as EtOH ppt. in Figure 4.26. A subsequent solvent exchange to water yielded a second solid (cf. H_2O ppt. in Figure 4.26). The analysis by Viell et al. (2013a) showed that EtOH ppt. is largely composed of carbohydrates, while H_2O ppt. is composed of lignin and extractives. Both solid phases add up to an extract of 6 g and imply that 6 wt % of the wood are purged with the washing liquor. The lost mass likely consists of non-structural components, acids from hemicellulose deacetylation and lignin. A proof of this hypothesis could have been realized easily in volatile solvents but the non-volatile ionic liquid, however, impedes concentration and analysis.

Nevertheless, the preservation of the complete amount of cellulose and xylan in the disintegrated beech is clearly promising for high yield conversion of the disintegrated wood to soluble sugars. A hydrolysis of 5 h yields 67 g of a water-soluble product. The analysis confirms that the product mainly contains reducing sugars (74 wt %).

Individual sugars, i.e., glucose, xylose, cellobiose and mannose, are detected with a content of 59 wt % altogether. The cellulose contained in the native beech chips is converted to glucose and cellobiose at a fraction of 69 wt %.

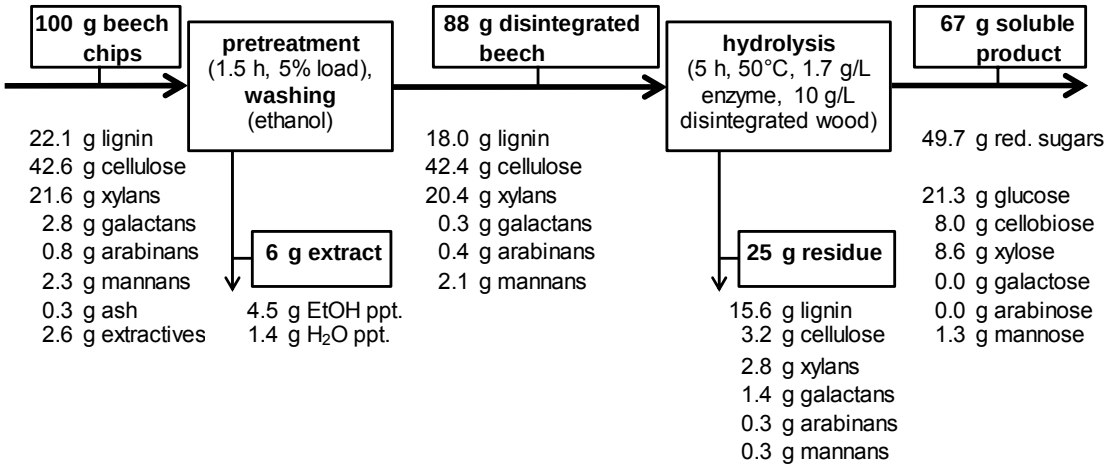

Figure 4.26. Block flow diagram of the combined pretreatment and enzymatic hydrolysis process to convert beech chips to sugars, including mass and composition data (based on 100g dry wood, ppt. = precipitate, Viell et al. (2013a)).

The (solid) residue left after hydrolysis contains the majority of the lignin from the original wood. In addition, it contains some cellulose, xylans, arabinans and mannans, in decreasing order. In particular, the content of galactans in the solid residue seems to be slightly overestimated, which could be due to an altered peak shape in the chromatogram. A small fraction of lignin (2.4 g) seems to be lost during hydrolysis, which is however in the order of the total error of approximately 5 wt % of the mass balance of hydrolysis.

Additional experiments were performed to explore the sensitivity of the sugar yields to the mutual effects of the residence time in pretreatment and in enzymatic hydrolysis (experimental results can be found in Viell et al. (2013a)). Basically, a hydrolysis time of 72 h after 1.5 h of pretreatment in EMIMAc results in a small increase in the yield of soluble solids (+2 g) with a slightly higher content of reducing sugars. The most remarkable difference observed after prolonged hydrolysis is a significant increase in glucose and cellobiose concentration, which corresponds to a cellulose conversion of 88 wt %.

Longer pretreatment with EMIMAc for 2 h increases the mass extracted during pretreatment and thus slightly decreases the mass of disintegrated wood. While cellulose and xylan are still recovered near-quantitatively in the disintegrated beech, the mass of the carbohydrate-rich ethanol precipitate is increased, which indicates that hemicelluloses, except xylans, are dissolved during pretreatment and precipitate with extracted lignin.

The hydrolyzed beech chips disintegrated by a pretreatment for 2 h lead to similar yields compared to those obtained after 1.5 h. The amount of soluble product is larger (73 g), but the mass of soluble sugars stays constant. The mass of the solid residue after pretreatment for 2 h in EMIMAc is equal to half the mass derived from the experiment with a pretreatment time of 1.5 h, although it retains a similar lignin content, which means that significantly less lignin was recovered from the sample pretreated for 2 h. A prolonged enzymatic hydrolysis time of 72 h increases the yields of reducing sugars and glucose although the mass of total soluble sugars does not vary considerably compared to a pretreatment for 1.5 h.

The results demonstrate that prolonged hydrolysis results in slightly more carbohydrates and in particular higher amounts of glucose in the soluble product. The conversion of cellulose into glucose and cellobiose is calculated as 68 wt % or 88 wt % after 5 h or 72 h of enzymatic hydrolysis respectively. This is similar to results from experiments under similar conditions (Lee et al., 2009). A pretreatment time of 3 h or more also results in similar yields from cellulose (cf. Xu et al., 2012; Torr et al., 2012).

The suggested process conditions in this work clearly achieve these yields at shorter overall process times. For comparison, an untreated spruce wood results in a yield of 10 wt % of sugars after 72 h of hydrolysis. After an Organosolv pretreatment, the enzymatic hydrolysis of cellulose still requires 48 h to gain 90 wt % conversion (Zhao et al., 2009) and 72h are a good estimate for a technical design (Humbird et al., 2011). This is due to the higher crystallinity as the amorphous fractions of cellulose are also reduced during Organosolv pretreatment.

Clearly, a considerable amount of carbohydrate is present as oligosaccharides after hydrolysis that are not detected using HPLC. A conservative estimation would be based on the yield of reducing sugars, which amounts to approximately 50 wt %, but the analysis likely underestimates the carbohydrate yield being calibrated with monomeric sugars (cf. Viell et al., 2013a). The upper bound can be assessed based

on the overall carbohydrate balance and calculates a maximum overall yield from beech wood of 65 wt % for the suggested combined pretreatment and hydrolysis. In any case, the suggested process concept achieves an improvement by an order of magnitude in yield and residence time during hydrolysis in comparison to other pretreatment concepts without decrystallization of the cellulose (cf. Section 2.4).

4.3.2 Concept of wood pretreatment based on ILs

The first important conclusion of this chapter is that the process concepts suggested in literature relying on the simple dissolution of wood, are infeasible. A complete dissolution of wood cannot be confirmed and the fractionation by precipitation is not quantitative. A considerable loss, however, does not seem acceptable in biomass utilization in view of the desired carbon efficiency and the required economic operations.

The second conclusion is that the individual ion combinations in the ILs result in different physico-chemical effects as evident by the differences observed in dissolution and disintegration. The systematic analysis revealed remarkable differences in the dissolution performance between the species of wood in the different ILs. DMIMDMP shows an inferior performance in wood dissolution but exhibits a shift of the dissociation equilibrium upon the addition of water towards an acid. BMIMCl dissolves preferentially cellulose. This process is very selective in case of spruce and likely due to the more acidic-resistant guaiacyl lignin. However, the process is clearly limited by mass transport resistances of the wooden ultrastructure.

In contrast, a pronounced disintegration of wood into fibers is unveiled in EMIMAc. This phenomenon is much faster than the dissolution of the main components and creates a large specific surface area, a feature that makes this IL very promising for a pretreatment process. The thorough analysis showed that the disintegration involves a reduction in the crystallinity of wood and a removal of syringyl lignin, which implies a change in the lignin structure as well. Concerning the hemicellulose fraction, the results suggest that only very small amounts are extracted during short-time pretreatment and preserve xylan nearly completely. Hence, the disintegration of beech wood in EMIMAc fulfills the requirements for a successful pretreatment without major removal of constituents and including the challenging decrystallization of the cellulose.

Consequently, this effect was exploited systematically as a pretreatment concept to determine the most important process parameters and mechanisms. The most beneficial pair of raw material and IL is the combination of beech wood and EMIMAc. Beech wood chips are disintegrated completely within 1.5 h at 115°C. The effect has been proven with particles up to 10 mm length and up to an upper critical water content of 8.5 wt % in the EMIMAc/H_2O mixture used for pretreatment.

The observed effects cannot be described comprehensively by the empirical Kamlet-Taft parameters but require more fundamental investigation to identify the molecular mechanism. The analysis implies that the strong interaction of IL with cellulose, which would have been dissolved when no hemicellulose and lignin were present, is likely the reason for the pronounced swelling in the confined structure of the cell wall. In combination with the cleavage and extraction of lignin, the mechanical pressure induced by swelling is likely the main mechanism of disintegration. The extraction of charged moieties is possibly also important in this process.

This hypothesis is also in line with the macroscopically observed differences between the wood species. While only the dense latewood in spruce is disintegrated readily, the open-lumened earlywood might simply result in too little force to liberate the fibers. The effects of selective lignin extraction and weakening of the compound middle lamella are also consistent with the alkaline conditions in EMIMAc. The implication of such reactivity in an ionic solvent in combination with the decrystallization of cellulose offers a possible means to design tailored solvent systems to the feedstock for maximum pretreatment effectiveness.

The developed pretreatment concept is eventually proven in a large scale experiment with beech chips in combination with enzymatic hydrolysis. After 1.5 h of pretreatment and disintegration at 115°C at a load of 5 wt %, the washed fibers are hydrolyzed within 5 h to reach up to 65 wt % of sugars. The effectiveness of hydrolysis is likely enhanced by the integrated pretreatment of recalcitrant, crystalline lignocellulose into an amorphous material. It is much easier to hydrolyze than the crystalline cellulose obtained with other pretreatment processes like Organosolv pretreatment as reported in literature.

The list of established pretreatment concepts offered in Table 2.3 can therefore be extended by an IL pretreatment concept. The lab-scale experiments show several parameters that could be optimized to enhance the process performance, for instance the described increase of the solids load to 10 wt %. To this end, the

performance has to be analyzed on the process level, which follows in the next chapter. At this point, the successful development of a feasible pretreatment for the conversion of wood into sugars based on an ionic liquid could be achieved. It is demonstrated that the outstanding capability of cellulose dissolution and reactive extraction by a particular reactivity of the ions is key to tailored pretreatment processes utilizing neoteric solvents.

5 Design and analysis of the pretreatment process

This chapter describes the design of a process to evaluate the potential of IL-based processing of wood derived from the process parameters inferred in the previous chapter. The objective is to cover the complete process including pretreatment, solvent recovery, enzymatic hydrolysis, and product purification. The process is simulated by established process simulation software and evaluated in terms of energy demand and cost. The latter is not meant to be a profit and loss statement but to identify economic bottlenecks at a very early stage of development and to show possible improvements in that regard. Similar investigations have been carried out with Organosolv-like processes (Viell et al., 2013b) that are used to benchmark the developed IL-based pretreatment process.

5.1 Modeling of the IL pretreatment process

The developed process flowsheet was set up with Aspen Plus (version 7.2, Aspen Technology, Inc.) to solve the mass and energy balances. The latter requires thermodynamic properties of each compound, which, in contrast to petroleum-based compounds, are scarce in case of biomass components and in particular of ILs. Wooley & Putsche (1996) compiled a database of biofuel components that includes data on biomass constituents. Cellulose, lignin and xylan are modeled as a conventional solid, i.e., they do not take part in the flash calculations and thus only require a heat of formation, density, and heat capacity. Glucose and xylose usually show up in diluted aqueous streams. They are modeled as liquids requiring a vapor pressure, enthalpy of formation, heat of vaporization, heat capacity, density and a critical point. The enthalpy of formation was obtained from experimental data and thus includes the heat of depolymerization in comparison to the macromolecule. Although the data on these liquid sugars are not intended to be used for the pure state, they will serve as a first estimate to isolate the products.

The properties for EMIMAc were taken from recent literature on vapor pressure and enthalpic data (Freire et al., 2011; Strechan et al., 2008; Liu et al., 2010; Shiflett et

al., 2010; Valderrama & Rojas, 2009). The mixture properties of EMIMAc/H_2O were modeled with activity coefficients using the non-random two-liquid (NRTL) equation that was regressed simultaneously to vapor-liquid equilibrium data and heat capacity data of EMIMAc/H_2O mixtures (Römich et al., 2012). The full set of properties and parameters are given in Appendix D.

Utilization of an IL in a process concept should account for a possible degradation of the IL during the process. The usual thermogravimetric analyses imply stability up to 180°C and above (Wendler et al., 2012) but the applied protocols do not cover the assessment of long-term stability (Maton et al., 2013). A beginning decomposition of ILs was detected at a temperature of 120°C (Meine et al., 2010; King et al., 2011). The decomposition was quantified recently by Brandt et al. (2013), with 1 wt % of a decomposed BMIMAc at a temperature of 102°C within 10 h. So far, there has been no mechanistic insight into the decomposition and it should be assumed that the combination of materials with ILs could readily influence the rate. For instance, after the exposition of EMIMAc to stainless steel at 100–130°C for four months, a transalkylation of 40 wt % of the $EMIM^+$ cations was observed (Keil et al., 2012).

EMIMAc is likely to be prone to decomposition and byproduct formation at the envisaged conditions, which has neither been understood nor quantified thoroughly up to now. An upper temperature limit of 120°C is recommended for the utilization of EMIMAc by a major manufacturer (Kupfer, 2012). Own measurements show that despite decomposition products of EMIMAc have been observed after 3 months at 105°C, the IL is still able to disintegrate wood (cf. Figure C.5 in Appendix C).

Decomposition thus might not require quantitative replacement of the lost solvent but has to be checked prior to technical implementation. For the conceptual design of an IL-based pretreatment process in this work it is assumed that decomposition of the solvent and biomass is negligible at a temperature of 115°C, which was set as the maximum processing temperature.

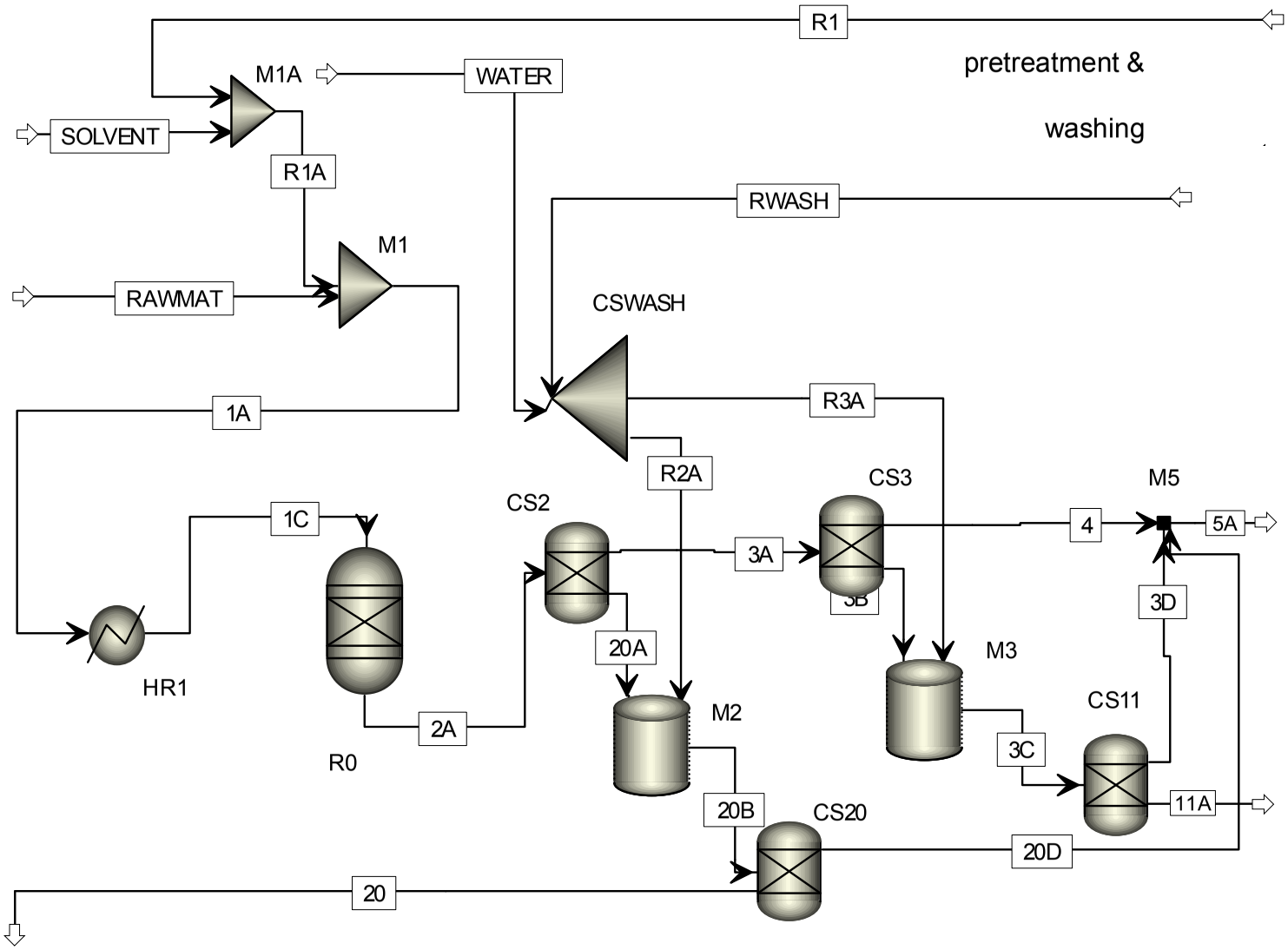

Figure 5.1. Flowsheet of the pretreatment and washing as part of the designed IL pretreatment process. The complete flowsheet of the simulation can be found in Appendix E, Figure E.1.

5.1.1 Process description

The flowsheet is depicted in three parts in Figure 5.1, Figure 5.3 and Figure 5.4; a complete flowsheet is available in Figure E.1 in Appendix E. The modeled process starts with a stream of 6250 $kg_{dry\ biomass}$/h of wood entering the process with stream RAWMAT in Figure 5.1. An exemplary hardwood with a moisture content of 6.6 wt % is utilized, which has a composition of 46 wt % cellulose, 21 wt % lignin, 27 wt % hemicelluloses, and 6 wt % other materials based on dry mass. It is mixed with 215 kg/h of fresh EMIMAc (stream SOLVENT) and with the recycle stream R1 consisting of 68,535 kg/h EMIMAc.

The recycled IL is at a temperature of 115°C, which results in a temperature of 110°C in stream 1A. Therefore, only little thermal energy is required in the heater HR1 to reach the pretreatment temperature of 115°C in the pretreatment reactor R0. In Section 4.2.3, it was shown that a higher load can decrease the yield in laboratory experiments (cf. Viell et al., 2013a). However, it is assumed to be a technological problem that might be overcome by a suitable technical reactor concept. Hence, a solid load of 1:10 (biomass:solvent) is chosen.

While the fresh IL has a water content of 1 wt %, the recycled IL also introduces 4 wt % of water. Altogether, it results in a water content during pretreatment of 4.2 wt %, which is well below the upper critical water content for disintegration of 8.5 wt % (cf. Section 4.2.3). If more moisture were introduced with the raw material into the process, the amount of water in the pretreatment would clearly increase. However, although a freshly logged tree (~60% moisture) would introduce 3750 kg/h of water instead of 412.5 kg/h at 6.6%, the water content in pretreatment would not change considerably due to the large solvent stream of 68,750 kg/h of EMIMAc in stream 1A.

During pretreatment in reactor R0, the wood is disintegrated for 1.5 h and exits the reactor in stream 2A. The subsequent separation unit CS2 realizes a separation of 88 wt % of the wood from the liquid using the yield factors given in Table E.1 in Appendix E. They have been calculated for each compound based on the mass balances determined in Section 4 to reflect the changes in composition during disintegration. The disintegrated wood is then subject to a further washing and separation step to remove residual IL from the solids (M2 and CS20).

Washing is realized according to the concept of displacement washing (Sixta, 2006). This concept is explained in Figure 5.2, which depicts the mass flows of the washing

step as an excerpt from Figure 5.1. The disintegrated wood in stream 20A is washed by the washing liquor (stream R2A), but some of the liquid leaves the washing stage with the washed, disintegrated wood in stream 20. The number of times this liquid is displaced or diluted by the washing liquor is described by the dilution factor (DF) (Sixta, 2006), i.e.,

$$DF = \frac{m_{R2A} - m_{20}^{liquid}}{m_{20A}^{wood}} = \frac{m_{20D} - m_{20A}^{liquid}}{m_{20A}^{wood}}. \quad (5.1)$$

A typical value of DF = 2 is chosen here. As the IL is to be removed in stream 20 after washing, the filtrate (stream 20D) contains the corresponding amount of IL.

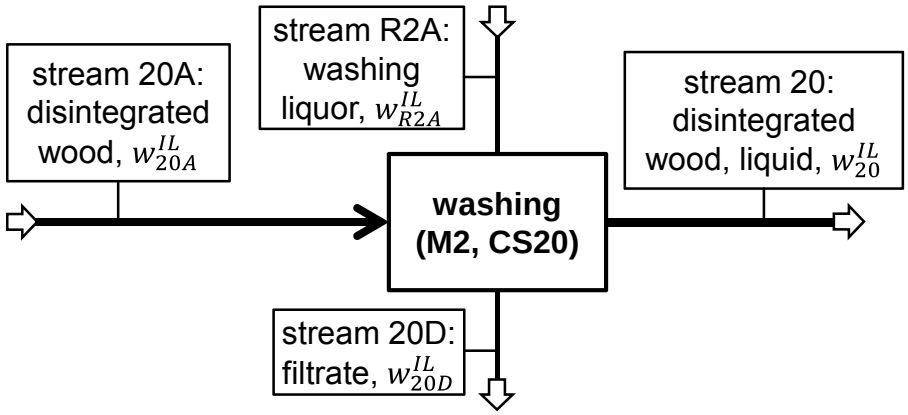

Figure 5.2. The block flow diagram of the washing realized in Figure 5.1 to separate the disintegrated wood from the IL. The disintegrated wood passes through the stage from stream 20A to 20, while the IL is washed into stream 20D.

The quantitative relation of the IL charge in the streams of the washing stage is described by the displacement ratio (DR),

$$\mathrm{DR} = \frac{w_{20A}^{IL} - w_{20}^{IL}}{w_{20A}^{IL} - w_{R2A}^{IL}}. \quad (5.2)$$

It relates the concentration difference across the washing stage ($w_{20A}^{IL} - w_{20}^{IL}$) to the maximum possible concentration difference ($w_{20A}^{IL} - w_{R2A}^{IL}$) due to the content of IL in the fresh washing liquor (w_{R2A}^{IL}). A value of DR = 0.89 is chosen, which is already at the upper bound of empirical displacement ratios in pulp washing (Mimms & Wright, 1989). Two washing stages realized in the virtual washing unit CS2 achieve a reduction of IL in the liquid to w_{20}^{IL}= 1.2 wt % in the liquid stream.

The separation of the pretreated wood from the IL in CS2 still leaves dissolved substances in the liquid IL stream 3A. They might precipitate and have been determined as extract in the process concept depicted in Figure 4.26. A second separation step (CS3) is therefore necessary to close the recycle of the IL and to separate all remaining 12 wt % of dissolved material as extract (stream 11A). Clearly this separation step is a hypothetical separation at this point. In order to assess a best case scenario, it is implemented as in unit CS2 a solid content of the extract of 25 wt % in stream 11A.

The cellulose-rich material in stream 20 is also discharged at a high solid load of 25 wt % from the pretreatment and is subject to enzymatic hydrolysis (Figure 5.3). An enzyme load of 2 wt % based on the cellulose content of the pretreated wood is chosen, both streams are fed to the hydrolysis reactor R22. Although this is much lower than the tested 17 wt % in the lab-scale experiment (Figure 4.26), it resembles technical conditions (Humbird et al., 2011); the manufacturer's recommendation of an enzyme load of 1.2 wt % (Nordisk, 1999) is taken as strong support for this choice.

The hydrolysis is carried out at a rather high solid load of 14 % (Zhang et al., 2009) to obtain a rather concentrated sugar stream after hydrolysis. The residual IL in stream 20 results in an IL content of 0.6 wt % that does not inhibit the enzymatic activity (Engel et al., 2010). A residence time of 5 h at 50°C is chosen as determined in Section 4.2.3. It is assumed that monosaccharides of xylose and glucose constitute the yield of soluble sugars, which is modeled with a conservative yield of 50 wt % of sugars from wood at first. In order to simplify the modeling, the product is assumed to consist only of monomeric sugars.

After the hydrolysis reactor, an enzyme recovery unit (CS23) is placed, which allows recycling of the enzymes while the hydrolyzate passes. The unit is inactive in the base case and will be discussed in the view of process improvements. The hydrolysis leaves a residual solid that is separated from the liquid hydrolyzate in CS24A as stream 17A, which is dried in F17 at 90°C and 700 mbar to give a lignin-rich stream with 60 wt % of lignin.

The liquid hydrolyzate stream 24A contains glucose (8.5 wt %) and is concentrated in F24 to 50 wt % sugars which is a storable concentration while accommodating the

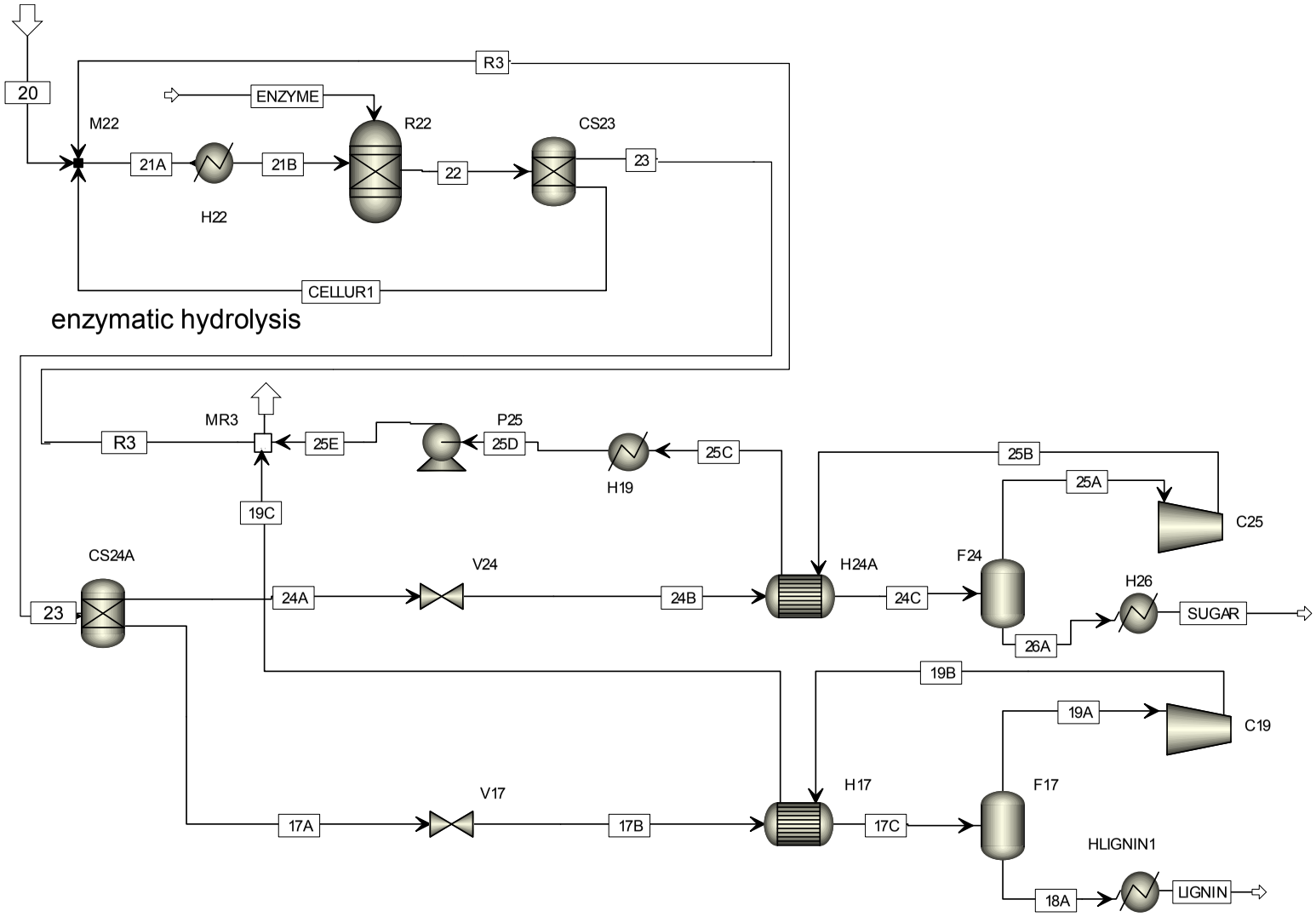

Figure 5.3. Flowsheet of the enzymatic hydrolysis as part of the designed IL pretreatment process. The complete flowsheet of the simulation can be found in Appendix E, Figure E.1.

thermal stability of sugars with a maximum drying temperature of 60°C. Both the concentration (F24) and the drying step (F17) employ evaporation and vapor recompression (C19 and C25) to preheat the feed to the unit in the heat exchangers H17 and H24A. The liquids are then recycled to hydrolysis and washing.

The liquid streams have to be recycled to minimize waste and costs. Combining the liquids after washing in Figure 5.1 result in stream 5A with 82,489 kg/h with a water content of 18.5 wt %. The recycling is established in the solvent recovery unit to recover the IL for pretreatment and the water for washing (Figure 5.4). A target specification of 4 wt % of water has been selected in the IL recycle in stream R1 to stay well below the limiting water content of 8.5 wt % during pretreatment.

Several unit operations can be employed to achieve such a separation. Membrane separation has shown to be unviable at such high concentrations due to the high osmotic pressure (Abels et al., 2012) or the large membrane areas required in pervaporation (García et al., 2013). Gas stripping of a chloride-based IL with nitrogen was investigated by Vitz et al. (2009), but the “dry” nitrogen stream resulted in a net water uptake of 6 wt % at 60°C. Hence, evaporation seems the only way to efficiently reduce the water content in the IL to the desired concentration, which is realized in a serial flash sequence (F5 and F7).

In detail, the flash sequence is designed as follows. A water stream of 5642 kg/h is evaporated at 113°C and 0.115 bar in F5. Then the pressure is further reduced to 0.014 bar in F7 to dry the EMIMAc at 115°C to 3.7 wt % for recycle in stream 9, while 7284 kg/h of water are removed. Both flash vapors are compressed to preheat the feed to the flash vessels via heat exchange in H5A and H7A. The subsequent heat exchangers H6 and H8A provide for complete vapor condensation to pump the liquid water at atmospheric pressure to the washing stage.

The process is designed at an annual capacity of 50,000 t/a of wood and an operation time of 8000 h/a. The full table of streams for the flowsheet shown in Figure 5.1, Figure 5.3 and Figure 5.4 can be found in Appendix E. All streams enter the process at 25°C and exit at 30°C. The heat exchangers in the simulation are designed using a heat transfer coefficient of 800 $W/m^2/K$ and a logarithmic mean temperature difference of 10 K. To reduce the primary energy demand, heat is integrated and vapor recompression is employed whenever possible. The necessary electrical power for the compressors is determined with an isentropic efficiency of 0.72.

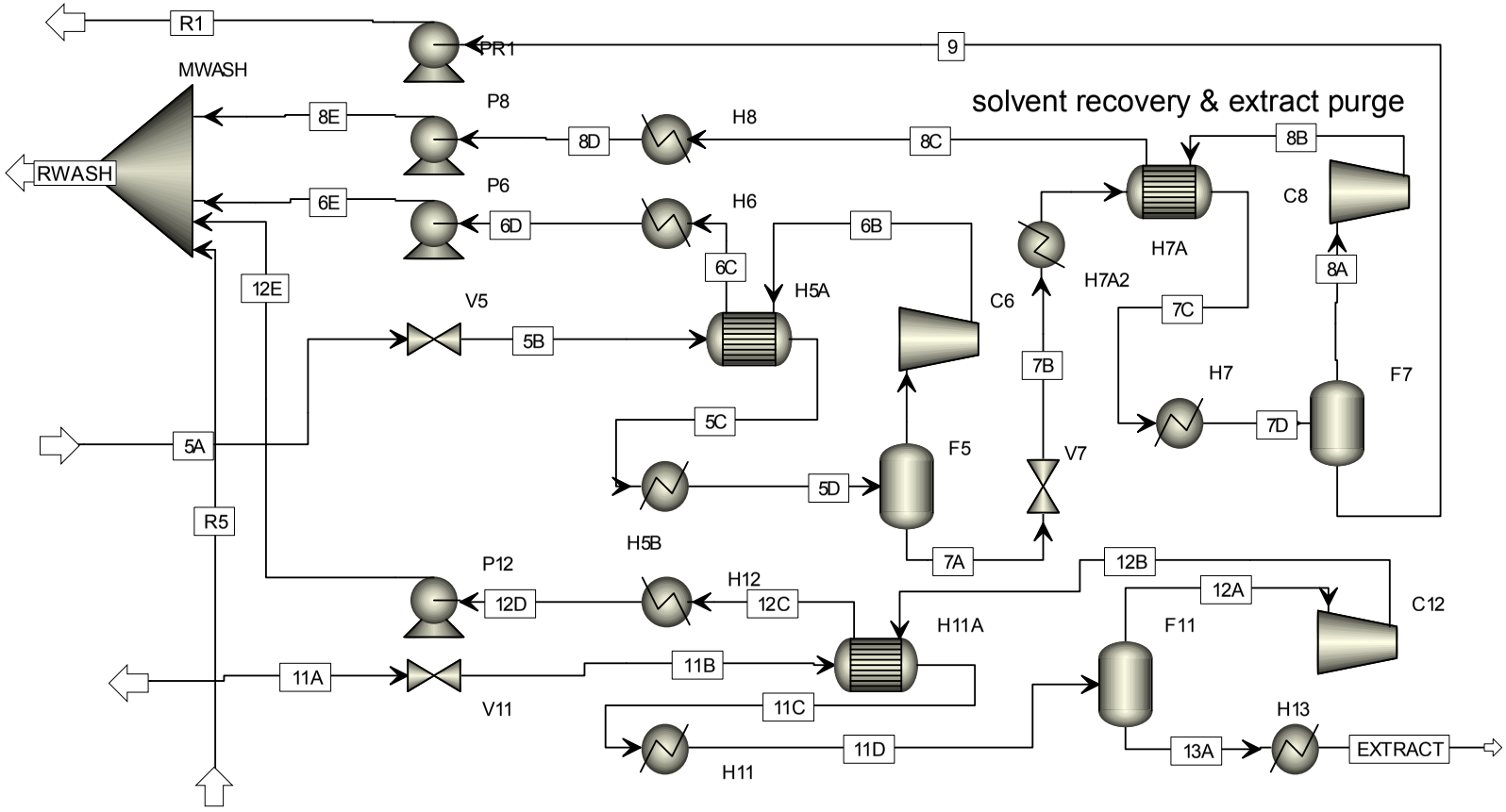

Figure 5.4. Flowsheet of the solvent recovery and extract purge as part of the designed IL pretreatment process. The complete flowsheet of the simulation can be found in Appendix E, Figure E.1.

5.1.2 Process evaluation

The mass balances and product streams from the simulation allow an economic analysis of material and energy streams. This analysis includes the determination of the capital cost, the cost of energy, utilities and raw materials, and the revenue due to product sales. The capital cost results from annualized investment cost through annuity payments for a given project life-time of 10 years and an interest rate of 10%. Investment costs for equipment are estimated based on non-linear cost functions (Guthrie, 1969) for pressure vessels, tanks, heat exchangers, pumps and compressors. All processing equipment is made of stainless steel. The cost data for the installed equipment is updated according to the Marshall and Swift Cost Index of 1457.4 for 2010 (Chemical Engineering, 2012).

The energy demand is based on the mass and energy balances that determine the energy demand for heating and the electricity for running the pumps and compressors. Although viscosity is clearly high in IL processing, no extra energy is considered for fluid mixing, because this depends on the particular design and implementation of the unit operations that is not yet known at this stage in conceptual design.

The energy requirement of washing unit operations is assessed based on the electricity consumption of rotary equipment (Peters et al., 2003). The process heat is supplied by natural gas. Cooling water is consumed to condense the water vapor and to cool the product streams. Heat exchange can only be realized between the two flash evaporation sequences (heat exchangers H6 and H7A2). Table 5.1 displays the specific costs for the different utilities electricity, heat, and cooling water.

Table 5.1. Utility prices taken from public databases (EEX, 2011; IChemE, 2011). The currency conversion 1 $ = 0.667 £ has been used where necessary.

utility	price [$/MWh]
electricity	70
natural gas	36
cooling water	1.61

The evaluation of the input and output streams requires the prices of raw materials and products (Table 5.2). While common chemicals are available in established databases (IChemE, 2011; ICIS, 2011), the prices of wood, cellulases, and products are discussed in Appendix F and have been chosen as in our previous work (Viell et al., 2013b).

Table 5.2. Prices of raw materials and products. All prices of solids are on a dry basis. The currency conversion 1 $ = 0.6942 € = 0.667 £ has been used where necessary.

material	reported range [$/t]	value [$/t]
water	0.75	0.75
wood	22–61,[1] 100[2]	100
xylose	300,[2] 450 (xylitol),[3] 493[4]	330
glucose	300,[2] 493[4]	330
lignin	275–465 (binder material)[4], 460 (adhesive resin)[4], 720,[2] 1540[5]–1760[4] (phenols), 13,250 (vanillin)[5]	1000
cellulases	1226,[5] 2848,[2] 4240[6]	3000
EMIMAc	2500–101,000	4500

[1] Galbe & Zacchi (2002)
[2] Michels (2009)
[3] Kadam, et al. (2008)
[4] OECD/FAO (2011)
[5] Shafiei et al. (2011)
[6] Humbird, et al. (2011)

The estimation of the IL price is a bit more difficult and is subject to high uncertainty. As a substance mainly used in academia, prices are not representative for large-scale utilization. In 2012, EMIMAc was priced slightly below 101 $/kg on a ton-scale as disclosed by a major chemical company (Kupfer, 2012). Wasserscheid & Welton (2007) gave a mid-term projection for ILs in general of 36–72 $/kg. The few economic scenarios in literature utilize even lower prices. Shiflett et al. (2010) chose a price of 20 $/kg for BMIMAc. Sen et al. (2012) assumed a price for EMIMCl of 10 $/kg without justification and even 2.16 $/kg were claimed for BMIMCl but without reference (Reddy, 2006). This range is in a sense confirmed by Klein-Marcuschamer, et al.

(2011), who report a range of 2.5 to 50 $/kg quoting anonymous IL manufacturers for an unspecified IL in biomass pretreatment. The range of envisaged IL prices from 2.16 to 50 $/kg is clearly not satisfactory for an economic assessment.

The possible IL prices can be narrowed further down by estimating the cost of IL synthesis based on the raw materials. A simple direct synthesis of an imidazolium-based IL with an acetate anion would at least require acetic acid (60.05 g/mol), selling at approximately 0.84 $/kg, and methylimidazole. The price of the latter substance can be estimated to be similar to methyl-2-pyrrolidone[2] (99.13 g/mol) at 4.1 $/kg (prices from ICIS (2011)). The stoichiometry for EMIMAc (170.21 g/mol) then calculates minimum costs of 2.7 $/kg just for the raw materials. In the production of chemicals, a typical cost structure shows a contribution of 30–60% by the raw materials (Peters et al., 2003). Thus, the minimum selling price of EMIMAc without any profit can be calculated to be 4.5–9 $/kg. Hence, even in a very optimistic scenario, the economy of IL-based pretreatment is to be assessed based on a price not lower than 4.5 $/kg.

The economic scenario includes the cost of IL inventory based on the mass flow of the exit stream of the pretreatment reactor (stream 2A) and the residence time. No decomposition of the ILs is considered (cf. Section 5.1) during processing. A general income tax of 36% is applied to a positive income to calculate net earnings.

5.2 Process simulation results

This chapter presents the results of the simulation of the designed pretreatment process. The efficiency of the process is computed in terms of the energy demand and an economic analysis. The latter balances the energy and material streams, based on their corresponding price discussed in the previous section. Such an analysis allows estimation of the process' potential in bioeconomy and identification of its bottlenecks. An analysis of Organosolv-like processes (Viell et al., 2013b) is taken as a reference to benchmark the designed process.

[2] BASF announced on their website that between "imidazolium […], pyridinium, pyrrolidinium, ammonium, phosphonium, etc. […] the differentiation in prices will be only small" (www.intermediates.basf.com/chemicals/ionic-liquids/faq), 30.12.2012.

5.2.1 Energy demand

The designed process mainly demands energy for heat in solvent recovery and the product drying section. Without heat integration, the process demands a total specific energy of 17.0 MJ/$kg_{dry\ biomass}$, which is much less than observed in Organosolv-like processing (28.8 to 40.7 MJ/$kg_{dry\ biomass}$, cf. Viell et al. (2013b)). Furthermore, the energy demand is also below the energy content of wood of 20.5 MJ/$kg_{dry\ biomass}$ (White, 1987), which is in contrast to the processes based on organic solvents as well. Thus, IL processing offers the chance to realize more energy-efficient processes than with organic solvents.

Nevertheless, the energy efficiency of industrial processes can be enhanced considerably by heat integration. Although an integration of hot and cold streams is largely impossible due to a heat demand above 100°C mainly in the solvent recovery section and a heat release at 60°C or below. The heat integration is therefore realized by preheating the feed streams of the evaporation units (cf. flowsheet in Figure 5.3 & Figure 5.4). This way, a reduction of up to 88% to approximately 5 MJ/$kg_{dry\ biomass}$ was reported in the primary energy demand of heat-integrated Organosolv-like processes (Viell et al., 2013b).

The heat integration of the IL process in Figure 5.1, Figure 5.3 and Figure 5.4, requires 5 heat exchanges and 5 compressors. It results in a specific demand of 2.9 MJ/$kg_{dry\ biomass}$ of electricity to power the pumps, the washing equipment, and most importantly the compressors. The pretreatment reactor requires only 0.1 MJ/$kg_{dry\ biomass}$ of heat. Assuming an efficiency of electricity generation of 40%, this gives an overall energy demand of 7.8 MJ/$kg_{dry\ biomass}$, which is surprisingly higher than the value obtained with heat-integrated Organosolv-like processes. The achievable reduction by heat integration of the IL process is consequently only 54%, which is considerably less compared to the mentioned processes. Hence, heat integration seems not to be effective in case of the designed IL process.

To shed light on this effect, the heat integration strategies are to be analyzed in the different processing section (Figure 5.1, Figure 5.3 and Figure 5.4). The pretreatment does not show reasonable chances for heat integration of the reactor streams. Organosolv-like processes recycle condensed solvents from solvent evaporation and product drying. As this requires a lower pressure to enable mild drying at moderate temperatures, the solvent is also recycled below the atmospheric boiling point and requires heating in order to reach reaction conditions. In case of IL processing, the IL

is recycled as bottom product at the process temperature of 115°C. This hot recycle results in a rather small heat demand of the pretreatment reaction; most of the heat is therefore required in the hydrolysis and solvent recovery, which is qualitatively very similar to the situation encountered in Organosolv-like processes.

The hydrolysis section in Figure 5.3 exhibits a slightly higher energy demand due to the utilization of more water in comparison to the Organosolv process. Since lignin and hemicelluloses are not separated prior to hydrolysis, they form a larger mass flow of solids that increases the water required in hydrolysis specified at 14 wt % solids. In fact, the solid content is increased by nearly 50%. As the additional water has to be removed by evaporation, this is also perceived in the energy demand of hydrolysis. However, the specific energy demand of hydrolysis in IL processing is 1.1 $MJ/kg_{dry\ Biomass}$, and the difference to hydrolysis in Organosolv processing (0.7 $MJ/kg_{dry\ Biomass}$) cannot be regarded as the cause for the difference in the total heat-integrated energy demand observed between both processes.

The solvent recycle makes up for approximately 75% of the heat-integrated energy demand and is actually considerably higher compared to the Organosolv process (5.5 $MJ/kg_{dry\ biomass}$ vs. 4.2 $MJ/kg_{dry\ biomass}$, respectively). Though both concepts mainly require energy in the solvent recovery, a particular influence of the IL is indicated, despite the IL being the non-volatile substance during thermal separation of water. To explore this in more detail, heat integration is studied with an EMIMAc/water mixture assuming ideal and non-ideal phase behavior. While the latter is described by a thermodynamic activity coefficient model (cf. Appendix D), the former exhibits an activity coefficient of unity, thus neglecting energetic IL/water interactions.

The investigation considers a flash separation sequence shown in Figure 5.5 as an excerpt from Figure 5.4, in particularly the second flash evaporation in F7 of water from EMIMAc is studied. The input stream is a total mass flow of 17,049.4 kg/h (stream 7B) with a water fraction of 12.5 wt % and a vapor fraction of 0.088. The heat exchangers (either H7A or H7) provide the heat to vaporize a vapor fraction of 0.425 that is separated in flash F7. The vapor is compressed in compressor C8 to condense the vapor in the heat exchanger H7A preheating the feed. The heat exchanger is designed at a logarithmic mean temperature difference of 17.6 K in both cases as in the original configuration in the flowsheet (cf. Figure 5.4). Any remaining vapor is condensed completely in the heat exchanger H8 to exit a liquid stream. The energy demand of the pumps is neglected in this case study.

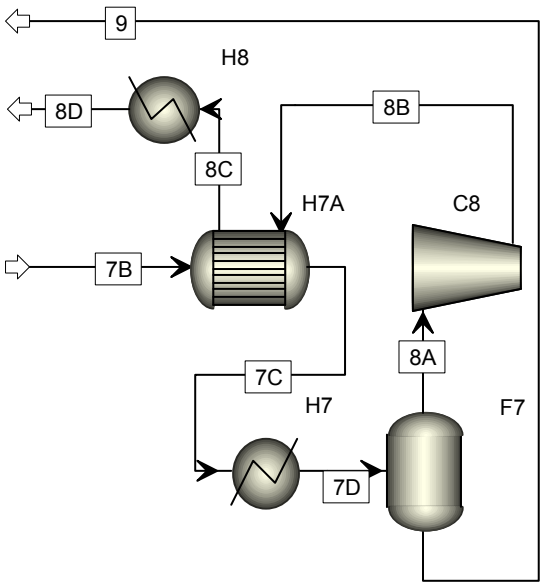

Figure 5.5. Model flowsheet to investigate heat integration by vapor recompression used in flash separation of water and EMIMAc. The structure is taken from Figure 5.4 and the process parameters are shown in Table 5.3.

The results obtained with the ideal IL/H_2O and the realistic EMIMAc/H_2O mixtures are compared in Table 5.3. The ideal mixture achieves the given vapor fraction at 70.1°C and 0.167 bar. Simple evaporation of the water stream requires 4525 kW of heat. Elevation of the dew point of the vapor requires a pressure ratio of $p_{out}/p_{in} = 3.34$. Using these parameters in the design method of Felbab et al. (2013) already identifies potential of vapor recompression. Indeed, the heat can be recovered from the pressurized vapor in the heat exchanger H7A at the expense of 651 kW of electrical power for the compressor C8. Using the efficiency of electricity production, a heat-integrated demand of 1628 kW is calculated that is 36% of the base case. This corresponds to a reduction of 74%; a value similar to what was obtained with Organosolv-like processes (Viell et al., 2013b). Hence, vapor recompression is clearly beneficial at the temperature and pressure ratios of the ideal IL/H_2O mixture.

In the case of the realistic mixture of EMIMAc with water, the stream 7A achieves the specified vapor fraction only at much lower pressure levels of 0.014 bar. A higher energy of 6349 kW of heat is required to evaporate the water, which is 140% of the energy demand calculated considering an ideal mixture. The difference obviously stems from the molecular interactions in realistic EMIMAc/water mixtures as a result of the strong hydrophilic interaction with EMIMAc. With heat integration, the

compressor requires nearly four times the power compared to the ideal mixture. This is due to the high pressure ratio of $p_{out}/p_{in} = 26.14$ required to match the temperature profiles in the heat exchanger H7A. Realization in a single compressor unit results in a high vapor temperature of 708°C; multistage compression with intercooling would be necessary in practice but it yields only a 10% improvement, which is not significant given the uncertainties of a conceptual design of ±30% (Marquardt, 2005). Altogether, the heat integration of the realistic EMIMAc/H_2O mixture results in an energy demand of 137% in comparison with the base case and achieves only a small reduction in comparison with the non-integrated EMIMAc/water separation.

Table 5.3. Simulation of the flash separation shown in Figure 5.5. Two cases are considered: an ideal mixture of water and a salt and a realistic mixture reflecting the hygroscopic nature of EMIMAc. Both evaporate the same vapor fraction.

	IL/H_2O, ideal mixture		EMIMAc/H_2O, realistic mixture	
stream	base	heat-integrated	base	heat-integrated
T(7A), p(7A)	70.1°C, 0.167 bar		70.1°C, 0.014 bar	
Q_{H7A} [kW], T [°C]	n/a	4525	n/a	6349
Q_{H7} [kW]	4525	0	6349	0
P_{C8} [kW]	n/a	651	n/a	2479
T(8B), pressure ratio ($\frac{p_{8B}}{p_{8A}}$)	n/a	228°C, 3.34	n/a	708°C, 26.14
Q_{min} [kW]	4525	1628	6349	6197
energy demand [%]	100%	36%	140%	137%

This shows that heat integration by vapor recompression only gives a small advantage in the case of the evaporation of a polar, volatile solvent from a homogenous mixture with a hydrophilic ILs. In Sections 4.1.2 and 4.2.3, the decrystallization and dissolution of the cellulose by the investigated IL molecules was traced to their effective hydrogen bonding. Water forms even stronger hydrogen bonds with the IL than with cellulose, which is the reason for precipitation. Here, the macroscopic result of this effect is seen, i.e., the high interaction in IL/water mixtures

decreases the vapor pressure of water. As the maximum temperature is set to 115°C, the pressure has to be reduced correspondingly to evaporate the water. The recovery of water from IL/water mixtures has to break these strong interactions by thermal energy. It is therefore the effect of the strong IL/water interaction in particular at high salt concentrations that cause the ineffectiveness of heat integration.

In sum, heat integration of the designed IL pretreatment process achieves reductions of the primary energy demand. The reductions are smaller compared to Organosolv-like processes due to the removal of water from concentrated IL systems. A fraction of 38% of the energy content of wood is required for the pretreatment. Nevertheless, the small benefit of vapor recompression has to be set off against the capital costs.

5.2.2 Economic analysis

The analysis of the technical potential of the designed IL pretreatment process includes the capital cost, energy and operating cost to balance the revenues from product sales. In particular, this section addresses the benefit of heat integration in IL processing and then analyzes the main drivers of process performance. Without any heat integration, the energy costs are 8.8 Mio $/a. They are due to process heat (8.5 Mio $/a), electricity (0.2 Mio $/a) and a small contribution due to the utilization of cooling water.

Concerning the application of heat integration, it is to be analyzed whether heat integration of the flash evaporators for IL recycling results in an economic benefit. Heat integration of the process with the exception of IL recycling calculates energy costs of 3.4 Mio $/a. With full heat integration, this figure is reduced by 0.2 Mio $/a but the compressors C6 and C8 (cf. Figure 5.4) require an additional investment of 9 Mio $. In view of the small savings, such an investment does not seem reasonable. Hence, no heat integration will be applied in the IL recycling section in the further economic analysis.

The investment for the heat-integrated process is 18.1 Mio $ including an IL inventory of 0.5 Mio $. The same capacity in Organosolv-like processing requires an investment of 30.8 to 34.8 Mio $ (Viell et al., 2013b).

The total economic balance in terms of costs for capital, energy and raw materials and revenues is presented in Figure 5.6 (top). It also depicts the results of the

Organosolv process as a benchmark (Figure 5.6, bottom). The heat-integrated IL process results in annual capital costs of 2.9 Mio $/a, which is much less than the Organosolv designs (≥5 Mio $/a) as a result of the lower investment cost. The energy cost total to 3.4 Mio $/a and are higher than calculated in Organosolv processing (2.5 Mio $/a) due to the larger specific energy demand despite heat integration.

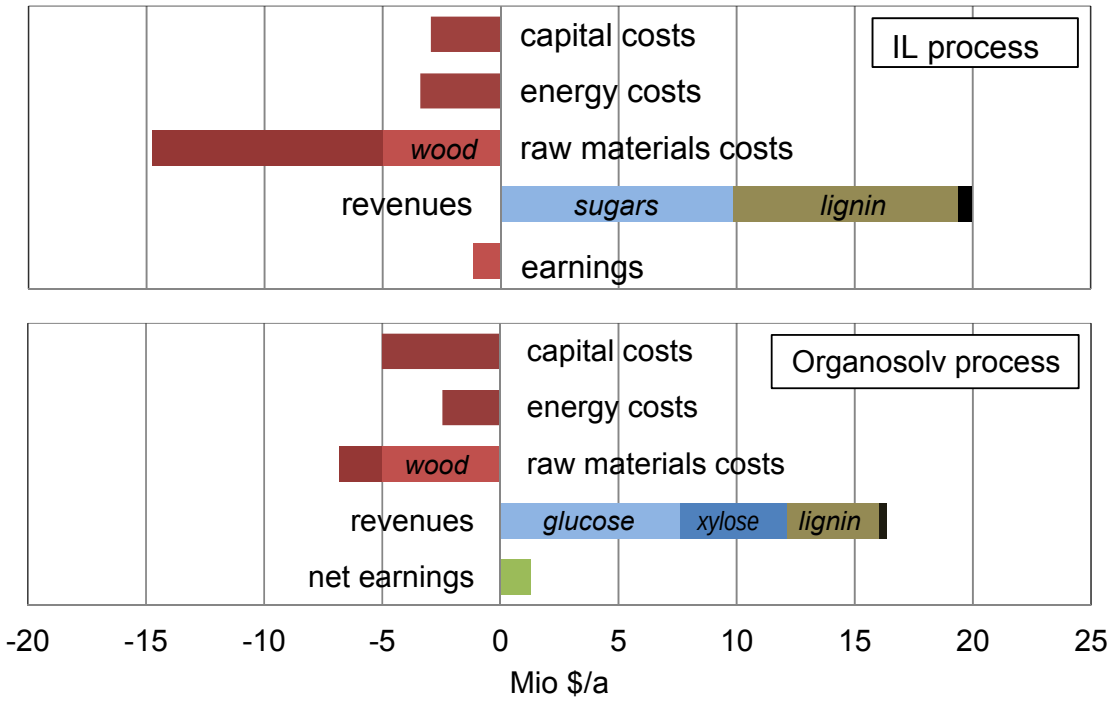

Figure 5.6. Economic analysis and comparison of the IL pretreatment processes designed in this work (top) and the Organosolv fractionation from Viell et al. (2013b, bottom). Most remarkably, the IL process exhibits very high raw materials costs largely due to the compensation of the IL losses.

The major difference is noticed in the costs for raw materials, which is 14.8 Mio $/a in total for IL processing but only 7 Mio $/a in case of the Organosolv process. While wood is bought for 5 Mio $/a in both cases and the cost of cellulases of 1.9 Mio $/a is comparable as well, the main contribution is the fresh IL cost of 7.8 Mio $/a despite the very optimistic IL price.

The revenues of 20.0 Mio $/a are achieved from selling sugars at 10 Mio $/a and lignin at 9.5 Mio $/a. The lower sugar yield in comparison to the Organosolv process

is clearly a result of the rather conservative assumption of sugar yield from wood and depicts the efficiency of the Organosolv process. The more optimistic yield of 65 wt % assessed in Section 4.2.3 can result in zero annual losses earnings. However, the lack of economic attractiveness is very clear.

Furthermore, the IL process does not achieve a carbohydrate fractionation. The hydrolysis of cellulose and hemicelluloses results in one stream of glucose and xylose. Although the equal sugar prices do not differentiate for a fractionation in this economic scenario, the subsequent sugar conversion process has to utilize both the C_6 and C_5 sugars. The applicability of such an operation can only be validated by integration of the pretreatment with downstream catalytic conversion.

Concerning the structure of the revenues, the production of lignin clearly has a considerable impact. In this economic scenario, the residue from hydrolysis is envisaged to provide a source for chemicals, i.e., aromatics. Clearly, if a chemical utilization of lignin cannot be achieved, the revenues would be nearly halved. The potential of a mere thermal utilization can be demonstrated by the small revenue from the extract. It exhibits a similar mass flow in comparison with the product stream of lignin (0.9 t/h vs. 1.2 t/h, respectively), but the substitution of (fossil) fuels according to its energy content accounts for only 0.6 Mio $/a which is less than an order of magnitude in comparison with the sale of lignin as a material.

Totaling the costs and revenues in Figure 5.6, it is obvious that even the high revenues from sugars and lignin cannot confidently balance the costs and calculate an annual loss of -1.2 Mio $/a with the IL process. Hence, the impact of the raw material costs and in particular the IL loss eats up the revenues. To demonstrate the impact of the individual costs of raw materials, a sensitivity analysis is shown in Figure 5.7. While the process shows a moderate sensitivity towards variations in the price of cellulases and wood, the market prices of lignin and sugar have a dominating effect. The uncertainty involved may be only improved when a chemical utilization of lignin is industrialized.

Instead, the most realistic approach to leverage the process' economic attractiveness is to optimize the utilization of costly auxiliary material, i.e. cellulases and EMIMAc. The enzyme loading is already adjusted to meet industrial values of 2 wt % cellulase per g of cellulose. An option would be the recovery of enzymes. If the separator CS23 in Figure 5.3 recycles 60% of active enzymes as for instance suggested by Steele et al. (2005), the annual cost for enzymes decreases by more than 1 Mio $/a.

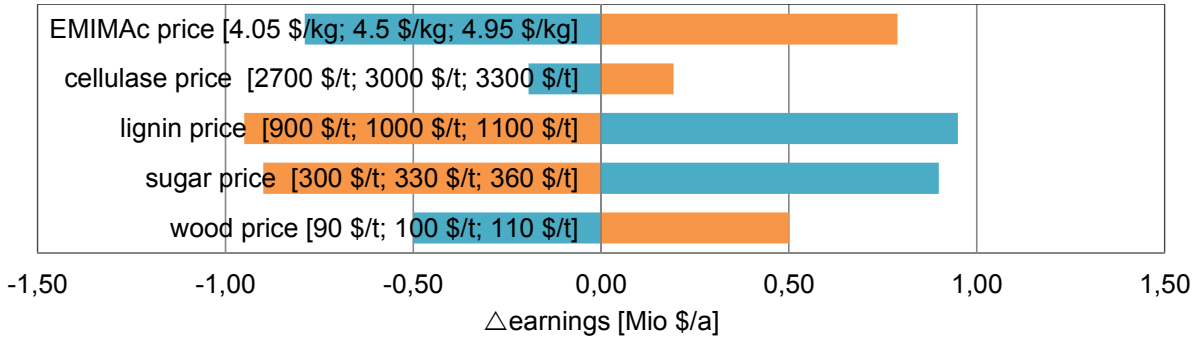

Figure 5.7. The result of a sensitivity analysis of raw material prices varying one parameter by 10% one at a time. Blue bars result from positive deviations in the raw material price, while negative ones are shown in orange.

Considering the much higher sensitivity of the process towards the IL price, a larger impact can be expected by either lowering the IL price or its recovery. At an IL price of 2.5 $/kg, which was sometimes reported in literature, the process achieves a net income of 1.5 Mio $/a. However, the reduction of the IL price seems no viable option as shown in Section 5.1.2. Hence, the solvent recovery is the only means to realize improvements in the current process.

The solvent recovery in the current design realizes a recovery of 99.7 wt %. It seems already rather high but obviously not high enough for economic operations of the IL process. The few techno-economic studies focusing on IL processing also noted the importance of IL recovery as key to efficient processing. Sen et al. (2012) suggested an experimentally unproven chromatographic separation step to recover the IL and simulated an IL recovery of 98 wt %. The produced sugars, however, failed to reach the market price by an order of magnitude. Klein-Marcuschamer et al. (2011) investigated an undisclosed IL process to convert lignocellulosic biomass into ethanol and lignin at an IL recovery of 99.6 wt %. At a realistic ethanol selling price of 2.5 $/gal (ICIS) and an IL price of 2.5 $/kg, they identified a lignin price of 1000 $/t to compensate for capital and operating cost but without any earnings. Both results agree with the results obtained in this work. Further potential thus may be anticipated by a more effective separation and recovery of the IL.

The designed IL pretreatment shows a loss of IL at the two solid separations CS2 and CS3 (cf. Figure 5.1). Both washing and filtration steps have been designed similarly based on empirical data. The rather low IL content of the liquid of 1.2 wt %

after washing in stream 20 translates into an IL fraction of 3.4 wt % based on the solid material.

Experimental validation of this step is clearly critical but there is very scarce data available in literature. Lozano et al. (2012), pretreating pure cellulose with BMIMCl, achieved a recovery of 99.7% with an integrated precipitation and washing step. Dibble et al. (2011) extensively washed corn stover pretreated with EMIMAc and determined a residual IL content on the solid of 2.7 wt % after the first washing series with ethanol, which is in good agreement with the values in this work. The authors also extended the washing for a second water washing, employing more than 10 times the mass of the IL but achieved a residual IL content on the corn stover of <0.2 wt %. Using these values in the designed process in this work, this translates into an IL loss of 12.5 kg/h or an IL recovery of 99.98 wt %. In fact, the economic analysis then calculates net earnings of 3.3 Mio $/a. However, the cited authors could only achieve a net recovery of 89 wt % of the IL despite the very clean solid material, which demonstrates the high uncertainty in these numbers. It also demonstrates that high recovery rates might be realistic but experimental work on larger scale seems necessary to close both mass balances of the solids and the IL to assess the IL loss in processing reliably. Basically, this will lead to an optimization problem between IL cost, washing effort and energy demand in solvent recovery in the current design of the IL-based pretreatment process.

5.3 The potential of an IL-based pretreatment

The simulation results allow a concluding discussion of the designed pretreatment process for wood based on ILs. The designed IL process demonstrates feasibility on process level and is successfully realized in a process simulator at industrial scale. The energy demand is higher in comparison to Organosolv processing due to unfavorable thermodynamics in the evaporation of water from the hygroscopic IL. The economic analysis confirms the process concept to be relatively simple with low capital costs. This result helps in realizing small scale capacities which meet the variable markets of biorenewables.

However, the analysis also discloses uneconomical operations despite the assumption of lignin as a high value product in the rather optimistic scenario. The loss of EMIMAc, despite being less than 1 percent, is identified to be the major

downside. Other factors like enzyme recovery might result in passing the break even, but do not result in considerable economic attractiveness. A strong effect is given by the price and the recovery rate of the IL. No advantage can be expected from economy of scale as operating costs increase linearly with process capacity.

The costly IL and the energy demand in the solvent recycle are probably an economic argument against the utilization of an IL in pretreatment. The potential of IL-based pretreatment concepts is therefore explored in the following paragraphs in a top-down approach: First the process concept is addressed, and then the influence of unit operations is discussed. The section finishes with possible measures on the level of process chemistry.

From a *process perspective*, the cost of ILs and the solvent recovery is identified as the highest burden in the designed pretreatment process. Although, the recovery of the IL can be taken as a design variable, a realistic assessment requires estimation of the recovery of the IL ions from the solid carbohydrates as a function of the effort, i.e. the washing stages. Since the current design achieves a high recovery in the solid-liquid separations, further improvements in that regard cannot be made without experimental validation. Dedicated experiments are therefore necessary to determine the achievable recovery from the biomacromolecules quantitatively and to optimize the recovery and the effort in solvent recycling.

The recycling was initially anticipated to benefit from the utilization of the ILs as a non-volatile class of solvents because no losses of costly volatile liquids would be faced. Given the findings presented in this thesis, the idea of complete dissolution (Sun et al., 2009) was abandoned and the disintegration was developed as an attractive short-time pretreatment. The concept of IL recycling from volatile solvents by evaporation however remains unchanged; both concepts involve a washing of solid (ligno-)celluloses by a hydrophilic solvent as practiced also in Organosolv-like processes (cf. Viell et al., 2013b). Consequently, the processing results in large liquid streams after the washing stage that contains the costly solvent, which has to be recovered. In case of ILs, this is more difficult than with volatile solvents because the field-tested technologies of solids drying and distillation are inapplicable and the vapor pressure of water is lowered by the strong hydrogen bonding in the particular IL. Hence, the reduction of the energy demand at high recovery requires the exploration of new strategies of IL recycling other than evaporation.

Concerning the economic argument of ILs being too expensive even at a recovery rate of 99.7%, the question is whether the application of solvents other than water can be considered beneficial in biomass processing in general. Similarly, concentrated acids are considered as being too expensive in biomass processing (Fan et al., 1987; Mosier et al., 2005), a statement which was made already by Locke et al. (1945). The reports offer, however, no quantitative justification. Concerning the much lower price of an acid (0.085 $/kg, ICIS (2011) for H_2SO_4) in comparison to 4.5 $/kg for IL, the claim of acids being too expensive does not seem obvious at first sight.

The economic analysis presented above sheds light on this fact by calculating the difference between maximum revenues and feedstock costs without any additional auxiliary material. The total carbohydrates in wood yield a revenue of 11 Mio $/a. The contribution of lignin can be confidently assigned to its heating value, which is then only 0.9 Mio $/a. This sums to a maximum total revenue of 12 Mio $/a from wood in any wood saccharification process. The set feedstock costs of 5 Mio $/a leave 7 Mio $/a to cover any additional expenses.

In case of IL processing, the capital costs have revealed to be rather low in comparison to other solvent-based fractionation processes (cf. also Viell et al., 2013b). The capital and energy costs of the IL and the Organosolv processes sum to 6.3 and 7.5 Mio $/a, respectively. Hence, even if all operating costs due to cellulases, IL or other solvents are neglected, the processes hardly pass the break even. The prerequisite of two digits return on investment (Peters et al., 2003) to realize new process technology is currently not achieved neither with the Organosolv nor the IL-based process.

Hence, the statements above concerning the uneconomic operations with concentrated acids need to be put differently. Any solvent that needs to be recovered will be problematic to reach the objective of economically attractive processing because the capital and energy costs are rather high. Hence, the cost structure seems unfavorable to accommodate a solvent other than water despite the nearly quantitative yield.

Analysis of the cost structure shows that feedstock costs without loss of IL make up approximately 48%. As feedstock costs in bulk chemicals or refineries make up for approximately 60–75% of the total costs (Lynd et al., 1999; Peters et al., 2003), a reduction of either capital or energy costs can be envisaged. The former are usually

reduced by economy of scale, which reduces capacity-specific capital cost. However, the world-scale capacities as established in petroleum-based processing likely do not match the more decentralized production in bio-based value chains. Hence, the only option will be to cut energy cost but without the application of expensive equipment. In fact, the separation technologies require most of the energy and capital cost in the processing concept. The application of solvents in biomass pretreatment thus requires a design of the solvent systems integrated with the recycling techniques.

These implications concern the employed *unit operations*. In the current design, there was no alternative to thermal evaporation in order to remove the water from the IL. Alternative separations are therefore to be explored in combination with any novel solvent system, in particular considering water that is continuously introduced into the processes at an amount of approximately 10–50 wt % per dry biomass. Despite the problematically high osmotic pressure encountered with membrane separations in concentrated ILs (cf. Abels et al. (2012)), membrane systems could possibly pre-concentrate dilute streams to purge undesired substances, concentrate products, and recover solvent molecules from purge streams prior to evaporation. This could result in a lower energy demand.

Further improvements can be made on the productivity of the costly solvent. A higher solid load allows processing of more raw material into products, thus more profit is generated per mass of solvent. Hence, the operating cost due to solvent loss becomes less pronounced in the overall balance. Klein-Marcuschamer et al. (2011) showed that this relation becomes particularly important in case ILs are used as solvent.

However, a higher solid load poses an engineering problem and requires other technical concepts of pretreatment reactors. Da Silva et al. (2011) recently demonstrated the integration of IL processing of bagasse in a twin-screw extruder and achieved a solid load of 25 wt %, a value more than twice than that proposed in this work. Furthermore, reactor designs of up to 40 wt % have been reported with other pretreatment concepts (Modenbach & Nokes, 2012). In this regard, the load determined with standard laboratory equipment can be likely improved.

Further improvements of the economic attractiveness can be expected from a different product range. Hence, *process chemistry* has to be explicitly integrated into the pretreatment. The vital advantage of lignin was already shown in Organosolv-like processes (Viell et al., 2013b). However, the revenue is still small if lignin and sugars

are produced and isolated. The utilization of sugars from wood in downstream catalysis will be only advantageous at minimum isolation steps. Therefore, the design of a reactive solvent system is proposed that is capable of biomass pretreatment while converting the intermediate carbohydrates into valuable products.

The investigations of the pretreatment in EMIMAc already indicate a reactivity to cleave and extract lignin. While these effects improve the downstream processes that are otherwise limited in terms of selectivity and conversion, the intrinsic mechanisms should be integrated with the subsequent conversion reactions. At the same time, the mechanisms of disintegration, decrystallization and extraction should be explored to design cheaper and tailored solvent systems. For instance, swelling of cellulose was also reported with other ionic systems even without complete dissolution, i.e., $NaOH{\cdot}H_2O$ or $LiCl{\cdot}H_2O$ (Fischer et al., 2003). The combination of ionic species with organic solvents without affecting their effectiveness was also shown (cf. Rinaldi, 2011; Rinaldi, 2012). An integrated dehydration and deoxygenation of cellulose with metal salt hydrates ($ZnCl{\cdot}H_2O$) to isosorbide (Sanders et al., 2012) or its conversion to HMF (Binder & Raines, 2010) has been shown.

Furthermore, the reaction could be possibly established in other types of ILs that form a thermodynamic cycle resulting in an immiscible IL for facilitated separation (Tang et al., 2012; Zakrzewska et al., 2010; Kamimura et al., 2012) or a switchable solvent (Jessop et al., 2012; Jessop et al., 2010; Reichardt & Welton, 2010). The investigation of the interplay between basic and acidic capabilities of ILs in particular with mixtures of molecular solvents is a first step towards the design of reactive solvent systems. Theoretically and indirect evidence for the reactivity of ILs and the in situ formation of catalytic species has been shown (Holloczki et al., 2010; Liu et al., 2012; Brehm et al., 2012). In combination with the mechanisms elucidated in this work, the catalytic activity is promising to design and tailor novel processing concepts for the valorization of biomass.

6 Conclusions

The utilization of wood requires an effective and sustainable pretreatment in order to access the complex ultrastructure and its embedded molecules as a renewable source for chemicals and energy. The known wood pretreatment and saccharification processes based on acids or organic solvents do not achieve near-quantitative yields or lack economic attractiveness. This thesis aims at the development of a pretreatment process for wood with ionic liquids (ILs) as a novel class of solvents.

The pretreatment and conversion should preserve the molecular structure. The selective conversion of wood into sugars is thus a central step and the highest selectivity can be expected with enzymatic hydrolysis. It requires, however, an effective pretreatment in order to gain access to celluloses for enzymatic hydrolysis.

The remarkable feature of the investigated ILs is the dissolution of cellulose. This motivated several authors to suggest process concepts based on the complete dissolution of wood and the subsequent precipitation of carbohydrates for fractionation. Consequently, the process development in this thesis starts with the idea of a complete dissolution of wood in ILs.

The basis for the experimental analysis is laid with an inventory of analytical techniques, i.e., the investigation by light and SEM microscopy, the determination of Kamlet-Taft parameters and wet chemical analysis of carbohydrates and lignin are established to accommodate the conditions encountered with the ILs. In addition, novel analytical methods have also been developed. In particular, the water content in ILs was determined precisely with infrared spectroscopy and a robust model-based spectral evaluation to close the mass balances during dissolution. Furthermore, the crystalline structure of celluloses was quantified using Raman spectroscopy and hard modeling of the overlapping spectral contributions.

The precise analysis of wood dissolution in ILs reveals that the suggested fractionation by precipitation does not offer high yields and involves a considerable loss of lignin. Furthermore, it is shown that the dissolution is very slow and incomplete within finite processing times. Hence, the idea of a complete dissolution of wood in ILs is infeasible and it was not considered further in this thesis.

The systematic experimental exploration of the wood dissolution in EMIMAc, however, reveals an interesting short-time effect causing the wood fibers to disintegrate. The fact that this disintegration works well with particles up to 10 mm in length and creates a remarkably increased specific surface area qualifies the effect for the sought pretreatment of wood.

The pretreatment concept is based on the disintegration of cells without substantial dissolution. Light microscopy shows swelling of the cell wall and disintegration at the compound middle lamella. The swelling of the cell wall seems to be related to the solvation capabilities of the IL for cellulose, which is supported by the reduced crystallinity after the pretreatment. The concerted syringyl extraction and the swelling of the secondary wall obviously cause the cells to disintegrate. A maximum water content of 8.5 wt % is acceptable. The process is successfully carried out with beech chips within 1.5 h at 115°C. It demonstrates the advantage of the disintegration in contrast to the dissolution, which would require at least 72 h.

An analysis of the ILs in mixtures with water based on Kamlet-Taft parameters indicates that the basicity of the anion is a prerequisite for the observed effects. However, the wood pretreatment in ILs cannot be described comprehensively using Kamlet-Taft parameters. Hence, although the basicity is a first mechanism of the interaction with cellulose, further mechanisms are essentially involved. In fact, each of the studied ILs exhibits a different physico-chemical behavior that might original from complex acid/base interactions in the concentrated ionic systems. Reactive processes of the IL are thus very likely but further studies are required to understand the disintegration on a molecular level.

The methods and results worked out in this thesis identified EMIMAc and beech as the most effective combination of IL and wood. The effectiveness is proven in combination with enzymatic hydrolysis. The cellulose and xylan are preserved during pretreatment and result in a near-quantitative yield of sugars within a hydrolysis for 5 h at 50°C. In detail, the overall mass balance shows a yield of up to 65 wt % of sugars, which is a near-quantitative conversion of the carbohydrates in beech wood.

Based on the experimental data and mass balances, the process is successfully simulated in the process simulation software Aspen Plus. It reveals feasible operations of the process at industrial scale and also two drawbacks. The first is the rather high energy demand in comparison to Organosolv processes. It is due to the hygroscopic nature of the IL being a liquid salt. As the solvent recycling relies

completely on thermal unit operations it becomes very energy-intensive. The effect is in particular obvious in comparison with state-of-the-art heat integration, which is not as effective as with organic solvents. The second downside is the loss of IL in the solid-liquid separations. The remarkably small loss of less than 1 percent of IL makes the whole process uneconomical.

Both downsides must be put into a fair perspective. The solvent recovery is an issue in any biomass pretreatment utilizing a solvent other than water and the uneconomic operations seem to be a general challenge. This problem will not be solved by incremental enhancements but requires fundamental improvements of the process concepts. This points on the one hand to the development of novel recycling and separation strategies for the non-volatile solvents and products. On the other hand, the separation of solids from an IL by washing should be minimized or avoided at best.

As the optimization of solvent loss is a technological problem beyond the scope of this thesis, the product range is identified to be a leverage for economic attractiveness. It is suggested to produce higher value products from carbohydrates and lignin in order to generate more revenue. Simultaneously, the products should be easy to isolate from the reaction medium.

In general, the results show that ILs should not be applied in one individual process step but have to be integrated into the process chain. The biomass pretreatment capability of EMIMAc for beech, as the best identified combination of wood and IL, is a successful step in that direction. It offers a unique perspective to make wood more attractive as a resource for fuels and chemicals. The objective of future works should further elucidate the underlying molecular mechanism of the pretreatment to design the solvent system and its reactivity to the biomass, the desired catalytic conversion, and the separation downstream. The design can exploit the diversity of ionic molecules to tailor the pretreatment processes to the feedstock and also to meet the needs of the process chains in future bioeconomy. The presented results provide a sound basis for this perspective.

Appendix

The appendix provides supplementary information. First, the dissolution of wood in an IL is investigated with light microscopy in Appendix A to depict the change of optical properties during penetration of wood with IL and to support the application of mass balances for the investigation of wood dissolution. Additional data and results of the experiments described in Section 4 are provided in Appendix B. Further supplementary experiments at different conditions that further support the experimental findings in Section 4 are presented in Appendix C.

The remaining Sections D to F give data on the process simulations. While the thermodynamic properties of EMIMAc and of its mixtures with water are compiled in Appendix D, the process simulation details are provided in Appendix E. The prices of the raw materials are discussed including references in Appendix F.

A Visual appearance of wood dissolution in ILs

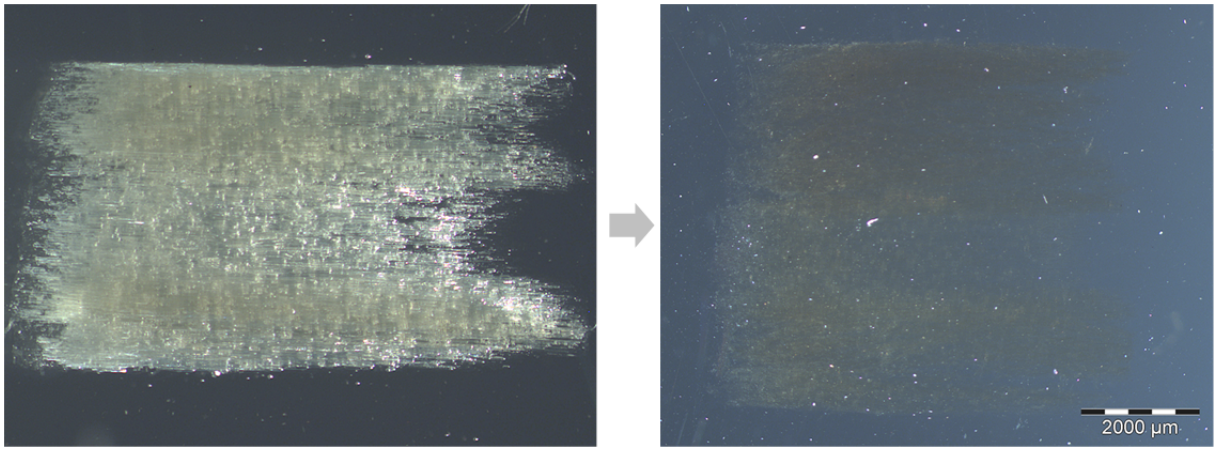

Figure A.1. The visual appearance of a slice of spruce in BMIMCl observed by reflected light microscopy on a heating stage (100°C). The slice was cut manually in a longitudinal direction at a thickness of ~100 µm. At the beginning of the experiment, the particle is readily visible in BMIMCl (left). After 8 days in BMIMCl at 100°C in an oven, the wood particle becomes hard to see but the contour of the particle is still identifiable (right).

B Supplementary data

The following figures show the appearance and composition of the residue after the dissolution experiments in ILs. Figure B.1 shows the material obtained with the fundamental mass balance in the case of small beech particles. Two fractions are shown as the protocol achieves separation of dissolved molecules from the residue. Thereafter, the material obtained with the simplified protocol is shown (Figure B.2 to Figure B.5, photos taken by Schlüter (2011)). The viscous mixtures were diluted with DMSO to facilitate separation of the liquid phase with dissolved molecules from the solid. A subsequent washing with DMSO, acetone and water was applied to remove the IL, thus a residual fraction is shown only.

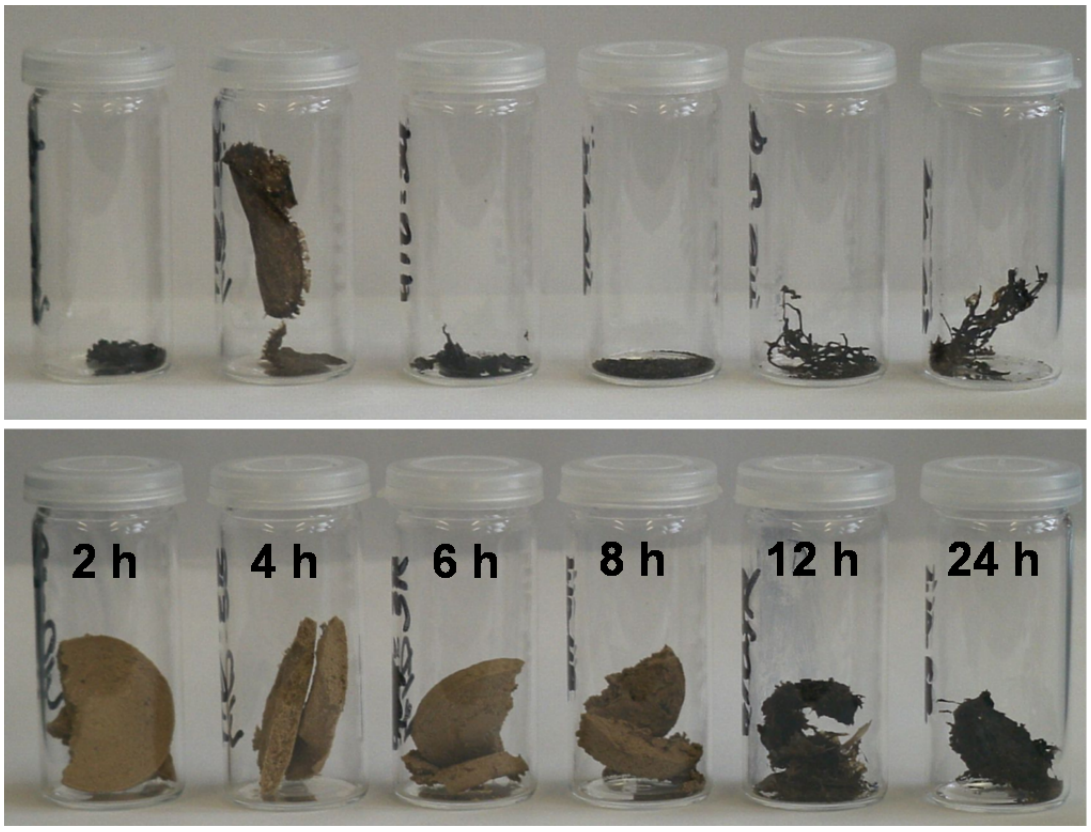

Figure B.1. Precipitated material from the supernatant (top) and the corresponding residue (bottom) after treatment of beech (0.1–0.5 mm) for the times indicated in the picture (EMIMAc, 115°C, 500 rpm). The material was processed without any additional chemicals by centrifugation, decantation, precipitation and washing with water according to the detailed protocol described in Section 3.2.

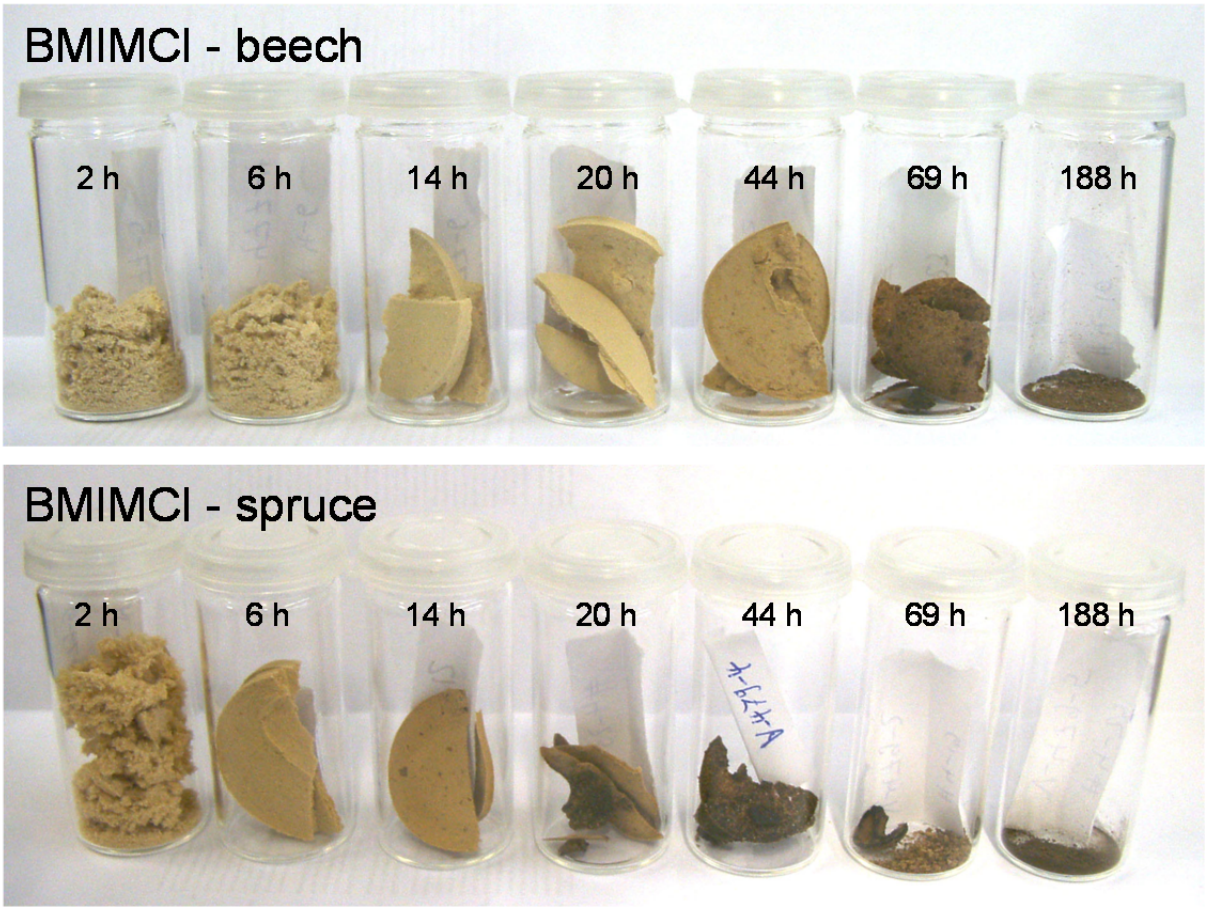

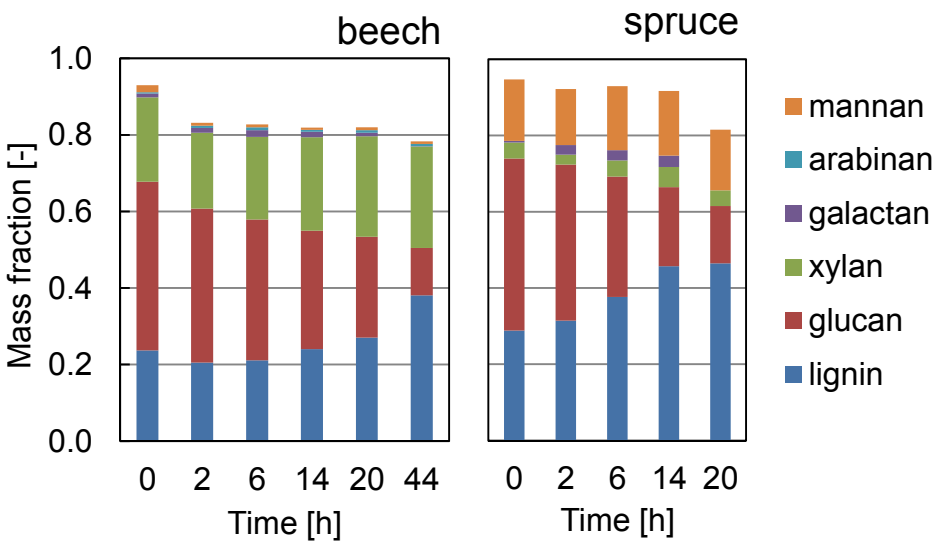

Figure B.2. Residue and its composition after dissolution in BMIMCl. The bar height is the total determined fraction. The preferential extraction of cellulose in both species of wood is clearly visible.

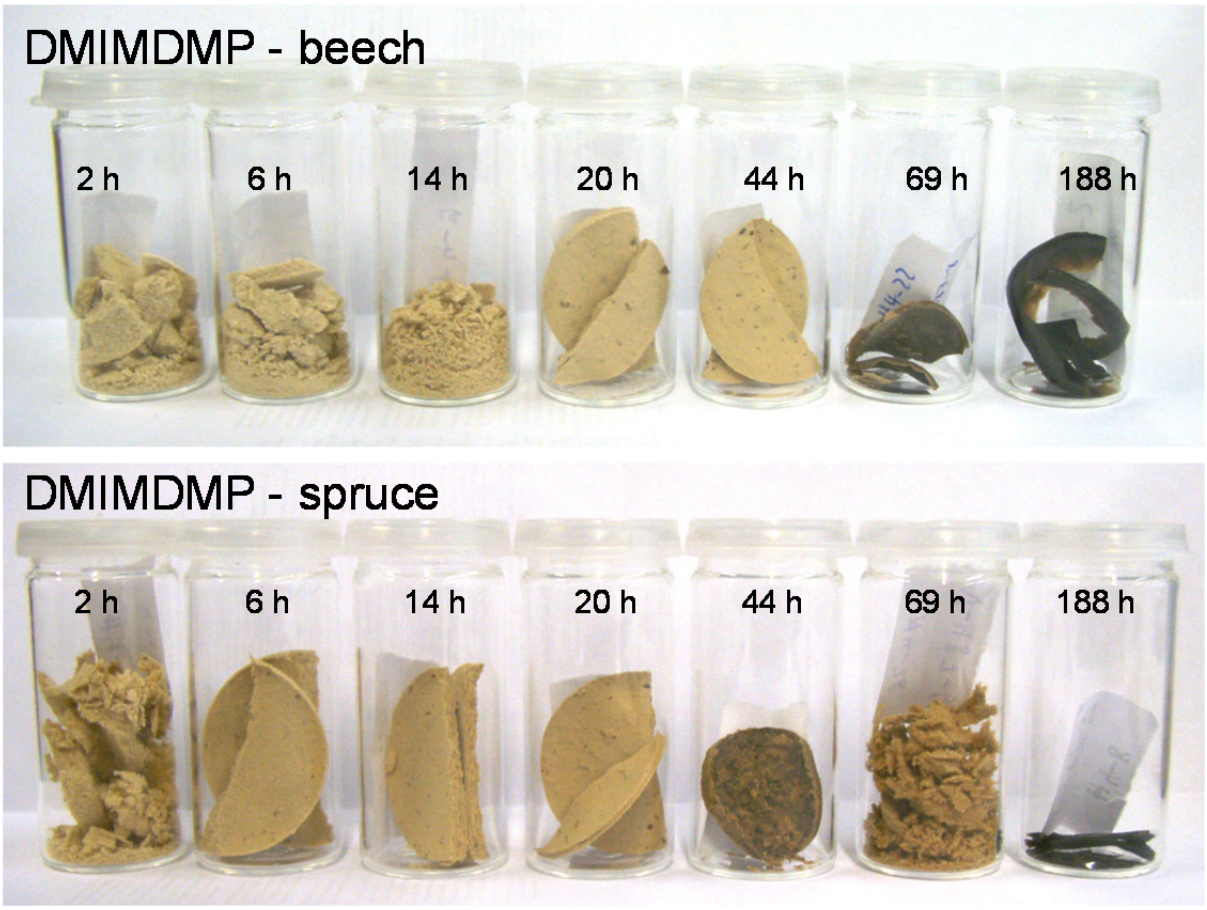

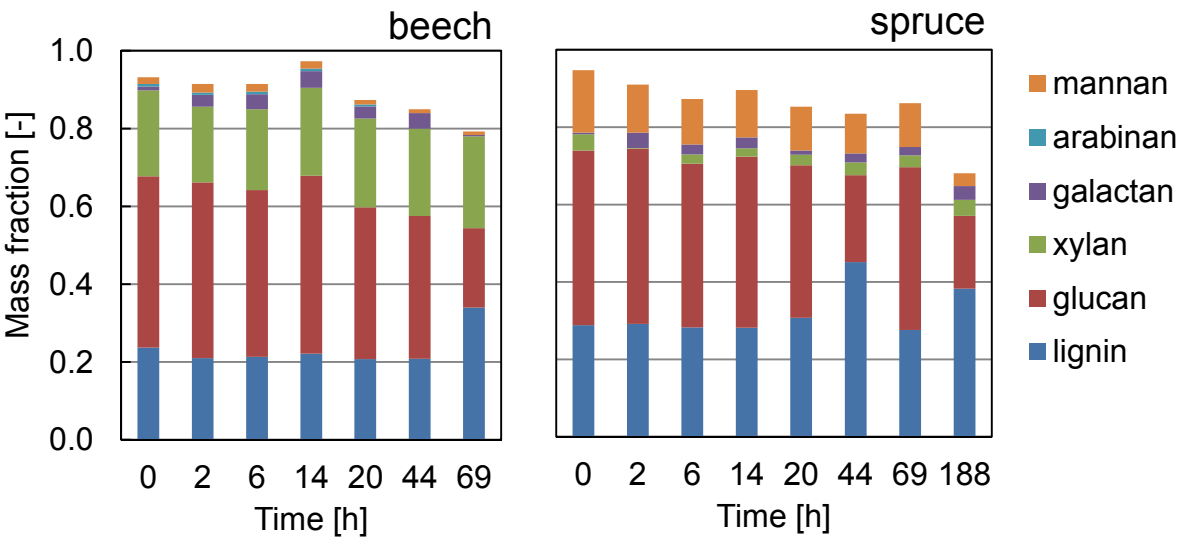

Figure B.3. Residue and its composition after dissolution in DMIMDMP. The bar height is the total determined fraction.

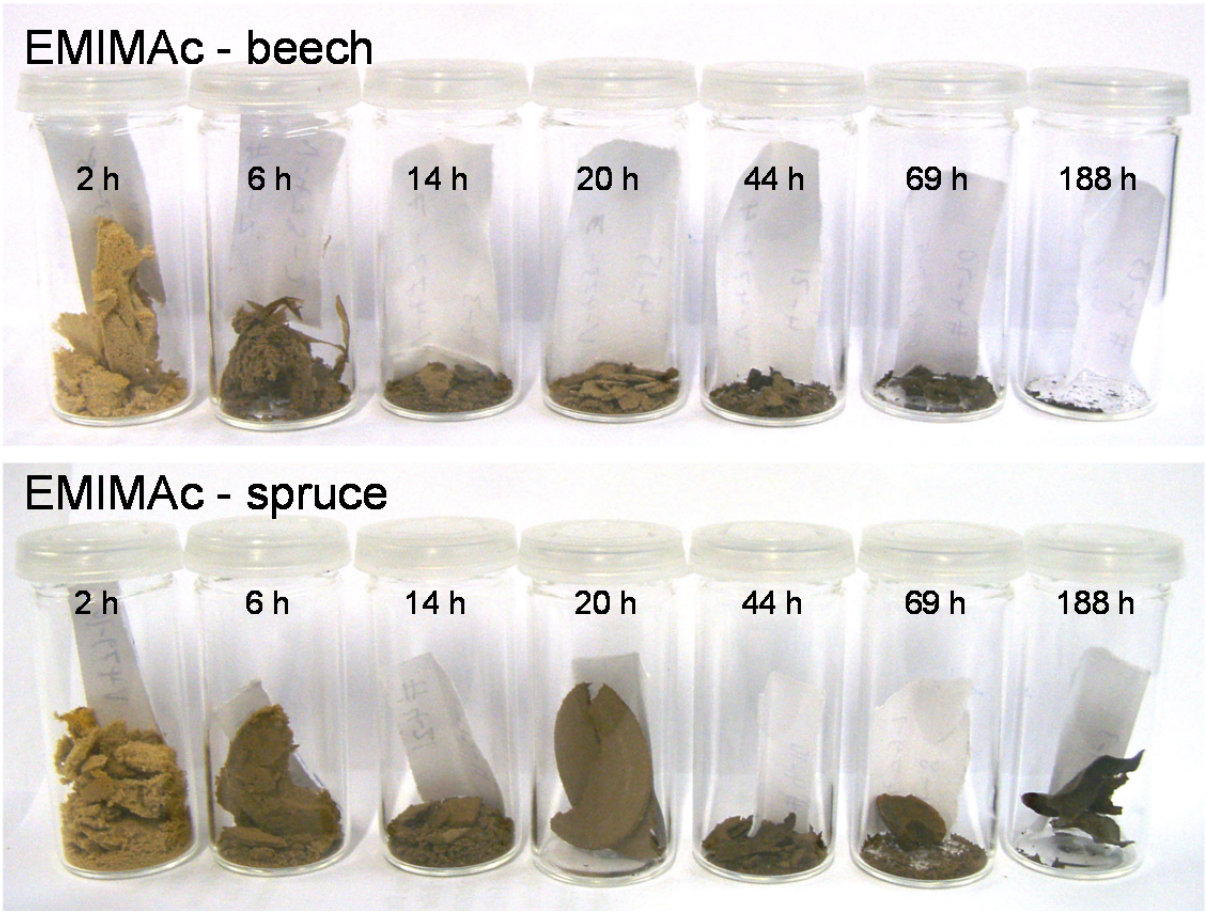

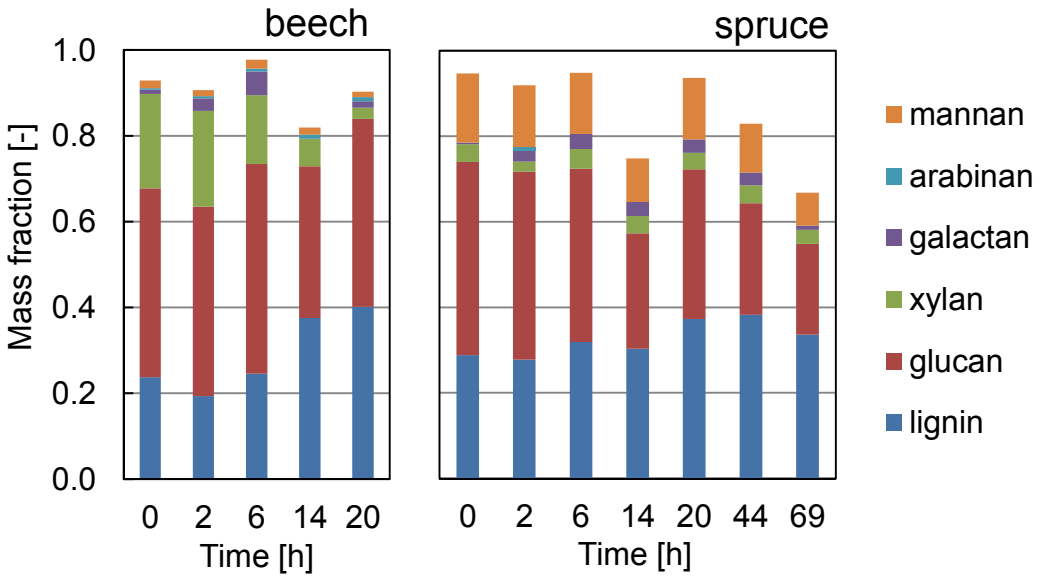

Figure B.4. Residue and its composition after dissolution in EMIMAc. The bar height is the total determined fraction. In the case of the data point at 14 h, the total mass fraction indicates an error in the determination of the cellulose fraction.

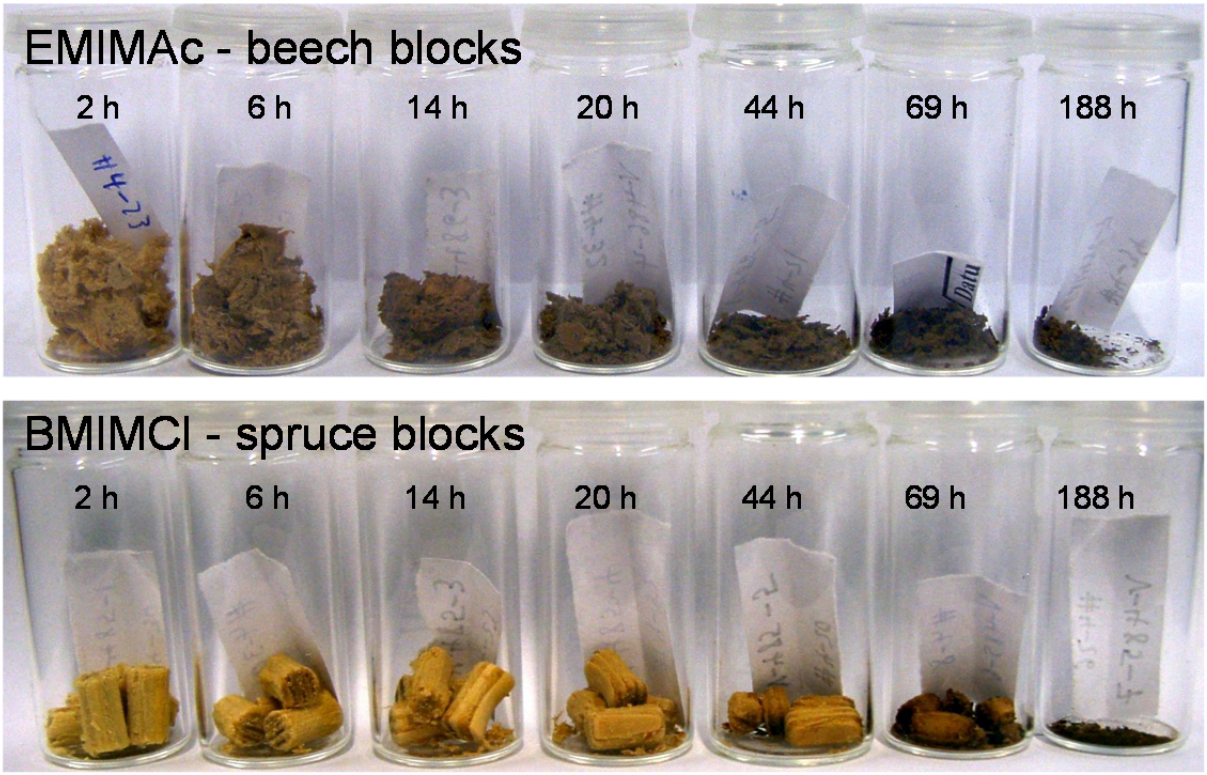

Figure B.5. Residue after dissolution of large blocks of beech in EMIMAc (top) and spruce in BMIMCl (bottom) at 115°C. The samples have been washed extensively with DMSO, acetone and water.

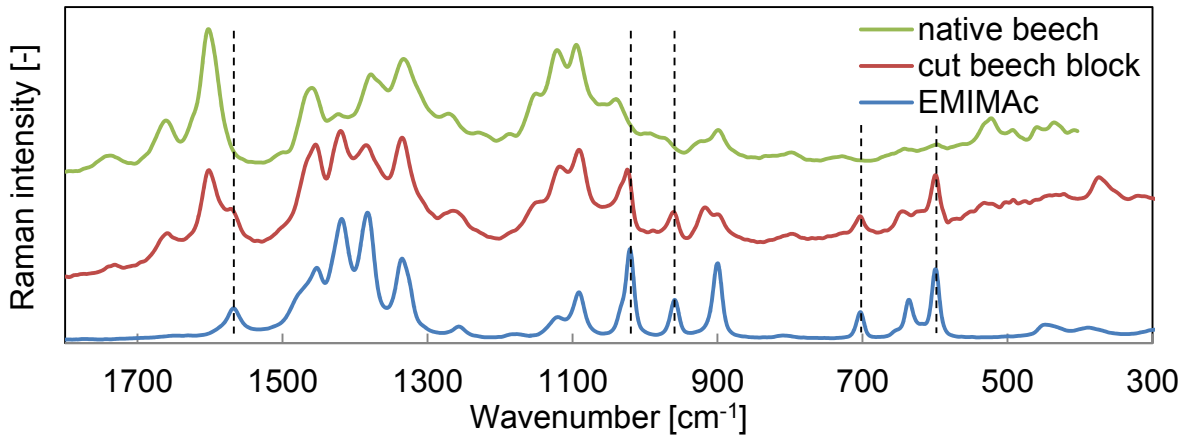

Figure B.6. Spectrum obtained from a block of beech after 2 h in EMIMAc (cf. Figure 4.13 & Figure B.) in comparison to a spectrum of native beech and EMIMAc. The block was cut into halves and probed on the inside. The spectral features marked by a dashed line identify the presence of EMIMAc in the tissue. It proves that a certain amount of IL cannot be removed from the inside of the intact blocks by washing.

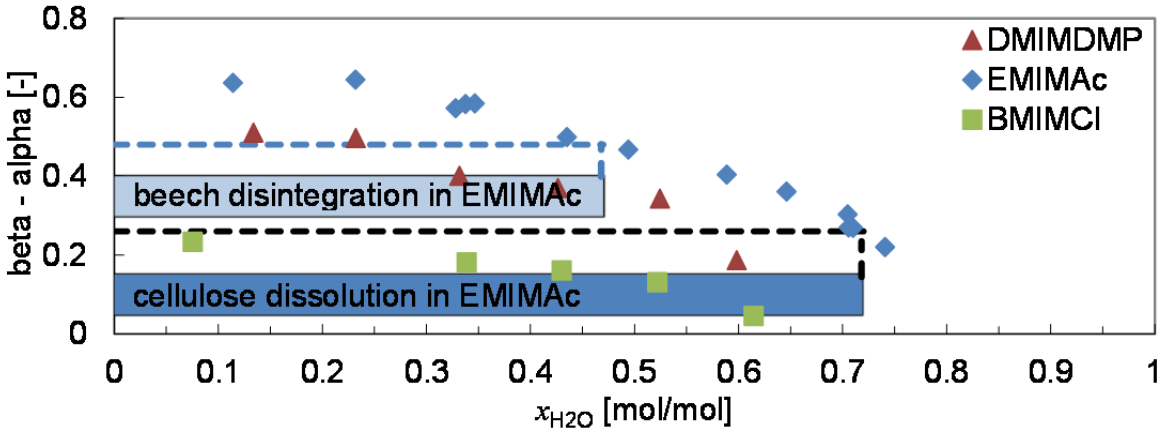

Figure B.7. The net basicity (difference between $\beta - \alpha$) for the three ILs over water content in comparison to disintegration and dissolution in EMIMAc/water systems. The suggested value at the limit of cellulose dissolution in EMIMAc is $\beta - \alpha = 0.27$ (dashed black line), which is a bit smaller than reported by Hauru et al. (2012). However, this value suggests that even concentrated BMIMCl cannot dissolve cellulose and erroneously predicts cellulose dissolution in DMIMDMP at much larger water contents than observed. In fact, the limiting water concentration in BMIMCl and DMIMDMP corresponds to $\beta - \alpha =$ 0.18 and 0.40, respectively. Further, the comparison with disintegration in EMIMAc predicts a similar effect also in DMIMDMP, which has not been observed with beech. Hence, the net basicity does not characterize the mechanisms the investigated IL systems comprehensively with regard to cellulose dissolution and beech disintegration.

C Supplementary experiments

The following figures show the morphology of the wood after treatment with ILs. The pictures provide additional data to compare the effect of other ILs to the effects of EMIMAc, which have been studied in the main text. Additionally, an experiment describes the changes of EMIMAc at 105°C after 3 months.

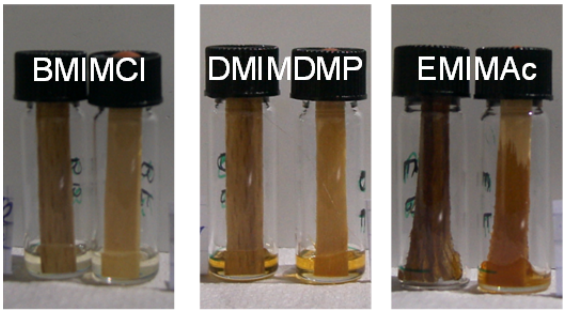

Figure C.1. Particles prepared from veneer (approximately 4 × 40 × 1 mm^3) after immersion in approximately 150 mg of IL for 20 min at 110°C (left beech, right spruce, respectively). Fast swelling and disintegration can be only observed in EMIMAc. In DMIMDMP, the disintegration of spruce latewood is slower than in EMIMAc and cannot be observed above.

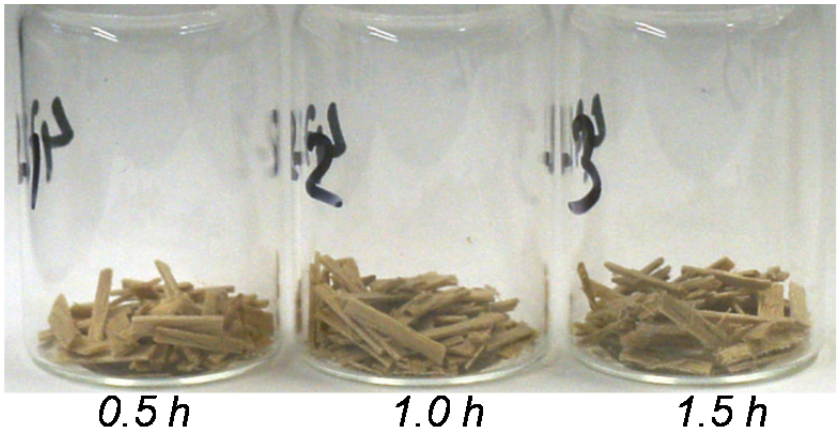

Figure C.2. The morphology of beech particles after treatment in BMIMCl after processing times up to 1.5 h. The shape and appearance of the wood is hardly changed (beech veneer 10 × 2 × 1 mm, 115°C, 500 rpm).

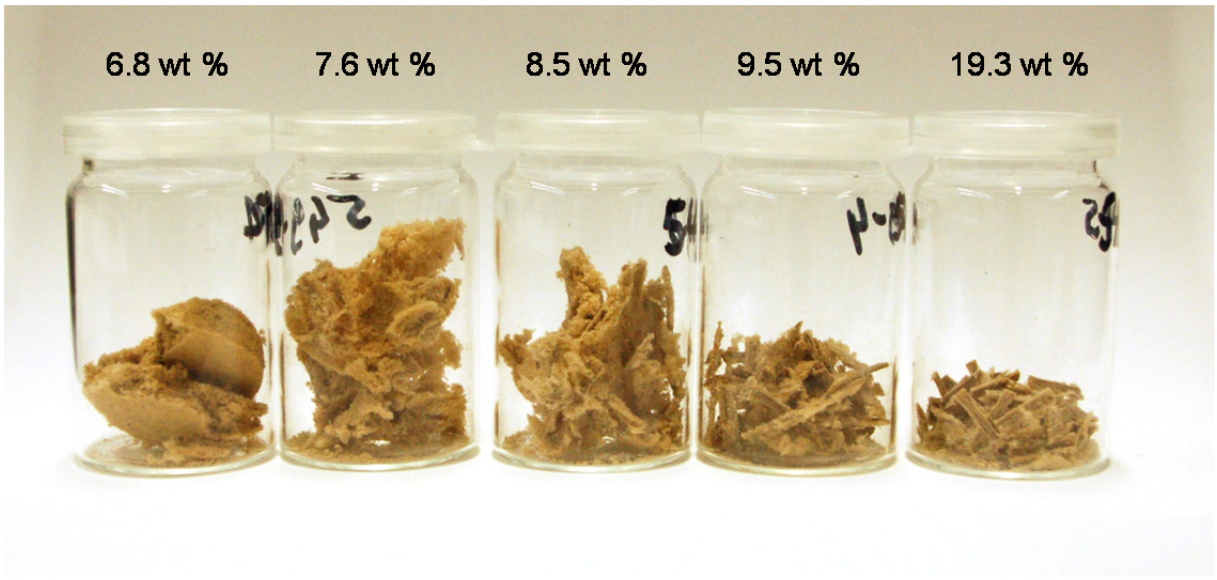

Figure C.3. Disintegration of beech chips at increasing water content. While the wood is completely disintegrated at 6.8 wt % of water in EMIMAc, the samples processed at 9.5 and 19.3 wt % are clearly not affected by the treatment. A transition is visible between 7.6 and 9.5 wt % so the limiting water concentration for disintegration is determined to be 8.5 wt % (EMIMAc, 115°C, 5 wt % load, 2 h, washed with acetone/water 1:1 (v/v)).

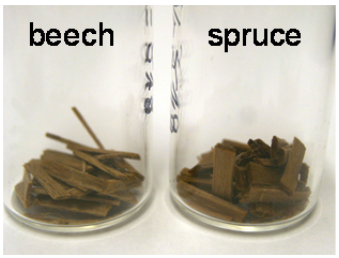

Figure C.4. Effect of 1-ethyl-2,3-dimethylimidazolium acetate on beech and spruce chips (10 × 2 × 1 mm^3). Except for a darkening, the treatment does not disintegrate beech or spruce as observed with EMIMAc. This demonstrates that the molecular effect of disintegration seems to be related to both the anion and the cation.

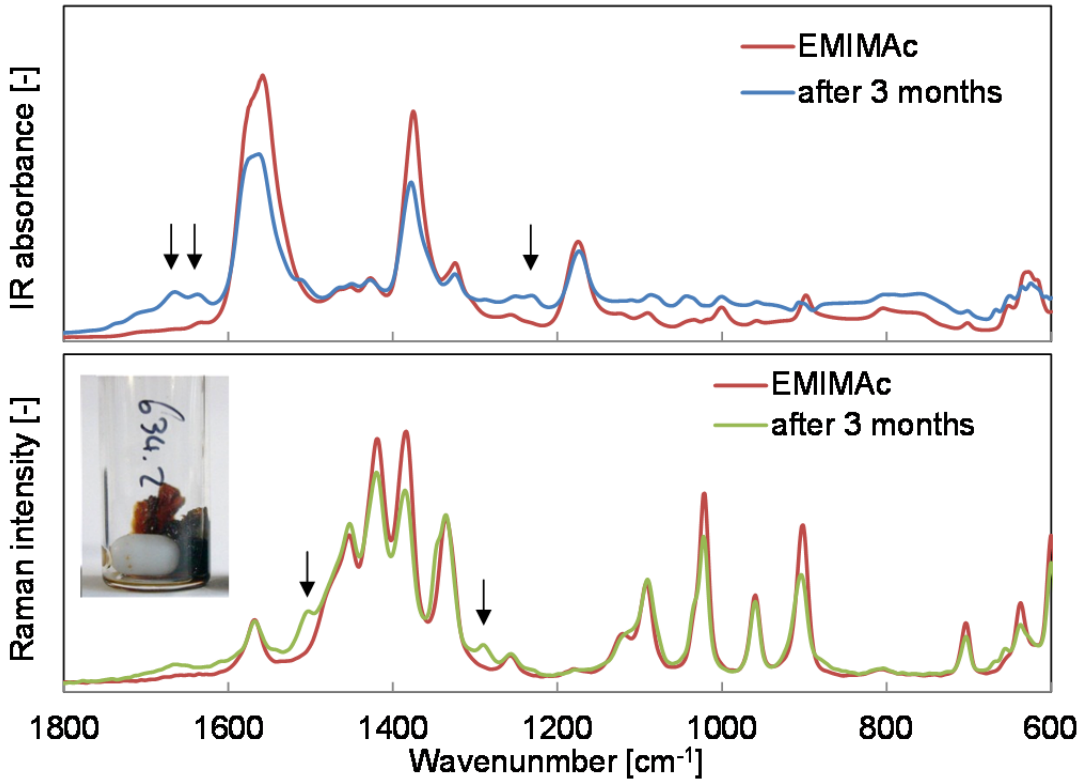

Figure C.5. FT IR spectra (top) and FT Raman spectra (bottom) of EMIMAc in its original state and after 3 months at 105°C. The latter spectra show differences in relative intensities and even peaks in addition to those of the original IL (indicated by the arrows). While the contribution in the IR spectrum at approximately 1639 cm^{-1} indicates the formation of water, the additional peaks at 1667 cm^{-1} and in the Raman spectrum clearly indicate the formation of other molecules after 3 months at 105°C, which implies a beginning decomposition of the EMIMAc. Nevertheless, the IL proved to disintegrate a beech chip after 3 months at 105°C as shown in the picture (cf. the original chip morphology in the preceding figures).

D Property data of EMIMAc and EMIMAc/H_2O

The following data are used to set up the property calculations for EMIMAc and its mixtures with water in Aspen Plus.

Properties of pure EMIMAc

The critical properties of T_C, V_C, p_C and ω were taken from estimations made by Valderrama & Rojas (2009) based on group contribution models. They pose consistent data as "if the properties were possible to be measured." The standard enthalpy of formation is taken from Shiflett et al. (2010), whose assumption is close to the value calculated by Verevkin et al. (2012). As no reaction with the IL is modeled, the Gibbs free energy of formation is set to zero; further values can be found in the paper of Preiss et al. (2010).

Table D.1. Miscellaneous properties of pure EMIMAc.

property	value
molecular weight M [-]	170.21
molecular structure	$C_8H_{14}N_2O_2$
density at 25°C ρ [g/cm^2]	1.1
normal boiling point T_B [K]	578.8
standard enthalpy of formation [J/kmol]	-200 × 10^6
standard Gibbs energy of formation G [J/kmol]	0
critical temperature T_C [K]	807.1
critical pressure p_C [bar]	29.2
critical compressibility factor Z_C [-]	0.2367
Pitzer acentric factor ω	0.5889
critical volume Vc [cm^3/mol]	544

Furthermore, the following model equations were utilized to calculate the temperature dependent properties. In some cases, the lack of data prompted to utilize parameters of other ILs, which is noted in the corresponding description. The identifier of the utilized property method in Aspen Plus is given in brackets; the choice of property equations in the property system is controlled by certain vectors (called THRSWT and TRNSWT) which settings are given when necessary.

The vapor pressure (PLXANT) of the IL is calculated using the extended Antoine equation.

$$\ln(p^{*,l}) = C_1 + \frac{C_2}{T + C_3} + C_4 T + C_5 \ln(T) + C_6 T^{C_7} \quad for\ C_8 \leq T \leq C_9$$

The vapor pressure is difficult to determine in the case of non-volatile ILs. However, a vapor pressure of ILs was detected, which is due to either a change in acid-base equilibrium or from evaporation of ion complexes (Earle et al., 2006). No such report could be found for EMIMAc. The normal boiling point T_B at atmospheric pressure and T_C at p_C did not give reliable data in the range 273–383 K, but overestimated the vapor pressure erroneously. Recently, a sophisticated setup with line-of-sight mass spectrometry enabled to obtain p,T data for $EMIMEtSO_4$ (Lovelock et al., 2010), which was used to approximate the vapor pressure of EMIMAc. The inferred parameters for the extended Antoine equation are displayed in the following table.

Table D.2. Antoine parameters to calculate the vapor pressure of EMIMAc.

parameter	value
C_1	28.661
C_2	-16,238
C_3	0
C_4	0
C_5	0
C_6	0
C_7	0
C_8	0
C_9	1000

The liquid molar volume (DNLDIP) is calculated using DIPPR, Eq. (105),

$$\rho^{*,l} = \frac{C_1}{C_2^{\left(1+\left(1-\frac{T}{C_3}\right)^{C_4}\right)}} \quad for\ C_6 \leq T \leq C_7 \ .$$

The parameters (cf. Table D.3) were fitted to data reported by Freire et al. (2011).

Table D.3. Parameters of DIPPR Eq. (105) to calculate the liquid volume (temperature in K, property units in kmol/m^3).

parameter	value
C_1	1.921
C_2	0.5071
C_3	807.1
C_4	0.5214
C_5	n/a
C_6	0
C_7	1000

The liquid heat capacity (CPLDIP) is calculated using DIPPR, Eq. (100),

$$c_p^{*,l} = C_1 + C_2 T + C_3 T^2 + C_4 T^3 + C_5 T^4 \ \ for\ C_6 \leq T \leq C_7.$$

The coefficients C_2 and C_3 were fitted to the temperature-dependent data for BMIMAc reported by Strechan et al. (2008). The parameter C_1 was determined by the heat capacity for EMIMAc given by Freire et al. (2011) (THRSWT/6=100, cf. Table D.4).

The heat of vaporization (DHVLDP) is calculated using DIPPR, Eq. (106),

$$\Delta H_{vap}^{*,l} = C_1 \left(1 - \frac{T}{T_c}\right)^{C_2 + C_3 \frac{T}{T_c} + C_4 \left(\frac{T}{T_c}\right)^2 + C_5 \left(\frac{T}{T_c}\right)^3} \quad for\ C_6 \leq T \leq C_7.$$

Similar to the vapor pressure, the heat of vaporization of ionic liquids is difficult to measure, but it has been calculated to describe the solvent-solute interaction (using the Hildebrandt parameter). Values of approximately 150 to 200 kJ/mol were reported for imidazolium-based ILs (Reichardt, 2005; Deyko et al., 2009), which exceeds the common values of molecular organic solvents by an order of magnitude. Revelli et al. (2009) estimated an enthalpy of vaporization of 124.2 kJ/mol at 333K.

Liu et al. (2010) calculated values of 189.578 kJ/kmol (300K) and 183.717 kJ/kmol (400K), which is very reasonable in this view and has been used for parameter estimation (THRSWT/4=106). Parameters are listed in Table D.5.

Table D.4. Parameters to calculate the liquid heat capacity (temperature in K, property units in kJ/kmol/K).

parameter	value
C_1	319.16222
C_2	-0.5123
C_3	0.001696
C_4	0
C_5	0
C_6	0
C_7	1000

Table D.5. Parameters to calculate the heat of vaporization (temperature in K, property units in kJ/kmol).

parameter	value
C_1	200100
C_2	0.1163
C_3	0
C_4	0
C_5	0
C_6	0
C_7	1000

Properties of EMIMAc/water mixtures

The activity coefficients of the EMIMAc/H_2O mixture are modeled using the NRTL equation (Renon & Prausnitz, 1968; Aspentech, 2012):

$$\ln(\gamma_i) = \frac{\sum_j x_j \tau_{ji} G_{ji}}{\sum_k x_k G_{ki}} + \sum_j \frac{x_j G_{ij}}{\sum_k x_k G_{kj}} \left(\tau_{ij} - \frac{\sum_m x_m \tau_{mj} G_{mj}}{\sum_k x_k G_{kj}} \right) \quad for\ C_7 \leq T \leq C_8,$$

$$G_{ij} = \exp\left(-\alpha_{ij}\tau_{ij}\right) \quad with\ G_{ii} = 1,$$

$$\tau_{ij} = a_{ij} + \frac{b_{ij}}{T} + e_{ij}\ln(T) + f_{ij}T \quad with\ \tau_{ii} = 0,$$

$$\alpha_{ij} = c_{ij} + d_{ij}(T - 273.15K).$$

The parameters a_{ij} and b_{ji} were obtained by simultaneous regression with data from VLE and heat capacity data of EMIMAc/H_2O mixtures as reported by Römich et al. (2012) at temperatures from 20–80°C. The regression employed the pure component vapor pressure of water only because the very small vapor pressures of EMIMAc caused numerical problems. The resulting parameters fit both the water vapor pressure and enthalpies very well (cf. Table D.6).

The property methods in Aspen Plus have to refer to the liquid reference state (cf. the routes DHL09, HV41 and HL09 in Aspen property routing). The change in enthalpy due to adiabatic mixing can be taken to validate the property data. For subcritical liquid mixtures, the specific enthalpy $h_m^l = \sum_i x_i h_i^{*,l} + h_m^{E,l}$ is then calculated from the

Table D.6. The NRTL parameters used to calculate the activity coefficient of EMIMAc/water mixtures (temperature in K, property units in J/mol).

parameter	value	value
i	water	EMIMAc
j	EMIMAc	water
a_{ij}	2.03326893	-4.03456924
b_{ij}	2834.64051	-443.034123
c_{ij}	0.251534977	0.251534977
d_{ij}	0	0
e_{ij}	0	0
f_{ij}	0	0
C_7	293.150	293.150
C_8	353.150	353.150

liquid pure component enthalpy h_i^l and the excess liquid enthalpy $h_m^{E,l}$. Real mixtures, and in particular ILs and water, exhibit rather high excess enthalpies during mixing. They are computed by using activity coefficients according to

$$h_m^{E,l} = -RT^2 \sum_i x_i \frac{\partial ln(\gamma_i)}{\partial T}.$$

To check the implemented property calculation, the temperature change during the mixing of EMIMAc and water was checked. The change of the liquid enthalpy of the mixture Δh_m^l and the temperature difference ΔT is related via the liquid mixture's heat capacity c_p^l as described by $\Delta h_m^l = m c_p \Delta T$. In the experiment, known quantities of water and EMIMAc were mixed at room temperature (~20°C) in an isolated centrifugal tube with slow stirring while the temperature was measured. The results are shown in Figure D.. Hall et al. (2012) conducted similar experiments at different mole fractions of water, which are given for comparison.

The activity coefficient model and the determined parameters compute a ΔT = 26°C, while the results of Hall et al. (2012) show an increase by 29°C. At other mole fractions of water the calculation gives comparable results as reported by the mentioned authors. Upon mixing the IL and water, an increase in the temperature of ΔT = 32 to 36°C at 90 mol % water is observed. Considering that the rough experiment is not conducted in a calorimeter, the difference seems acceptable. The small difference to literature data confirms the appropriate modeling of EMIMAc/water properties.

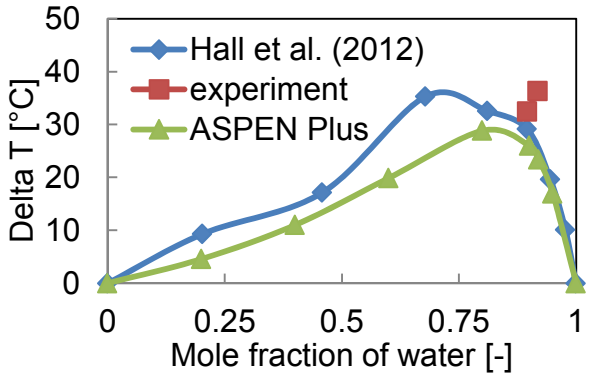

Figure D.1. The excess temperature $\Delta T = (T - T_{RT})$ as the difference to room temperature due to mixing of EMIMAc and water at different mole fractions.

E Process simulation data

This section provides supplementary data on the process simulation. In particular, the data utilized in the design of the pretreatment reaction is given to set up the pretreatment reactor R0. The complete flowsheet with all streams and unit operations is then shown (Figure E.1) to complement Figure 5.1, Figure 5.3 and Figure 5.4. The state and composition of all the streams in the simulation are given in Table E.2.

Table E.1. Conversion and yield data of wood components during pretreatment. The conversion shows how much lignin and hemicellulose are converted into liquid lignin or soluble components by hydrolysis of hemicellulose. The reactor yield is then calculated based on all components including water for implementation in the process simulation.

raw component	product component	conversion [wt %]	reactor yield [-]
cellulose	cellulose (solid)	100.00	0.3102
lignin	lignin (liquid)	9.52	0.0135
	lignin (solid)	90.48	0.1281
hemicellulose	hemicellulose	96.74	0.1761
	C_6 sugars	0.04	0.00
	C_5 sugars	5.17	0.0067
	furfural	0.00	0.00
	hydroxymethylfurfural	0.00	0.00
	acetic acid	0.00	0.00
others	others (solid)	0.00	0.00
	others (liquid)	100.00	0.0405
	water	100.00	0.3248

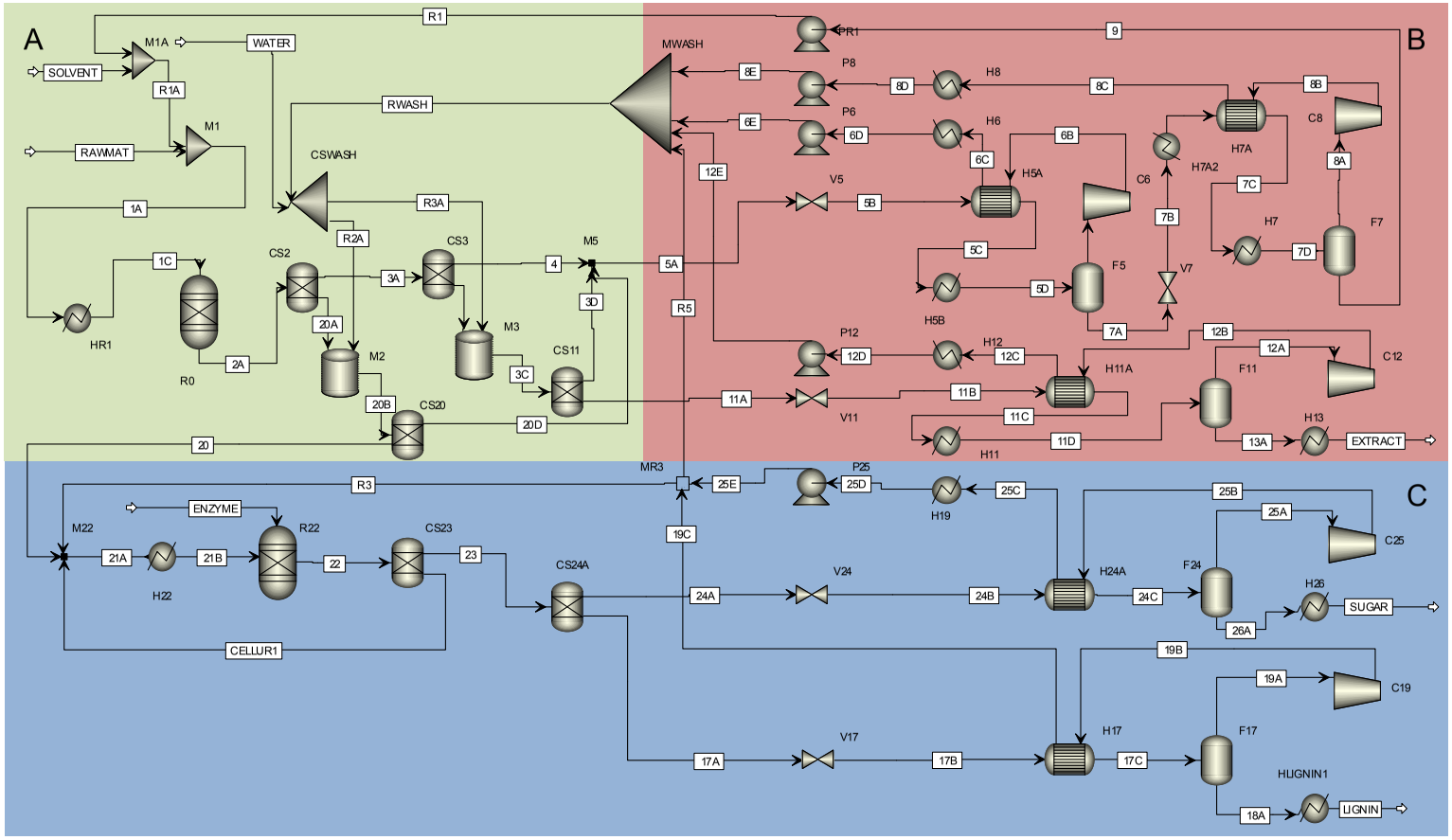

Figure E.1. Complete flowsheet of the designed IL pretreatment process including recycles and full energy integration. The different colors indicate different sections, i.e., pretreatment and fractionation (A), solvent recovery and extract purge (B), and enzymatic hydrolysis (C).

Table E.2. Process streams of the designed IL process depicted in Figure E.1.

	1A	1C	2A	3A	3B	3C	3D	4
Temperature [C]	110	115	115	115	115	71	71	115
Pressure [bar]	1.0	1.0	1.0	1.0	1.0	1.0	1.0	1.0
Vapor Frac	0.0	0.0	0.0	0.0	0.0	0.0	0.0	0.0
Mole Flow [kmol/hr]	577.7	577.7	577.8	576.8	7.0	319.3	125.0	569.7
Mass Flow [kg/hr]	72140.7	72140.7	72197.2	72016.5	471.6	6097.9	2251.9	71545.0
Volume Flow [m/hr]	70.5	70.8	70.8	70.7	0.3	6.0	2.4	70.8
Enthalpy [Gcal/hr]	-46.7	-46.5	-46.6	-46.5	-0.6	-21.7	-8.4	-45.9
Mass Flow [kg/hr]								
WATER	3015.7	3015.7	3009.9	3009.9	0.0	5626.3	2251.9	3009.9
CELLULOS	2875.0	2875.0	2874.3	0.0	0.0	0.0	0.0	0.0
LIGNIN	1312.5	1312.5	1312.2	125.0	125.0	125.0	0.0	0.0
HEMICELL	1687.5	1687.5	1632.1	562.4	562.4	562.4	0.0	0.0
GLUCOSE	0.0	0.0	0.0	0.0	0.0	0.0	0.0	0.0
OTHERS	375.0	375.0	374.9	374.9	374.9	374.9	0.0	0.0
EMIMAC	68750.0	68750.0	68750.0	68569.3	34.2	34.2	0.0	68535.1
CELLULASE	0.0	0.0	0.0	0.0	0.0	0.0	0.0	0.0
FURFURAL	0.0	0.0	0.0	0.0	0.0	0.0	0.0	0.0
XYLOSE	0.0	0.0	62.5	62.5	62.5	62.5	0.0	0.0

	5A	5B	5C	5D	6A	6B	6C	6D
Temperature [C]	120	98	113	113	113	464	100	100
Pressure [bar]	1.0	0.1	0.1	0.1	0.1	1.0	1.0	1.0
Vapor Frac	0.0	0.1	0.2	0.2	1.0	1.0	0.4	0.0
Mole Flow [kmol/hr]	1264.5	1264.5	1264.5	1264.5	313.2	313.2	313.2	313.2
Mass Flow [kg/hr]	84061.8	84061.8	84061.8	84061.8	5641.6	5641.6	5641.6	5641.6
Volume Flow [m/hr]	87.2	28611.2	87467.8	87467.8	87388.1	19186.6	3447.3	6.1
Enthalpy [Gcal/hr]	-92.7	-92.7	-89.8	-89.8	-17.9	-16.9	-19.9	-20.9
Mass Flow [kg/hr]								
WATER	15526.7	15526.7	15526.7	15526.7	5641.6	5641.6	5641.6	5641.6
CELLULOS	0.0	0.0	0.0	0.0	0.0	0.0	0.0	0.0
LIGNIN	0.0	0.0	0.0	0.0	0.0	0.0	0.0	0.0
HEMICELL	0.0	0.0	0.0	0.0	0.0	0.0	0.0	0.0
GLUCOSE	0.0	0.0	0.0	0.0	0.0	0.0	0.0	0.0
OTHERS	0.0	0.0	0.0	0.0	0.0	0.0	0.0	0.0
EMIMAC	68535.1	68535.1	68535.1	68535.1	0.0	0.0	0.0	0.0
CELLULASE	0.0	0.0	0.0	0.0	0.0	0.0	0.0	0.0
FURFURAL	0.0	0.0	0.0	0.0	0.0	0.0	0.0	0.0
XYLOSE	0.0	0.0	0.0	0.0	0.0	0.0	0.0	0.0

	6E	7A	7B	7C	7D	8A	8B	8C
Temperature [C]	100	113	76	115	115	115	733	77
Pressure [bar]	1.0	0.1	0.0	0.0	0.0	0.0	0.4	0.4
Vapor Frac	0.0	0.0	0.2	0.4	0.4	1.0	1.0	0.5
Mole Flow [kmol/hr]	313.2	951.4	951.4	951.4	951.4	404.3	404.3	404.3
Mass Flow [kg/hr]	5641.6	78420.2	78420.2	78420.2	78420.2	7284.1	7284.1	7284.1
Volume Flow [m/hr]	6.1	79.6	305778.0	930434.3	930434.3	934455.9	81511.5	13252.1
Enthalpy [Gcal/hr]	-20.9	-71.9	-71.9	-67.4	-67.4	-23.1	-20.8	-25.3
Mass Flow [kg/hr]								
WATER	5641.6	9885.1	9885.1	9885.1	9885.1	7284.1	7284.1	7284.1
CELLULOS	0.0	0.0	0.0	0.0	0.0	0.0	0.0	0.0
LIGNIN	0.0	0.0	0.0	0.0	0.0	0.0	0.0	0.0
HEMICELL	0.0	0.0	0.0	0.0	0.0	0.0	0.0	0.0
GLUCOSE	0.0	0.0	0.0	0.0	0.0	0.0	0.0	0.0
OTHERS	0.0	0.0	0.0	0.0	0.0	0.0	0.0	0.0
EMIMAC	0.0	68535.1	68535.1	68535.1	68535.1	0.0	0.0	0.0
CELLULASE	0.0	0.0	0.0	0.0	0.0	0.0	0.0	0.0
FURFURAL	0.0	0.0	0.0	0.0	0.0	0.0	0.0	0.0
XYLOSE	0.0	0.0	0.0	0.0	0.0	0.0	0.0	0.0

	8D	8E	9	11A	11B	11C	11D	12A
Temperature [C]	77	77	115	71	34	60	60	60
Pressure [bar]	0.4	1.0	0.0	1.0	0.1	0.1	0.1	0.1
Vapor Frac	0.0	0.0	0.0	0.0	0.1	0.9	0.9	1.0
Mole Flow [kmol/hr]	404.3	404.3	547.0	194.3	194.3	194.3	194.3	183.9
Mass Flow [kg/hr]	7284.1	7284.1	71136	3846.0	3846.0	3846.0	3846	3313.8
Volume Flow [m/hr]	7.7	7.7	70.2	3.7	6859.1	100607	100607	100606
Enthalpy [Gcal/hr]	-27.2	-27.2	-44.3	-13.3	-13.2	-11.4	-11.4	-10.6
Mass Flow [kg/hr]								
WATER	7284.1	7284.1	2601.1	3374.4	3374.4	3374.4	3374.4	3313.8
CELLULOS	0.0	0.0	0.0	0.0	0.0	0.0	0.0	0.0
LIGNIN	0.0	0.0	0.0	125.0	125.0	125.0	125.0	0.0
HEMICELL	0.0	0.0	0.0	562.4	562.4	562.4	562.4	0.0
GLUCOSE	0.0	0.0	0.0	0.0	0.0	0.0	0.0	0.0
OTHERS	0.0	0.0	0.0	374.9	374.9	374.9	374.9	0.0
EMIMAC	0.0	0.0	68535.1	34.2	34.2	34.2	34.2	0.0
CELLULASE	0.0	0.0	0.0	0.0	0.0	0.0	0.0	0.0
FURFURAL	0.0	0.0	0.0	0.0	0.0	0.0	0.0	0.0
XYLOSE	0.0	0.0	0.0	62.5	62.5	62.5	62.5	0.0

	12B	12C	12D	12E	13A	17A	17B	17C
Temperature [C]	144	46	46	46	60	50	50	90
Pressure [bar]	0.1	0.1	0.1	1.0	0.1	1.0	0.7	0.7
Vapor Frac	1.0	0.1	0.0	0.0	0.0	0.0	0.0	1.0
Mole Flow [kmol/hr]	183.9	183.9	183.9	183.9	10.4	194.1	194.1	194.1
Mass Flow [kg/hr]	3313.8	3313.8	3313.8	3313.8	532.2	3495.9	3495.9	3495.9
Volume Flow [m/hr]	63743.6	5532.4	3.4	3.4	0.4	3.6	3.6	8202.1
Enthalpy [Gcal/hr]	-10.4	-12.3	-12.5	-12.5	-0.9	-13.2	-13.2	-11.1
Mass Flow [kg/hr]								
WATER	3313.8	3313.8	3313.8	3313.8	60.6	3495.9	3495.9	3495.9
CELLULOS	0.0	0.0	0.0	0.0	0.0	83.0	83.0	83.0
LIGNIN	0.0	0.0	0.0	0.0	125.0	1187.2	1187.2	1187.2
HEMICELL	0.0	0.0	0.0	0.0	562.4	60.9	60.9	60.9
GLUCOSE	0.0	0.0	0.0	0.0	0.0	0.0	0.0	0.0
OTHERS	0.0	0.0	0.0	0.0	374.9	0.0	0.0	0.0
EMIMAC	0.0	0.0	0.0	0.0	34.2	0.0	0.0	0.0
CELLULASE	0.0	0.0	0.0	0.0	0.0	0.0	0.0	0.0
FURFURAL	0.0	0.0	0.0	0.0	0.0	0.0	0.0	0.0
XYLOSE	0.0	0.0	0.0	0.0	62.5	0.0	0.0	0.0

	18A	19A	19B	19C	20	20A	20B	20D
Temperature [C]	90	90	136	65	71	115	71	71
Pressure [bar]	0.7	0.7	1.0	1.0	1.0	1.0	1.0	1.0
Vapor Frac	0.0	1.0	1.0	0.0	0.0	0.0	0.0	0.0
Mole Flow [kmol/hr]	3.9	190.2	190.2	190.2	855.8	1.1	1425.5	569.8
Mass Flow [kg/hr]	69.9	3426.0	3426.0	3426.0	15578.3	180.7	25843.2	10265.0
Volume Flow [m/hr]	0.1	8202.1	6465.3	3.6	16.4	0.2	27.3	10.8
Enthalpy [Gcal/hr]	-0.3	-10.9	-10.8	-12.8	-57.7	-0.1	-96.1	-38.4
Mass Flow [kg/hr]								
WATER	69.9	3426.0	3426.0	3426.0	15397.5	0.0	25663	10265
CELLULOS	83.0	0.0	0.0	0.0	2874.3	2874.3	2874.3	0.0
LIGNIN	1187.2	0.0	0.0	0.0	1187.2	1187.2	1187.2	0.0
HEMICELL	60.9	0.0	0.0	0.0	1069.7	1069.7	1069.7	0.0
GLUCOSE	0.0	0.0	0.0	0.0	0.0	0.0	0.0	0.0
OTHERS	0.0	0.0	0.0	0.0	0.0	0.0	0.0	0.0
EMIMAC	0.0	0.0	0.0	0.0	180.7	180.7	180.7	0.0
CELLULASE	0.0	0.0	0.0	0.0	0.0	0.0	0.0	0.0
FURFURAL	0.0	0.0	0.0	0.0	0.0	0.0	0.0	0.0
XYLOSE	0.0	0.0	0.0	0.0	0.0	0.0	0.0	0.0

	21A	21B	22	23	24A	24B	24C	25A
Temperature [C]	69	50	50	50	50	50	60	60
Pressure [bar]	1.0	1.0	1.0	1.0	1.0	0.2	0.2	0.2
Vapor Frac	0.0	0.0	0.0		0.0	0.0	0.8	1.0
Mole Flow [kmol/hr]	1762.2	1762.2	1787.1	1787.1	1593.0	1593.0	1593.0	1346.1
Mass Flow [kg/hr]	31908	31907.6	35708	35708	32211.7	32212	32212	24251
Volume Flow [m/hr]	33.6	32.9	35.3		31.7	31.7	206400.9	205564.0
Enthalpy [Gcal/hr]	-118.9	-119.5	-125.9		-112.7	-112.7	-98.8	-77.4
Mass Flow [kg/hr]								
WATER	31727	31726.9	31781	31781	28285.4	28285	28285	24251
CELLULOS	2874.3	2874.3	83.0	83.0	0.0	0.0	0.0	0.0
LIGNIN	1187.2	1187.2	1187.2	1187.2	0.0	0.0	0.0	0.0
HEMICELL	1069.7	1069.7	60.9	60.9	0.0	0.0	0.0	0.0
GLUCOSE	0.0	0.0	2740.7	2740.7	2740.7	2740.7	2740.7	0.0
OTHERS	0.0	0.0	0.0	0.0	0.0	0.0	0.0	0.0
EMIMAC	180.7	180.7	180.7	180.7	180.7	180.7	180.7	0.0
CELLULASE	48.3	48.3	80.5	32.2	32.2	32.2	32.2	0.0
FURFURAL	0.0	0.0	0.0	0.0	0.0	0.0	0.0	0.0
XYLOSE	0.0	0.0	1004.9	1004.9	1004.9	1004.9	1004.9	0.0

	25B	25C	25D	25E	26A	CELLU	ENZY	EXTR
Temperature [C]	112	68	68	68	60			30
Pressure [bar]	0.3	0.3	0.3	1.0	0.2	1.0	1.0	1.0
Vapor Frac	1.0	0.0	0.0	0.0	0.0			0.0
Mole Flow [kmol/hr]	1346.1	1346.1	1346.1	1346.1	246.9	0.0	0.0	10.4
Mass Flow [kg/hr]	24251	24251	24251	24251	7960.9	0.0	0.0	532.2
Volume Flow [m/hr]	153931	982.7	25.5	25.5	6.8	0.0	0.0	0.4
Enthalpy [Gcal/hr]	-76.8	-90.7	-90.8	-90.8	-21.4			-0.9
Mass Flow [kg/hr]								
WATER	24251	24251	24251	24251	4034.6	0.0	0.0	60.6
CELLULOS	0.0	0.0	0.0	0.0	0.0	0.0	0.0	0.0
LIGNIN	0.0	0.0	0.0	0.0	0.0	0.0	0.0	125.0
HEMICELL	0.0	0.0	0.0	0.0	0.0	0.0	0.0	562.4
GLUCOSE	0.0	0.0	0.0	0.0	2740.7	0.0	0.0	0.0
OTHERS	0.0	0.0	0.0	0.0	0.0	0.0	0.0	374.9
EMIMAC	0.0	0.0	0.0	0.0	180.7	0.0	0.0	34.2
CELLULASE	0.0	0.0	0.0	0.0	32.2	48.3	32.2	0.0
FURFURAL	0.0	0.0	0.0	0.0	0.0	0.0	0.0	0.0
XYLOSE	0.0	0.0	0.0	0.0	1004.9	0.0	0.0	62.5

	LIGNI	R1	R1A	R2A	R3	R3A	R5	RAWM
Temperature [C]	30	115	115	68	67	68	67	25
Pressure [bar]	1.0	1.0	1.0	1.0	1.0	1.0	1.0	1.0
Vapor Frac	0.0	0.0	0.0	0.0	0.0	0.0	0.0	0.0
Mole Flow [kmol/hr]	3.9	547.0	548.4	1424.5	906.4	312.3	629.9	29.3
Mass Flow [kg/hr]	69.9	71136.2	71353.2	25662.5	16329.3	5626.3	11347.5	787.5
Volume Flow [m/hr]	0.1	70.2	70.4	27.0	17.1	5.9	11.9	0.6
Enthalpy [Gcal/hr]	-0.3	-44.3	-44.5	-96.1	-61.2	-21.1	-42.5	-2.1
Mass Flow [kg/hr]								
WATER	69.9	2601.1	2603.2	25662.5	16329.3	5626.3	11347.5	412.5
CELLULOS	83.0	0.0	0.0	0.0	0.0	0.0	0.0	2875.0
LIGNIN	1187.2	0.0	0.0	0.0	0.0	0.0	0.0	1312.5
HEMICELL	60.9	0.0	0.0	0.0	0.0	0.0	0.0	1687.5
GLUCOSE	0.0	0.0	0.0	0.0	0.0	0.0	0.0	0.0
OTHERS	0.0	0.0	0.0	0.0	0.0	0.0	0.0	375.0
EMIMAC	0.0	68535.1	68750.0	0.0	0.0	0.0	0.0	0.0
CELLULASE	0.0	0.0	0.0	0.0	0.0	0.0	0.0	0.0
FURFURAL	0.0	0.0	0.0	0.0	0.0	0.0	0.0	0.0
XYLOSE	0.0	0.0	0.0	0.0	0.0	0.0	0.0	0.0

	RWAS	SOLVE	SUGAR	WATE				
Temperature [C]	74	25	30	25				
Pressure [bar]	1.0	1.0	1.0	1.0				
Vapor Frac	0.0	0.0	0.0	0.0				
Mole Flow [kmol/hr]	1531.3	1.4	246.9	205.5				
Mass Flow [kg/hr]	27587	217.1	7960.9	3701.9				
Volume Flow [m/hr]	29.2	0.2	6.6	3.7				
Enthalpy [Gcal/hr]	-103.1	-0.1	-21.6	-14.0				
Mass Flow [kg/hr]								
WATER	27587	2.2	4034.6	3701.9				
CELLULOS	0.0	0.0	0.0	0.0				
LIGNIN	0.0	0.0	0.0	0.0				
HEMICELL	0.0	0.0	0.0	0.0				
GLUCOSE	0.0	0.0	2740.7	0.0				
OTHERS	0.0	0.0	0.0	0.0				
EMIMAC	0.0	214.9	180.7	0.0				
CELLULASE	0.0	0.0	32.2	0.0				
FURFURAL	0.0	0.0	0.0	0.0				
XYLOSE	0.0	0.0	1004.9	0.0				

F Pricing of raw materials

In addition to the discussion of a feasible price of EMIMAc in Section 5.1.2, this section compiles the prices of the other raw materials. As they are an essential part of the economic analysis to identify the potential of the designed process, a reasonable price of the raw materials is a perquisite for adequate evaluation. Therefore, the pricing is carried out by reviewing several references, which is depicted in the following.

Wood shows a rather broad range in the assumed price. Older publications report values of 22–61 $/t (Elliott et al., 1990; Galbe & Zacchi, 2002), but a projection of 92 $/t was made for Europe in 2020 (Wiesenthal et al., 2006). More recent results indicate prices of approximately 100 $/t (Michels, 2009; Perlack & Stokes, 2011). In this view, a price of 100 $/t is a reasonable value to assess realistic feedstock prices.

The main products are fermentable sugars and lignin. Whereas northern-bleached softwood pulp sells for approximately 900 $/t, the average world market price of raw sugars realized 493 $/t between 2008 and 2011 (OECD/FAO, 2011), but prices are projected to settle at approximately 400 $/t in the longer term. However, the purity of the produced sugars from wood fractionation processes in this work will be hardly competitive with conventional raw sugars. A more reasonable unit price can be based on molasses, which are priced at 165 $/t in the case of a sugar content of 50 wt % (Fischer & Zeier, 2011). This justifies a price of 330 $/t for both the pure C_6 and C_5 sugars produced. This price is also assumed for oligomeric hemicelluloses as they can be fed directly into fermentation processes as well.

Cellulases costs have decreased drastically in the last decade (Arato et al., 2005). The reported numbers still range from 1226 (Shafiei et al., 2011) to 4240 $/t, (Humbird et al., 2011). The lower bound seems to be too optimistic, hence, a value of 3000 $/t seems to be appropriate. After hydrolysis, the residual material consists mainly of lignin and some residual cellulose. Such a material would be utilized to substitute fossil fuels today, which would therefore value the residue according to its higher heating value of 26 MJ/kg for lignin and 16 MJ/kg for cellulose (Clymer, 2009). A revenue can then be calculated based on the price for coal of 90 $/t (ICIS, 2011).

However, the lignin might become a valuable source in the future. High value products such as vanillin can be envisioned in principle, which would sell at a price of 13,250 $/t. However, only low-value products are currently derived from (sulfonated)

bulk lignin without chemical utilization such as binder materials or additives selling at a price of 370 $/t have been successfully placed in the market place. Both types of products do not seem to be appropriate for biorefinery applications due to either the small market volume for vanillin of approximately 8000 t/a (Hocking, 1997) or the lack of exploiting the aromatic nature of lignin for producing higher valuable products chemically. The utilization of lignin as a surrogate in plastics is more valuable. A fraction of 22% of Kraft lignin was used in polybutadiene thermoplastics (Saito et al., 2012). Phenolic resins sell at approximately 4000 $/t (ICIS, 2011), which motivated a target price of 720 $/t of lignin in a recent study (Galbe & Zacchi, 2002). However, the substitution of 20–30 wt % of the resin by lignin (corresponding to an upper bound of 1200 $/t) as a filler can also be achieved with sulfonated lignin material (Kadam et al., 2008). Thus, the non-derivatized phenolic structure of lignin might substitute phenols (1540–1760 $/t) directly in polymerization. Clearly, the quality of lignin will be lower in comparison to phenols, so an average selling price of non-sulfonated lignin of 1000 $/t is assumed.

References

Ab Rani, M. A., Brant, A., Crowhurst, L., Dolan, A., Lui, M., Hassan, N. H., Hallett, J. P., Hunt, P. A., Niedermeyer, H., Perez–Arlandis, J. M., Schrems, M., Welton, T. & Wilding, R., 2011. Understanding the polarity of ionic liquids. *Phys. Chem. Chem. Phys.* 13, 16831–16840.

Abels, C., Redepenning, C., Moll, A., Melin, T. & Wessling, M., 2012. Simple purification of ionic liquid solvents by nanofiltration in biorefining of lignocellulosic substrates. *J. Membr. Sci.* 405–406, 1–10.

Abe, M., Fukaya, Y. & Ohno, H., 2010. Extraction of polysaccharides from bran with phosphonate or phosphinate-derived ionic liquids under short mixing time and low temperature. *Green Chem.* 12, 1274–1280.

Abraham, M. H., Grellier, P. L., Abboud, J. M., Doherty, R. M. & Taft, R. W., 1988. Solvent effects in organic chemistry – recent developments. *Can. J. Chem.* 66, 2673–2686.

Agarwal, U., Reiner, R. & Ralph, S., 2009. *Determination of cellulose I crystallinity by FT-Raman spectroscopy.* Oslo, Norway, Proceedings of the 15th International Symposium on Wood, Fiber and Pulping Chemistry, June 15 – 18.

Agarwal, U., Weinstock, I. & Atalla, R., 2003. FT-Raman spectroscopy for direct measurement of lignin concentrations in kraft pulps. *Tappi J.* 2, 22–26.

Alsmeyer, F., Koß, H. & Marquardt, W., 2004. Indirect spectral hard modeling for the analysis of reactive and interacting mixtures. *Appl. Spectrosc.* 58, 975–985.

Anantharaj, R. & Banerjee, T., 2012. Phase behavior of catalytic deactivated compounds and water with 1-ethyl-3-methylimidazolium acetate [EMIM][OAc] ionic liquid at T= 298.15 – 323.15 K and p = 1 bar. *J. Ind. Eng. Chem.* 18, 331–343.

Andersson, S., Serimaa, R., Paakkari, T., Saranpää, P. & Pesonen, E., 2003. Crystallinity of wood and the size of cellulose crystallites in Norway spruce (Picea abies). *J. Wood Sci.* 49, 531–537.

Arato, C., Pye, E. & Gjennestad, G., 2005. The lignol approach to biorefining of woody biomass to produce ethanol and chemicals. *Appl. Biochem. Biotechnol.* 123, 871–882.

Archer, W. L., 1991. Determination of Hansen solubility parameters for selected cellulose ether derivatives. *Ind. Eng. Chem. Res.* 30, 2292–2298.

Argyropoulos, D. & Menachem, S., 1997. Lignin. In: K. Eriksson, et al. eds. *Biotechnology in the Pulp and Paper Industry.* Springer: Berlin, pp 127–158.

Aspentech, 2012. *Aspen Physical Property System V7.3.2,* Aspen Technology: Burlington.

Atkins, P. & Julio, D. P., 2006. *Physical Chemistry.* Oxford University Press: New York.

Balensiefer, T., Schroeder, H., Freyer, S., D'andola, G. & Massonne, K., 2008. Method for producing glucose by enzymatic hydrolysis of cellulose that is obtained from material containing ligno-cellulose using and ionic liquic that comprises a polyatomic anion. DE Patent: WO 2008090156 A1.

Balogh, D., Curvelo, A. & De Groote, R., 1992. Solvent effects on organosolv lignin from Pinus caribaea hondurensis. *Holzforschung* 46, 343–348.

Bansal, P., Hall, M., Realff, M. J., Lee, J. H. & Bommarius, A. S., 2010. Multivariate statistical analysis of X-ray data from cellulose: A new method to determine degree of crystallinity and predict hydrolysis rates. *Bioresour. Technol.* 101, 4461-4471.

Barton, A., 1991. *CRC Handbook of Solubility Parameters and other Cohesion Parameters.* CRC Press: Boca Raton.

Beckham, G. T., Matthews, J. F., Peters, B., Bomble, Y. J., Himmel, M. E. & Crowley, M. F., 2011. Molecular-level origins of biomass recalcitrance: Decrystallization free energies for four common cellulose polymorphs. *J. Phys. Chem. B* 115, 4118–4127.

Belitz, H., Grosch, W. & Schieberle, P., 2008. *Lehrbuch der Lebensmittelchemie.* Springer: Berlin.

Bergius, F., 1933. The utilization of wood for the production of foodstuffs, alcohol, and glucose. *J. Soc. Chem. Ind.* 52, 1045–1052.

Bergius, F., 1937. Conversion of wood to carbohydrates. *Ind. Eng. Chem.* 29, 247–253.

Binder, J. B. & Raines, R. T., 2010. Fermentable sugars by chemical hydrolysis of biomass. *P. Natl. A. Sci.* 107, 4516–4521.

Blanch, H. W., Simmons, B. A. & Klein–Marcuschamer, D., 2011. Biomass deconstruction to sugars. *Biotechnol. J.* 6, 1086–1102.

Blechschmidt, J., Engert, P. & Stephan, M., 1986. The glass transition of wood from the viewpoint of mechanical pulping. *Wood Sci. Technol.* 20, 263–272.

Bochek, A., 2003. Effect of hydrogen bonding on cellulose solubility in aqueous and nonaqueous solvents. *Russ. J. Appl. Chem.* 76, 1711–1719.

Brandt, A., Grasvik, J., Hallett, J. P. & Welton, T., 2013. Deconstruction of lignocellulosic biomass with ionic liquids. *Green Chem.* 15, 550–583.

Brandt, A., Hallett, J., Leak, D., Murphy, R. & Welton, T., 2010. The effect of the ionic liquid anion in the pretreatment of pine wood chips. *Green Chemistry* 12, 672–679.

Brehm, M., Weber, H., Pensado, A. S., Stark, A. & Kirchner, B., 2012. Proton transfer and polarity changes in ionic liquid-water mixtures: a perspective on hydrogen bonds from ab initio molecular dynamics at the example of 1-ethyl-3-methylimidazolium acetate-water mixtures – Part 1. *Phys. Chem. Chem. Phys.* 14, 5030–5044.

Bunton, C. A., Mhala, M. M., Oldham, K. G. & Vernon, C. A., 1960. 660. The reactions of organic phosphates. Part III. The hydrolysis of dimethyl phosphate. *J. Chem. Soc.* 3293–3301.

Caffall, K. H. & Mohnen, D., 2009. The structure, function, and biosynthesis of plant cell wall pectic polysaccharides. *Carbohyd. Res.* 344, 1879–1900.

Casas, A., Omar, S., Palomar, J., Oliet, M., Alonso, M. V. & Rodriguez, F., 2013. Relation between differential solubility of cellulose and lignin in ionic liquids and activity coefficients. *RSC Adv.* 3, 3453–3460.

Cedergren, A. & Oraedd, C., 1994. Coulometric study of the influence of aldehydes and ketones on the Karl Fischer titration of water using standard pyridine/methanol reagents. *Anal. Chem.* 66, 2010–2016.

Cetinkol, Ö., Dibble, D., Cheng, G., Kent, M., Knierim, B., Auer, M., Wemmer, D., Pelton, J., Melnichenko, J., Ralph, J., Simmons, B. & Holmes, B., 2010. Understanding the impact of ionic liquid pretreatment on eucalyptus. *Biofuels* 1, 33–46.

Chang, V. S. & Holtzapple, M. T., 2000. Fundamental factors affecting biomass enzymatic reactivity. *Appl. Biochem. Biotechnol.* 84–86, 5–37.

Chemical Engineering, 2012. Economic indicators. *Chemical Engineering* 1, 56.

Chen, Q., Takao, K., Shinjiro, O., Masahiro, H. & Noriyuki, N., 2012. Dissolution and acetylation of ball-milled birch (Betula platyphylla) and bamboo (Phyllostachys nigra) in the ionic liquid [Bmim]Cl for HSQC NMR analysis. *Holzforschung* 66, 607–614.

Chen, T., Chidambaram, M., Liu, Z., Smit, B. & Bell, A., 2010. Viscosities of the mixtures of 1-ethyl-3-methylimidazolium chloride with water, acetonitrile and glucose: A molecular dynamics simulation and experimental study. *J. Phys. Chem. B* 114, 5790–5794.

Chrapava, S., Touraud, D., Rosenau, T., Potthast, A. & Kunz, W., 2003. The investigation of the influence of water and temperature on the LiCl/DMAc/cellulose system. *Phys. Chem. Chem. Phys.* 5, 1842–1847.

Clymer, J., 2009. *Heat of combustion & respiratory quotient calculation.* [Online] available at: http://home.fuse.net/clymer/rq/ [accessed 25.10.2012].

Colthup, N. B., Daly, L. H. & Wiberley, S. E., 1990. *Introduction to Infrared and Raman Spectroscopy, Third Edition.* Academic Press: New York.

Cox, B. J. & Ekerdt, J. G., 2013. Pretreatment of yellow pine in an acidic ionic liquid: Extraction of hemicellulose and lignin to facilitate enzymatic digestion. *Bioresource Technology* 134, 59–65.

Cremer, T., Kolbeck, C., Lovelock, K. R., Paape, N., Wölfel, R., Schulz, P. S., Wasserscheid, P., Weber, H., Thar, J., Kirchner, B., Maier, F. & Steinrück, H., 2010. Towards a molecular understanding of cation-anion interactions – probing the electronic structure of imidazolium ionic liquids by NMR spectroscopy, X-ray photoelectron spectroscopy and theoretical calculations. *Chem. Eur. J.* 16, 9018–9033.

Crowhurst, L., Mawdsley, P. R., Perez–Arlandis, J. M., Salter, P. A. & Welton, T., 2003. Solvent–solute interactions in ionic liquids. *Phys. Chem. Chem. Phys.* 5, 2790–2794.

Cruz, H., Fanselow, M., Holbrey, J. D. & Seddon, K. R., 2012. Determining relative rates of cellulose dissolution in ionic liquids through in situ viscosity measurement. *Chem. Commun.* 48, 5620–5622.

Cuissinat, C. & Navard, P., 2008a. Swelling and dissolution of cellulose, Part III: plant fibres in aqueous systems. *Cellulose* 15, 67–74.

Cuissinat, C., Navard, P. & Heinze, T., 2008b. Swelling and dissolution of cellulose, Part IV: Free floating cotton and wood fibres in ionic liquids. *Carbohydr. Polym.* 72, 590–596.

da Silva, A. S., Lee, S.-H., Endo, T. & Bon, E. P., 2011. Major improvement in the rate and yield of enzymatic saccharification of sugarcane bagasse via pretreatment with the ionic liquid 1-ethyl-3-methylimidazolium acetate ([Emim] [Ac]). *Bioresour. Technol.* 102, 10505–10509.

Dadi, A., Varanasi, S. & Schall, C., 2006. Enhancement of cellulose saccharification kinetics using an ionic liquid pretreatment step. *Biotechnol. Bioeng.* 5, 904–910.

Davidson, D., 1942. The indicator method of classifying acids and bases in qualitative organic analysis. *Journal of Chemical Education* 19, 221-226.

Deyko, A., Lovelock, K. R. J., Corfield, J., Taylor, A. W., Gooden, P. N., Villar–Garcia, I. J., Licence, P., Jones, R. G., Krasovskiy, V. G., Chernikova, E. A. & Kustov, L. M., 2009. Measuring and predicting $\Delta_{\mathrm{vap}}\mathrm{H}^{298}$ values of ionic liquids. *Phys. Chem. Chem. Phys.* 11, 8544–8555.

Dibble, D. C., Li, C., Sun, L., George, A., Cheng, A., Cetinkol, O. P., Benke, P., Holmes, B. M., Singh, S. & Simmons, B. A., 2011. A facile method for the recovery of ionic liquid and lignin from biomass pretreatment. *Green Chem.* 13, 3255–3264.

Ding, S. & Himmel, M., 2006. The maize primary cell wall microfibril: A new model derived from direct visualization. *J. Agric. Food Chem.* 54, 597–606.

Ding, Z., Chi, Z., Gu, W., Gu, S., Liu, J. & Wang, H., 2012. Theoretical and experimental investigation on dissolution and regeneration of cellulose in ionic liquid. *Carbohydr. Polym.* 89, 7–16.

Doherty, T. V., Mora–Pale, M., Foley, S. E., Linhardt, R. J. & Dordick, J. S., 2010. Ionic liquid solvent properties as predictors of lignocellulose pretreatment efficacy. *Green Chemistry* 12, 1967–1975.

Donaldson, L., 1985. Critical assessment of interference microscopy as a technique for measuring lignin distribution in cell walls. *New Zeal. J. For. Sci.* 15, 349–360.

Donaldson, L., 2001. Lignification and lignin topochemistry – an ultrastructural view. *Phytochemistry* 57, 859–873.

Dong, K. & Zhang, S., 2012. Hydrogen bonds: A structural insight into ionic liquids. *Chem. Eur. J.* 18, 2748–2761.

Du, H. & Qian, X., 2011. The effects of acetate anion on cellulose dissolution and reaction in imidazolium ionic liquids. *Carbohydr. Res.* 346, 1985–1990.

Earle, M., Esperanca, J., Gilea, M., Canongia Lopes, J., Rebelo, L., Magee, J., Seddon, K. & Widegreen, J., 2006. The distillation and volatility of ionic liquids. *Nature* 439, 831–834.

Ebner, G., Schiehser, S., Potthast, A. & Rosenau, T., 2008. Side reaction of cellulose with common 1-alkyl-3-methylimidazolium-based ionic liquids. *Tetrahedron Lett.* 49, 7322–7324.

EEX, 2011. *European Energy Exchange AG.* [Online] available at: http://www.eex.com/de [accessed 25.08.2011].

Eggemann, T. & Elander, R., 2005. Process and economic analysis of pretreatment technologies. *Bioresour. Technol.* 96, 2019–2025.

Ekenstam, A., 1936. Über das Verhalten der Cellulose in Mineralsäure-Lösungen, I. Mitteil.: Die Bestimmung des Molekulargewichts in Phosphorsäure-Lösung. *Ber. Dtsch. Chem. Ges. (A and B Series)* 69, 549–552.

El Seoud, O. A., da Silva, V. C., Possidonio, S., Casarano, R., Areas, E. P. G. & Gimenes, P., 2011. Microwave–assisted derivatization of cellulose, 2 – The surprising effect of the structure of ionic liquids on the dissolution and acylation of the biopolymer. *Macromol. Chem. Phys.* 212, 2541–2550.

Elliott, D., Baker, E., Beckman, D., Solantausta, Y., Tolenhiemo, V., Gevert, S., Hörnell, C., Östman, A. & Kjellström, B., 1990. Technoeconomic assessment of direct biomass liquefaction to transportation fuels. *Biomass* 22, 251–269.

Engel, P., Mladenov, R., Wulfhorst, H., Jäger, G. & Spiess, A., 2010. Point by point analysis: how ionic liquid affects the enzymatic hydrolysis of native and modified cellulose. *Green Chemistry* 12, 1959–1966.

Faith, W. L., 1945. Development of the Scholler process in the United States. *Ind. Eng. Chem.* 37, 9–11.

Fan, L., Gharpuray, M. M. & Lee, Y., 1987. *Cellulose Hydrolysis (Biotechnology Monographs).* Springer: Berlin.

Felbab, N., Patel, B., El–Halwagi, M., Hildebrandt, D. & Glasser, D., 2013. Vapor recompression for efficient distillation. 1. A new synthesis perspective on standard configurations. *AIChE J.* 59, 2977–2992.

Fendt, S., Padmanabhan, S., Blanch, H. & Prausnitz, J., 2011. Viscosities of acetate or chloride–based ionic liquids and some of their mixtures with water or other common solvents. *J. Chem. Eng. Data* 56, 31–34.

Fengel, D. & Wegener, G., 1989. *Wood: chemistry, ultrastructure, reactions.* de Gruyter: Berlin.

Ficke, L. E., Rodríguez, H. & Brennecke, J. F., 2008. Heat capacities and excess enthalpies of 1-ethyl-3-methylimidazolium-based ionic liquids and water. *J. Chem. Eng. Data* 53, 2112–2119.

Fidale, L., Köhler, S., Prechtl, M., Heinze, T. & Seoud, O., 2006. Simple, expedient methods for the determination of water and electrolyte contents of cellulose solvent systems. *Cellulose* 13, 581–592.

Fink, H., Hofmann, D. & Philipp, B., 1995. Some aspects of lateral chain order in cellulosics from X-ray scattering. *Cellulose* 2, 51–70.

Fischer, M. & Zeier, J., 2011. *Marktbericht Melasse September 2011,* DMH Deutsche Melasse Handelsgesellschaft mbH: Hamburg.

Fischer, S., Leipner, H., Thümmler, K., Brendler, E. & Peters, J., 2003. Inorganic molten salts as solvents for cellulose. *Cellulose* 10, 227–236.

Flory, P. J., 1942. Thermodynamics of high polymer solutions. *J. Chem. Phys.* 10, 51–61.

Fort, D., Remsing, R., Swatloski, R., Moyna, P., Moyna, G. & Rogers, R., 2007. Can ionic liquids dissolve wood? Processing and analysis of lignocellulosic materials with 1-n-butyl-3-methylimidazolium chloride. *Green Chem.* 9, 63–69.

Freire, M. G., Teles, A. R. R., Rocha, M. A. A., Schröder, B., Neves, C. M. S. S., Carvalho, P. J., Evtuguin, D. V., Santos, L. M. N. B. F. & Coutinho, J. A. P., 2011. Thermophysical characterization of ionic liquids able to dissolve biomass. *J. Chem. Eng. Data* 56, 4813–4822.

Fröba, A., Rausch, M., Krzeminski, K., Assenbaum, D., Wasserscheid, P. & Leipertz, A., 2010. Thermal conductivity of ionic liquids: Measurement and prediction. *Int. J. Thermophys.* 31, 2059–2077.

Fromm, J., Rockel, B., Lautner, S., Windeisen, E. & Wanner, G., 2003. Lignin distribution in wood cell walls determined by TEM and backscattered SEM techniques. *J. Struct. Biol.* 143, 77–84.

Froschauer, C., Hummel, M., Iakovlev, M., Roselli, A., Schottenberger, H. & Sixta, H., 2013. Separation of Hemicellulose and Cellulose from Wood Pulp by Means of Ionic Liquid/Cosolvent Systems. *Biomacromolecules* 14, 1741–1750.

Froschauer, C., Hummel, M., Laus, G., Schottenberger, H., Sixta, H., Weber, H. K. & Zuckerstätter, G., 2012. Dialkyl phosphate-related ionic liquids as selective solvents for xylan. *Biomacromolecules* 13, 1973-1980.

Fujita, M. & Harada, H., 2000. Ultrastructure and formation of wood cell wall. In: D. N. Hon, ed. *Wood and Cellulosic Chemistry.* Marcel Dekker: New York. pp 1–50.

Fukaya, Y., Hayashi, K., Wada, M. & Ohno, H., 2008. Cellulose dissolution with ionic liquids under mild conditions: required factors for anions. *Green Chem.* 10, 44–46.

Fukaya, Y., Sugimoto, A. & Ohno, H., 2006. Superior solubility of polysaccharides in low viscosity, polar, and halogen-free 1,3-dialkylimidazolium formates. *Biomacromolecules* 7, 3295–3297.

Fukazawa, K., Revol, J.-F., Jurasek, L. & Goring, D., 1982. Relationship between ball milling and the susceptibility of wood to digestion by cellulase. *Wood Sci. Technol.* 16, 279–285.

Galbe, M. & Zacchi, G., 2002. A review of the production of ethanol from softwood. *Appl. Microbiol. Biotechnol.* 59, 618–628.

Galbe, M. & Zacchi, G., 2007. Pretreatment of Lignocellulosic Materials for Efficient Bioethanol Production. In: L. Olsson, ed. *Biofuels.* Springer, Berlin. pp 41–65.

García, V., Valkama, H., Sliz, R., King, A. W., Myllylä, R., Kilpeläinen, I. & Keiski, R. L., 2013. Pervaporation recovery of [AMIM]Cl during wood dissolution; effect of [AMIM]Cl properties on the membrane performance. *J. Membr. Sci.* 444, 9–15.

Gazit, O. M. & Katz, A., 2012. Dialkylimidazolium ionic liquids hydrolyze cellulose under mild conditions. *ChemSusChem* 5, 1542–1548.

George, A., Tran, K., Morgan, T. J., Benke, P. I., Berrueco, C., Lorente, E., Wu, B. C., Keasling, J. D., Simmons, B. A. & Holmes, B. M., 2011. The effect of ionic liquid cation and anion combinations on the macromolecular structure of lignins. *Green Chem.* 13, 3375–3385.

Gericke, M., Liebert, T., El Seoud, O. A. & Heinze, T., 2011. Tailored media for homogeneous cellulose chemistry: Ionic liquid/co–solvent mixtures. *Macromol. Mater. Eng.* 296, 483–493.

Girisuta, B., Janssen, L. P. B. M. & Heeres, H. J., 2007. Kinetic study on the acid–catalyzed hydrolysis of cellulose to levulinic acid. *Ind. Eng. Chem. Res.* 46, 1696–1708.

Glasser, W. G., Atalla, R. H., Blackwell, J., Malcolm Brown, R. J., Burchard, W., French, A. D., Klemm, D. O. & Nishiyama, Y., 2012. About the structure of cellulose: debating the Lindman hypothesis. *Cellulose* 19, 589–598.

Goldstein, I., 1980. The hydrolysis of wood. *Tappi J.* 63, 141–143.

Goldstein, I. & Easter, J., 1992. An improved process for converting cellulose to ethanol. *Tappi J.* 75, 135–140.

Gray, M. C., Converse, A. O. & Wyman, C. E., 2007. Solubilities of oligomer mixtures produced by the hydrolysis of xylans and corn stover in water at 180°C. *Ind. Eng. Chem. Res.* 46, 2383–2391.

Green, D. & Perry, R., 2008. *Perry's Chemical Engineers' Handbook, Eighth Edition.* McGraw–Hill Professional: New York.

Guo, J., Zhang, D., Duan, C. & Liu, C., 2010. Probing anion-cellulose interactions in imidazolium-based room temperature ionic liquids: a density functional study. *Carbohydr. Res.* 345, 2201–2205.

Guthrie, K., 1969. Data and techniques for preliminary capital cost estimating. *Chem. Eng.* 76, 114–142.

Hall, C. A., Le, K. A., Rudaz, C., Radhi, A., Lovell, C. S., Damion, R. A., Budtova, T. & Ries, M. E., 2012. Macroscopic and microscopic study of 1-ethyl-3-methylimidazolium acetate-water mixtures. *J. Phys. Chem. B* 116, 12810–12818.

Hallett, J. P. & Welton, T., 2011. Room-temperature ionic liquids: Solvents for synthesis and catalysis. 2. *Chem. Rev.* 111, 3508–3576.

Hall, M., Bansal, P., Lee, J., Realff, M. & Bommarius, A., 2010. Cellulose crystallinity – a key predictor of the enzymatic hydrolysis rate. *FEBS J.* 277, 1571–1582.

Hansen, C. & Björkman, A., 1998. The ultrastructure of wood from a solubility parameter point of view. *Holzforschung* 52, 335–344.

Hanus, J. & Mazeau, K., 2006. The xyloglucan–cellulose assembly at the atomic scale. *Biopolymers* 82, 59–73.

Harris, E. E. & Beglinger, E., 1946. Madison wood sugar process. *Ind. Eng. Chem.* 38, 890–895.

Hauru, L. K. J., Hummel, M., King, A. W. T., Kilpeläinen, I. & Sixta, H., 2012. Role of solvent parameters in the regeneration of cellulose from ionic liquid solutions. *Biomacromolecules* 13, 2896–2905.

Heinze, T., Schwikal, K. & Barthel, S., 2005. Ionic liquids as reaction medium in cellulose functionalization. *Macromol. Biosci.* 5, 520–525.

Hergert, H. L., 1997. Developments in organosolv pulping – An overview. In: M. Akhtar & R. A. Young, eds. *Environmentally Friendly Technologies for the Pulp and Paper Industry.* Wiley, New York, pp 5–68.

Hildebrand, J. H., 1916. Solubility. *J. Am. Chem. Soc.* 38, 1452–1473.

Hocking, M. B., 1997. Vanillin: Synthetic flavoring from spent sulfite liquor. *J. Chem. Educ.* 74, 1055–1059.

Holladay, J., Bozell, J., Johnson, D. & White, J., 2007. *Top value-added chemicals from biomass, II: Results of screening for potential candidates from biorefinery lignin,* Pacific Northwest National Laboratory (PNNL) and the National Renewable Energy Laboratory (NREL): Richland.

Holloczki, O., Gerhard, D., Massone, K., Szarvas, L., Nemeth, B., Veszpremi, T. & Nyulaszi, L., 2010. Carbenes in ionic liquids. *New J. Chem.* 34, 3004–3009.

Hon, D. N., 2000. *Wood and Cellulosic Chemistry.* Marcel Dekker: New York.

Huddleston, J., Visser, A., Reichert, W., Willauer, H., Broker, G. & Rogers, R., 2001. Characterization and comparison of hydrophilic and hydrophobic room temperature ionic liquids incorporating the imidazolium cation. *Green Chem.* 3, 156–164.

Hudson, S. M. & Cuculo, J. A., 1980. The solubility of unmodified cellulose: A critique of the literature. *J. Macromol. Sci. C: Pol. R.* 18, 1–82.

Hu, F., Jung, S. & Ragauskas, A., 2012. Pseudo-lignin formation and its impact on enzymatic hydrolysis. *Bioresour. Technol.* 117, 7–12.

Humbird, D., Davis, R., Tao, L., Kinchin, C., Hsu, D., Aden, A., Schoen, P., Lukas, J., Olthof, B., Worley, M., Sexton, D. & Dudgeon, D., 2011. Process design and economics for biochemical conversion of lignocellulosic biomass to ethanol: Dilute–acid pretreatment and enzymatic hydrolysis of corn stover, National Renewable Energy Laboratory (NREL): Golden.

Hyvärinen, S., Virtanen, P., Murzin, D. Y. & Mikkola, J., 2010. Towards ionic liquid fractionation of lignocellulosics for fermentable sugars. *Cellul. Chem. Technol.* 44, 187–195.

IChemE, 2011. *Cost of process utilities.* [Online] available at: http://ed.icheme.org/costutil.html [accessed 25.08.2011].

ICIS, 2011. *Indicative chemical prices.* [Online] available at: http://www.icis.com [accessed 25.08.2011].

Iguchi, M., Aida, T. M., Watanabe, M. & Smith Jr, R., 2013. Dissolution and recovery of cellulose from 1-butyl-3-methylimidazolium chloride in presence of water. *Carbohyd. Polym.* 92, 651–658.

Ikeda, T., Holtman, K., Kadla, J., Chang, H. & Jameel, H., 2002. Studies on the effect of ball milling on lignin structure using a modified DFRC method. *J. Agr. Food Chem.* 50, 129–135.

Ishii, T. & Shimizu, K., 2000. Chemistry of Cell Wall Polysaccharides. In: D. N. Hon, ed. *Wood and Cellulosic Chemistry.* Marcel Dekker: New York, pp 175–212.

Isogai, A. & Atalla, R., 1998. Dissolution of Cellulose in aqueous NaOH solutions. *Cellulose* 5, 309–319.

Jäger, G., Wu, Z., Garschhammer, K., Engel, P., Klement, T., Rinaldi, R., Spiess, A. & Büchs, J., 2010. Practical screening of purified cellobiohydrolases and endoglucanases with alpha–cellulose and specification of hydrodynamics. *Biotechnol. Biofuels* 3, 1–12.

Janesko, B. G., 2011. Modeling interactions between lignocellulose and ionic liquids using DFT-D. *Phys. Chem. Chem. Phys.* 13, 11393–11401.

Jayme, G. & Azzola, F. K., 1965. Textur und Topochemie der Tüpfel und Tüpfelschließhäute von Buchenholzzellen (Fagus sylvatica L.). *Holz Roh. Werkst.* 23, 41–49.

Jessop, P. G., Jessop, D. A., Fu, D. & Phan, L., 2012. Solvatochromic parameters for solvents of interest in green chemistry. *Green Chem.* 14, 1245–1259.

Jessop, P., Phan, L., Carrier, A., Robinson, S., Dürr, C. & Harjani, J., 2010. A solvent having switchable hydrophilicity. *Green Chem.* 12, 809–814.

Jimenez de la Parra, C., Navarrete, A., Dolores Bermejo, M. & Jose Cocero, M., 2012. Patents Review on Lignocellulosic Biomass Processing Using Ionic Liquids. *Recent Patents on Engineering* 6, 159–181.

Ji, W., Ding, Z., Liu, J., Song, Q., Xia, X., Gao, H., Wang, H. & Gu, W., 2012. Mechanism of lignin dissolution and regeneration in ionic liquid. *Energy Fuels* 26, 6393–6403.

Kacuráková, M., Wellner, N., Ebringerová, A., Hromadková, Z., Wilson, R. & Belton, P., 1999. Characterisation of xylan-type polysaccharides and associated cell wall components by FT-IR and FT-Raman spectroscopies. *Food Hydrocolloid.* 13, 35–41.

Kadam, K., Chin, C. & Brown, L., 2008. Flexible biorefinery for producing fermentation sugars, lignin and pulp from corn stover. *J. Ind. Microbiol. Biot.* 35, 331–341.

Kadla, J. & Dai, Q., 2006. Pulp. In: *Kirk–Othmer Encyclopedia of Chemical Technology.* John Wiley & Sons: New York.

Kahlen, J., Masuch, K. & Leonhard, K., 2010. Modelling cellulose solubilities in ionic liquids using COSMO–RS. *Green Chem.* 12, 2172–2181.

Kail, N., Marquardt, W. & Briesen, H., 2009. Process analysis by means of focused beam reflectance measurements. *Ind. Eng. Chem. Res.* 48, 2936–2946.

Kamimura, A., Okagawa, T., Oyama, N., Otsuka, T. & Yoshimoto, M., 2012. Combination use of hydrophobic ionic liquids and LiCl as a good reaction system for the chemical conversion of cellulose to glucose. *Green Chem.* 14, 2816–2820.

Kamlet, M. J., Abboud, J. L. & Taft, R. W., 1977. The solvatochromic comparison method. 6. The pi* scale of solvent polarities. *J. Am. Chem. Soc.* 99, 6027–6038.

Kamlet, M. J., Doherty, R. M., Famini, G. R. & Taft, R. W., 1987. Linear solvation energy relationships. Local empirical rules – or fundamental laws of chemistry? The dialogue continues. A challenge to the chemometricians. *Acta Chem. Scand. B* 41, 589–598.

Kamlet, M. J., Kayser, E. G., Eastes, J. W. & Gilligan, W. H., 1973. Hydrogen bonding by protic solvents to nitro oxygens. Effects on electronic spectra of nitroaniline derivatives. *J. Am. Chem. Soc.* 95, 5210–5214.

Kamlet, M. & Taft, R., 1976a. The solvatochromic comparison method. I. The beta scale of solvent hydrogen–bond acceptor (HBA) basicities. *J. Am. Chem. Soc.* 98, 377–383.

Kamlet, M. & Taft, R., 1976b. The solvatochromic comparison method. I. The alpha scale of solvent hydrogen–bond donor (HBA) acidities. *J. Am. Chem. Soc.* 98, 2886–2894.

Kamm, B., Kamm, M., Gruber, P. & Kromus, S., 2006. Biorefinery systems – an overview. In: *Biorefineries – Industrial Processes and Products.* Wiley–VCH: Weinheim, pp 3–40.

Kasarova, S. N., Sultanova, N. G., Ivanov, C. D. & Nikolov, I. D., 2007. Analysis of the dispersion of optical plastic materials. *Opt. Mater.* 29, 1481–1490.

Katritzky, A. R., Fara, D. C., Yang, H., Tämm, K., Tamm, T. & Karelson, M., 2004. Quantitative measures of solvent polarity. *Chem. Rev.* 104, 175–198.

Katzen, R. & Othmer, D. F., 1942. Wood hydrolysis. A continuous process. *Ind. Eng. Chem.* 34, 314–322.

Keil, P., Kick, M. & König, A., 2012. Long-term stability, regeneration and recycling of imidazolium–based ionic liquids. *Chem. Ing. Tech.* 84, 859–866.

Kessler, M. A. & Wolfbeis, O. S., 1989. ET(33), a solvatochromic polarity and micellar probe for neutral aqueous solutions. *Chem. Phys. Lipids* 50, 51–56.

Khupse, N. D. & Kumar, A., 2011. Delineating solute-solvent interactions in binary mixtures of ionic liquids in molecular solvents and preferential solvation approach. *J. Phys. Chem. B* 115, 711–718.

Kilpeläinen, I., Xie, H., King, A., Grainstrom, M., Heikkinen, S. & Argyropoulos, D., 2007. Dissolution of wood in ionic liquids. *J. Agric. Food Chem.* 55, 9142–9148.

King, A. W. T., Asikkala, J., Mutikainen, I., Järvi, P. & Kilpeläinen, I., 2011. Distillable acid-base conjugate ionic liquids for cellulose dissolution and processing. *Angew. Chem. Int. Edit.* 50, 6301–6305.

Klähn, M., Stüber, C., Seduraman, A. & Wu, P., 2010. What determines the miscibility of ionic liquids with water? Identification of the underlying factors to enable a straightforward prediction. *J. Phys. Chem. B* 114, 2856–2868.

Kleinert, T. & v. Tayenthal, K., 1931. Über neuere Versuche zur Trennung von Cellulose und Inkrusten verschiedener Hölzer. *Angew. Chem.* 44, 788–791.

Klein–Marcuschamer, D., Simmons, B. A. & Blanch, H. W., 2011. Techno-economic analysis of a lignocellulosic ethanol biorefinery with ionic liquid pre-treatment. *Biofuels, Bioprod. Bioref.* 5, 562–569.

Klemm, D., Heublein, B., Fink, H. & Bohn, A., 2005. Cellulose: Fascinating biopolymer and sustainable raw material. *Angew. Chem. Int. Edit.* 44, 3358–3393.

Klemm, D., Phili, B., Heinze, T., Heinze, U. & Wagenknecht, W., 1998. *Comprehensive Cellulose Chemistry, Volume 1.* Wiley–VCH: Weinheim.

Klotz, E., Doyle, R., Gross, E. & Mattson, B., 2011. The equilibrium constant for bromothymol blue: A general chemistry laboratory experiment using spectroscopy. *J. Chem. Educ.* 88, 637–639.

Köhler, S., Liebert, T., Schöbitz, M., Schaller, J., Meister, F., Günther, W. & Heinze, T., 2007. Interactions of ionic liquids with polysaccharides 1. Unexpected acetylation of cellulose with 1-ethyl-3-methylimidazolium acetate. *Macromol. Rapid Commun.* 28, 2311–2317.

Kosan, B., Michels, C. & Meister, F., 2008. Dissolution and forming of cellulose with ionic liquids. *Cellulose* 15, 59–66.

Kosan, B., Schwikal, K. & Meister, F., 2010. Solution states of cellulose in selected direct dissolution agents. *Cellulose* 17, 495–506.

Kumler, W. & Eiler, J. J., 1943. The acid strength of mono and diesters of phosphoric acid. The n–alkyl esters from methyl to butyl, the esters of biological importance, and the natural guanidine phosphoric acids. *J. Am. Chem. Soc.* 65, 2355–2361.

Kuo, C. & Lee, C., 2009. Enhancement of enzymatic saccharification of cellulose by cellulose dissolution pretreatments. *Carbohydr. Polym.* 77, 41–46.

Kupfer, H., 2012. *personal communication.* BASF SE: Ludwigshafen.

Kuzmina, O., Sashina, E., Troshenkowa, S. & Wawro, D., 2010. Dissolved state of cellulose in ionic liquids – the impact of water. *Fibres Text. East. Eur.* 18, 32–37.

Labbé, N., Kline, L. M., Moens, L., Kim, K., Kim, P. C. & Hayes, D. G., 2012. Activation of lignocellulosic biomass by ionic liquid for biorefinery fractionation. *Bioresour. Technol.* 104, 701–707.

Ladisch, M., Ladisch, C. & Tsao, G., 1978. Cellulose to sugars: New path gives quantitative yield. *Science* 201, 743–745.

Langan, P., Nishiyama, Y. & Chanzy, H., 1999. A revised structure and hydrogen-bonding system in cellulose II from a neutron fiber diffraction analysis. *J. Am. Chem. Soc.* 121, 9940–9946.

Larsen, K. L. & Barsberg, S., 2010. Theoretical and Raman spectroscopic studies of phenolic lignin model monomers. *J. Phys. Chem. B* 114, 8009–8021.

Laurence, C., Nicolet, P., Dalati, M. T., Abboud, J. M. & Notario, R., 1994. The empirical treatment of solvent-solute interactions: 15 Years of pi*. *J. Phys. Chem.* 98, 5807–5816.

Laus, G., Bentivoglio, G., Schottenberger, H., Kahlenberg, v., Kopacka, H., Röder, T. & Sixta, H., 2005. Ionic liquids: Current developments, potential and drawbacks for industrial applications. *Lenzinger Berichte* 84, 71–85.

Lebo, S. E., Gargulak, J. D. & McNally, T. J., 2001. Lignin. In: *Kirk–Othmer Encyclopedia of Chemical Technology.* John Wiley & Sons New: York.

Lee, S., Doherty, T., Linhardt, R. & Dordick, J., 2009. Ionic liquid–mediated selective extraction of lignin from wood leading to enhanced enzymatic cellulose hydrolysis. *Biotechnol. Bioeng.* 102, 1368–1376.

Le, K., Sescousse, R. & Budtova, T., 2012. Influence of water on cellulose–EMIMAc solution properties: a viscometric study. *Cellulose* 19, 45–54.

Leskinen, T., King, A. W. T., Kilpeläinen, I. & Argyropoulos, D. S., 2011. Fractionation of lignocellulosic materials with ionic liquids. 1. Effect of mechanical treatment. *Ind. Eng. Chem. Res.* 50, 12349–12357.

Li, C., Sun, L., Simmons, B. A. & Singh, S., 2013. Comparing the recalcitrance of eucalyptus, pine, and switchgrass using ionic liquid and dilute acid pretreatments. *Bioenerg. Res.* 6, 14–23.

Liebert, T., 2010. Cellulose Solvents – Remarkable History, Bright Future. In: T. Liebert, T. Heinze & K. J. Edgar, eds. *Cellulose Solvents: For Analysis, Shaping and Chemical Modification.* American Chemical Society, Washington. 3–54.

Liebert, T. & Heinze, T., 2008. Interaction of ionic liquids with polysaccharides. 5. Solvents and reaction media for the modification of cellulose. *Bioresources* 3, 576–601.

Liu, D., Zhang, Y. & Chen, E. Y., 2012. Organocatalytic upgrading of the key biorefining building block by a catalytic ionic liquid and N-heterocyclic carbenes. *Green Chem.* 14, 2738–2746.

Liu, H., Sale, K., Holmes, B., Simmons, B. & Singh, S., 2010. Understanding the interactions of cellulose with ionic liquids: A molecular dynamics study. *J. Phys. Chem. B* 114, 4293–4301.

Locke, E., Saeman, J. & Dickerman, G., 1945. *The Production of wood sugar in Germany and its conversion to yeast and alcohol,* US Army: Field Information Agency, Technical.

Lovelock, K. R. J., Deyko, A., Licence, P. & Jones, R. G., 2010. Vaporisation of an ionic liquid near room temperature. *Phys. Chem. Chem. Phys.* 12, 8893–8901.

Lozano, P., Bernal, B., Recio, I. & Belleville, M., 2012. A cyclic process for full enzymatic saccharification of pretreated cellulose with full recovery and reuse of the ionic liquid 1-butyl-3-methylimidazolium chloride. *Green Chem.* 14, 2631–2637.

Lucas, M., Wagner, G., Nishiyama, Y., Hanson, L., Samayam, I., Schall, C., Langan, P. & Rector, K., 2011. Reversible swelling of the cell wall of poplar biomass by ionic liquid at room temperature. *Bioresour. Technol.* 102, 4518–4523.

Lüers, H., 1930. Das Celluloseverzuckerungsverfahren von H. Scholler. *Angew. Chem.* 43, 455–458.

Lüers, H., 1937. Der heutige Stand der Holzverzuckerung. *Holz Roh. Werkst.* 1, 35–40.

Lungwitz, R., Friedrich, M., Linert, W. & Spange, S., 2008. New aspects on the hydrogen bond donor (HBD) strength of 1-butyl-3-methylimidazolium room temperature ionic liquids. *New J. Chem.* 32, 1493–1499.

Lungwitz, R., Strehmel, V. & Spange, S., 2010. The dipolarity/polarisability of 1-alkyl-3-methylimidazolium ionic liquids as function of anion structure and the alkyl chain length. *New J. Chem.* 34, 1135–1140.

Lv, Y., Wu, J., Zhang, J., Niu, Y., Liu, C., He, J. & Zhang, J., 2012. Rheological properties of cellulose/ionic liquid/dimethylsulfoxide (DMSO) solutions. *Polymer* 53, 2524–2531.

Lynd, L., Wyman, C. & Gerngross, T., 1999. Biocommodity engineering. *Biotechnol. Prog.* 15, 777–793.

MacFarlane, D., Pringle, J., Johansson, K., Forsyth, S. & Forsyth, M., 2006. Lewis base ionic liquids. *Chem. Commun.* 1905–1917.

Magill, A. M., Cavell, K. J. & Yates, B. F., 2004. Basicity of nucleophilic carbenes in aqueous and nonaqueous solvents theoretical predictions. *J. Am. Chem. Soc.* 126, 8717–8724.

Marcus, Y., 1993. The properties of organic liquids that are relevant to their use as solvating solvents. *Chem. Soc. Rev.* 22, 409–416.

Marquardt, W., 2005. *Prozessentwicklung in der Verfahrenstechnik.* RWTH Aachen University.

Marquardt, W., Harwardt, A., Hechinger, M., Kraemer, K., Viell, J. & Voll, A., 2010. The biorenewables opportunity – toward next generation process and product systems. *AIChE J.* 56, 2228–2235.

Marson, G. A. & El Seoud, O. A., 1999. Cellulose dissolution in lithium chloride/N,N-dimethylacetamide solvent system: Relevance of kinetics of decrystallization to cellulose derivatization under homogeneous solution conditions. *J. Polym. Sci. A1* 37, 3738–3744.

Maton, C., De Vos, N. & Stevens, C. V., 2013. Ionic liquid thermal stabilities: decomposition mechanisms and analysis tools. *Chem. Soc. Rev.* 42, 5963–5977.

Matthews, J. F., Bergenstrahle, M., Beckham, G. T., Himmel, M. E., Nimlos, M. R., Brady, J. W. & Crowley, M. F., 2011. High-temperature behavior of cellulose I. *J. Phys. Chem. B* 115, 2155–2166.

Mazza, M., Catana, D.-A., Vaca-Garcia, C. & Cecutti, C., 2009. Influence of water on the dissolution of cellulose in selected ionic liquids. *Cellulose* 16, 207–215.

McDonough, T., 1992. *The chemistry of Organosolv delignification,* The Institute of Paper Science and Technology: Atlanta.

McMillan, J., 1994. Pretreatment of Lignocellulosic Biomass. In: M. Himmel, J. Baker & R. Overend, eds. *Enzymatic Conversion of Biomass for Fuels Production.* American Chemical Society, Washington, pp 292–324.

Meine, N., Benedito, F. & Rinaldi, R., 2010. Thermal stability of ionic liquids assessed by potentiometric titration. *Green Chem.* 12, 1711–1714.

Michels, C. & Kosan, B., 2005. Contribution to the dissolution state of cellulose and cellulose derivatives. *Lenzinger Berichte* 84, 62–70.

Michels, J., 2009. *Pilotprojekt "Lignocellulose-Bioraffinerie",* DECHEMA: Frankfurt.

Michels, J. & Wagemann, K., 2010. The German lignocellulose feedstock biorefinery project. *Biofuel. Bioprod. Bior.* 4, 263–267.

Mikkola, J.-P., Kirilin, A., Tuuf, J.-C., Pranovich, A., Holmbom, B., Kustov, L., Murzin, D. & Salmi, T., 2007. Ultrasound enhancement of cellulose processing in ionic liquids: from dissulution towards functionalization. *Green Chem.* 9, 1229–1237.

Mimms, A. K. M. P. J. & Wright, E., 1989. *Kraft pulping: a compilation of notes.* Tappi Press: Atlanta.

Miyafuji, H., Miyata, K., Saka, S., Ueda, F. & Mori, M., 2009. Reaction behavior of wood in an ionic liquid, 1-ethyl-3-methylimidazolium chloride. *J. Wood Sci.* 15, 215–219.

Miyafuji, H. & Suzuki, N., 2011. Observation by light microscope of sugi (Cryptomeria japonica) treated with the ionic liquid 1-ethyl-3-methylimidazolium chloride. *J. Wood Sci.* 57, 459–461.

Miyafuji, H. & Suzuki, N., 2012. Morphological changes in sugi (Cryptomeria japonica) wood after treatment with the ionic liquid, 1-ethyl-3-methylimidazolium chloride. *J. Wood Sci.* 58, 222–230.

Modenbach, A. A. & Nokes, S. E., 2012. The use of high-solids loadings in biomass pretreatment – a review. *Biotechnol. Bioeng.* 109, 1430–1442.

Mora-Pale, M., Meli, L., Doherty, T. V., Linhardt, R. J. & Dordick, J. S., 2011. Room temperature ionic liquids as emerging solvents for the pretreatment of lignocellulosic biomass. *Biotechnol. Bioeng.* 108, 1229–1245.

Mosier, N., Wyman, C., Dale, B., Elander, R., Lee, Y., Holtzale, M. & Ladisch, M., 2005. Features of promising technologies for pretreatment of lignocellulosic biomass. *Bioresource Technol.* 96, 673–686.

Nakamura, A., Miyafuji, H. & Saka, S., 2010a. Liquefaction behavior of Western red cedar and Japanese beech in the ionic liquid 1-ethyl-3-methylimidazolium chloride. *Holzforschung* 64, 289–294.

Nakamura, A., Miyafuji, H., Saka, S., Mori, M. & Takahashi, H., 2010b. Recovery of cellulose and xylan liquefied in ionic liquids by precipitation in anti-solvents. *Holzforschung* 64, 77–79.

Nic, M., Jirat, J., Kosata, B. & Jenkins, A., 2006. *IUPAC compendium of chemical terminology, 2nd ed. (the "Gold Book").* International Union of Pure and Applied Chemistry: Oxford.

Nishiyama, Y., Langan, P. & Chanzy, H., 2002. Crystal structure and hydrogen-bonding system in cellulose I from synchrotron X-ray and neutron fiber diffraction. *J. Am. Chem. Soc.* 124, 9074–9082.

Ni, Y. & Hu, Q., 1995. Alcell lignin solubility in ethanol-water mixtures. *J. Appl. Polym. Sci.* 57, 1441–1446.

Nordisk, N., 1999. *Product sheet Celluclast 1.5 L,* Novo Nordisk Ferment Ltd.: Dittingen, Switzerland.

Novoselov, N., Sashina, E., Petrenko, V. & Zaborsky, M., 2007. Study of dissolution of cellulose in ionic liquids by computer modeling. *Fibre Chem.* 39, 153–158.

OECD/FAO, 2011. *OECD–FAO Agricultural outlook 2011–2020,* OECD Publishing and FAO: Paris.

Ohno, H. & Fukaya, Y., 2009. Task specific ionic liquids for cellulose technology. *Chem. Lett.* 38, 2–7.

Ohtani, J. & Ishaya, S., 1973. An observation of the sculptures of the vessel wall of fagus crenata BL. using scanning electron microscopy. *Reaseach Bulletins of the college experiment forrests, Hokkaido University* 30, 125–143.

Oliet, M., Rodriguez, F., Santos, A., Gilarranz, M., Garcia–Ochoa, F. & Tijero, J., 2000. Organosolv delignification of Eucolyptus globulus: Kinetic study of autocatalyzed ethanol pulping. *Ind. Eng. Chem. Res.* 39, 34–39.

Padmanabhan, S., Kim, M., Blanch, H. W. & Prausnitz, J. M., 2011. Solubility and rate of dissolution for Miscanthus in hydrophilic ionic liquids. *Fluid Phase Equilib.* 309, 89–96.

Papa, G., Varanasi, P., Sun, L., Cheng, G., Stavila, V., Holmes, B., Simmons, B., Adani, F. & Singh, S., 2012. Exploring the effect of different plant lignin content and

composition on ionic liquid pretreatment efficiency and enzymatic saccharification of Eucalyptus globulus L. mutants. *Bioresour. Technol.* 117, 352–359.

Park, J. I., Steen, E. J., Burd, H. D., Evans, S. S., Redding–Johnson, A. M., Batth, T., Benke, P. I., D'haeseleer, P., Sun, N., Sale, K. L., Keasling, J. D., Lee, T. S., Petzold, C. J., Mukhopadhyay, A., Singer, S. W., Simmons, B. A. & Gladden, J. M., 2012. A thermophilic ionic liquid–tolerant cellulase cocktail for the production of cellulosic biofuels. *PLoS ONE* 7(5), 1–10.

Park, S., Baker, J. O., Himmel, M. E., Parilla, P. A. & Johnson, D. K., 2010. Cellulose crystallinity index: measurement techniques and their impact on interpreting cellulase performance. *Biotechnology for Biofuels* 3, 1–10.

Pauly, M. & Keegstra, K., 2008. Cell–wall carbohydrates and their modification as a resource for biofuels. *The Plant Journal* 54, 559–568.

Perlack, R. & Stokes, B., 2011. *U.S. billion-ton update: Biomass supply for a bioenergy and bioproducts industry.,* U.S. Department of Energy: Oak Ridge.

Peters, M. S., Timmerhaus, K. & West, R. E., 2003. *Plant Design and Economics for Chemical Engineers.* Mcgraw Hill Inc: New York.

Phillips, M., 1934. The chemistry of lignin. *Chemical Reviews* 14, 103–170.

Pinkert, A., 2012. Comment on "Instantaneous dissolution of cellulose in organic electrolyte solutions". *J. Chem. Eng. Data* 57, 1338–1340.

Pinkert, A., Marsh, K. N. & Pang, S., 2010. Reflections on the solubility of cellulose. *Ind. Eng. Chem. Res.* 49, 11121–11130.

Plechkova, N. & Seddon, K., 2008. Applications of ionic liquids in the chemical industry. *Chem. Soc. Rev.* 37, 123–150.

Politzer, P. & Murray, J., 2006. Quantitative approaches to solute-solvent interactions. In: C. G. Vayenas, R. E. White & M. E. Gamboa-Adelco, eds. *Modern Aspects of Electrochemistry.* Springer, New York, pp 1–63.

Preiss, U., Emel'yanenko, V. N., Verevkin, S. P., Himmel, D., Paulechka, Y. U. & Krossing, I., 2010. Temperature–dependent prediction of the liquid entropy of ionic liquids. *ChemPhysChem* 11, 3425–3431.

Pu, Y., Jiang, N. & Ragauskas, A., 2007. Ionic liquids as a green solvent for lignin. *J. Wood Chem. Technol.* 27, 23–33.

Rabideau, B. D., Agarwal, A. & Ismail, A. E., 2013. Observed mechanism for the breakup of small bundles of cellulose Ialpha and Ibeta in ionic liquids from molecular dynamics simulations. *J. Phys. Chem. B* 117, 3469–3479.

Rahman, M., Rodriguez, H., Sun, N., Swatloski, R. P., Daly, D. T. & Rogers, R. D., 2009. *Ionic liquid systems for the processing of biomass, their components and/or derivatives, and mixtures thereof,* US Patent: WO2009105236 A1.

Rayne, S. & Mazza, G., 2007. Rapid dissolution of lignocellulosic plant materials in an ionic liquid. *Nature Precedings.*

Reddy, R. G., 2006. Ionic liquids: How well do we know them? *J. Phase Equilib. Diff.* 27, 210–211.

Reese, E., 1976. The history of cellulases. In: E. Gaden, M. Mandels, E. Reese & L. Spano, eds. *Enzymatic Conversion of Cellulosic Materials: Technology and Applications.* Wiley: New York, pp 9–20.

Reichardt, C., 1994. Solvatochromic dyes as solvent polarity indicators. *Chem. Rev.* 94, 2319–2358.

Reichardt, C., 2005. Polarity of ionic liquids determined empirically by means of solvatochromic pyridinium N-phenolate betaine dyes. *Green Chem.* 7, 339–351.

Reichardt, C. & Welton, T., 2010. *Solvents and Solvent Effects in Organic Chemistry.* Wiley–VCH: Weinheim.

Remsing, R., Hernandez, G., Swatloski, R., Massefski, W., Rogers, R. & Moyna, G., 2008. Solvation of carbohydrates in N,N'-dialkylimidazolium ionic liquids: A multinuclear NMR spectroscopy study. *J. Phys. Chem. B* 112, 11071–11078.

Renon, H. & Prausnitz, J. M., 1968. Local compositions in thermodynamic excess functions for liquid mixtures. *AIChE J.* 14, 135–144.

Revelli, A., Mutelet, F. & Jaubert, J., 2009. Partition coefficients of organic compounds in new imidazolium based ionic liquids using inverse gas chromatography. *J. Chromatogr. A* 1216, 4775–4786.

Rinaldi, R., 2011. Instantaneous dissolution of cellulose in organic electrolyte solutions. *Chem. Commun.* 47, 511–513.

Rinaldi, R., 2012. Reply to "Comment on 'Instantaneous dissolution of cellulose in organic electrolyte solutions' ". *J. Chem. Eng. Data* 57, 1341–1343.

Rinaldi, R. & Schüth, F., 2010. Acid hydrolysis of cellulose as the entry point into biorefinery schemes. *ChemSusChem* 3, 296–296.

Roberts, R. & Rowe, R., 1993. The solubility parameter and fractional polarity of microcrystalline cellulose as determined by mechanical measurement. *Int. J. Pharm.* 99, 157–164.

Röder, T., Moosbauer, J., Fasching, M., Bohn, A., Fink, H., Baldinger, T. & Sixta, H., 2006. Crystallinity determination of native cellulose – comparison of analytical methods. *Lenzinger Berichte* 86, 85–89.

Rodriguez, H., Gurau, G., Holbrey, J. D. & Rogers, R. D., 2011. Reaction of elemental chalcogens with imidazolium acetates to yield imidazole-2-chalcogenones: direct evidence for ionic liquids as proto-carbenes. *Chem. Commun.* 47, 3222–3224.

Rogers, R. D. & Seddon, K. R., 2003. Ionic liquids – solvents of the future?. *Science* 302, 792–793.

Römich, C., Merkel, N. C., Valbonesi, A., Schaber, K., Sauer, S. & Schubert, T. J. S., 2012. Thermodynamic properties of binary mixtures of water and room-temperature ionic liquids: Vapor pressures, heat capacities, densities and viscosities of water + 1-ethyl-3-methylimidazolium acetate and water + diethylmethylammonium methane sulfonate. *J. Chem. Eng. Data* 57, 2258–2264.

Saake, B. & Lehnen, R., 2007. Lignin. In: *Ullmann's Encyclopedia of Industrial Chemistry.* Wiley–VCH, Weinheim, pp 21–36.

Saeman, J., 1949. Zur Kinetik der Hydrolyse des Holzes und der Zersetzung der Zucker in verdünnten Säuren bei hohen Temperaturen. *Holzforschung* 4, 1–14.

Saito, T., Brown, R. H., Hunt, M. A., Pickel, D. L., Pickel, J. M., Messman, J. M., Baker, F. S., Keller, M. & Naskar, A. K., 2012. Turning renewable resources into value-added polymer: development of lignin-based thermoplastic. *Green Chem.* 14, 3295–3303.

Sakakibara, A. & Sana, Y., 2000. Chemistry of Lignin. In: D. N. Hon, ed. *Wood and Cellulosic Chemistry.* Marcel Dekker: New York, pp 109–174.

Salmén, L. & Burgert, I., 2009. Cell wall features with regard to mechanical performance. A review. *Holzforschung* 63, 121–129.

Sanders, J., Clark, J., Harmsen, G., Heeres, H., Heijnen, J., Kersten, S., van Swaaij, W. & Moulijn, J., 2012. Process intensification in the future production of base chemicals from biomass. *Chem. Eng. Process.* 51, 117–136.

Sarkar, A. & Pandey, S., 2006. Solvatochromic absorbance probe behavior and preferential solvation in aqueous 1-butyl-3-methylimidazolium tetrafluoroborate. *J. Chem. Eng. Data* 51, 2051–2055.

Sashina, E. & Novoselov, N., 2009. Effect of structure of ionic liquids on their dissolving power toward natural polymers. *Russ. J. Gen. Chem.* 79, 1057–1062.

Schenzel, K., Almlöf, H. & Germgard, U., 2009. Quantitative analysis of the transformation process of cellulose I [to] cellulose II using NIR FT Raman spectroscopy and chemometric methods. *Cellulose* 16, 407–415.

Schenzel, K. & Fischer, S., 2001. NIR FT Raman spectroscopy – a rapid analytical tool for detecting the transformation of cellulose polymorphs. *Cellulose* 8, 49–57.

Schliephake, 1990. Umweltschonende Aufschlußverfahren von pflanzlichem Material zur Gewinnung von Faserzellstoffen. *Lenzinger Berichte* 69, 21–28.

Schlüter, F., 2011. Lösungsvermögen ionischer Flüssigkeiten für Holz. Bachelor Thesis, RWTH Aachen University.

Schmeisser, M., Illner, P., Puchta, R., Zahl, A. & van Eldik, R., 2012. Gutmann donor and acceptor numbers for ionic liquids. *Chem. – Eur. J.* 18, 10969–10982.

Schubert, H., 2006. Probleme der Umsetzung neuer Technologie in die industrielle Praxis, dargestellt am Beispiel des alkalischen Suflitverfahrens mit AQ und Methanol – ASAM. *Lenzinger Berichte* 86, 24–31.

Schuerch, C., 1952. The solvent properties of liquids and their relation to the solubility, swelling, isolation and fractionation of lignin. *J. Am. Chem. Soc.* 74, 5061–5067.

Schulz, G. V. & Löhmann, H. J., 1941. Über die Kinetik des hydrolytischen Abbaus der Cellulose. 261. Mitteilung über makromolekulare Verbindungen. *J. Prakt. Chem.* 157, 238–282.

Schütt, F., Puls, J. & Saake, B., 2011. Optimization of steam pretreatment conditions for enzymatic hydrolysis of poplar wood. *Holzforschung* 65, 453–459.

Schütt, F., Westereng, B., Horn, S. J., Puls, J. & Saake, B., 2012. Steam refining as an alternative to steam explosion. *Bioresource Technology* 111, 476–481.

Seddon, K., Stark, A. & Torres, M., 2000. Influence of chloride, water, and organic solvents on the physical properties of ionic liquids. *Pure Appl. Chem.* 72, 2275–2287.

Sen, S. M., Binder, J. B., Raines, R. T. & Maravelias, C. T., 2012. Conversion of biomass to sugars via ionic liquid hydrolysis: process synthesis and economic evaluation. *Biofuel. Bioprod. Bior.* 6, 444–452.

Sescousse, R., Le, K. A., Ries, M. & Budtova, T., 2010. Viscosity of cellulose-imidazolium-based ionic liquid solutions. *J. Phys. Chem. B* 114, 7222–7228.

Shafiei, M., Karimi, K. & Taherzadeh, M. J., 2011. Techno–economical study of ethanol and biogas from spruce wood by NMMO–pretreatment and rapid fermentation and digestion. *Bioresour. Technol.* 102, 7879–7886.

Shiflett, M. B., Drew, D. W., Cantini, R. A. & Yokozeki, A., 2010. Carbon dioxide capture using ionic liquid 1-butyl-3-methylimidazolium acetate. *Energ. Fuel.* 24, 5781–5789.

Shimizu, K., Sudo, K., Ono, H., Ishihara, M., Fujii, T. & Hishiyama, S., 1998. Integrated process for total utilization of wood components by steam–explosion pretreatment. *Biomass and Bioenergy* 14, 195–203.

Shukla, S. K., Khupse, N. D. & Kumar, A., 2012. Do anions influence the polarity of protic ionic liquids?. *Phys. Chem. Chem. Phys.* 14, 2754–2761.

Singh, S., Sammons, B. & Vogel, K., 2009. Visualization of biomass solubilization and cellulose regeneration during ionic liquid pretreatment of switchgrass. *Biotechnol. Bioeng.* 104, 68–75.

Sixta, H., ed., 2006. *Handbook of Pulp.* Wiley–VCH: Weinheim.

Sixta, H., Potthast, A. & Krotschek, A. W., 2006. Chemical Pulping Processes. In: H. Sixta, ed. *Handbook of Pulp.* Wiley-VCH: Weinheim, pp 109–510.

Sjostrom, E., 1993. *Wood Chemistry, Second Edition: Fundamentals and Applications.* Academic Press: San Diego.

Sluiter, A., Hames, B., Hyman, D., Payne, C., Ruiz, R., Scarlata, C., Sluiter, J., Templeton, D. & Wolfe, J., 2008. *Determination of total solids in biomass and total dissolved solids in liquid process samples,* National Renewable Energy Laboratory: Golden.

Sluiter, A., Hames, B., Ruiz, R., Scarlata, C., Sluiter, J. & Templeton, D., 2005a. *Determination of ash in biomass,* National Renewable Energy Laboratory: Golden.

Sluiter, A., Hames, B., Ruiz, R., Scarlata, C., Sluiter, J., Templeton, D. & Crocker, D., 2011. *Determination of structural carbohydrates and lignin in biomass,* National Renewable Energy Laboratory: Golden.

Sluiter, A., Ruiz, R., Scarlata, C., Sluiter, J. & Templeton, D., 2005b. *Determination of extractives in biomass,* National Renewable Energy Laboratory: Golden.

Sluiter, J. B., Ruiz, R. O., Scarlata, C. J., Sluiter, A. D. & Templeton, D. W., 2010. Compositional analysis of lignocellulosic feedstocks. 1. Review and description of methods. *J. Agric. Food Chem.* 58, 9043–9053.

Sorvari, J., Sjöström, E., Klemola, A. & Laine, J., 1986. Chemical characterization of wood constituents, especially lignin, in fractions separated from middle lamella and secondary wall of Norway spruce (Picea abies). *Wood Sci. Technol.* 20, 35–51.

Spange, S., K., F., Prause, S. & Heinze, T., 2003. Empirical polarity parameters of celluloses and related materials. *Cellulose* 10, 201–212.

Spange, S., Reuter, A., Vilsmeier, E., Heinze, T., Keutel, D. & Linert, W., 1998. Determination of empirical polarity parameters of the cellulose solvent N,N–dimethylacetamide/LiCl by means of the solvatochromic technique. *J. Polym. Sci. A1* 36, 1945–1955.

Steele, B., Raj, S., Nghiem, J. & Stowers, M., 2005. Enzyme recovery and recycling following hydrolysis of ammonia fiber explosion–treated corn stover. *Applied Biochemistry and Biotechnology* 124, 901–910.

Strechan, A., Paulechka, Y., Blokhin, A. & Kabo, G., 2008. Low-temperature heat capacity of hydrophilic ionic liquids [BMIM][CF3COO] and [BMIM][CH3COO] and a correlation scheme for estimation of heat capacity of ionic liquids. *J. Chem. Thermodyn.* 40, 632–639.

Sugiyama, J., Vuong, R. & Chanzy, H., 1991. Electron diffraction study on the two crystalline phases occurring in native cellulose from an algal cell wall. *Macromolecules* 24, 4168–4175.

Sun, N., Rahman, M., Qin, Y., Maxim, M., Rodríguez, H. & Rogers, R., 2009. Complete dissolution and partial delignification of wood in the ionic liquid 1-ethyl-3-methylimidazolium acetate. *Green Chem.* 11, 646–655.

Suresh, S. J. & Naik, V. M., 2000. Hydrogen bond thermodynamic properties of water from dielectric constant data. *J. Chem. Phys.* 113, 9727–9732.

Swatloski, R., Spear, S., Holbrey, J. & Rogers, R., 2002. Dissolution of cellose with ionic liquids. *J. Am. Chem. Soc.* 124, 4974–4975.

Taft, R. W. & Kamlet, M. J., 1979. Linear solvation energy relationships. Part 4. Correlations with and limitations of the alpha scale of solvent hydrogen bond donor acidities. *J. Chem. Soc., Perkin Trans. 2* 12, 1723–1729.

Taherzadeh, M. J. & Karimi, K., 2007. Acid–based hydrolysis processes for ethanol from lignocellulosic materials: A review. *BioResources* 2, 472–499.

Takayama, M., Johjima, T., Yamanaka, T., Wariishi, H. & Tanaka, H., 1997. Fourier transform Raman assignment of guaiacyl and syringyl marker bands for lignin determination. *Spectrochim. Acta A* 53, 1621–1628.

Tang, S., Baker, G. A. & Zhao, H., 2012. Ether- and alcohol-functionalized task-specific ionic liquids: attractive properties and applications. *Chem. Soc. Rev.* 41, 4030–4066.

Timell, T. E., 1967. Recent progress in the chemistry of wood hemicelluloses. *Wood Sci. Technol.* 1, 45–70.

Torr, K. M., Love, K. T., Cetinkol, O. P., Donaldson, L. A., George, A., Holmes, B. M. & Simmons, B. A., 2012. The impact of ionic liquid pretreatment on the chemistry and enzymatic digestibility of Pinus Radiata compression wood. *Green Chem.* 14, 778–787.

Trivedi, S., Malek, N., Behera, K. & Pandey, S., 2010. Temperature–dependent solvatochromic probe behavior within ionic liquids and (ionic liquid + water) mixtures. *J. Phys. Chem. B* 114, 8118–8125.

Tuck, C. O., Pérez, E., Horváth, I. T., Sheldon, R. A. & Poliakoff, M., 2012. Valorization of biomass: Deriving more value from waste. *Science* 337, 695–699.

Valderrama, J. O. & Rojas, R. E., 2009. Critical properties of ionic liquids. Revisited. *Ind. Eng. Chem. Res.* 48, 6890–6900.

Varanasi, P., Singh, P., Arora, R., Adams, P. D., Auer, M., Simmons, B. A. & Singh, S., 2012. Understanding changes in lignin of Panicum virgatum and Eucalyptus globulus as a function of ionic liquid pretreatment. *Bioresource Technol.* 126, 156–161.

Verevkin, S. P., Zaitsau, D. H., Emel'yanenko, V. N., Schick, C., Jayaraman, S. & Maginn, E. J., 2012. An elegant access to formation and vaporization enthalpies of ionic liquids by indirect DSC experiment and "in silico" calculations. *Chem. Commun.* 48, 6915–6917.

Viell, J., Fajzulin, I. & Marquardt, W., 2013. Monitoring of the dissolution of crystalline cellulose in mixtures of ionic liquids and H2O by FT Raman spectroscopy and indirect hard modeling. *in preparation.*

Viell, J., Harwardt, A., Seiler, J. & Marquardt, W., 2013b. Is biomass fractionation by Organosolv–like processes economically viable? A conceptual design study. *Bioresour. Technol.* 150, 89–97.

Viell, J. & Marquardt, W., 2011. Disintegration and dissolution kinetics of wood chips in ionic liquids. *Holzforschung* 65, 519–525.

Viell, J. & Marquardt, W., 2012. Concentration measurements in ionic liquid-water mixtures by mid-infrared spectroscopy and indirect hard modeling. *Appl. Spectrosc.* 66, 208–217.

Viell, J., Wulfhorst, H., Schmidt, T., Commandeur, U., Fischer, R., Spiess, A. & Marquardt, W., 2013a. An efficient process for the saccharification of wood chips by combined ionic liquid pretreatment and enzymatic hydrolysis. *Bioresour. Technol.* 146, 144–151.

Vitha, M. & Carr, P. W., 2006. The chemical interpretation and practice of linear solvation energy relationships in chromatography. *J. Chromatogr. A* 1126, 143–194.

Vitz, J., Erdmenger, T., Haenscha, C. & Schubert, U., 2009. Extended dissolution studies of cellulose in imidazolium based ionic liquids. *Green Chem.* 11, 417–424.

Wada, M., Ike, M. & Tokuyasu, K., 2010. Enzymatic hydrolysis of cellulose I is greatly accelerated via its conversion to the cellulose II hydrate form. *Polym. Degrad. Stab.* 95, 543–548.

Wang, H., Gurau, G. & Rogers, R. D., 2012. Ionic liquid processing of cellulose. *Chem. Soc. Rev.* 41, 1519–1537.

Wang, J., Ren, J., Liu, X., Lu, G. & Wang, Y., 2013. High yield production and purification of 5-hydroxymethylfurfural. *AIChE J.* 59, 2558–2566.

Wasserscheid, P. & Welton, T. eds., 2007. *Ionic Liquids in Synthesis.* Wiley–VCH: Weinheim.

Weerachanchai, P., Chen, Z., Leong, S. S. J., Chang, M. W. & Lee, J., 2012. Hildebrand solubility parameters of ionic liquids: Effects of ionic liquid type, temperature and DMA fraction in ionic liquid. *Chem. Eng. J.* 213, 356–362.

Weingärtner, H., 2008. Zum Verständnis ionischer Flüssigkeiten auf molekularer Ebene: Fakten, Probleme und Kontroversen. *Angew. Chem.* 120, 664–682.

Wendler, F., Todi, L. & Meister, F., 2012. Thermostability of imidazolium ionic liquids as direct solvents for cellulose. *Thermochim. Acta* 528, 76–84.

Wen, J., Sun, S., Xue, B. & Sun, R., 2013. Quantitative structures and thermal properties of birch lignins after ionic liquid pretreatment. *J. Agr. Food Chem.* 61, 635–645.

Wenzl, H., 1970. *The Chemical Technology of Wood.* Academic Press: New York.

White, R. H., 1987. Effect of lignin content and extractives on the higher heating value of wood. *Wood Fiber Sci.* 19, 446–452.

Wiesenthal, T., Mourelatou, A., Peterson, J. & Taylor, P., 2006. *How much bioenergy can Europe produce without harming the environment?* European Environment Agency: Copenhagen, Denmark.

Wiley, J. & Atalla, R., 1987. Band assignments in the Raman spectra of celluloses. *Carbohydr. Res.* 160, 113–129.

Willför, S., Pranouich, A., Tamminen, T., Puls, J., Lained, C., Suurniikki, A., Saake, B., Uotila, K., Simolin, H., Hemminga, J. & Holmbom, B., 2009. Carbohydrate analysis of plant materials with uronic acid-containing polysaccharides – A comparison between different hydrolysis and subsequent chromatographic analytical techniques. *Ind. Crop.Prod.* 29, 571–580.

Willför, S., Sundberg, A., Hemming, J. & Holmbom, B., 2005a. Polysaccharides in some industrially important softwood species. *Wood Sci. Technol.* 39, 245–257.

Willför, S., Sundberg, A., Pranovich, A. & Holmbom, B., 2005b. Polysaccharides in some industrially important hardwood species. *Wood Sci. Technol.* 39, 601–617.

Willför, S., Sundberg, K., Tenkanen, M. & Holmbom, B., 2008. Spruce-derived mannans – A potential raw material for hydrocolloids and novel advanced natural materials. *Carbohydr. Polym.* 72, 197–210.

Wooley, R. J. & Putsche, V., 1996. *Development of an Aspen Plus physical property database for biofuels components, NREL/MP–425–20685,* National renewable energy laboratory (NREL)/US Department of Energy: Golden.

Xiao, W., Yin, W., Xia, S. & Ma, P., 2012. The study of factors affecting the enzymatic hydrolysis of cellulose after ionic liquid pretreatment. *Carbohydr. Polym.* 87, 2019–2023.

Xu, A., Wang, J. & Wang, H., 2010. Effects of anionic structure and lithium salts addition on the dissolution of cellulose in 1-butyl-3-methylimidazolium-based ionic liquid solvent systems. *Green Chem.* 12, 268–275.

Xu, A., Zhang, Y., Zhao, Y. & Wang, J., 2013. Cellulose dissolution at ambient temperature: Role of preferential solvation of cations of ionic liquids by a cosolvent. *Carbohydrate Polymers* 92, 540–544.

Xu, F., Shi, Y.-C. & Wang, D., 2012. Enhanced production of glucose and xylose with partial dissolution of corn stover in ionic liquid, 1-ethyl-3-methylimidazolium acetate. *Bioresour. Technol.* 114, 720–724.

Xu, H., Pan, W., Wang, R., Zhang, D. & Liu, C., 2012b. Understanding the mechanism of cellulose dissolution in 1-butyl-3-methylimidazolium chloride ionic

liquid via quantum chemistry calculations and molecular dynamics simulations. *J. Comput. Aided Mol. Des.* 26, 329–337.

Yang, B. & Wyman, C., 2008. Pretreatment: the key to unlocking low-cost cellulosic ethanol. *Biofuel. Bioprod. Bior.* 2, 26–40.

Yawalata, D. & Paszner, L., 2004. Cationic effect in high concentration alcohol organosolv pulping: The next generation biorefinery. *Holzforschung* 58, 7–13.

Yoo, B., Afzal, W. & Prausnitz, J. M., 2012. Solubility parameters for nine ionic liquids. *Ind. Eng. Chem. Res.* 51, 9913–9917.

Yuan, T., Wang, W., Xu, F. & Sun, R., 2012. Synergistic benefits of ionic liquid and alkaline pretreatments of poplar wood. Part 1: Effect of integrated pretreatment on enzymatic hydrolysis. *Bioresour. Technol.* 144, 429–434.

Yu, G., Zhao, D., Wen, L., Yang, S. & Chen, X., 2012. Viscosity of ionic liquids: Database, observation, and quantitative structure-property relationship analysis. *AIChE J.* 58, 2885–2899.

Yu, H., Hu, J. & Chang, J., 2011. Selective separation of wood components based on Hansen's theory of solubility. *Ind. Eng. Chem. Res.* 50, 7513–7519.

Zakrzewska, M., Bogel–Lukasik, E. & Bogel–Lukasik, R., 2010. Solubility of carbohydrates in ionic liquids. *Energ. Fuel.* 24, 737–745.

Zakzeski, J., Bruijnincx, P., Jongerius, A. & Weckhuysen, B., 2010. The catalytic valorization of lignin for the production of renewable chemicals. *Chem. Rev.* 110, 3552–3599.

Zanuttini, M., Marzocchi, V., Mocchiutti, P. & Inalbon, M., 2005. Deacetylation consequences in pulping processes. *Eur. J. Wood Wood Prod.* 63, 149–153.

Zavrel, M., Bross, D., Funke, M., Büchs, J. & Spiess, A., 2008. High-throughput screening for ionic liquids dissolving (ligno-)cellulose. *Bioresour. Technol.* 100, 2580–2587.

Zechmeister, L., 1913. Zur Kenntnis der Cellulose und des Lignins, PhD Thesis, ETH Zürich.

Zhang, H., Wu, J., Zhang, J. & He, J., 2005. 1-Allyl-3-methylimidazolium chloride room temperature ionic liquid: A new and powerful nonderivatizing solvent for cellulose. *Macromolecules* 38, 8272–8277.

Zhang, J., Zhang, H., Wu, J., Zhang, J., He, J. & Xiang, J., 2010c. Reply to "Comment on ‘NMR spectroscopic studies of cellobiose solvation in EmimAc aimed to understand the dissolution mechanism of cellulose in ionic liquids' ". *Phys. Chem. Chem. Phys.* 12, 14829–14830.

Zhang, S., Qi, X., Ma, X., Lu, L. & Deng, Y., 2010b. Hydroxyl ionic liquids: The differentiating effect of hydroxyl on polarity due to ionic hydrogen bonds between hydroxyl and anions. *J. Phys. Chem. B* 114, 3912–3920.

Zhang, Y. a. H., Qian, X. & Chen, E., 2010a. Ionic liquid–water mixtures: Enhanced Kw for efficient cellulosic biomass conversion. *Energ. Fuel.* 24, 2410–2417.

Zhang, Y., Xu, J. & Yuan, Z., 2009. Stimuli–responsive materials applied as carriers of immobilized enzymes. *Mater. Sci. Forum* 610–613, 1198–1202.

Zhao, X., Cheng, K. & Liu, D., 2009. Organosolv pretreatment of lignocellulosic biomass for enzymatic hydrolysis. *Appl. Microbiol.Biot.* 82, 815–827.

Zhao, Y., Liu, X., Wang, J. & Zhang, S., 2013. Effects of anionic structure on the dissolution of cellulose in ionic liquids revealed by molecular simulation. *Carbohydrate Polymers* 94, 723–730.

Zugenmaier, P., 2008. *Crystalline Cellulose and Cellulose Derivatives – Characterization and Structures.* Springer: Berlin.